

# **Modelling extraterrestrial habitability, biomass and biosignatures through the bioenergetic lens**

Peter M. Higgins

Doctor of Philosophy  
The University of Edinburgh  
2022



---

# Abstract

---

In order to survive, evolve and thrive, life requires a biologically useful supply of energy and nutrients. While there is evidence for both throughout the solar system and beyond, quantifying the energetic threshold at which a given environment can be described as habitable remains difficult. This thesis explores how power (energy per unit time) can be used as a habitability predictor in extraterrestrial environments. The behaviour of life is simplified into a series of chemical processes which use energy and nutrients to create and maintain complexity — order from disorder — all while obeying the fundamental laws of thermodynamics. Crucially, the underlying thermodynamics of biology is split into two clear habitability-defining terms: the available power supply and the power demand posed by the environment.

We developed a new computational model for assessing the energetic and nutrient availability of the weakly constrained environments that are typical of astrobiology, astronomy and planetary science. NutMEG [Nutrients, Maintenance, Energy and Growth] can be used to estimate how much biomass an environment could provide were it exposed to life and how a microbial community might affect the local chemistry. We used the model to characterise the behaviour of methanogens in optimal conditions, and examine how the predictions change in energy- or nutrient-limited settings. For this application, NutMEG was configured to replicate methanogen growth behaviour from laboratory data available in the literature. As temperature rises from 280 to 330 K, NutMEG predicts exponential drops in final biomass ( $10^9$ – $10^6$  cells  $L^{-1}$ ) and total methane production from a growth cycle (62–3  $\mu$ M) despite an increase in peak growth rates (0.007–0.14  $hr^{-1}$ ). This owes to the increasing cost of survival diverting energy away from growth processes. Restricting energy and nutrients exacerbates this trend. With minimal assumptions NutMEG can reliably replicate microbial growth behaviour, but better understanding of the synthesis and maintenance costs life must overcome in different extremes is required to improve its results further.

We used NutMEG to examine the habitability of Enceladus’ subsurface ocean. The oceanic composition is difficult to characterise with current data and estimates are highly dependent on model-based interpretations, informed by Cassini measurements, which are also not yet tightly constrained. In light of these ambiguities, we considered a wide selection of parameter spaces to quantify the available energy for

putative methanogens on Enceladus. We estimated the spontaneous power supply their metabolism could provide and compared it to expected power demands in order to map the icy moon's habitability. On the one hand, Enceladus' parameter space contains pockets in which life could thrive. On the other, there are swathes of the parameter space which appear uninhabitable. Enceladean habitability appears to be a delicate balance between the ocean's temperature, pH, salinity and concentrations of carbonates, nutrients and dissolved gases (particularly  $H_2$ ); many of which are co-dependent. Variation in any one of these can tip the balance into uninhabitable conditions. These results do not aim to be pessimistic, but reflect how astrobiologists should be cautiously pragmatic in their approach to calculating the theoretical habitability of bodies which are not yet well characterised.

Finally, we extend this to explore the energetic controls on possible biomass and biosignatures on Enceladus. Peak methanogenic growth rates and biomass estimates for the ocean's parameter space are defined, ranging from completely devoid of life to bustling with biology. We then consider hydrothermal activity as a source of hydrogen and carbon dioxide and quantify how this could improve methanogens' chances of survival in Enceladus' ocean. Using measurements from the Cassini mission and predictions of hydrothermal productivity we constrain the levels of biomass which could be supported in the bulk ocean in a steady state and discuss whether associated biosignatures could be detectable with future instruments. Much of the ocean is inflexible to small changes in biological behaviour, implying that methanogens fitting neatly into such conditions is improbable. However, some pockets of the parameter space at pH 8.5–9 are flexible, and tantalisingly coincide with the current best estimate of bulk ocean pH. In such regions, methanogens could occupy habitable niches in an ocean which behaves as-observed with biomasses of up to  $\sim 10^{10}$  cells  $L^{-1}$ , but this requires such life to be near the  $H_2$  source. Whether biosignatures could be detectable via an amino acid chirality analysis depends on the temperature of the habitat and the flow of material through the ocean, neither of which are understood well enough to draw concrete conclusions yet. At hydrothermal temperatures  $>370$  K these biosignatures decay within months, but in the cool bulk ocean they could be preserved for millennia.

---

## Lay summary

---

To survive, evolve and thrive, life requires a steady supply of energy and nutrients. Both are abundant throughout the universe and can be delivered in many forms — such as food or light — but they must be consistently available over long time periods to be useful for biology. In this thesis we explore how power (the flow of energy through time) can be used to indicate whether or not extraterrestrial environments are able to host Earth-like life. We separate biological energy flows into two groups: the power supply available from an organism’s surroundings, and the power demand associated with surviving there. These settings are considered habitable when supply exceeds demand.

To streamline these calculations we created a new computational model called **NutMEG** [**N**utrients, **M**aintenance, **E**nergy and **G**rowth] which unifies numerous theories about how life behaves under one easy-to-use hood. NutMEG considers the energy and nutrient content of a system to predict its:

1. **Habitability** — whether a community of organisms could survive there.
2. **Biomass** — how many of them we can expect.
3. **Biosignatures** — chemical markers they could be leaving for us to detect with telescopes or space missions.

To begin, we use NutMEG to characterise methanogens — an ancient species which survives on chemicals that are readily available throughout the universe — and examine how their behaviour changes in different conditions. We find that as temperature increases, methanogens grow faster but they create less biomass overall. This is predominantly because in hotter settings they need to use more energy to survive and hence cannot use as much to grow. This has important implications for how much life we could expect in hot extraterrestrial environments.

We then turn our attention to Saturn’s icy moon Enceladus. Observations by NASA’s Cassini spacecraft have revealed tantalising details of its potentially habitable subsurface ocean, allowing it to be resolved in unprecedented detail. Even so, the possible conditions beneath its icy shell are vast, ranging from cold Earth-like seawater to scalding vents of alkaline fluid. One thing we are sure of is that the ocean contains all the ingredients methanogens need to get their energy. We use NutMEG

to search for habitable windows within the uncertainty of available Enceladus data. We find that some regions appear habitable, but not all of them are suitable for methanogens as we know them on Earth.

Finally, we extend this work to estimate how much life Enceladus can sustain and what markers it might be leaving for future space missions to discover. Expected conditions within the ocean range from habitable pockets bustling with life to hellish zones which are completely devoid of life. We test whether small adjustments in biological behaviour (representing evolution) change the ocean chemistry so much that it alters what Cassini would have observed. Interestingly, the conditions which host the most energy would appear significantly different if life were well-adapted to such surroundings. This suggests that if such environments exist they are habitable but not inhabited. On the other hand, the conditions which do not change significantly when biology is introduced are those which we are most confident do exist on Enceladus. This raises the exciting prospect that the pockets of Enceladus' ocean most likely to be inhabited are the ones most likely to be present. Whether biosignatures could be detected on the icy moon remains an open question. Our results suggest they could be preserved in the ocean for anywhere between months and millennia. To hone these results further we need more data on the geochemical processes occurring at the bottom of the ocean. Elucidating them will help determine the feasibility of a life detection mission to Enceladus.

---

# Declaration

---

I declare that this thesis was composed by myself, that the work contained herein is my own except where explicitly stated otherwise in the text, and that this work has not been submitted for any other degree or professional qualification except as specified.

At the time of writing, outcomes of this work and research directly related to it have been published in academic journals, submitted for publication in academic journals, are in preparation for submission to academic journals, and/or have been made freely available online:

- [1] P. M. Higgins and C. S. Cockell. “A bioenergetic model to predict habitability, biomass and biosignatures in astrobiology and extreme conditions”. *Journal of The Royal Society Interface* **17**.171 (2020), p. 20200588. DOI: 10 . 1098 / rsif . 2020 . 0588.
- [2] P. M. Higgins, C. R. Glein, and C. S. Cockell. “Instantaneous Habitable Windows in the Parameter Space of Enceladus’ Ocean”. *Journal of Geophysical Research: Planets* **126**.11 (2021), e2021JE006951. DOI: 10 . 1029 / 2021JE006951.
- [3] P. M. Higgins. “NutMEG”. *Python package*. Available at: <https://github.com/pmhiggins/NutMEG>; Documentation: <https://nutmeg-astrobiology.readthedocs.io> (2021). DOI: 10.5281/zenodo.4746771.
- [4] C. S. Cockell, P. M. Higgins, and A. A. Johnstone. “Biologically Available Chemical Energy in the Temperate but Uninhabitable Venusian Cloud Layer: What Do We Want to Know?” *Astrobiology* **21**.10 (2021). DOI: 10 . 1089 / ast . 2020 . 2280.
- [5] L. M. R. Seeburger, P. M. Higgins, N. P. Whiteford, et al. “Linking methanogenesis in low-temperature hydrothermal systems to planetary spectra: CH<sub>4</sub> biosignatures on an Archean-Earth-like exoplanet”. *Astrobiology (in review)* (2022).
- [6] C. S. Cockell, R. Wordsworth, N. Whiteford, et al. “Minimum Units of Habitability and Their Abundance in the Universe”. *Astrobiology* **21**.4 (2021), pp. 481–489. DOI: 10 . 1089 / ast . 2020 . 2350.

- [7] S. Gault, P. M. Higgins, C. S. Cockell, et al. “A meta-analysis of the activity, stability, and mutational characteristics of temperature-adapted enzymes”. *Bioscience Reports* **41**.BSR20210336 (2021). DOI: 10.1042/BSR20210336.
- [8] E. J. Ortega Arzola, P. M. Higgins, and C. S. Cockell. “Energetics of building cell structures: synthesizing proteomes, genomes, transcriptomes, and membranes”. *PNAS (in preparation)* (2022).

signature.jpg

*(Peter M. Higgins, 2022)*



---

# Acknowledgements

---

Let it be beyond doubt that my gratitude extends to all my friends, family and colleagues who have been right at my side over the past four years. There are of course too many of you to name, but you know who you are. Except perhaps Casper the cat who, although a pacifying companion in my thesis writing days, spent most of that time asleep.

I express particular thanks to my supervisor Charles Cockell, whose boundless and infectious enthusiasm for all things astrobiology has kept me motivated and engaged; an effect that I am sure will last for many years to come. Charles' support and encouragement regarding my scatterbrained ideas for student projects and often questionable side-hustles has helped my personal development in ways I never thought studying for a PhD would. Thanks also to the whole gang at the UK Centre for Astrobiology through my tenure of 2017–2022. There are too many of you to name, but special mention goes to the best office mates in the business — at least in the days we were allowed in the office — Andy Dickinson, Rosie Cane and Liam Perera. Between our discussions about chicken wings, LEGO technique, bingeable TV and Korean cuisine, we also got some great science chats in which enriched this work to no end. I also thank each of my coauthors on the papers listed in the declaration, particularly Chris Glein, whose chemical modelling was instrumental in what makes chapters six and seven of this thesis shine.

I want to thank the UKRI and STFC for funding this research, and for offering an extension when the coronavirus pandemic hit. I also thank the University of Edinburgh for their support of home working and regular testing such that we could maintain some sense of normality whenever possible.

Most importantly, there are two individuals to whom I am unequivocally indebted. The first is Niall Whiteford, my lockdown buddy, bringer of Netflix, countless coffees to fuel thesis writing, and of course the resolve and support that only a fellow flatmate undertaking his PhD from his bedroom could provide. Finally, I cannot express enough the appreciation I have for my partner Sooji Choi. You were there for all the highs and lows, never doubting when I stumbled, cheering me on whilst feeding me snacks each and every step of the way. I hope that our new life together across the Atlantic is only the beginnings of your return on investment. Thank you.



---

# Contents

---

<b>List of figures</b>	----- xvii
<b>List of tables</b>	----- xxiii
<b>List of code listings</b>	----- xxv
<b>1 Overview</b>	----- 1
<b>2 Modelling microbial behaviour and habitability</b>	----- 5
<b>2.1 Habitability</b>	..... 6
2.1.1 An energetic approach to habitability	..... 7
2.1.2 Low-energy and low-nutrient environments	..... 8
2.1.3 Extreme conditions and the limits of life	..... 10
<b>2.2 Microbial modelling in astrobiology</b>	..... 17
2.2.1 Developing models from empirical data	..... 18
2.2.2 An agnostic, theoretical growth model	..... 20
<b>2.3 Case study: Enceladus' subsurface ocean</b>	..... 21
2.3.1 A brief overview of icy moon habitability	..... 22
2.3.2 Geophysical properties	..... 26
2.3.3 (Geo)chemistry of the subsurface ocean	..... 29

2.3.4	The prospects for life .....	31
<b>2.4</b>	<b>Other locations of astrobiological interest.....</b>	<b>34</b>
2.4.1	Earth's extremes.....	34
2.4.2	Mars .....	34
2.4.3	Venus.....	36
2.4.4	Exoplanets .....	36
<b>2.5</b>	<b>Summary.....</b>	<b>37</b>
<b>3</b>	<b>Bioenergetics of adaptation, survival and growth – – – – –</b>	<b>39</b>
<b>3.1</b>	<b>Microbial energy flows: an agnostic overview.....</b>	<b>40</b>
3.1.1	Gibbs free energy and chemical thermodynamics .....	41
3.1.2	Gibbs free energy of electrochemical cells.....	44
3.1.3	How life acquires and processes energy.....	46
3.1.4	Kinetics of metabolism .....	49
<b>3.2</b>	<b>Energetics of biosynthesis .....</b>	<b>51</b>
<b>3.3</b>	<b>Quantifying adaptation to extremes.....</b>	<b>54</b>
3.3.1	Defending against temperature effects.....	55
3.3.2	Defending against pH effects.....	60
3.3.3	Combining temperature and pH adaptations .....	70
<b>3.4</b>	<b>Summary and outlook .....</b>	<b>72</b>
<b>4</b>	<b>NutMEG: an energetic habitability model – – – – –</b>	<b>77</b>

<b>4.1</b>	<b>Nutrients, maintenance, energy and growth</b>	78
4.1.1	The core concept	78
4.1.2	Habitability assessments	80
4.1.3	Growth rates and biomass estimates	80
<b>4.2</b>	<b>Computational design</b>	81
4.2.1	Overall structure	81
4.2.2	The environment	83
4.2.3	The reaction module	83
4.2.4	The reactor and saved_systems	88
4.2.5	A culture of organisms	90
4.2.6	Altogether, an ecosystem	98
4.2.7	The applications module	98
4.2.8	Data Management	100
<b>4.3</b>	<b>Implementing a growth simulation</b>	102
4.3.1	Walk-through of a simulation step	102
4.3.2	Stopping a simulation	105
<b>4.4</b>	<b>Example applications</b>	106
4.4.1	Microbial competition	106
4.4.2	Biologically available energy in the Venusian clouds	111
4.4.3	Exoplanets and biosignature detection	113

4.5	Summary .....	116
5	<b>A typical optimal methanogen</b> - - - - -	119
5.1	Introduction .....	122
5.2	Methods .....	124
5.2.1	An efficiency based model for microbial growth .....	124
5.2.2	Configuration against empirical methanogenic growth data .....	127
5.3	Results .....	131
5.3.1	Maintenance costs of methanogens .....	131
5.3.2	Energy and nutrient limitation of the TOM .....	133
5.3.3	Alternative explanation: synthesis energy .....	139
5.4	Discussion and conclusions .....	140
5.5	Extended methods .....	144
5.5.1	Implementation of growth prediction .....	144
5.5.2	Free energy availability in natural systems .....	144
5.5.3	Thermodynamically limited biochemical kinetics .....	145
5.5.4	The energetic cost of cell synthesis .....	145
5.5.5	Nutrient limitation .....	145
5.6	Remarks on the rate constant .....	147
6	<b>Habitable windows for methanogens on Enceladus</b> - - - -	151
6.1	Introduction .....	155

<b>6.2</b>	<b>Methods</b> .....	156
6.2.1	Geochemical model.....	157
6.2.2	Bioenergetic model.....	158
<b>6.3</b>	<b>Parameter space selection</b> .....	160
6.3.1	Temperature and pressure.....	160
6.3.2	Chemical composition and pH.....	162
6.3.3	Methanogen parameter space .....	163
<b>6.4</b>	<b>Results</b> .....	164
6.4.1	Free energy availability .....	164
6.4.2	Net power supply .....	166
6.4.3	Variance in power supply from the parameter space.....	169
6.4.4	Energetic habitability of the parameter space .....	172
<b>6.5</b>	<b>Discussion</b> .....	176
6.5.1	Implications for Enceladus' habitability .....	176
6.5.2	Uncertainties in composition owing to hydrothermal activity .....	177
6.5.3	Other limitations of the parameter space and model.....	179
6.5.4	Recommendations for future work and missions .....	182
<b>6.6</b>	<b>Summary</b> .....	183
<b>7</b>	<b>Enceladus' biomass and biosignatures</b> – – – – –	185
<b>7.1</b>	<b>Introduction</b> .....	186

<b>7.2</b>	<b>Methods</b> .....	187
7.2.1	Refining the parameter space.....	187
7.2.2	Towards a steady state .....	194
7.2.3	Biomass turnover and racemization .....	199
<b>7.3</b>	<b>Results</b> .....	201
7.3.1	Steady state case studies.....	201
7.3.2	Biomass turnover from a NutMEG-derived steady state.....	210
7.3.3	Racemization and biosignature detectability .....	217
<b>7.4</b>	<b>Discussion and conclusions</b> .....	221
<b>8</b>	<b>Outlook</b> - - - - -	227
<b>A</b>	<b>Supplemental theory</b> - - - - -	233
A.1	Calculating free energies .....	234
A.2	Relating biological and chemical standards.....	241
A.3	Alternative proton flux calculation.....	243
A.4	Dissolved gases in solution .....	245
<b>B</b>	<b>Availability of code and data</b> - - - - -	247
B.1	pH variation with temperature (Box 3.5).....	249
B.2	T adaptation calculations (Figure 3.4) .....	250
B.3	pH adaptation calculations (Figures 3.5–3.7) .....	251
<b>C</b>	<b>Supplemental material for Chapter 6</b> - - - - -	253



<b>C.1 Captions for the data set .....</b>	<b>254</b>
<b>C.2 Supplemental tables .....</b>	<b>255</b>
<b>C.3 Supplementary figures .....</b>	<b>256</b>
<b>Bibliography -----</b>	<b>269</b>



---

## List of figures

---

2.1	Illustrative plot of the various phases of microbial growth. . . . .	9
2.2	Example isokineticity diagram for some biomacromolecules in solution.	12
2.3	Three-dimensional maps showing the known limits for microbial growth . . . . .	16
2.4	Linear behaviour of microbial growth in the exponential phase . . . . .	24
2.5	The NASA roadmap for icy worlds . . . . .	25
2.6	The structure of Enceladus' interior . . . . .	27
2.7	Inferred activity of CO <sub>2</sub> in Enceladus' bulk ocean . . . . .	31
2.8	Inferred Gibbs free energy of methanogenesis in Enceladus' bulk ocean	32
2.9	Possible geological context of Mars . . . . .	35
3.1	Variation in the standard Gibbs free energy of methanogenesis and ATP production with temperature and pressure . . . . .	47
3.2	The Gibbs free energy yield per mole of ATP at various cell conditions.	48
3.3	Energetic cost of protein synthesis . . . . .	51
3.4	Estimates of the maintenance power owing to temperature . . . . .	57
3.5	Flux of protons and hydroxide across a cell membrane and the corresponding power demand required to pump them back . . . . .	64

3.6	Variability in the flux of protons and hydroxide across a cell membrane and the corresponding power demand required to pump them back . . . . .	67
3.7	The power demand required to pump unwanted protons and hydroxide ions back across a cell membrane . . . . .	70
3.8	Heatmaps of the combined maintenance power owing to temperature and pressure . . . . .	71
4.1	Flowchart to demonstrate the concept behind NutMEG. . . . .	79
4.2	Simplified class diagram to show how the major objects in NutMEG interact and depend on each other . . . . .	82
4.3	Class diagram of the reaction module . . . . .	86
4.4	Class diagram of the culture module . . . . .	91
4.5	Class diagram of the base_organism namespace . . . . .	94
4.6	Simple example results showing microbial competition . . . . .	108
4.7	Molar free energies of metabolic pathways that could be feasible in the Venusian clouds . . . . .	112
4.8	Methane production and detectability on an Earth-like exoplanet . . .	115
5.1	The rate of CH <sub>4</sub> consumption and growth rate of real methanogens in optimal settings, with those of the ‘typical optimal methanogen’ for comparison. . . . .	130
5.2	Predicted maintenance power required for real methanogens and the ‘typical optimal methanogen’ . . . . .	132
5.3	Growth curves of simulated typical optimal methanogens under energy or nutrient limitation. . . . .	135

5.4	Peak growth rates, final biomass values and total CH <sub>4</sub> production of the simulated typical optimal methanogens when growing under energy or nutrient limitation. . . . .	136
5.5	Concentration of dissolved CO <sub>2</sub> and H <sub>2</sub> at different temperatures from a typical laboratory setup for methanogens. . . . .	138
5.6	Contour to show the factor by which the synthesis energy of the typical optimal methanogen needs to be increased for the optimal maintenance power to be zero. . . . .	139
5.7	The methanogenesis rate constant of both simulated and empirical methanogens . . . . .	149
5.8	How variable rate constants can be used to cover the entire range of methanogenic growth behaviour . . . . .	150
6.1	The Gibbs free energy of methanogenesis in seawater throughout the Enceladus ocean parameter space . . . . .	165
6.2	Power supply available to a methanogen at various seawater temperatures and bulk ocean pH values . . . . .	167
6.3	Limiting bounds of power supply for a methanogen on Enceladus . . . .	168
6.4	Variance in power supply for methanogens on Enceladus . . . . .	170
6.5	Representative instantaneous power supplies and demands in the Enceladus ocean . . . . .	173
6.6	Areas of the Enceladus ocean parameter space which meet various criteria for habitability. . . . .	175
7.1	The optimum ATP yield for methanogens throughout Enceladus' ocean.	189
7.2	Simple inflow and outflow model for Enceladus' ocean . . . . .	192
7.3	Feasibility of different chemical inflows and outflows on Enceladus based on observations. . . . .	193

7.4	Rate constants of racemization for select amino acids . . . . .	200
7.5	Maps of the death rate required for a steady state on Enceladus . . . . .	202
7.6	The incoming power supply to Enceladus at different temperatures, bulk ocean pH, salt-level and rates of H <sub>2</sub> inflow . . . . .	203
7.7	New biomass which can be sustained from an incoming power supply on Enceladus . . . . .	204
7.8	Biomass which can be created in Cassini-derived uninhabitable con- ditions . . . . .	206
7.9	Maps of the H <sub>2</sub> inflow required to make the uninhabitable regions of the Enceladus parameter space habitable . . . . .	207
7.10	The number of methanogens required to preserve the reaction quo- tient of methanogenesis in Enceladus conditions . . . . .	209
7.11	Characteristic NutMEG simulation results which were flexible in Enceladus- like conditions . . . . .	211
7.12	Characteristic NutMEG simulation results which enter limit cycles. . .	212
7.13	The steady state biomass, death rates and biomass turnover rates in Enceladus' ocean when H <sub>2</sub> inflow is 10 <sup>-12</sup> mol (L s) <sup>-1</sup> . . . . .	215
7.14	The steady state biomass, death rates and biomass turnover rates in Enceladus' ocean when H <sub>2</sub> inflow is 10 <sup>-10</sup> mol (L s) <sup>-1</sup> . . . . .	216
7.15	Ratio of amino acids enantiomers with time in different Enceladus conditions . . . . .	218
7.16	The time it takes for the buildup from a constant input of biological amino acids to appear indistinguishable from those with an abiotic origin . . . . .	218
7.17	Total cell death required for the overall amino acid content to be indistinguishable from an abiotic mixture when H <sub>2</sub> inflow is 10 <sup>-12</sup> mol (L s) <sup>-1</sup> . . . . .	219

7.18	Total cell death required for the overall amino acid content to be indistinguishable from an abiotic mixture when $\text{H}_2$ inflow is $10^{-10} \text{ mol (L s)}^{-1}$ . . . . .	220
------	--	-----





---

## List of tables

---

2.1	Summary of typical extremophile nomenclature . . . . .	11
2.2	Summary of the ecological limits for life . . . . .	17
2.3	Select Cassini measurements from the Enceladus south polar plume .	26
4.1	Typical CHNOPS makeup of a microbe . . . . .	95
4.2	The variables which are recorded in the NutMEG database at each time step. . . . .	101
5.1	Minimal organism and environment parameters required to initialise a NutMEG growth prediction. . . . .	126
6.1	Parameter ranges of Enceladus' subsurface ocean and hydrogenotrophic methanogens . . . . .	161
6.2	Best- and worst-case variation in Enceladus' parameter space for life .	171
7.1	A refined parameter space for the 'habitable' regions of Enceladus' ocean. . . . .	188
7.2	Steps to compute the mean molar inflow and outflow of H <sub>2</sub> , CO <sub>2</sub> and CH <sub>4</sub> in Enceladus' ocean. . . . .	193



---

## List of code listings

---

4.1	Initialising a reaction object . . . . .	84
4.2	Dictionary showing criteria for ending a NutMEG simulation . . . . .	104
4.3	Example of running a simulation with two organisms. . . . .	109
4.4	Implementation of the <code>simulate_competition</code> method . . . . .	110
4.5	Example of extracting the free energy of sulfate reduction in a Venusian cloud droplet. . . . .	111



# CHAPTER 1

---

## Overview

---

Where to begin? The research that led to this thesis spans multiple disciplines so it is important to first capture the scope of our work and outline our goals.

At the core of this work is the concept of habitability, but what does life actually require? The fundamental laws of physics dictate that life needs entropy. To a chemist, it needs continuous chemical disequilibrium. To biologists, it needs substrates, nutrients, and maybe a reproductive partner. As far as many astronomers are concerned, apparently all life needs is water. Some ecologists would even scoff at the question. After all, why ask if there isn't an obvious complete ecosystem? As far as we know, no natural environments on Earth only host one organism.

In this brief introduction we first offer an energy and nutrient-based definition of habitability. We then outline how in this thesis we use a bioenergetic approach to build quantitative habitability models and from them estimate how much biomass extraterrestrial environments could host and what biosignatures they may be leaving for us to find.

An environment is **habitable** when it provides the means for an organism to survive, maintain itself and grow or reproduce [9]. This is a relatively simple concept in a qualitative sense, but quantifying whether an environment can be considered habitable or not remains a difficult endeavour. This is because the material requirements for life to survive, grow and evolve are complex, vary significantly between organisms and depend on what one even considers alive. One way to cast habitability into a quantitative framework is by taking an energetic approach [10–12]. The **energetic habitability concept** states that an environment can be deemed habitable if enough energy and nutrients are available for an organism to maintain itself, offsetting any adverse effects caused by its local environment. This arises from the notion that the fundamental principles of **thermodynamics** act as both an absolute limiter on whether life can maintain its intrinsic structure, and a throttle to the kinetic accessibility of energy, whatever form it may take.

The concept splits the question of habitability into two simple parameters (at first order), the organismic **power supply**  $P_S$  [ $\text{W cell}^{-1}$ ] and **demand**  $P_M$  [ $\text{W cell}^{-1}$ ] (also known as **maintenance**), where power is the rate of change of energy. If  $P_S \geq P_M$  then an environment is **energetically habitable** and the organism can access more energy than it needs to survive. If instead  $P_S < P_M$  the organism cannot maintain itself with the available energy and the environment is **energetically uninhabitable** [10].

The notion above underpins all of the research presented in this thesis. We use this quantitative framework for microbial behaviour to build a computational model for astrobiology. We then use it to determine whether Saturn's moon **Enceladus** could host habitable spaces for Earth-like **methanogens** — ancient species which consume chemicals that are common throughout the universe. Enceladus is a unique and important target for astrobiology in the solar system. Since the detection of plumes from Enceladus' southern hemisphere demonstrated that some source of liquid water must reside below the surface, interest in the moon as a candidate for life has blossomed [e.g. 13–21]. Many have been keen to point out that there appears to be energy available for life in the ocean, but direct considerations of whether this is enough to outweigh the stresses of the Enceladean environment are needed. We set out to assess whether this could be the case within the icy moon's expected parameter space. And if so, find out how much **biomass** (biological material) it could host and what **biosignatures** (indicators of biological activity) it could be leaving for us to detect. The path to answer these questions requires understanding of the underlying microbiology, bioenergetics, chemical thermodynamics, planetary/space science and geochemistry. Below we outline how we make it happen in this thesis, following the broad assessment of the current literature in Chapter 2.

---

### **i) Bioenergetics of adaptation, survival and growth**

There is far more underpinning the energetic habitability concept than we summarised in the paragraphs above. Chapter 3 explores the energetic parameters which are important for microbial growth models. We first outline how energy is parameterised in a biological context and how life extracts and processes energy from its environment. We then discuss the energetic costs associated with synthesising large biomolecules (which is necessary for maintenance and growth), and introduce some methods to determine the power demand owing to temperature (the inevitable breakdown of these large molecules) and pH (the costs associated with maintaining a constant internal pH).

### **ii) Nutrients, maintenance, energy and growth**

To translate the ideas and theory presented in Chapters 2 & 3 into a useful form for the wider scientific community, we created **NutMEG** [Nutrients, Maintenance, Energy and Growth]: a Python package bringing such considerations all under the same hood. In Chapter 4 we introduce the concepts behind its implementation and how microbial growth models were incorporated into a flexible computational algorithm. It has been used to various levels of specificity, from estimating just the energetic availability in an environment [e.g. 4], to the energetic habitability of better understood settings [e.g. 2], and predicting their possible biomass and biosignature levels (e.g. Chapter 7 & [5]).

### **iii) An empirical basis for Earth-like life**

**Hydrogenotrophic methanogens** are organisms of particular interest in astrobiology. They have an ancient, simple metabolism the basic ingredients of which can be found across the universe. In Chapter 5 we parameterise methanogens using data from laboratory studies on Earth for use with NutMEG. With this data, we can make estimates of the habitability (with respect to methanogens) for any location that contains these ingredients. Importantly, this is ‘throttled’ to the limits of Earth-like life. While one could argue putative extraterrestrial life might take any form permitted by the laws of thermodynamics, we restrict ourselves to what we can observe to avoid any possible cognitive biases such ideas could introduce.

### **iv) Energetic habitability of Enceladus**

In Chapter 6 we turn to Enceladus and its energetic habitability. We explore the spontaneous habitability of the icy moon’s subsurface ocean to the methanogens parameterised above using a range of environmental parameters informed by data from NASA’s Cassini mission. This requires modelling the carbonate geochemistry throughout the ocean. We ask: if Cassini’s observations offered a ‘snapshot’ view of

the ocean, does a habitable window exist within the uncertainty of the data, without considering as-yet unconstrained (but still important) variables such as a supply of nutrients?

### **v) Biomass and biosignatures on Enceladus**

Establishing regions of the ocean which could be habitable is a useful first step, but leaves much to be desired. The pathway to life detection is through observable biosignatures, which are markers that can only be produced by biological activity. In Chapter 7 we attempt to quantify the possible amount of biomass and biosignatures produced by life in Enceladus' ocean — should it be inhabited, of course.

Each chapter of this thesis is designed as a self-contained work, but symbols and definitions are consistent throughout. A glossary of symbols can be found at the back of this thesis for reference. Each of the research stages above have their own conclusions, limitations and proposals for future work which are examined in detail in the chapters' respective discussion sections. A broad outlook on our results, summarising our conclusions and recommendations for future research can be found in Chapter 8.



# CHAPTER 2

---

## Modelling microbial behaviour and habitability

---

It is quite remarkable how hardy life can be. Some species can survive at temperatures well below freezing, others at over 120 °C, pressures higher than the bottom of the Mariana trench, or at environmental pH values as low as zero. As far as the extremes of life go, humans are incredibly fragile.

In this chapter we explore what it means for an environment to be habitable, map out the known limits of life, learn the basics of modelling microbial behaviour in weakly constrained environments, and introduce Saturn's moon Enceladus as a possible host for extraterrestrial life, with its tantalisingly 'habitable' ocean.

### Subchapters

2.1	Habitability .....	6
2.2	Microbial modelling in astrobiology .....	17
2.3	Case study: Enceladus' subsurface ocean .....	21
2.4	Other locations of astrobiological interest .....	34
2.5	Summary .....	37

## 2.1 Habitability

---

The fundamental principles of thermodynamics act as an absolute limiter on whether life can build the complex structures required for it to reproduce and thrive (**entropy**), as well as throttling the accessibility of nutrients which are vital to survival (**chemical kinetics**). Traditionally, a habitat has been defined as an environment which provides the means for an organism to undergo **metabolic activity** and survive, maintain itself, and grow or reproduce [22]. Exploring the thermodynamic constraints on such processes can help us build upon this new method of assessing habitability by considering life as dependent on a series of energetic and physicochemical processes [10]. Some examples of these include nutrient uptake, general maintenance, coping with environmental stresses, and growth. Of course, the energetic demand of these processes varies from organism to organism [10, 23]. A standard model for examining the habitability of various environments is yet to be realised.

One could argue that the most direct definition of a potential habitat comes from empirical evidence — covering the range of environments between the extremes seen on Earth within which it is known life can survive. However, this understanding is rather linear. In reality the problem is more complex, with the competing effects of temperature [24, 25], pressure [26], salinity [27], pH [28], nutrient availability [29] *etc.* each contributing to the ultimate fate of an unsuspecting organism [9, 10]. Fluctuations in these parameters can lead to the rise and fall of short-lived periods of **instantaneous habitability** or even **continuous planetary habitability** lasting over geological timescales [9]. Empirical data for microbial growth while under multiple stresses is limited and a topic of active research, so a comprehensive understanding of how they intertwine remains a challenge. In this thesis, we focus on assessing habitability using an energetic and kinetic approach. Further discussion of habitability in the general sense can be found in the review by Cockell et al. (2016) [9].

In recent years, debate has emerged as to whether habitability is a discrete or continuous property [30–33]. For this work, we define habitability as a discrete property of an environment with respect to a given organism. To give a crude example the ocean is habitable for fish but not dogs. Adding more water does not make it ‘more habitable’ to fish, nor does it make it ‘less habitable’ to dogs.

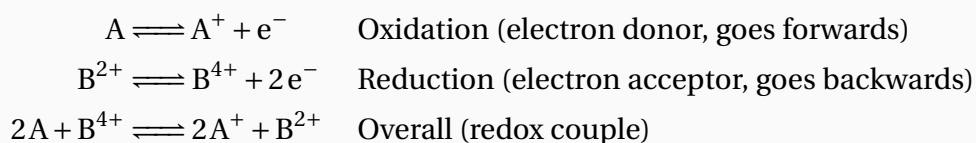
### 2.1.1 | An energetic approach to habitability

As a first approximation, the survival of an organism can be reduced to it having access to a usable energy source and key nutrients, providing a means for it to sustain itself in its settings. This is the core concept behind **energetic habitability**, which postulates that (i) life requires complexity, and (ii) energy is required to build and maintain that complexity. The latter is a consequence of the **second law of thermodynamics**<sup>1</sup>, whereby incoming energy must counteract the natural degradation of the molecules via entropy. We define the energy used to deal with environmental stresses (and any other energetic processes which are *not* involved in reproduction) as the **maintenance energy** [J cell<sup>-1</sup>] or, more specifically for this thesis the **maintenance power**  $P_M$  [W cell<sup>-1</sup>]. Power is the flow of energy through time, where one Watt is equivalent to one joule per second. Hoehler (2007) [10] suggests that by this definition life requires:

1. Raw materials.
2. Energy to rearrange those materials as needed.
3. A medium to house this construction/rearrangement.
4. An environment with acceptable conditions for life such that this can take place and which allows reactions to proceed at a reasonable rate.

#### Box 2.1: Redox couples

A redox couple or redox reaction is a chemical reaction in which electrons have been transferred. The nomenclature comes from it being the pairing of **reduction** and **oxidation** chemical reactions where the former involves gaining electrons and the latter involves losing electrons. A redox reaction is made of two half-reactions, for example:



Life makes use of this flow of electrons via the electron transport chain, which is described in Chapter 3.

<sup>1</sup>The second law states that in an isolated system, the **entropy**, which parameterises disorder, can only increase.

Life can use a multitude of energy sources, but typically it is fuelled via energy-yielding chemical pathways built from so-called **redox couples** (Box 2.1), occasionally featuring the absorption of radiation [10]. Other sources play a more indirect role, such as tidal heating or geothermal energy mediating the temperature of an environment. This energetic uptake can be quantified by calculating the **Gibbs free energy**<sup>2</sup> of a process  $\Delta G$  [ $\text{J mol}^{-1}$ ]. In chemistry, this is a measure of an interaction's spontaneity, and tells us whether it is a net source or sink of energy. A negative  $\Delta G$  denotes a spontaneous process, in which energy is released such as breaking down polymers or simple metabolisms (reducing chemical complexity and/or releasing heat). Conversely, a positive  $\Delta G$  is a process which requires net energetic input such as building long chain proteins (Subchapter 3.2) or maintaining a potential gradient (Subchapter 3.3). Processes with negative  $\Delta G$  are known as **exergonic**, and those with positive  $\Delta G$  are **endergonic**. Provided there is a balance in energetic availability and energetic requirements (maintenance), there is no thermodynamic reason that a putative organism cannot survive or even grow, provided there is surplus energy.

For a chemical reaction the Gibbs free energy can be calculated a number of ways, but is typically done with the following equation:

$$\Delta G = \Delta G_r^\circ + RT \ln Q \quad (2.1)$$

where  $\Delta G_r^\circ$  is the **standard Gibbs free energy** [ $\text{J mol}^{-1}$ ] of the reaction. This is equivalent to  $\Delta G$  when the activity of all chemical constituents is 1 and varies with **temperature**  $T$  and **pressure**  $P$ . It can typically be calculated using thermodynamic software or looked up in tables [e.g. 34].  $Q$  is the **quotient** of the reaction<sup>3</sup> and  $R$  [ $\text{J mol}^{-1} \text{K}^{-1}$ ] is the **universal gas constant**. Further information on methods to calculate  $Q$ ,  $\Delta G$ ,  $\Delta G_r^\circ$  and related thermodynamic parameters are discussed in Chapter 3 and Appendix A. Chapter 3 also gives an overview of how simple life forms use redox couples to extract energy from their environment.

## 2.1.2 | Low-energy and low-nutrient environments

The reality of microbial life outside the laboratory is that it often spends the majority of its time exhibiting little or no growth, having reached an approximate equilibrium with its environment [23, 35]. Under such **growth arrest**, underlying mechanisms of microbial metabolisms change, such as a diversion of resources to protect [36] and repair [35] DNA, and after just a few weeks of starvation a variety of fitness-

<sup>2</sup>also referred to as simply the **free energy** or the IUPAC recommended **Gibbs energy**

<sup>3</sup>For a chemical reaction this is the ratio of the activities of the product species over those of the reactant species involved, taking stoichiometric coefficients of the reaction into account as exponents of the concentrations. See Chapter 3 for more information.

enhancing genetic traits can begin to emerge [37]. Such scenarios are likely brought on by a low thermodynamic availability (or complete lack) of a key nutrient, and when conditions become more favourable microbes are poised to embark on rapid growth cycles [35].

Environments that are low in energy and/or nutrients are often described as **oligotrophic**. Throughout the microbial ecology literature, the line between ‘nutrients’ and ‘energy’ is often blurred. Indeed, a nutrient source can be an energy source also (such as dissolved organic carbon), but not all energy sources are nutrient sources. For the purposes of this thesis the term oligotrophic will be used to describe environments which are deficient in one or both of nutrients and energy [38].

The majority of Earth’s biosphere is oligotrophic [38–43]. This means that most of the biomass on the planet is not in the exponential phase of growth (which is often measured in the laboratory; Figure 2.1 shows a typical laboratory growth experiment result), but rather in a state of starvation where the main goal is survival. It can thus be difficult to draw comparisons between laboratory data, which is mostly obtained in the exponential phase, and observations of natural systems. This does not mean that organisms in these environments are always slow growers; as soon as a surplus of energy becomes available the microbes tend to utilise that surplus until the environment is back in an energy-limited state [35, 38]. In this way the instantaneous viability of any organism is heavily influenced by other organisms in its vicinity and the physico-chemical environment [38].

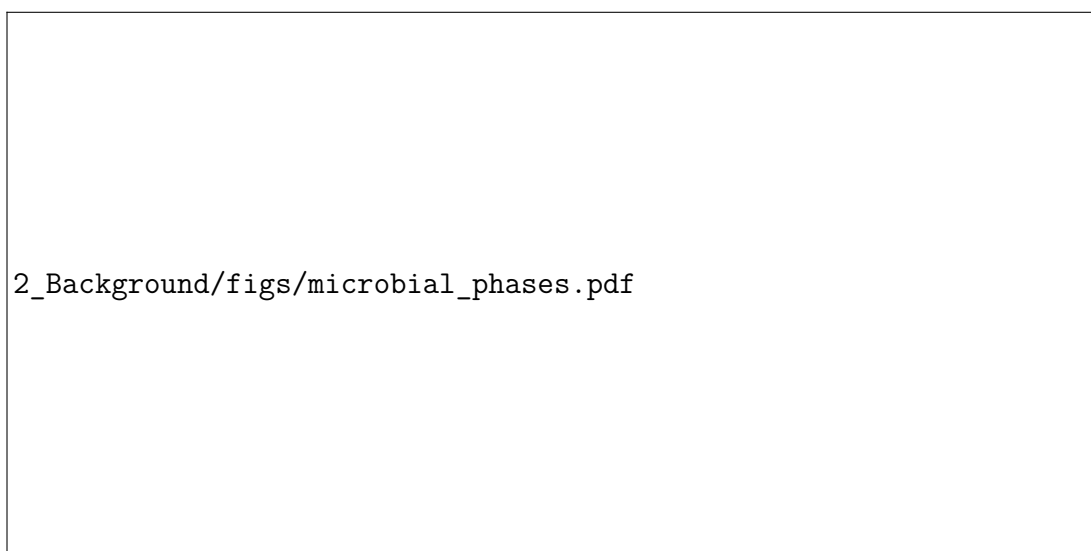


**Figure 2.1** Illustrative plot of the various phases of microbial growth.

For these starved systems, it is important to address the type, amount and quality of the available energy, as well as its turnover rate and replenishment. There is always a ‘survival’ energy requirement for given physico-chemical conditions, which is often referred to in the literature as the **basal metabolism** or **basal energy requirement** [10, 23, 38]. This is easy to confuse with the cost of maintenance — the basal energy requirement is the absolute thermodynamic limit, accounting for unavoidable processes which must be dealt with such as **amino acid racemization** and **DNA depurination** (discussed in Section 2.1.3 & Chapter 3), and the maintenance contribution is defined for this thesis as the energy used for all processes apart from growth, including those which may not be strictly necessary.

Organisms which survive in low-energy and/or low-nutrient environments are often referred to as **oligotrophs**. Physiologically they usually have the following properties [44]:

1. **Enzymes with a greater substrate affinity** allowing for higher **rate constants**<sup>4</sup> of energy extraction and nutrient uptake/processing.
2. **More economical metabolisms** in general, reducing the required maintenance cost.
3. **A specific rate-determining step** which controls the whole metabolism.

Oligotrophs also tend to be small (sub- $\mu\text{m}$ ) because a larger surface to volume ratio favours substrate uptake [38]. There are also benefits to a reduced cell size as it leads to a lower basal power requirement [45].

### 2.1.3 | Extreme conditions and the limits of life

There are many environmental effects which can inhibit a microbe’s viability. Most of these have been well-examined individually and a plethora of in-depth reviews can be found in the literature [e.g. 9, 25, 27, 46, 47]. Organisms which can tolerate adverse conditions such as pH, temperature, pressure and/or salinity are known as **extremophiles**. Those which are adapted to a particular extreme have specific nomenclature, summarised in Table 2.1. This section gives an overview of some ways in which the major-playing physico-chemical parameters can affect (or even end) the lives of organisms. More specific adaptations and methods of computing their bioenergetic consequences can be found in Chapter 3.

---

<sup>4</sup>The rate constant  $k$  relates the rate of a reaction to the activities of its constituents.

**Table 2.1 Summary of typical extremophile nomenclature.** Throughout the literature these lines are often blurred (e.g. what one author considers a thermophile, another may think of as a hyperthermophile). The suffix -tolerant should be appended for species which tolerate these extremes, and -phile for species which require these conditions. These terms can be 'stacked', so a hyperthermoalkaliphile is an alkaliphile which requires very high temperatures. Populated with ranges identified by Capece et al. (2013) [48].

Prefix	Threshold
<b>thermo-</b>	$T > 60^{\circ}\text{C}$ (hyper- at $T > 80^{\circ}\text{C}$ )
<b>psychro-</b>	$T < 15^{\circ}\text{C}$
<b>acido-</b>	$\text{pH} < 3$
<b>alkali-</b>	$\text{pH} > 9$
<b>halo-</b>	$> 5\%$ (hyper- at $> 20\text{--}30\%$ )
<b>piezo-</b>	$P > 60 \text{ MPa}$

### 2.1.3.1 | Temperature and pressure

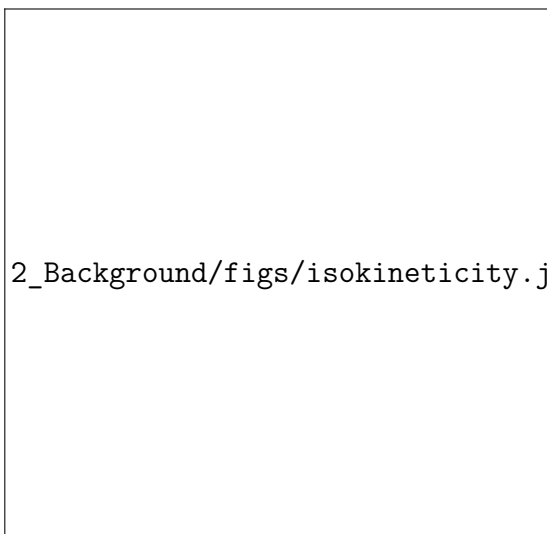
#### i) The limits

Initial constraints on temperature and pressure can be made through a few assumptions. As liquid water is a good starting point in the search for a habitat, the region of interest can be limited to the temperatures and pressures corresponding to that phase. Depending on the local salt composition, small veins of liquid water can be also be found well below the standard freezing point [49, 50]. On the other end of the spectrum, biodecomposition begins to have a major effect on structured molecules at  $\sim 140^{\circ}\text{C}$  and by  $\sim 150^{\circ}\text{C}$  the stability of amino acids — the building blocks of life — falters [51] meaning the search would probably be futile at temperatures higher than this. An archaeal isolate has been shown to exhibit growth at  $121^{\circ}\text{C}$  [24], and another at  $122^{\circ}\text{C}$  at high pressure (40 MPa) [52]. At present, these are the highest observed temperatures for microbial growth.

Certain microbes have been shown to survive in very cold environments (such as permafrost) for millennia. Sometimes, when low on available nutrients this requires defensive measures such as becoming dormant, engaging in cannibalism or synthesising stress proteins. To cope with the effects of low temperature some can shrink in size, change their fatty acid and phospholipid composition, lose some

**Figure 2.2 Example isokineticity diagram for some biomacromolecules in solution.**

The ellipses act like a contour plot to represent temperatures and pressures for which the degradation rate is constant and demonstrates a way to push up the temperature limit for a molecule by changing the pressure, or vice versa. From Knorr et al. (2006) [54].



2\_Background/figs/isokineticity.jpg

water, or make use of redox couples in small aqueous veins in the ice. From these adaptations, studies predict that metabolism can be maintained down to at least  $-40^{\circ}\text{C}$  [25].

Much like high temperatures, high pressures can lead to the degradation of biomacromolecules by deforming their structural properties [26]. For over two decades, high hydrostatic pressures have been used in food manufacturing to render microorganisms, viruses, and enzymes inactive while limiting damage to nutrients in the food, supplanting the thermal techniques of yesteryear [53–55]. Often, a combination of high pressure and temperature can be convenient to an extremophile, such as for the methanogen *Methanopyrus kandleri*, which can have its maximum temperature for growth increased from  $116^{\circ}\text{C}$  to  $122^{\circ}\text{C}$  by increasing local pressure to 40 MPa [52]. The stability of biomacromolecules can be visualised with an isokineticity diagram (Figure 2.2), in general the combinations of temperature and pressure appear to provide elliptical regions of biomacromolecular stability [54].

As with temperature, a fundamental lower limit of pressure for life is unknown due to the lack of low pressure environments on the Earth. Empirical studies suggest that lowering the pressure by 1–2 orders of magnitude compared to a microbe's 'comfort zone' can drastically reduce growth, be it a typical surface organism (e.g. *Bacillus subtilis* [56]) or a piezophile (e.g. *Methanococcus jannaschii* [57]).

## ii) Effects on energetics and kinetics

Temperature and pressure have an important effect on the energy yield and kinetics of (bio)chemical pathways as they are intertwined with the fundamental laws of thermodynamics. The **enthalpy** and **entropy** of a chemical reaction,  $\Delta H$  [ $\text{J mol}^{-1}$ ]



and  $\Delta S$  [J (mol K)<sup>-1</sup>] respectively, both depend on temperature and pressure when significantly deviating from standard conditions, and pass those dependencies on to  $\Delta G$  (Chapter 3). Thankfully, in most cases the free energy yield of a given reaction can be estimated using the revised Helgeson-Kirkham-Flowers (HKF) equations of state [34], which are now easily solvable through computational chemistry packages such as cantera<sup>5</sup> and reaktoro<sup>6</sup> [58]. Chemical influences such as ionic strength and solvation effects can affect the validity of this approach (Section 2.1.3.2, Appendix A), but temperature and pressure always play a key role in chemical theory [59].

As a first approximation, chemical reaction rate constants have an exponential relationship with temperature:

$$k \sim \exp \left[ \frac{-E_a}{RT} \right] \quad (2.2)$$

where  $E_a$  is the reaction's **activation energy** (which is weakly temperature dependent), and  $R$  the universal gas constant. Metabolic rates could be assumed to have approximately this dependency on temperature if the concentration of the reaction constituents do not appreciably change. This means it could also be shared with complexity destroying pathways, and thus biological expenditure of energy in order to maintain viability is expected to scale exponentially with temperature. There is evidence to support this [60]. It should be stressed that these thermochemical calculations place limits on how fast a reaction can take place. As biological processes to extract energy are often catalytically controlled and feature sub-processes to collect the energy, their kinetics are rarely directly calculable. However, rates of uptake are typically much lower than may be thermodynamically possible so empirical data can be used to predict expected reaction rates, and these can then be capped at the **thermodynamically limited** rates. We parameterise such a microbial reaction rate — novel for microbial modelling — in Chapter 5.

### iii) Astrobiological relevance

Although Earth has environments spanning a wide range of temperatures — at least, for those in which water can exist as a liquid — and plenty with medium (the surface) to high (the subsurface, deep in the ocean) pressure, the extremes of these are often difficult to sample, and specialist equipment is necessary to study them in the laboratory. Nonetheless, the individual extremes of temperature and pressure are well characterised for a number of organisms, particularly piezophiles, psychrophiles, and thermophiles [55, 61, 62]. For many extraterrestrial environments, controlled analogues of temperature and pressure are obtainable for empirical study in the laboratory with scale and chemistry being more difficult to

<sup>5</sup>Cantera: available for Python, Matlab, Fortran and C/C++ — <https://www.cantera.org/>

<sup>6</sup>Reaktoro: available for Python and C++ — <http://www.reaktoro.org/>

simulate confidently in these environments. However, for the vast majority of the microbiology literature, experiments are undergone in standard conditions. While the literature for growth in extraterrestrial analogues is small, it is growing [61]. Using the well documented rules of chemical thermodynamics, these gaps in the concrete knowledge can be filled in to pave the way for astrobiological models.

### 2.1.3.2 | Salinity and pH

#### i) Coping mechanisms

As salt content in water increases, so too does the resultant **osmotic stress** an organism must endure, less it make specific adaptations. Ordinarily, the interior of a ‘generic’ microorganism will have a low ionic content, encouraging the water to flow out of the microbe and into the saline environment [63]. Two strategies are often employed to balance a microbe’s cytoplasm with its settings. The first is **high salt-in**, in which ions (e.g.  $K^+$ ) are allowed inside the membrane. Because of changes in the structure of internal proteins to accommodate this, often high salt-in organisms cannot function in the absence of salt. The second method is **low salt-in**, which instead synthesises (or borrows from the medium) organic compatible solutes which are less damaging than small ions. This gives them more adaptability to a range of salt concentrations at the cost of larger energy expenditure — particularly when they need to produce their own solutes. [27, 64].

Most biological processes are best-suited to pH-neutral conditions, and variations from that are often detrimental [10, 28]. From a purely chemical angle, extremes of high and low pH can catalyse the hydrolytic cleavage of biopolymers. It is no wonder then that most known organisms, including alkaliphiles and acidophiles, regulate their internal pH at some energetic cost [63]. This is achieved by having a semi-permeable membrane which permits nutrient exchange with the environment, and the ‘pumping’ of protons into or out of the cell as necessary [10]. Another observed adaptation for acidophiles is the evolution of acid-stable proteins, which are more capable of handling heightened  $H^+$  concentrations. Similarly, some alkaliphiles have adaptations including negatively charged cell walls to reduce the accidental uptake of potentially harmful  $OH^-$  ions [63].

#### ii) Effects on energetics and kinetics

Often saline and extreme non-neutral pH systems go hand-in-hand. Many of the metabolic processes performed by halophiles described by Oren (2011) [27] have several dependencies on proton concentration, meaning the kinetics and free energy yield of these processes is intricately linked with pH. As redox chemistry is the

main method of energy uptake for chemotrophs [63], in many cases calculating the Gibbs free energy by using **electrochemical cell potentials**  $E$  [V] may be beneficial. Corrections to **standard cell potentials**  $E^\circ$  [V] with changing temperature  $T$  are available [65], which can then be corrected to non-standard conditions using:

$$E = E^\circ - \frac{RT}{nF} \ln Q \quad (2.3)$$

where  $n$  is the number of moles of electrons transferred,  $F$  is **Faraday's constant** and  $Q$  is the reaction quotient. As ions are often present, there are significant corrections to their activities which changes based on local salinity [59]. Examples of these corrections include **Debye-Hückle Theory** for dilute solutions and the **mean square approximation** for more ion-rich concentrations [66]. Neither of these approaches are perfect, but at least give some corrections to the deviation from ideality that salinity brings. For many of the parameters that arise in these theories, temperature scaling can be implemented but pressure effects are not fully understood. This limits the reliability of these theories to environments without excessively high pressures [59]. An overview of the chemical considerations required when considering ions in solution, and how these relate to the free energy is provided in Chapter 3 and Appendix A.

On the other hand, because many organisms try to limit salt content and excessive pH within the cells, many of their other biochemical processes can proceed more-or-less as normal. The requirement is then a coping mechanism which would generally require some kind of energetic cost to maintain. For pH a first estimate could be the energy required to pump protons against a pH gradient of  $\Delta\text{pH}$  [28]:

$$\Delta G_{pH} = -2.3RT\Delta\text{pH} \quad (2.4)$$


The rate of this would vary with the amount of pumping required [10]. A review of the effect of high salinity on free energy yields is provided by Oren (2011) [27].

### iii) Astrobiological relevance

High-salt Martian brines have direct links with these extremes, and the growth of microbes in analogues of these environments is a topic of current research. The Martian subsurface could provide available redox couples [67–69], and measurements from the Enceladean plumes imply a weakly saline subsurface ocean [15]. Recent studies suggest it may be strongly saline deep in the ocean [70]. Honing the ideas summarised in this section and tying it in with the ever-growing set of empirical data can help to predict the true energetic cost of living in such environments, and make predictions for elsewhere.

### 2.1.3.3 | Survival under multiple extremes

Owing to the limits described in this section, habitability at extremes is a multi-dimensional problem — even more so when considering other limiters such as ionising radiation, UV, heavy metal effects and water activity [9, 61]. Empirical data can be collected for multiple extremes and collected into ‘maps’ of habitability (Figure 2.3) in order to give a visualisation of for which extremes it is known that *something* could grow. While this does not tie in to energetic explanations it is a useful way of viewing the whole scope of life and instances where one parameter dominates and causes a fundamental limit. Table 2.2 summarises the limits for various extremes, as compiled by McKay (2014) [71].



2\_Background/figs/habitabilitymaps4.pdf

**Figure 2.3** Three-dimensional maps showing the known limits for microbial growth. Specifically, these show the limits of temperature, pH, pressure and NaCl concentration. From Harrison et al. (2013) [61].

**Table 2.2 Summary of the ecological limits for life.** Adapted from McKay (2014) [71].

Parameter	Limit
Lower temperature	$\sim -15^{\circ}\text{C}$
Upper temperature	$122^{\circ}\text{C}$
Maximum pressure	1100 atm
Low light	$\sim \mu\text{mol m}^{-2}\text{s}^{-1}$
pH	0–12.5
Salinity	Saturated NaCl
Water activity	0.6 (yeast and mold) 0.8 (bacteria)
UV	$>1000 \text{ J m}^{-2}$
Radiation	$50 \text{ Gy hr}^{-1}$

## 2.2 Microbial modelling in astrobiology

Historically, **microbial growth models** — theoretical and/or computational methods used to describe microbial behaviour — were developed to understand how microbial life behaves when observed in the laboratory. Because laboratory experiments typically focus on the exponential phase of optimal growth where energy and nutrients are plentiful, these are rarely applicable to natural environments [23]. Astrobiologists require modelling procedures that can better reflect the environments low in energy and nutrients that exist throughout the universe [6].

There are many model structures for understanding the energetics of microbial behaviour [72]. In this thesis we focus on the simple maintenance/growth relationship. Using this method, the energetics of a microbe’s behaviour can loosely be split into two categories: **maintenance** and **growth** [40]. As we shall see, these are key to assessing the habitability, biomass and biosignatures of poorly characterised environments [1, 10, 11, 23, 39].

Maintenance can include the energetic input to maintain overall structure [10], the cost of adaptations to a particular environment (e.g. those discussed in Section 2.1.3), energy loss due to spillage (discussed overleaf), or even stored away for use when starving [35]. In a way then, the maintenance requirement encapsulates the energetic cost of all biological processes which are not directly related to growth.

Spillage is a factor historically used when calculating maintenance contributions, which accounts for the energy used in generally non-constructive processes. It can be shown [72, references therein] that spillage tends to zero as a microbe is quenched of energy and is generally a complex, but increasing, function of the microbial power supply. There are some interesting ideas about the reasons behind spillage; it may just be a harmless evolutionary inefficiency, but perhaps consuming extra energy could be to the advantage of the organism, ousting a competitor. Some contribution from spillage can also be used to compensate for other mechanisms that have not been considered in general maintenance calculations.

### 2.2.1 | Developing models from empirical data

By far the most widely used microbial growth model is the **Monod model** [73] which applied the Michaelis-Menten equation, originally derived to calculate the kinetics of enzyme-catalysed reactions, to microbial growth. The equation takes the form:

$$\mu = \mu_{\max} \left( \frac{s}{K_s + s} \right) \quad (2.5)$$

where  $\mu$  is the observed **growth rate**<sup>7</sup> [ $s^{-1}$ ],  $\mu_{\max}$  is the maximum growth rate e.g. if it were not limited by the substrate with concentration  $s$ .  $K_s$  is the Michaelis-Menten constant (also known as the half-saturation constant) for substrate  $s$ . It is unique to the substrate and organism, and often varies with environmental parameters such as temperature and pH [74].

What if there are multiple limiting substrates? There are a number of ways to combine multiple terms of the expression within parentheses above, for instance one could simply only account for the most significant reduction (the well-known **Liebig's law of the minimum**), or multiply the fractions together like so:

$$\text{Minimum:} \quad \mu = \mu_{\max} \left[ \min \left\{ \frac{s_i}{K_{s_i} + s_i} \right\}_i \right] \quad (2.6)$$

$$\text{Multiplicative:} \quad \mu = \mu_{\max} \left[ \prod \frac{s_i}{K_{s_i} + s_i} \right] \quad (2.7)$$

Other options that have been proposed include a simple average or harmonic mean, and each of these four can be shown to be successful with various empirical datasets [75].

<sup>7</sup>Microbial growth can also reported in terms of the **doubling time**, which is the time required for the population to double.

A key problem with the Monod model for astrobiologists is the dependence of half-saturation constants on environmental variables such as temperature and pH, and their organism specificity. It is an excellent technique for analysing empirical data but is not suitable for conditions which are poorly understood and/or are largely inaccessible (such as those of interest to astrobiologists).

A more flexible method to fit empirical data is provided by the classical **Tempest model** [72, 76]. It is a re-parameterisation of the Pirt model [77], which in turn extended the traditional Monod model above by recognising the importance of an explicit maintenance power rather than including a string of growth-limiting constants. For a constant maintenance requirement per cell  $m$  [W cell<sup>-1</sup>], the relationship:

$$q = \frac{\mu}{Y_T} = m + \frac{\mu}{Y_G} \quad (2.8)$$

is linear in  $\mu$ , where  $q$  is the rate of energy consumption per cell,  $Y_T$  is the actual yield of bacteria [classically with units g biomass per g energy source] and  $Y_G$  is the maximum theoretical yield (i.e. with no maintenance). If we consider each of the terms in Equation 2.8 as powers with units W cell<sup>-1</sup>, the total rate of energy consumption per cell is the **power supply**,  $q = P_S$ ,  $m$  can be rewritten as the **maintenance power**  $P_M$ , and Equation 2.8 is equivalent to:

$$P_S = P_M + P_G \quad (2.9)$$

where  $P_G = \mu/Y_G$ , the power going into growth processes or **growth power**.

On a plot of  $q$  vs  $\mu$  [ $P_S$  vs  $P_G Y_G$ ] the gradient  $1/Y_G$  will change should the power supply vary with growth rate. The maintenance power  $m$  [ $P_M$ ] can be gathered from the intercept (Figure 2.4, left hand side). There have been several further adaptations to Tempest-like models, in order to account for maintenance changing as a function of power supply, including the introduction of an **endogenous metabolism**<sup>8</sup> or splitting the maintenance coefficient into multiple factors [72]. With each of these corrections, however, comes a further reliance on empirical data for specific organisms in specific environments, limiting theoretical generalisations of these models.

<sup>8</sup>The endogenous metabolism encapsulates the metabolic processes which occur in cells in the absence of any energy of nutrient supply.

## 2.2.2 | An agnostic, theoretical growth model

There are many routes to estimating biomass yields from a more theoretical basis [e.g. 78, 79], but often little attention is paid to differing environments and the effect of the extremes described in Section 2.1.3 are unaccounted for. In geomicrobiology and environmental microbiology many of these extremes are more commonplace, and this is reflected in the attempts to model growth in Earth's natural settings. A fairly comprehensive method of modelling growth energetically has been described by LaRowe and Amend [39, 40], in which the rate of change in total **biomass**  $B$  [cells],  $dB/dt$ , is calculated by considering the balance between cell-specific energetic supply and demand:

$$\frac{dB}{dt} = Y_{LA} B(t) (P_S(t) - P_M(t)) \quad (2.10)$$

$$\frac{dB}{dt} = Y_{LA} B(t) \left( \frac{-\Delta G_{cat}(t)}{v} r_{cat}(t) - P_M(t) \right) \quad (2.11)$$

where  $P_S$  [W cell<sup>-1</sup>] and  $P_M$  [W cell<sup>-1</sup>] are the cell-specific power supply and demand (maintenance power) respectively,  $\Delta G_{cat}$  [J mol<sup>-1</sup>] is the free energy of the catabolic reaction (see Box 2.2),  $v$  is a stoichiometric coefficient such that the Gibbs stoichiometry matches the rate of the catabolic reaction per unit biomass,  $r_{cat}$  [mol s<sup>-1</sup>]. The yield coefficient is  $Y_{LA}$  [cell J<sup>-1</sup>], and determines how much biomass the energy available can produce. For a biomass in cells, it can be represented by:

$$Y_{LA} = \left( \frac{\text{gram. biomass}}{\text{J}} \right) \left( \frac{\text{cells}}{\text{gram. biomass}} \right) \quad (2.12)$$

where the left term is the mass of dry cells that can be made per joule of energy, and the right term the number of cells in a gram of dry biomass. For other extraneous losses of biomass, such as predation, death rates or disease additional terms can be added to Equations 2.10–2.11 [39]. This differential equation is equivalent to the Tempest model (Equation 2.8), because the growth rate  $\mu$  is equivalent to the rate of change of biomass per unit biomass, for example:

$$\mu(t) = \frac{dB}{dt} \frac{1}{B(t)} \quad (2.13)$$

It follows that the maximum theoretical yield and the LaRowe & Amend yield are equivalent (biomass units permitting). This yield with units as in Equation 2.12 is analogous to a cell-specific **energetic cost of biomass synthesis** in J cell<sup>-1</sup>:

$$E_{syn} = \frac{1}{Y_{LA}} \quad (2.14)$$



Hence, under this model a growth rate can be defined for a given catabolic **power supply** [ $P_S$ ] maintenance **power demand** [ $P_M$ ], and **energetic cost of biomass synthesis** [ $E_{\text{syn}}$ ]:

$$\mu(t) = \frac{dB}{dt} \frac{1}{B(t)} = \frac{1}{E_{\text{syn}}} \left( P_S(t) - P_M(t) \right) \quad (2.15)$$

Figure 2.4 shows the linear relationships that can be drawn from the Tempest and LaRowe & Amend models for qualitative purposes. On the left, in the typical Tempest format (e.g. Equation 2.8) where the 'base' has no maintenance power — a classical Monod fit [72]. Introducing a maintenance power shifts the y-intercept (dashed line), and adding a dependency to that maintenance power making it increase linearly with growth rate increases the gradient (dotted line). On the right is a representation of Equation 2.10. The  $x$ -intercept shows the point at which maintenance power exceeds power supply (i.e.  $\mu = 0$ ). If the yield is halved — a doubling of  $E_{\text{syn}}$  by Equation 2.12 — this is still met but the gradient is reduced by half (dotted line). Increasing the power supply by 50% shifts both intercepts proportionally such that growth can be achieved at higher maintenance powers (dashed line).

The main takeaway of this brief overview of relevant microbial energetic models is that theoretical estimates of  $P_S$ ,  $P_G$  and  $P_M$  can be linked to empirical data, specifically microbial growth rates and yields. In Chapter 3 we will explore how the power supply can be computed from a single overall catabolic reaction and examine some techniques to estimate the maintenance power associated with temperature and pH. In Chapters 4 and 5 a numerical model of Equation 2.10 is developed and applied to methanogens.

## 2.3 Case study: Enceladus' subsurface ocean

---

In the 2000s a subsurface ocean was inferred under Saturn's icy moon Enceladus [80]. Since then, it has become a tantalising case-study for potentially habitable conditions in the outer solar system. This came to a head in the 2010s when it became apparent that all of the reactants and products of the **hydrogenotrophic methanogenesis** metabolism feature in the ocean's composition [e.g. 13, 15]. On

the whole however, the parameters of the icy moon remain weakly constrained and there is still much for us to discover. Nonetheless, what we know about the ocean now could be enough to infer whether or not it contains habitable regions [16].

### 2.3.1 | A brief overview of icy moon habitability

Since evidence began to suggest the existence a subsurface ocean on Europa [81], and more recently the direct observation of plumes from the southern hemisphere of Enceladus [80], icy moons have perhaps become the most promising candidates for exobiological activity in the solar system. Owing to their greater distance from the Earth, and having fewer dedicated missions with no direct access to the subsurface water, modelling has played a large role in predicting their structure, composition, and astrobiological potential [e.g. 19–21, 70, 82–84].

Europa was the first of the two moons for which indirect evidence of a subsurface ocean was found [81], and the discovery turned the traditional notion of a habitable zone on its head [63]. Since then, a large number of studies have investigated the structure, composition and potential role of biology on the icy moon [e.g. 82–84]. Since direct evidence of the ocean's composition is unavailable, there is little empirical data available to assess these models' predictions. This will hopefully change should the planned Europa Clipper mission go ahead; one of its priorities is to better characterise the ocean.

When the detection of plumes from Enceladus' southern hemisphere demonstrated some source of liquid water must reside below the surface [81], the icy satellite promptly joined Europa as a candidate for extraterrestrial life in the solar system. Enceladus benefits from direct measurements of its composition from the plumes, and they were discovered to contain  $\text{CH}_4$ ,  $\text{CO}_2$  and  $\text{H}_2$  — the net reagents of hydrogenotrophic methanogenesis [15], an ancient metabolism used by life on Earth. Various salts, silicates and short-chain alkanes were also detected. A summary of inorganic constituents in the Enceladus plume and E-ring observations is shown in Table 2.3 as mixing ratios. One should not be tempted to say that these observations reflect the exact composition of the ocean, but geological and geochemical models can use them to constrain what its physico-chemical parameters may be [2, 85–87].

Nowadays, for each of these moons emphasis is put on both their potential habitability and the possibility of life independently emerging on them, owing to proposed **hydrothermal systems**<sup>9</sup> similar to the Earth [88]. These moons are not

---

<sup>9</sup>These are regions where water is circulated near rock at very high temperatures, producing a plethora of chemical species and diverse energy sources for life.

### 2.3. Case study: Enceladus' subsurface ocean

---

unique in the solar system for having salty subsurface oceans. They have also been inferred beneath the surfaces of Ganymede, Callisto and Titan, and tentatively could exist on Triton, Pluto, Dione and Ceres [89]. Some of these bodies are also suspected to support significant water-rock interactions but Enceladus and Europa stand out as the strongest candidates for such interactions allowing persistent redox **disequilibria**<sup>10</sup> [17].

The NASA roadmap for icy worlds [18] has assessed the state of knowledge for icy moons throughout the solar system to prioritise future space missions. They describe Enceladus as an ocean world with a solid foundation of 'Energy for life' but only a basic foundation of the 'physico-chemical conditions for life' (Figure 2.5). This means a possible next step in characterising its habitability is determining whether the energy that it provides is enough for life to survive and grow.

---

<sup>10</sup>At chemical equilibrium, the energy in the system is minimised. In simple terms disequilibrium may allow for reactions to take place and energy to be extracted by life. Further discussion of chemical kinetics and bioenergetics can be found in Chapter 3.

2\_Background/figs/Tempest\_LA2.pdf

**Figure 2.4 Linear behaviour of microbial growth in the exponential phase.** These plots show the linearity of equations for bacterial growth in the exponential phase (Equations 2.8 & 2.10), and the effects of changing parameters as indicated in the legend.

#### Box 2.2: Metabolism, catabolism and anabolism

It is important to define some key terms for the way life processes energy and nutrients for the non-biologist reader. As a general rule, **catabolism** breaks larger molecules down into smaller ones — releasing energy — and **anabolism** builds big molecules up — consuming energy. Together they broadly define **metabolism**. When you eat, food is catabolised into usable chunks of energy (such as adenosine triphosphate [ATP], the universal energy currency of life). Your body then uses anabolic processes which utilise this energy for building biomass, like storing fat or repairing muscle.

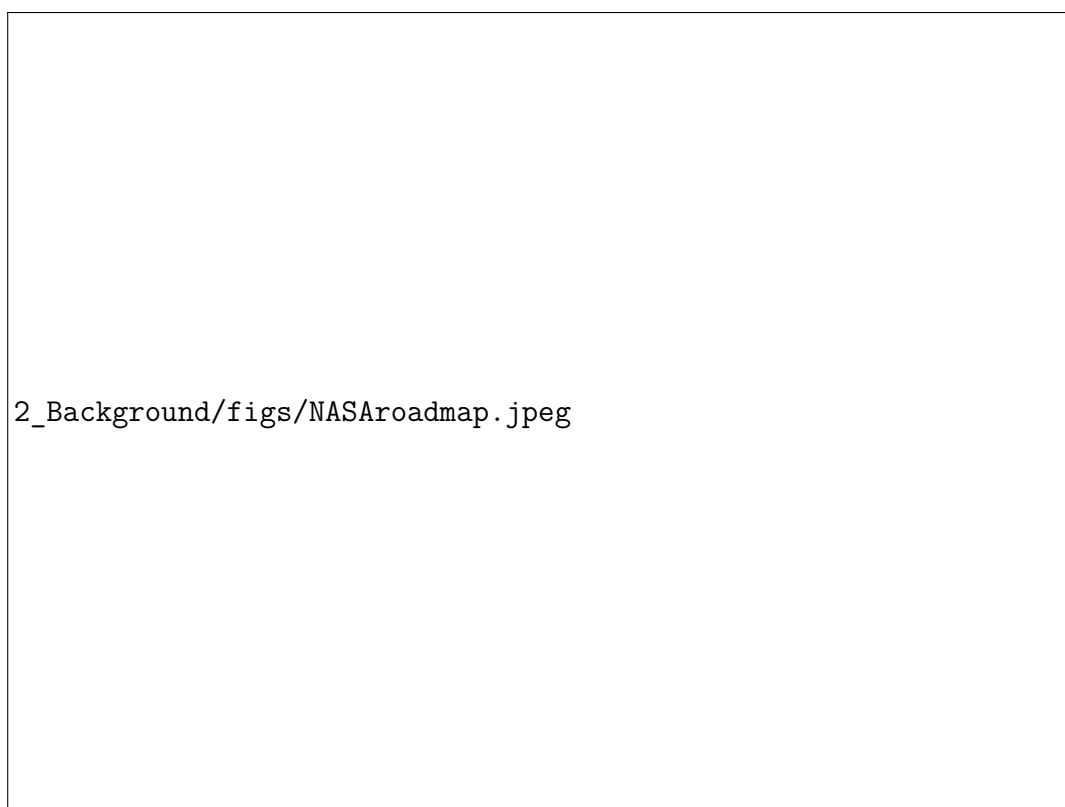


**Figure 2.5 The NASA roadmap for icy worlds** compiled by Hendrix et al. (2018) [18]. This plot visualises what we know about the habitability of icy bodies in the solar system.

**Table 2.3 Select Cassini measurements from the Enceladus south polar plume**

These volume mixing ratios are from Cassini observations E14 E18 E17 and E21.

Species	Mixing ratio (%)	Reference
H <sub>2</sub> O	97.5±1.5	[15]
CO <sub>2</sub>	0.55±0.25	[15]
CH <sub>4</sub>	0.2±0.1	[15]
H <sub>2</sub>	0.9±0.5	[15]
NH <sub>3</sub>	0.85±0.45	[15]
H <sub>2</sub> S*	0.0021±0.001	[13]

\* While H<sub>2</sub>S was reported in 2009 [13], the same group later declared its detection too ambiguous to be confident in [90].

### 2.3.2 | Geophysical properties

Much was revealed about the geological activity below the surface following the detection of Enceladus' south polar plumes [80]. This is the only confirmed example of active cryovolcanism in the solar system [89, 91, 92]. A number of models have been put forward to determine the geological structure of the icy moon and have been well-reviewed in recent years [17, 18, 89]. The broad consensus of the global geophysical properties will be summarised here along with the key unknowns, by starting at the surface and working our way down.

#### i) An icy exterior

On Enceladus' surface lies a thick layer of ice. On average, the ice sheet is around 30–40 km thick [85, 93, 94], though recent studies suggest it may be much thinner (an average of 21 km [95]), but this is only part of the story. The ice layer is differentiated and appears to be warmer and thinner at the south pole compared to the rest of the surface [93], with some models suggesting that the ice may make contact with the rocky core in its thickest equatorial regions and be only a few km thick at the south pole [94]. Ultimately the ice thickness depends on the composition of the core and the extent of geothermal heating caused by tidal effects.

Cosmetically, the defining feature of the satellite's surface is the so-called 'tiger stripes' at its south pole. These are the fractures from which the plume emanates. The temperature at the top of these tiger stripes is expected to be between 177–217 K [96], in contrast to the rest of the surface which is much cooler at between 33–145 K [91, 97]. The plumes themselves are variable with Enceladus' orbit, peaking as it



**Figure 2.6 The structure of Enceladus' interior.** Image credit: NASA/JPL.

undergoes the strongest tidal forces. They are likely driven by some combination of liquid flowing within the ice and boiling up from below, much like geysers on Earth [89]. Most of the expelled ice grains fall back down onto the surface and are eventually recycled back through the ice sheet [98]. This is among the reasons why Enceladus is the most reflective body in the solar system. Finer vapour particles which escape the gravitational pull of the satellite form Saturn's E-ring [99].

### ii) A subsurface ocean

Beneath the icy cloak lies a vast subsurface ocean. Its extent is still not entirely clear, but is now widely expected to be a global, albeit differentiated salty ocean with a depth of up to  $\approx 15$  km [15, 85, 87, 93, 94, 100], though recent analyses suggest it may be even deeper, to an average of 37 km [95]. The majority of the ocean has a temperature of approximately 273 K, but could be lower if it is highly saline [83, 86]. The composition of the ocean is discussed in Section 2.3.3 and modelled in Chapter 6.

The extent of convection and temperature gradients between 'hot-spots' at the water-rock interface [94, 100] and the cooler wider ocean is unclear. This owes to the unknown rock-water temperatures and core composition (discussed below). Understanding the convective processes at play on Enceladus is key to determining the age and ultimate fate of the ocean. If the ocean pH is high, it means that either

the ocean is relatively young (<100 Myr) or **serpentinisation**<sup>11</sup> reactions have been proceeding very slowly [83]. Moreover, if the ocean were to freeze, the effects of tidal heating will reduce and it may never be able to become liquid again [17].

### iii) A rocky core

The presence of water-rock interactions, which were inferred when non-water components were observed in the E-ring, implies that Enceladus has a rocky core [14]. Determining the composition of the core will help illuminate the nature of the water-rock interactions, the heat generated in the core by tidal forces, and consequently the physico-chemical parameters of the ocean itself [17].

Vance et al (2018) [83] used the interior density, temperature, sound speed, and electrical conductivity of icy moon interiors to characterise their habitability from a geophysical perspective. They conclude that Enceladus has a low-density rocky interior, with low levels of metals in the core. Decreasing core density correlates with thinner ice shell thickness. In this model a porous low-density core may allow fluids to flow throughout it. Such a process, converting anhydrous to hydrous rock, could explain the production of hydrogen to this day [83, 85]. Glein & Waite (2020) [87] examined various rock compositions, including whether they were reduced or oxidised, and explored whether their CO<sub>2</sub> production could meet Cassini-derived constraints. A combination of quartz, talc and carbonate was found to agree with these constraints in both reduced and oxidised cases. This introduces a new question as to the ratio of ferric/ferrous iron in the core, which requires further analysis on the plume measurements to determine [87]. This composition can also explain the generation of silica particles [85], but would be unfavourable for significant H<sub>2</sub> production. For a **heterogeneous**<sup>12</sup> core with 'hot-spots', as is expected [94, 100], a carbonated upper layer and serpentinising lower layer could produce the necessary CO<sub>2</sub>, H<sub>2</sub>, and SiO<sub>2</sub> levels to corroborate Cassini measurements [87].

The temperature of the water-rock interface influences convective processes in the ocean and its chemical composition. As briefly discussed above, one way to estimate the temperature of the water-rock interface proposed by Hsu et al. (2015) [85] is to calculate the temperature required to form silica nanoparticles of the size observed by Cassini. This temperature also depends on the pH of the interface and the cooler surrounding ocean. They predict it to vary from ~363 K at high pH to over

---

<sup>11</sup>Serpentinisation is the geological process which creates serpentine minerals, such as serpentinite, from silicates. This process is particularly important for astrobiologists because it embellishes hydrothermal fluids on Earth with methane and hydrogen.

<sup>12</sup>Heterogeneous systems are not uniform throughout; the opposite of a homogeneous system.



500 K at low pH. If the pH of the cooler ocean is one unit lower, these temperatures are much higher [85]. Temperatures of 363 K can be met by 'hot-spots' generated through tidal heating [94].

### 2.3.3 | (Geo)chemistry of the subsurface ocean

Despite Cassini's plume observations we have no direct samples of the ocean. Its chemistry must be inferred from the icy particles and gases detected by the spacecraft's Cosmic Dust Analyzer [CDA] and Ion Neutral Mass Spectrometer [INMS] instruments, and coupled to the water-rock interactions described above.

The pH is the key source of uncertainty when determining the composition [86]. A number of estimates of the bulk ocean pH have been put forward ranging between 8 and 12 [14, 85–87, 101, 102]. Most recently, a pH value of 8.5–9 for the ocean at 273 K appears most likely [87].

The ocean is weakly saline. Postberg et al. (2009) [14] identified grains in the E-ring that were rich in sodium salts (~0.5–2% by mass), which can arise only if the plumes originate from alkaline liquid water. They also suggested that the ocean may be rich in carbonates and constrained limits on the salt content at 0.2 molal (m) Cl and 0.1 m DIC, or 0.05 m Cl and 0.01 m DIC. Here DIC refers to **dissolved inorganic carbon** (sum of the molalities of  $\text{CO}_2(\text{aq})$ ,  $\text{HCO}_3^- (\text{aq})$  and  $\text{CO}_3^{2-} (\text{aq})$ ). Glein et al. (2015) [86] note that this should be a 'useful but not rigid constraint'. If all of the core chloride is dissolved in the ocean, which is feasible because of the low core density discussed above, the possible upper limit for dissolved chloride is  $1.4 \times 10^{18}$  mol in the ocean, corresponding to 0.2–1.2 mol  $\text{kg}^{-1}$  on average [86]. Silicon and traces of metal were detected by the CDA, which Hsu et al. (2015) [85] used to constrain the salinity of the ocean to 4% at the rock-water interface and 0.5% in the cooler bulk ocean. A recent study into the depth stratification of the ocean suggests that the bulk ocean salinity may be significantly higher than previously thought, though these results are at present only qualitative [70].

Carbon dioxide was a predominant detection in the plume, so predictions of the ocean composition have attempted to match potential carbonate-based chemical systems to the Cassini measurements [15, 86, 87]. In short, if the activity of  $\text{CO}_2$  in the ocean [ $a_{\text{CO}_2}$ ] can be estimated, the mixing ratio (Table 2.3) can be used to estimate the activity of the other constituents near to the water-ice boundary. In an aqueous system,  $a_{\text{CO}_2}$  and pH are codependent because a change in the pH of

the system shifts the carbonate **buffer**<sup>13</sup>, and likewise a change in  $a_{CO_2}$  affects the pH. To select one with confidence requires knowing the other. As discussed above, pH constraints can be estimated by a number of methods — such as considering water-rock interactions — and  $a_{CO_2}$  can be corroborated with INMS and CDA data.

This corroboration has been done a few ways. One comes from taking the molar ratio recorded by the INMS and relating that to the molar ratio in the ocean by considering how it has changed as it travels from the ocean, through the tiger stripe and into the plume [86, 87]. The main source of this change is water vapour condensation as the species traverse the tiger stripes. Once the gas exits, it is likely **quenched**<sup>14</sup>, and does not change significantly before detection [87]. The condensation effects can be quantified:

$$\log_{10}(a_{CO_2}) \approx \log_{10}\left(\frac{CO_2}{H_2O}\right)_{\text{plume}} + \left[9.429 - \frac{2574}{T_{\text{tiger}}}\right] \quad (2.16)$$

where  $T_{\text{tiger}}$  is the temperature of the tiger stripes ( $197 \pm 20$  K) [96] and  $\left(\frac{CO_2}{H_2O}\right)_{\text{plume}}$  is the molar ratio of  $CO_2$  to  $H_2O$  in the plume observations; i.e. the ratio of their mixing ratios (Table 2.3).

Another way to estimate  $a_{CO_2}$  uses salt observations from the CDA. NaCl and  $NaHCO_3/Na_2CO_3$  salts are particularly abundant [14, 103]. Glein et al. (2015) [86] tested carbonate speciation models based on this salt content (varying  $[Cl^-]$  and [DIC]) using specialist software. Waite et al. (2017) [15] provide an approximate fit to the  $[Cl^-] = 0.1$  m, [DIC] = 0.01 m case which is accurate to within 20% for pH values between 7 and 14:

$$\log_{10}(a_{CO_2}) = -0.1213(pH^2) + 0.9832pH - 3.1741 \quad (2.17)$$

By comparing Equations 2.16 and 2.17 one could now estimate the pH of the ocean and  $a_{CO_2}$  constrained by Cassini measurements (e.g. Figure 2.7). This is a simplified example of the much more complex real systems which must be considered, for instance one must also consider the other possible values of  $[Cl^-]$ , [DIC] and the effects of other chemical species. These computations are also only strictly valid near the water-ice boundary. Increasing the temperature affects the chemical speciation results, and if there is significant water-rock interaction as discussed above, proximity to such systems will also affect the chemical composition. A more robust chemical speciation model is developed and discussed as part of Chapter 6.

<sup>13</sup>A buffer solution is one whose pH only changes a small amount when an acid or base is added to it.

<sup>14</sup>Quenching is a term used in chemistry when an external process or agent, unrelated to the one studying, stops a reaction.

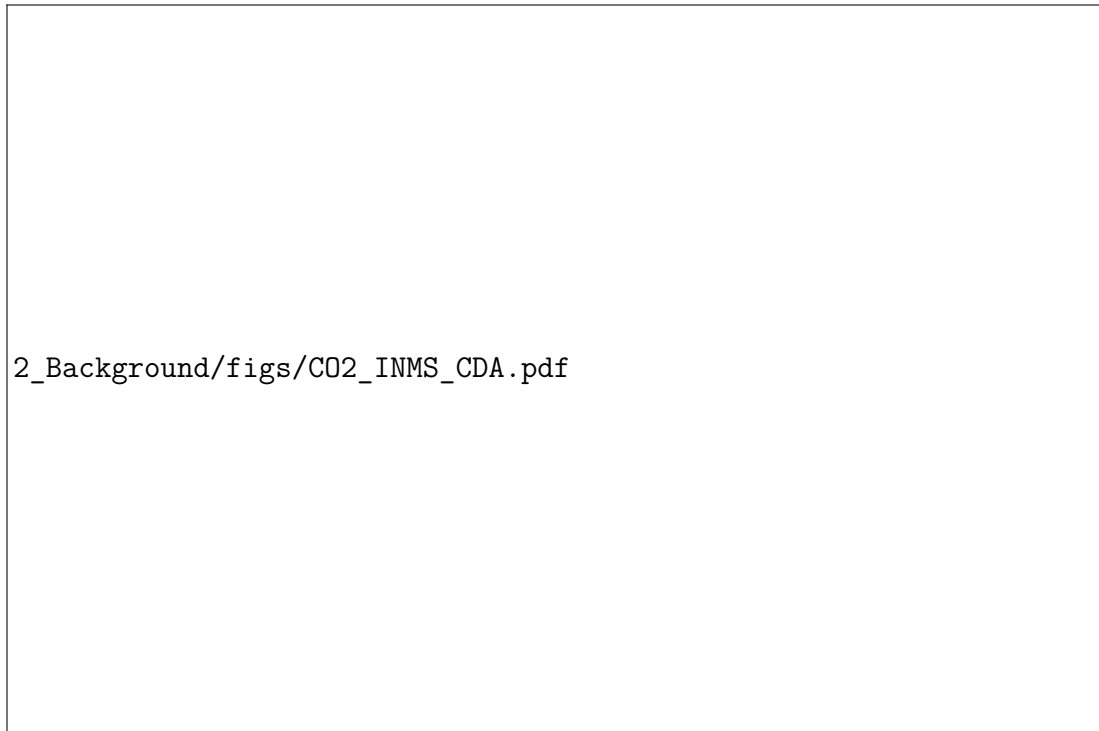


**Figure 2.7 Activity of CO<sub>2</sub> as inferred from INMS and CDA data** from Equations 2.17 and 2.16 in the main text. Uncertainty bounds in the INMS plot (blue bar) are due to variation in the tiger stripe temperature. Uncertainty in the CDA plot (green line) is in the fit to the data.

### 2.3.4 | The prospects for life

Most simple life forms require a redox couple, consisting of an electron donor and acceptor in an energy-yielding configuration [10]. A notable exception is phototrophs, which also use energy from light. There are two proposed major sources of electron acceptors on icy moons. One is from radiolytic processing, in which the surface ice interacts with local radiation creating electron acceptors such as O<sub>2</sub> and H<sub>2</sub>O<sub>2</sub>. Another is high temperature water-rock interactions at the bottom of the ocean, producing CO<sub>2</sub>, CH<sub>4</sub> or others. Contrary to Europa, electron acceptors are unlikely to be produced in large amounts on Enceladus' surface due to weak interaction with Saturn's **magnetosphere**<sup>15</sup>, meaning the only source of electron acceptors may be through hydrothermal activity [17]. In a recent study Ray et al. (2021) [19] computed possible oxidant concentrations in the ocean from these two

<sup>15</sup>Magnetospheres represent the magnetic fields and plasma environments of planets. Ions from magnetospheres can interact with the surface or atmospheres of planets and their satellites.

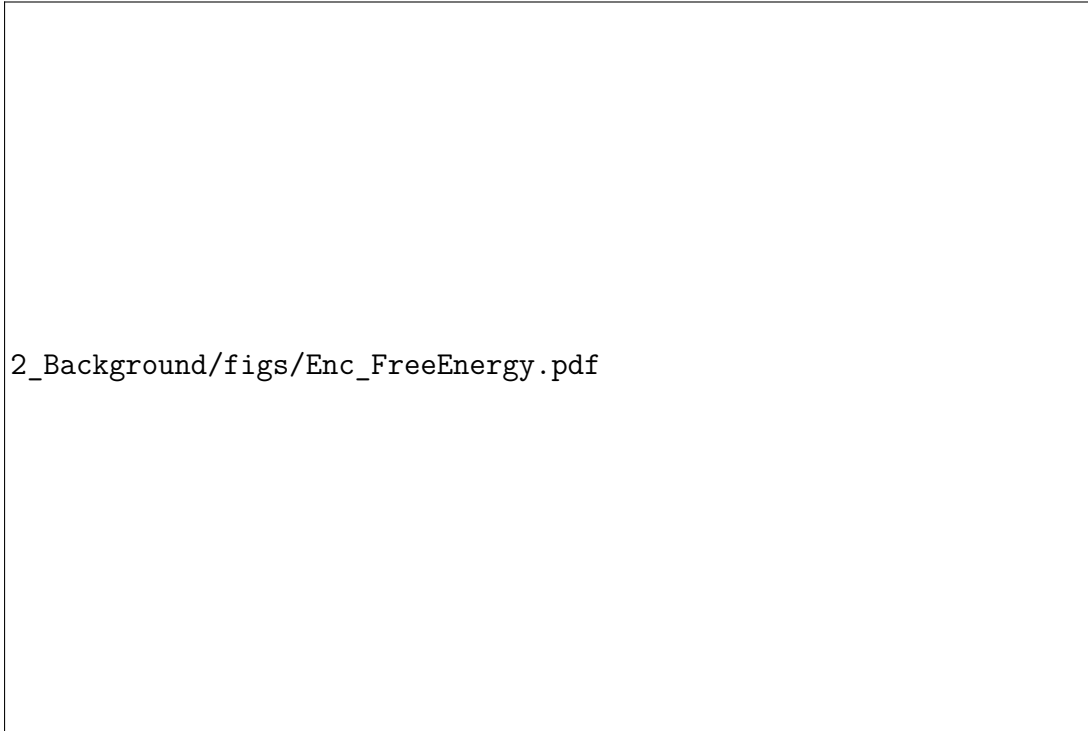


**Figure 2.8 Gibbs free energy of methanogenesis from INMS and CDA data.**  
Computed using the  $\text{CO}_2$  activities in Figure 2.7 and the mixing ratios in Table 2.3.

sources, which allows for more metabolisms to be considered. To date,  $\text{CO}_2$  is the only biologically useful electron acceptor confirmed to exist in the ocean [17] and ultimately alternative oxidants will only be assured by future visits to the icy moon.

The detection of  $\text{H}_2$  in the plumes sparked the possibility of methanogenesis occurring in Enceladus' subsurface ocean [15]. The viability of this metabolism can be assessed using Equation 2.1, which requires the activity of all reagents in the following reaction:



Each of these have been detected by Cassini at various mixing ratios (Table 2.3) and their activities can be inferred from the  $a_{\text{CO}_2}$  calculated above [15]. Figure 2.8 shows the free energy ranges permissible at the  $a_{\text{CO}_2}$  values presented in Figure 2.7 for the range of mixing ratios in Table 2.3. Configurations which have a negative free energy could be viable energy sources for life. Whether the power this provides exceeds the power demands of the environment to permit long-term microbial growth and survival remains to be seen, and is the focus of Chapters 6 & 7.

Also important for habitability is a suitable nutrient inventory. The minimum requirement typically considered is the availability of **CHNOPS** (carbon, hydrogen, nitrogen, oxygen, phosphorus, and sulfur) elements and transition metals such as Fe [6, 9]. C, H, N, O and S have been identified as constituents in the south pole plumes (Table 2.3), though whether S was the correct interpretation has been disputed since their observation by Waite et al. (2009) [13] and other molecules could also pose a fit to the data [90]. Carbon sources other than CO<sub>2</sub> and CH<sub>4</sub> have also been reported in the form of diverse types of organic compounds that span a spectrum from simple to complex [13, 104, 105]. Enceladus is expected to have formed from **chondritic**<sup>16</sup> material which means it should have a S, P and Fe endowment, completing the set. With no direct measurements of these three nutrients, it is difficult to quantify their abundance in the ocean and hydrothermal systems. Modelling analyses have estimated the dissolved concentration of phosphorus [106] and sulfates [19] in the bulk ocean, and laboratory experiments are underway to more tightly constrain these values.

The plausibility of an origin (or delivery) of life on Enceladus is also of interest. The global nature of Enceladus' ocean is a promising feature for this. It is more likely that a global ocean will persist long enough for life to emerge than a regional sea due to the rate of persistent heating (in Enceladus' case, tidal heating) it would be subjected to [16]. Interestingly, if Enceladus' ocean is relatively young (~100 Myr) [107], material exchange with the inner solar system is unlikely. This means that if life were to appear on the icy moon, it must have done so independently of life on Earth [16].

---

<sup>16</sup>Chondrites are non-metallic meteorites which have not undergone any external processing.

## 2.4 Other locations of astrobiological interest

---

### 2.4.1 | Earth's extremes

Biogeochemical modelling has been used extensively in an attempt to understand regions of the Earth that are not easily accessible, such as deep-sea hydrothermal vents [108–110], the deep subsurface [39, 41, 111], drylands [112], and the atmosphere [113] (though the latter generally focus on transport rather than survival explicitly). Two approaches to modelling are often utilised: the biogeochemical approach (ignoring the identity of organisms) and the ecological approach (focusing on growth and biomass of organisms), and the two can be shown to be consistent on long time scales [114].

### 2.4.2 | Mars

The general consensus is that most of the surface of Mars (in its current state) is inhospitable to life, not least because of the lack in shelter from solar UV radiation, and any available water is either frozen or in highly saline brines [63]. On the brighter side though, the subsurface remains of interest due to a tantalising concoction of nutrients and available redox couples, protected from radiation and with potential sources of groundwater [63, 67, 68]. Areas of interest are in the rocks of the subsurface, which should be less porous than their Earth analogues [63], and deeper down in the hydrothermal fluid [115]. Figure 2.9 shows the geologic structure and availability of certain nutrients in the Martian crust.

The number of explicit models of biological activity on Mars is limited, with the highest profile study conducted by Weiss et al. in (2000) [116]. This is mostly due to large uncertainties in the composition and structure of the planet which remain to this day. While a number of models have been proposed regarding the chemical and physical structure of Mars and its subsurface [e.g. 117], the assessment of the red planet's habitability has mostly been limited to laboratory experiments in Mars-analogue environments and media. An attempt to model microbial activity in the subsurface using similar techniques to that of the Earth (see above), either globally, in local porous media or hydrothermal systems, could prove useful for the further characterisation of Mars' geological structure by explicit consideration of a biological source for the methane observed in the atmosphere [e.g. 118, 119]. This would also need to account for the delayed diffusion of methane to the surface [120]. Iron-oxidising organisms could also be considered [121].



**Figure 2.9 Possible geological context of Mars** a: Proposal for the potential geologic contexts of Martian groundwater, on a logarithmic scale down to depths of 10 km. b: The distribution of energy sources and nutrients at these depths. Both from Michalski et al. (2013) [68].

The history of Martian habitability is also of interest. It has been long suggested that Mars may have gone through three epochs, starting not unlike the Earth but with each one becoming more and more hostile to life as we know it [63]. Earth analogues can be selected for each of these epochs [122] and possible trajectories that Mars could have taken were pockets of it inhabited in the past hypothesised [123]. Perhaps a model set over geological timescales could help to quantify the biogeochemical effects caused by an inhabited habitat on Mars during these periods — and whether detectable biosignatures could be preserved.

### 2.4.3 | Venus

Earth's sister planet is a hellish place but that has not omitted it from the radar of some astrobiologists, which has been met with controversy. A runaway greenhouse effect has rendered the surface inhospitable to known life with temperatures over 300 K higher than the maximum limit for life [4]. Attention has hence focused on a temperate region of the cloud layer between altitudes of 48 and 60 km. In 2020, the astrobiology of the Venusian atmosphere took centre stage when Greaves et al. (2020) [124] reported a detection of phosphine in the clouds, a molecule which is only known to be produced by biology on Earth and is a possible biosignature considered by exoplanet scientists [125]. The authors could not isolate a non-biological means of producing this phosphine, but it should be noted the detection has recently been strongly disputed and may have been erroneous. From a microbiology perspective, the cloud droplets are uninhabitable [4]. They are at least 81% sulfuric acid resulting in a pH of less than 0 and water activity of less than 0.1, both of which far exceed the known limits of life on Earth (Table 2.2). Venus is sterile according to our current understanding of life. An interesting question though is just how far from habitable is it? We explored this question as part of an undergraduate research project. It is summarised in Section 4.4.2 and an article produced from this work has been published in the journal *Astrobiology* [4].

### 2.4.4 | Exoplanets

One could take the slightly more ambitious approach of considering the possibility of habitable extrasolar planets or moons. McKay (2014) [71] reviewed the limits for life in an exoplanetary context, using similar requirements and limits to those discussed in Section 2.1.3. The prospect of Earth-like planets is tantalising, but at present the amount of data available is limited to atmospheric spectra (if even that is available). As a result, models exploring the habitability of exoplanets often simulate the atmospheres to elucidate the surface's characteristics [e.g. 126] or instead focus on life in the atmospheres themselves [e.g. 127]. Predicting the appearance of spectra which contain biosignatures is also of interest in target selection for higher-resolution future telescopes such as JWST [e.g. 128]. In another project related to this thesis, we worked with a summer student to explore what is needed to bridge the gap between microbial modelling and observations of exoplanet atmospheres. This is summarised in Section 4.4.3 and is under review for the journal *Astrobiology* [5].



---

## 2.5 Summary

---

A standard, agnostic model for examining the habitability of various environments is yet to be realised. A possible route towards building one is by taking an energetic approach to habitability, in which we consider life's behaviour as a series of chemical processes, which use energy and nutrients to build and maintain complexity. This reduces the complications of biological activity to physical fundamentals in which our main concern is asserting the availability of energy and nutrients in a system. What remains is for these processes to be quantified and verified. The groundwork for this has in many ways already been laid out, and in this thesis we will bring together an energetic overview of biological adaptation, survival and growth processes (Chapter 3) into one catch-all python package for quantitative habitability predictions (Chapter 4).

This approach can be applied to bodies throughout the solar system and beyond. In general it is the physico-chemical parameters which planetary scientists and astronomers first determine on any extraterrestrial body, and with the energetic approach to habitability these are all that is needed to begin making assessments. We introduced the Enceladus subsurface ocean as a case study for this approach, and briefly reviewed the prospects of some other bodies. The variation in possible parameters below Enceladus' icy shell is huge, ranging from the cold bulk ocean with a pH similar to seawater on Earth to scalding alkaline fluids at its depths. But, with geochemical and geophysical modelling these parameters could be constrained, and we may be able to quantitatively assess its habitability for methanogens, organisms which use an ancient metabolism on Earth whose reagents are common throughout the universe. In Chapter 5 we configure our model to predict methanogenic behaviour based on energetic and nutrient availability using data gathered in laboratories on Earth, and in Chapters 6 and 7 apply it to Enceladus' ocean to predict its habitability, possible biomass and biosignatures.



# CHAPTER 3

---

## Bioenergetics of adaptation, survival and growth

---

In Erwin Schrödinger's 1944 book "What is Life?" [129], he asks: "*What then is that precious something contained in our food which keeps us from death?*". Ultimately, that precious something is entropy. This is because when we eat our bodies use the energy and nutrients released in breaking down food to build and repair the complex biomolecules that we are made from. This process is known broadly as metabolism, and many facets of it can be quantified using bioenergetic ideas.

This chapter explains the theory that has been developed and used to quantify microbial adaptation and energetics in a bioenergetic context for life on Earth. Each subchapter explores a different parameter which is important for microbial growth models, and presents how we unify them to the same standard.

### Subchapters

3.1	Microbial energy flows: an agnostic overview ..	40
3.2	Energetics of biosynthesis .....	51
3.3	Quantifying adaptation to extremes .....	54
3.4	Summary and outlook .....	72

In Chapter 2, an agnostic, energy and time based solution to simple microbial behaviour was introduced, in which the growth rates  $\mu$  [ $\text{s}^{-1}$ ] of biomass  $B$  [cells] were characterised by an expression in terms of cell-specific maintenance power  $P_M$  [ $\text{W cell}^{-1}$ ], cell-specific power supply  $P_S$  [ $\text{W cell}^{-1}$ ], and the synthesis cost of biomass  $E_{\text{syn}}$  [ $\text{J cell}^{-1}$ ]:

$$\mu(t) = \frac{dB}{dt} \frac{1}{B(t)} = \frac{1}{E_{\text{syn}}} \left( P_S(t) - P_M(t) \right) \quad (2.15 \text{ revisited})$$

Each of these is dependent on the local physico-chemical conditions [10] and some quantifiable cell-specific properties such as size, proteomic and genomics structure [8] or internal pH [37, 45]. In this chapter we will bring together some theory for computing these variables such that a bioenergetic microbial growth model for astrobiology can be realised.

## 3.1 Microbial energy flows: an agnostic overview

---

Astrobiology needs a flexible, agnostic method to assess whether or not an environment has a useful supply of energy for life. Finding a suitable method is difficult, because life as-we-know-it on Earth has developed complex biochemical mechanisms to extract energy from its environment over billions of years of evolution. The Gibbs ‘free’ energy of a process  $\Delta G$  represents the maximum amount of useful work which can be done by that process i.e. the maximum amount of energy which can be extracted from it while still obeying the laws of thermodynamics [59]. Because it represents work done by the system, energy is available when  $\Delta G < 0$ . In a sense, if a chemical reaction has a negative  $\Delta G$  this energy is up-for-grabs and can be used to drive other energy consuming processes. Fundamentally, this is how life appears to ‘break’ the second law of thermodynamics<sup>1</sup> when it builds huge biomacromolecules such as proteins or DNA — a decrease in entropy. Overall there *has* been an increase in entropy, in the form of all the ‘food’ consumed and broken down to build up that biomacromolecule.

Life *must* follow the laws of thermodynamics, so Gibbs free energies are a useful measure of what biology can and cannot achieve. If a simple life form in a closed system only has the microbial machinery to perform one energy-yielding metabolic pathway (overall, a chemical reaction), its energetic resources are finite and can be

---

<sup>1</sup>The second law states that in an isolated system, the entropy, which in lay terms quantifies the degree of disorder, can only increase.

quantified. We can use the Gibbs free energy of chemical reactions to work out whether a chemical composition can yield useful energy for life, and this technique has even been used to identify metabolisms which appear missing in nature [130]. To convert this to a useful power supply  $P_S$  requires more information about how fast the organism can process that energy and convert it into a usable form. In this subchapter we present some methods for calculating the Gibbs free energy available from chemical reactions in known environments, give an overview of how life on Earth converts this into a usable form, and finally show how this can be coupled with microbially limited chemical kinetics to calculate the power supply available for life.

### 3.1.1 | Gibbs free energy and chemical thermodynamics

This section contains a brief overview of how molar Gibbs free energies can be calculated in chemistry and biology. It is not designed to be exhaustive, but should bring the reader up-to-speed for following the model and results presented in Chapters 4–7. The equations presented here are classical and available in many undergraduate textbooks [e.g. 59]. The typical method for calculating  $\Delta G$  was introduced in Chapter 2:

$$\Delta G = \Delta G_r^\circ + RT \ln Q \quad (2.1 \text{ revisited})$$

where  $\Delta G_r^\circ$  [J mol<sup>-1</sup>] is the standard Gibbs free energy change of the interaction, which is  $\Delta G$  in some reference frame, usually that in which the activity of all constituents is 1. Contrary to what one might find in the literature (even in textbooks),  $\Delta G_r^\circ$  is a function of temperature and pressure and beholden to the standard of choice [131]. The reaction quotient  $Q$  takes the form:

$$Q = \frac{a_C^c a_D^d}{a_A^a a_B^b} \quad (3.1)$$

for a generic chemical equation:



in which  $a_x$  is the **chemical activity** of species  $x$ . Often with chemical problems it can be approximated that the activity is equivalent to the molarity  $M$  [mol L<sup>-1</sup>] or molality  $m$  [mol (kg H<sub>2</sub>O)<sup>-1</sup>] if  $m$  and  $M$  are suitably small. When this is not the case, **activity coefficients**  $\gamma_x$  are used to correct between  $m_x$  or  $M_x$  with  $a$ . Methods for calculating and using activity coefficients relating to neutral solutes and electrolytes are introduced in Appendix A.1.

More formally, the Gibbs free energy is the maximum amount of energy which can be extracted from a reversible process in a thermodynamically closed system at constant temperature and pressure. It is defined by:

$$\Delta G = \Delta H - T\Delta S \quad (3.3)$$

where  $\Delta H$  is the change in **enthalpy**, which is equivalent to the change in the internal energy of the constituents during the process; and  $\Delta S$  is the change in **entropy**, a measure of how much constituents are 'spread out' by the process.

In the context of a chemical reaction one can think of the enthalpy change as referring to the release or consumption of energy due to different bond energies in the reactants compared to the products. Usually one would simplify this to the heat lost or consumed by the reaction — whether it is exothermic or endothermic. Entropy can be thought of as a measure of disorder for a chemical system. Generally speaking, entropy increases as the phase of molecules 'spreads out', so from solid to liquid to gas. The entropy is also likely to increase if more molecules are produced by a reaction than are consumed by it. An example of a chemical reaction with negative entropy change is the building of proteins, whereby on the order of hundreds of amino acids are assembled into one long chain. If basic information about the enthalpic and entropic changes associated with a reaction are known, we may be able to infer the spontaneity of a reaction at a given pressure using Equation 3.3:

- When a reaction is exothermic and entropy increases, i.e.  $\Delta H < 0$  and  $\Delta S > 0$  the Gibbs free energy change will always be negative and the reaction will always be spontaneous.
- When a reaction is exothermic and entropy decreases, i.e.  $\Delta H < 0$  and  $\Delta S < 0$  the reaction will be spontaneous below some critical temperature, but not spontaneous above that temperature.
- When a reaction is endothermic and entropy increases, i.e.  $\Delta H > 0$  and  $\Delta S > 0$  the reaction will be spontaneous above some critical temperature, but not spontaneous below that temperature.
- When a reaction is endothermic and entropy decreases, i.e.  $\Delta H > 0$  and  $\Delta S < 0$  the Gibbs free energy change will always be positive and the reaction will never be spontaneous.

It follows that enthalpy and entropy each contribute to the spontaneity of a reaction but neither one is a definitive measure of the Gibbs free energy alone. However, it is worth noting that any entropy releasing process will have a negative Gibbs free energy at a large enough temperature. Further examination of these quantities as drivers of metabolism in their own right would make for interesting analysis.

Equation 3.3 also holds in the standard reference frame, provided equivalent standards are chosen for the three variables:

$$\Delta G_r^\circ = \Delta H_r^\circ - T \Delta S_r^\circ \quad (3.4)$$

By the definition of  $\Delta G$ , at **chemical equilibrium**  $\Delta G = 0$  because no energy can be extracted<sup>2</sup>. This means that:

$$\Delta G_r^\circ = -RT \ln K \quad (3.5)$$

where  $K$  is the **equilibrium constant**, the reaction quotient at chemical equilibrium. This expression is particularly useful, because it relates a property of equilibrium ( $K$ ) to that of a reference frame ( $\Delta G_r^\circ$ ) which is *very rarely at equilibrium* in nature. If the equilibrium constant for a process is known, then  $\Delta G$  can also be calculated for a given composition like so:

$$\Delta G = RT \ln \left( \frac{Q}{K} \right) \quad (3.6)$$

Often,  $\Delta G_r^\circ$  and/or  $K$  are tabulated for common interactions at RTP<sup>3</sup>. However, their use in this way is limited if energetic calculations are to be performed at temperatures or pressures other than 298.15 K and 1 bar. An alternative, more flexible method of calculating  $\Delta G_r^\circ$  takes advantage of  $\Delta G$ ,  $\Delta H$  and  $\Delta S$  being defined as **state variables**. This means they are variables which define the thermodynamic state of the system, but are invariant of the path taken to get that state.

For example, by considering three states of a chemical reaction — the reactants, products, and elements in their standard phases — the standard free energy of that reaction can be written:

$$\Delta G_r^\circ = \sum \Delta G_f^\circ(\text{products}) - \sum \Delta G_f^\circ(\text{reactants}) \quad (3.7)$$

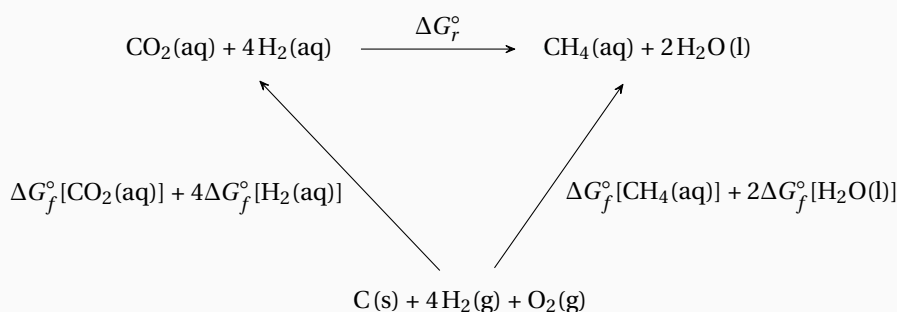
where  $\Delta G_f^\circ$  is the **standard Gibbs free energy of formation** of a chemical species. This is the standard free energy change when a chemical species is formed from its constituent elements in their standard phases. For example, the  $\Delta G_f^\circ$  for water is the  $\Delta G_r^\circ$  of the reaction  $\text{H}_2(\text{g}) + \text{O}_2(\text{g}) \rightleftharpoons \text{H}_2\text{O}(\text{l})$ . An example of how Equation 3.7 is derived from these three interactions is summarised in Box 3.1. This is useful because the quantity of Gibbs free energies that need to be tabulated drops significantly from having to empirically measure  $\Delta G_r^\circ$  for every possible reaction, to only requiring the  $\Delta G_f^\circ$  of the reacting species.

<sup>2</sup>This is because at chemical equilibrium, the system has reached some energetic minimum state, any change will require an input of energy.

<sup>3</sup>RTP stands for room temperature and pressure, traditionally 298.15 K and 1 bar

**Box 3.1: Using free energy as a state variable**

The origin of Equation 3.7 is best demonstrated by an example. Consider the methanogenesis metabolism (Equation 2.18), the focus of many chapters in this thesis. Let us also consider the constituent elements in their standard states. Because the Gibbs free energy is a state variable, we can take a path from the reagents to the products via the standard elements, and the energy change of the path will be identical as if we went straight from reactants to products.



In essence, this is the reverse of the formation of the reagents, and then the forward of the formation of the products. So overall:

$$\begin{aligned}
 \Delta G_r^\circ = & -(\Delta G_f^\circ[\text{CO}_2(\text{aq})] + 4\Delta G_f^\circ[\text{H}_2(\text{aq})]) \\
 & + (\Delta G_f^\circ[\text{CH}_4(\text{aq})] + 2\Delta G_f^\circ[\text{H}_2\text{O}(\text{l})])
 \end{aligned}$$

### 3.1.2 | Gibbs free energy of electrochemical cells

Life extracts energy by catalysing chemical (occasionally photochemical) reactions which have a negative Gibbs free energy change. This is done via an **electron transport chain** where, in lay terms, electrons are passed along an energetic production line from an electron donor species to an electron acceptor species (Section 3.1.3). This flow of electrons bears a likeness to electrochemical cells. In electrochemistry, the Nernst equation relates the so-called cell potential  $E$  [V] to some standard  $E^\circ$  [V] and its environment:

$$E = E^\circ - \frac{RT}{nF} \ln Q \quad (2.3 \text{ revisited})$$

where  $n$  is the number of moles of electrons passed and  $F$  is the Faraday constant which is approximately  $96485 \text{ C mol}^{-1}$ . This expression strongly resembles Equation 2.1, and an equivalency can be drawn between the Gibbs free energy and the



cell potential:

$$\Delta G = -nFE \quad (3.8)$$

$$\Delta G_r^\circ = -nFE^\circ \quad (3.9)$$

The pairing of an electron donor molecule and an electron acceptor molecule is known as a redox couple. In Box 3.2 an example of calculating the free energy of the same equation as in Box 3.1 — only as a redox couple — is presented.

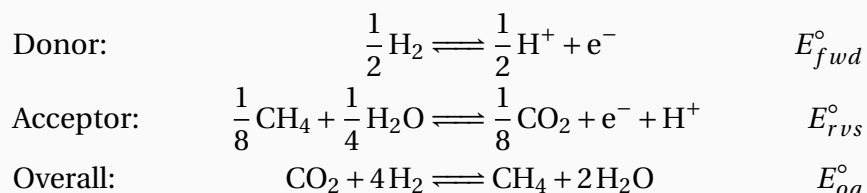
In microbiology and biochemistry, it is common to use a slightly different standard to chemistry and physics. It is referred to in this thesis as the **biological standard** and shown on parameters with a ' notation. For example, a biological standard Gibbs free energy is written  $\Delta G_r'^\circ$ . Both are computed as the respective variable with the activity of all constituents as 1, and often tabulated values represent those at 298.15 K and 1 bar (RTP). The difference between them is that the biological standard also specifies a pH and **ionic strength**<sup>4</sup> to be more representative of biological systems. The pH of choice is usually 7 (e.g.  $[\text{H}^+] = 10^{-7}$  M as opposed to 1 M) [131]. This becomes complex at pressures and temperatures outwith RTP because changing these parameters changes the 'neutral' pH (Box 3.5). It can be demonstrated that there is an equivalency between standards at RTP and an ionic strength of 0 when a reaction does not depend on  $[\text{H}^+]$  (Appendix A.2).

Standard Gibbs free energies vary with temperature and pressure, but often only values at RTP are directly available in the literature. Large databases in models such as SUPCRT92 [132] tabulate thermodynamic parameters (including  $\Delta G_f^\circ$ ) for a huge number of species and software packages are available which can approximate  $\Delta G_f^\circ$  at a given temperature and pressure. The reaktoro Python module [58] is used for the thermochemical calculations performed in this thesis. This module contains code to implement the revised Helgeson-Kirkham-Flowers (HKF) equations of state [34] to compute the standard thermodynamic values at the temperatures and pressures needed (e.g.  $\Delta G_f^\circ$ ,  $\Delta G_r^\circ$ ,  $\Delta H_f^\circ$ ,  $\Delta S_f^\circ$ ). An example of this variation for methanogenesis and ATP production (which is introduced in the next section) is shown in Figure 3.1. It is also possible to correct standard cell potentials with temperature; an example of doing so is summarised in Appendix A.1. Computing the dependence of the biological standards on temperature and pressure is more difficult and less widely accessible as for the chemical standards [131].

<sup>4</sup>The ionic strength  $I_n$  is a measure of the total concentration of ions and charge in a solution. It is useful in much of the theory around electrolytes (Appendix A).

### Box 3.2: Calculating the free energy from a redox reaction

The methanogenesis reaction from Box 3.1 can be written in terms of an electron donor in  $H_2$  and an electron acceptor in  $CO_2$ :



The first reaction proceeds to the right, (each  $H_2$  molecule *donates* 2 electrons) and the second reaction proceeds to the left (each  $CO_2$  molecule *accepts* 8 electrons). Combining the two gets the third equation, in which 8 electrons are transferred. The cell potential of the overall reaction is:

$$\Delta E^\circ = E_{oa}^\circ = E_{fwd}^\circ - E_{rvs}^\circ$$

so the standard free energy is, in units of [J (mol  $CO_2$ )<sup>-1</sup>]:

$$\Delta G_r^\circ = -8F\Delta E^\circ$$

Thus far, the equations presented here and in Section 3.1.1 only show us the maximum amount of energy that can be extracted from a chemical interaction. Life cannot use *all* of the Gibbs energy released through the electron transport chain. As we will see in section 3.1.4, the thermodynamic drive for energy extraction diminishes the larger the fraction of energy that life tries to capture.

### 3.1.3 | How life acquires and processes energy

The universal energy currency for life is **adenosine triphosphate** [ATP]. While other molecules can be used for energy storage, such as lipids, ATP is typically used as the intermediary because of its small size and high-energy phosphate bond. While ATP can be produced a number of ways, the quintessential reaction is the phosphorylation of adenosine diphosphate [ADP] by reaction with an inorganic phosphate  $P_i$ , which can be generalised to:



3\_Theory/figs/stds\_Meth\_ATP.pdf

**Figure 3.1 Variation in the standard Gibbs free energy of methanogenesis and ATP production with temperature and pressure.** These temperatures and pressures are representative of the Enceladus subsurface ocean. From Higgins et al. (2021) [2], where this is supplemental figure S1.

This represents the severance and restoration of the aforementioned high energy phosphate bond. The variance in  $\Delta G_r^\circ$  for this reaction is shown in Figure 3.1. Life uses the low stability of ATP to drive energetically expensive reactions (e.g. using the reaction above in reverse to build biomacromolecules), and reforms ATP from the energetic input of its metabolism.

The processes by which life gathers energy are complex and vary significantly between species but the overall system can be simplified to the movement of electrons in an electron transport chain. Most organisms use a redox couple consisting of an electron donor and an electron acceptor to extract energy from their surroundings. The electron is passed from the donor through a series of proteins until it reaches the acceptor and the overall reaction is complete. Each step through this chain stabilises the electron further, and the free energy released from this is used to drive mechanisms which pump protons across a cell membrane, in turn generating and maintaining a proton gradient across it. This gradient and the induced potential across the membrane lend a tendency for protons to diffuse back across the membrane to equalise again, generating a **proton motive force** [pmf] measured in V. It is this pmf that is used to generate ATP. Protons pass through a gateway of sorts via an ATP synthase protein which acts as a ratchet, driven by

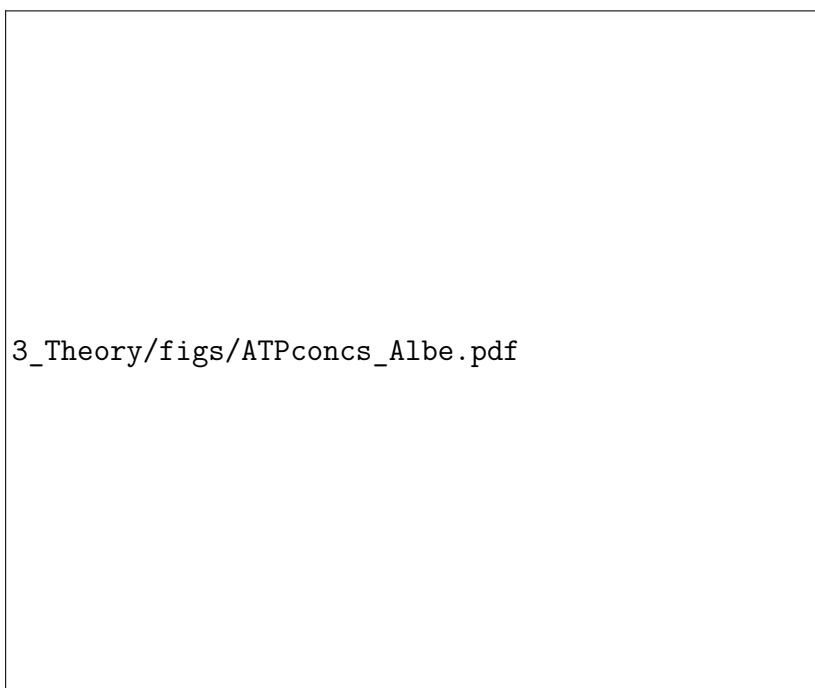


**Figure 3.2 The Gibbs free energy yield per mole of ATP at various cell conditions.** These encapsulate a range of microbial ATP, ADP and  $P_i$  concentrations [133] and changing temperature.

the pmf to stitch together ADP and  $P_i$ . Typically 3–5 protons are required to form one ATP molecule, dependent on the ATP synthase, potential difference, and  $H^+$  gradient.

One can define a minimum energy quanta that life needs to be able to extract from its overall metabolic reaction in order to pump one proton across the membrane. Because there are 3–5 protons required to form each molecule of ATP, this is the amount of energy held in 20–33% of an ATP phosphate bond [10, 134]. This will depend on the physico-chemical parameters and intra-cellular concentrations of ADP,  $P_i$  and ATP, but if in typical cell conditions one mole of ATP holds around 40 kJ of energy, this places the so-called **biological energy quantum** at 8–13 kJ mol<sup>-1</sup>. This is somewhat limited however, because thermodynamically speaking ATP hydrolysis can yield more or less energy per molecule ( $\Delta G_{ATP}$ ) in some conditions compared to others (e.g. Figure 3.2).

### 3.1.4 | Kinetics of metabolism

#### Excerpt from Higgins & Cockell (2020) [1]

The free energy of a process is not enough to be used by an organism as is, it must first be converted and stored as a ‘fuel’ to use for future processes. All currently understood life forms use the molecule ATP for this purpose, utilising the high-energy phosphorylation reaction of ADP. This phosphorylation must be considered to calculate the rate of a multi-step (bio)chemical process, and activated complex theory<sup>a</sup> can be used to both calculate this and correct for non-standard thermodynamic conditions using a thermodynamic limiter  $F_T$  [135]. The thermodynamic limiter is applied as a correction to the forward reaction rate:

$$r = r_+ F_T \quad (3.10)$$

$$F_T = 1 - e^{-f/\chi RT} \quad (3.11)$$

$$f = \Delta G_{net} = -(\Delta G_A + \Delta G_C) \quad (3.12)$$

where  $f$  is the ‘thermodynamic driving force’ or the difference between the amount of free energy released by the overall mechanism  $\Delta G_A$  and the amount of free energy conserved by the organism during the pathway  $\Delta G_C$ .  $\chi$  is the ‘average stoichiometric number’, i.e. the average number of times each step has taken place in the pathway (usually 1) [135]. This could be thought of as akin to a heat engine. It is impossible for the cell to be 100% efficient because

otherwise there would be little thermodynamic reason for the reaction to take place resulting in very slow kinetics. Hence, an organism must find a sweet-spot of energetic efficiency against rate of uptake.

<sup>a</sup>Also known as transition state theory

Jin & Bethke (2007) [135] summarise how an energy or nutrient consumption rate can be thermodynamically limited for various mechanisms. For example, in fermentation, where larger molecules are broken down into smaller, more useful ones which can be conserved in ATP synthesis  $\Delta G_C$  can be written  $n_{ATP}\Delta G_P$  where  $n_{ATP}$  is the number of moles of ATP that can be produced and  $\Delta G_P$  the free energy of each formation. For respiration pathways, energy can be captured directly by ATP synthesis within the pathway, or indirectly through creating a proton motive force and coupling it with ATP synthesis. Hence in this case  $\Delta G_C = \left(n_p + \frac{n_H^R}{n_H^P}\right)\Delta G_P$ , where  $n_p$  is the total number of ATP molecules formed in the reaction pathway,  $n_H^P$  is the total number of protons that must pass through the membrane for an ATP synthesis, and  $n_H^R$  is the number that are moved across the membrane [135]. In this respiration example, the **total yield of ATP per mole of reaction**  $n_{ATP}$  can be written:

$$n_{ATP} = \left(n_p + \frac{n_H^R}{n_H^P}\right) \quad (3.13)$$

This method can also be used to thermodynamically drive a process that is energetically unfavourable but necessary, such as the uptake of a key nutrient. An organism can counterbalance the energy difference by using ATP hydrolysis  $n_{ut}$  times as a catalyst meaning effectively a negative amount of energy is conserved by the organism:  $\Delta G_C = -n_{ut}\Delta G_P$ . As long as this counterbalances  $\Delta G_A$  and  $f < 0$ , the reaction can proceed [135].

Beyond the free energies of the overall reaction and ATP synthesis, Equation 3.10 requires the forward rate of the chemical reaction. For a generic reaction of the form  $aA + bB \rightleftharpoons cC$ , this is given by:

$$r_+ = k_+[A]^a[B]^b \quad (3.14)$$

where  $k_+$  is the forward rate constant of the reaction and typically varies with temperature and pressure. Due to the influence of life in these interactions, many interactions are enzymatically controlled, so  $k_+$  is unlikely to be the same as would be expected from the chemical reaction alone. It must be derived from experiments featuring the organism in question. In Chapter 5,  $k_+$  is calculated for methanogenesis at a range of temperatures and pressures.

## 3.2 Energetics of biosynthesis

A major hurdle for the theoretical growth models introduced in Chapter 2 is quantifying exactly how much energy is required for one cell to ‘build’ another. As microbes come in all shapes and sizes, with a huge variety in composition, computing the energy required to build all of those molecules for each individual species can appear daunting. LaRowe and Amend (2016) [40] propose that many biomacromolecules have a similar structure to proteins and hence cost approximately the same amount of energy to synthesise per unit mass. For example, *Escherichia coli* (*E. coli*) has a dry weight of 55% protein, so as a first approximation the total energy to synthesise an *E. coli* cell is  $E_{pro}/0.55$  where  $E_{pro}$  is the total cost of synthesising its constituent proteins. This cost can then be calculated on a protein-by-protein basis using a **group contribution algorithm** which combines the free energies of formation of a protein’s constituent groups. The overall free energy of

3\_Theory/figs/MG\_FS1\_ESynth.pdf

**Figure 3.3 Energetic cost of protein synthesis.** This approximates the synthesis energy cost per dry gram in anoxic conditions as described in the paper excerpt. From Higgins & Cockell (2020) [1], where this was supplemental figure S1.

formation of the protein in any given conditions can then be calculated, providing the concentration of all the amino acids in the cell are known [136]. Using this method, scaling up cellular average protein lengths rather than each individually, Amend *et al.* (2013) [137] predicted a cost of 191 J per dry gram of cells for *E. coli*, but this was independent of the amino acid content of the proteins. By taking into account each individual amino acid, this peptide formation energy cost increases to  $\sim 500 \text{ J (dry g)}^{-1}$  (see excerpt overleaf).

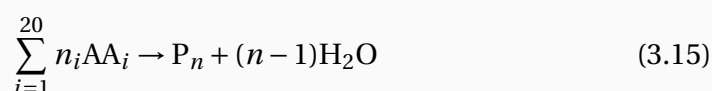
For the synthesis energy calculations used throughout this thesis we consider one or both of the following:

1. The energy required to **build all of the amino acids** in one cell (based on calculations in McCollom and Amend (2005) [138]).
2. The energy required to **form all of the biomacromolecules** in a cell from their constituent amino acids [136, 137].

The result of these calculations is shown in Figure 3.3.

**Excerpt from Higgins & Cockell (2020) [1]**

For the latter calculation, it is assumed that the total cost of polymerisation of one dry gram of cells is broadly comparable to the cost of polymerisation of one dry gram of that organism's constituent proteins [37, 139]. If the synthesis of protein  $P_n$  is a string of condensation reactions of amino acids AA, the overall reaction will take the form:



where  $n = \sum n_i$  is the number of amino acids in the chain. The free energy of this reaction can be estimated using a group contribution algorithm [136]. The standard free energy of formation of protein  $P_n$   $\Delta G_f^\circ[P]$  can be estimated as the sum of the standard free energies of formation of its constituent parts:

$$\begin{aligned} \Delta G_f^\circ[P] = & \Delta G_f^\circ[AABB] + (n_{AA} - n_{GLY} - 1) \Delta G_f^\circ[PBB] + \\ & \sum_{i=1}^{19} m_i \Delta G_f^\circ[R_i] + n_{GLY} \Delta G_f^\circ[GLY] \end{aligned} \quad (3.16)$$

where AABB, PBB, GLY, and R represent the amino acid 'backbone' ( $\text{H}_2\text{N}-\text{CH}-\text{COOH}$ ), protein 'backbone' ( $\text{HN}-\text{CH}-\text{C=O}$ ), glycine, and the R group of non-glycine amino acids respectively.  $n_{GLY}$  is the number of glycines in the



chain,  $n_{AA}$  is the number of non-GLY amino acids in the chain, and  $m_i$  acts as a counter for the number of occurrences of each non-GLY amino acid  $i$  in the chain.

Overall, the standard free energy of reaction for this protein synthesis is:

$$\Delta G_r^\circ = (n - 1)\Delta G_f^\circ[\text{H}_2\text{O}] + \Delta G_f^\circ[P] - \sum_{i=1}^{20} n_i \Delta G_f^\circ[\text{AA}_i] \quad (3.17)$$

In principle Equation 3.17 should be used for every single protein in the cell, but the reality is that any cell can contain millions or hundreds of millions of proteins, the exact structures of which is largely unknown if they are even detected [140, 141].

The model builds the mean constituent protein of the organism, for this study<sup>a</sup> *E. coli* was used [140]. The free energy of synthesis of a protein with the mean length of amino acids (144), built proportional to the typical abundances of amino acids was calculated per Equation 3.17, corrected to nonstandard conditions using the local temperature, amino acid abundance and a protein concentration of  $10^{-12}$  M (both from [138]) and then converted to be the cost to produce one dry gram. This is then taken to approximate the cost of polymerisation of one dry gram of cells.

<sup>a</sup>and, in turn, all results in this thesis which utilise  $E_{\text{syn}}$

In 2020 an MSc student in our group, E. J. Ortega Arzola worked on a project to improve these estimates by using a group contribution algorithm to estimate the energetic cost of synthesising the protein, DNA and membrane content of an organism using proteomic and genomic data as an input. While their MSc dissertation is complete, we have continued to work on this project and are preparing a publication for the journal *PNAS*. Our results suggest that the energetic cost of building DNA and RNA strands are of a similar order of magnitude to the cost of protein building [8].

The group contribution approach has some limitations, however. It assumes that each new appendage to the chain when ‘building’ a protein has equal energetic cost, while it has been demonstrated that subsequent addition of amino acid groups to polypeptide chains becomes more efficient with chain length [142, addition of glycine only]. Further, the distribution of proteins in cells is a constantly changing estimate (e.g. [143] compared to [140] for *E. coli*), which may significantly affect the energy prediction. The true composition of the proteins should also be taken into account — the calculation presented above scaled up the average chain length

and amino acid link contributions rather than consider the true structure in each case. Unfortunately, as there are potentially millions of proteins in a typical cell [e.g. 140], even if we had the empirical data for their structure this is unlikely to be computationally feasible.

### 3.3 Quantifying adaptation to extremes

---

Now that we have identified methods to estimate the cell specific power supply  $P_S$  and the energetic cost of biomass synthesis  $E_{\text{syn}}$ , the final key parameter to determine is the maintenance cost in a given set of conditions  $P_M$ .

For this work, the maintenance contribution encapsulates all mechanisms of energetic loss which are not directly related to growth. This includes the maintenance of overall cell structure [10], such as coping with the degradation of biomacromolecules, motility and preserving proton gradients [45]. Other mechanisms sometimes considered include spillage [discussed by 72], energy stored away for use while starving [35], or perhaps most importantly for astrobiology and extreme conditions, the cost of adaptations to a particular environment [10]. For many of these adaptations individual coping mechanisms have been identified. This is the case for high salinity [27, 64], and pH [28] but it should be noted that for these two only the energy gradients have been calculated and not the rate at which this energy is needed. Temperature (and to a lesser extent pressure) significantly affect chemical kinetics, most importantly the rate of degradation of biomacromolecules assuming they follow an Arrhenius relationship [10], which would require a larger power output to cope with [45]. However, in extreme energy-limited systems the maintenance of protein structure may reduce by up to 95% as the organism focuses on other processes [37].

For combined extremes and the cost of their relevant adaptations, we employ an additive approach. For example, if a species needs to deal with three significant energy sinks  $X$ ,  $Y$  and  $Z$  the total maintenance power could be written:

$$P_M = P_X + P_Y + P_Z \quad (3.18)$$

Often, these contributions to  $P_M$  have shared dependencies, typically on temperature. Despite this it can be useful to consider these adaptations as ‘owing to’ a specific extreme. In this subchapter we will corroborate possible maintenance powers owing to temperature and pH and then explore what happens when they are combined.

#### 3.3.1 | Defending against temperature effects

Temperature plays a key role in all chemical theory [59]. This is evident from the arguments so far in this chapter regarding computation of  $\Delta G$ ,  $k$  and  $E_{\text{syn}}$ . We have seen that building biomacromolecules becomes ever-more difficult at increasing temperature (Figure 3.3), standard Gibbs free energies may increase or decrease (Figure 3.1) but the kinetics of a viable biologically mediated interaction and hence  $P_S$  tend to increase exponentially with  $T$ .

In general, the thermal stability of biomolecules in a microbe increases with their maximum tolerable environmental temperature [62]. So, a thermophile with an optimal growth temperature of  $\sim 80^\circ\text{C}$  will have biomolecules which are more resistant to breakdown at such temperature than a **mesophile**<sup>5</sup> with an optimal growth temperature of  $\sim 35^\circ\text{C}$ . One could predict that the biomolecules of that thermophile may not be viable at the lower temperature, but this is not necessarily the case. In their review of life at high temperatures, Jaenicke & Sterner (2006) [62] identify “hyperthermophilic enzymes with high intrinsic thermostability that are more active than their mesophilic counterparts, even at room temperature, thus combining high catalytic efficiency with high overall rigidity.” This means that the heightened stability from adapting to hyperthermal environments is not necessarily a detriment when returning to lower temperatures.

There can also be benefits to psychrophiles in the opposite direction. In a study led by S. Gault we explored the activity, stability and mutational characteristics of temperature-adapted enzymes [7]. We found that the gap between the optimum and melting temperatures for enzymes was broadly consistent between mesophiles and thermophiles at  $0\text{--}20^\circ\text{C}$  but for psychrophiles was much larger (up to  $60^\circ\text{C}$ ). This indicates that the adaptations required for psychrophilic enzymes can remain viable at much warmer temperatures than their optimum [7]. We also found that the average mutation to an enzyme becomes more deleterious at higher temperatures [7].

<sup>5</sup>Mesophiles are organisms which prefer non-extreme temperatures, typically between around  $15\text{--}50^\circ\text{C}$

Jaenicke & Sterner (2006) [62] assert that “it is essentially impossible to predict how temperature changes may affect viability” for any given organism, owing to the complexity in metabolic pathways and the enzymatically controlled kinetics of all ongoing reactions. Agnosticising these processes such that they could work across all biomacromolecules and all microorganisms is clearly a grand, if not impossible challenge. What we can do however, is draw lines of comparison across well-adapted species to quantify how a well-suited organism might cope with extremes of temperature. This can be done through meta-analyses of empirical data [e.g. 1, 37, 60].

The most well-known and widely-cited empirical determination of the maintenance power due to temperature is the paper by Tijhuis et al. (1993) [60]. They computed the maintenance powers as only dependent on temperature for aerobic and anaerobic bacteria whose optimal growth temperatures were between 5–57°C:

$$\text{Aerobe:} \quad = \quad 60.9m_c \times \exp \left[ \frac{-6.94 \times 10^4}{R} \left( \frac{1}{T} - \frac{1}{298} \right) \right] \quad 41\% \text{ conf.} \quad (3.19)$$

$$\text{Anaerobe:} \quad = \quad 35.3m_c \times \exp \left[ \frac{-6.94 \times 10^4}{R} \left( \frac{1}{T} - \frac{1}{298} \right) \right] \quad 32\% \text{ conf.} \quad (3.20)$$

$$\text{Mean:} \quad = \quad 48.1m_c \times \exp \left[ \frac{-6.94 \times 10^4}{R} \left( \frac{1}{T} - \frac{1}{298} \right) \right] \quad 29\% \text{ conf.} \quad (3.21)$$

The units here have been converted to  $\text{W cell}^{-1}$ , which necessitates knowing the mass of the cell  $m_c$  [kg]. Confidence values for each reflect the accuracy of their fit in correspondence to the data, and the confidence value for the mean was estimated by propagating these errors. These estimates are plotted with temperature in Figure 3.4.

One key drawback with using these values for astrobiological interest is that they are in optimal conditions in the exponential phase of growth. This is useful for characterising microbial growth in the laboratory, but in natural settings life is usually energy and/or nutrient limited and in a constant fight for survival [23]. This has led to the search for minimum (or basal) energy requirements, which quantify only the cost of mechanisms which are absolutely necessary to survival. One example of this is amino acid racemization (Box 3.3) which necessitates the replacement of an affected biomacromolecule because its function may be compromised [37].



**Figure 3.4 The maintenance power owing to temperature** predicted by Tijhuis et al. (1993) [60] and Lever et al. (2015) [37]. For fair comparison, both of these are for a cell of the same size ( $3.44 \times 10^{-18} \text{ m}^3$ ). For the Lever et al. (2015) estimates, both the original authors' synthesis energies and our synthesis energies (temperature dependent) are shown. Code to recreate this data is available in Appendix B.2.

### Box 3.3: Chirality and racemization

In chemistry, **chiral molecules** have a specific type of isomer, known as an **enantiomer**. They cannot be superimposed on their mirror image by any combination of rotations and translations. Another object with this property is the human hand. Despite appearing the same and being mirror images of one another, a right hand cannot be transformed in space to appear exactly like a left hand without a reflection.

A **racemic mixture** is one which is made up of 50% of each enantiomer. When one enantiomer is transformed into another it is known as **racemization**, a spontaneous process for most non-racemic mixtures. Life is selective in chirality, so inherently *not* racemic. This means that when the amino acids it relies on become racemized, they may need to be replaced to maintain their desired function. Racemization rates and enantiometric ratios can also be used as potential biosignatures (examined in Chapter 7).

In a review of life when severely energy limited, Lever et al. (2015) [37] calculated the energetic costs of some unavoidable processes including amino acid racemization and DNA depurination<sup>6</sup>. They calculated the cost of racemization from the rate at which it occurs,  $r_{rmz}$ , which is assumed to proceed as a first-order chemical reaction:

$$r_{rmz}(T) = [AA]k_{rmz}(T) \quad (3.22)$$

where  $[AA]$  is the mean amino acid concentration and  $k_{rmz}(T)$  is the mean first-order rate constant of racemization of amino acids, which is a function of temperature. Lever et al. (2015) [37] constrain this to be:

$$k_{rmz}(T) = 0.00012e^{0.10174 \times (T[^\circ\text{C}])} \quad (3.23)$$

Allow us to set a factor  $F_{rmz}$  which is the cut-off fraction for protein replacement. For example, if a protein were replaced after 2% of its constituent amino acids are racemized,  $F_{rmz}$  would be 0.02. The reason such a factor is needed is because the degree of racemization which needs to occur before replacement in microbes remains unknown. Then, the time required for the entire protein content of a cell to need replacing is:

$$t_R = \frac{F_{rmz}[AA]}{r_{rmz}(T)} = \frac{F_{rmz}}{k_{rmz}(T)} \quad (3.24)$$

<sup>6</sup>Depurination is the removal of a purine ring containing base from one segment of DNA through a reaction with  $\text{H}_2\text{O}$ .

Then, we can say that the replacement cost per unit time ( $P_{rmz}$  [W (protein)<sup>-1</sup>]) is:

$$P_{rmz} = \frac{E_{pro}}{t_R} = \frac{E_{pro}k_{rmz}(T)}{F_{rmz}} \quad (3.25)$$

where  $E_{pro}$  is the energy required to replace the protein, which we computed in Subchapter 3.2. The results presented by Lever et al. (2015) [37] rely on a few assumptions, namely:

1. All amino acids in the cell are protein bound.
2. There are 250 amino acids per protein.
3. The cost of amino acid polymerisation does not change with temperature.
4. The cost of amino acid synthesis does not change with temperature.

By using methods presented in Subchapter 3.2, we can account for points 3 and 4 above. Point 1 remains a sticking-point, and results from the concentration of amino acids [AA] being used in the rate and replacement equations. Point 2 may also be problematic, but our use of the group contribution algorithm assumes that the Gibbs free energy of polymerisation scales linearly with protein length.

Figure 3.4 shows the energetic cost of repairing protein racemization using this technique adjusted for a cell volume of  $3.44 \times 10^{-18} \text{ m}^3$  for two scenarios: the  $E_{syn}$  presented in the original study ( $586 \text{ J (dry g)}^{-1}$ , not temperature dependent), and the  $E_{syn}$  value we derived in Subchapter 3.2. The temperature dependence of the rate constant of racemization dominates the trend, but including the increase in  $E_{syn}$  with temperature may increase the cost of replacement due to racemization by an order of magnitude when approaching 400 K. This would not be the case if the cost of amino acid formation were not considered, as the polymerisation cost does not significantly change with temperature (Figure 3.3).

In the same study, the authors computed the energetic cost of another thermodynamically inevitable process, DNA depurination. It was found that this cost is 3–4 orders of magnitude lower than the racemization cost, particularly for replacement fractions less than 0.1. However, it does become significant at high temperatures. The authors identify three reasons for this:

1. There are 50 times fewer DNA nucleotides per cell than the number of amino acids per cell (recall their racemization calculation assumed all amino acids were in proteins).
2. Racemization rate constants are higher than depurination rate constants at temperatures less than 74°C.
3. The cost of racemization is higher because the entire protein needs replacing rather than single amino acids.

We do not include DNA depurination in Figure 3.4, or  $P_T$  calculations for this work. This is because of uncertainty in the depurination rate's dependence on temperature and the synthesis costs of DNA. With the outcomes of the MSc project outlined in Subchapter 3.2 hopefully this will become clearer in the future. Furthermore, depurination is not the only source of DNA damage and simple replacement is not necessarily the method used. More broadly, the types of DNA repair undergone by cells can include: [144]:

1. **Direct repair:** Restoration of damage via a deliberate chemical or photochemical interaction.
2. **Nucleotide excision repair:** Removal and replacement of a damaged site.
3. **Base excision repair:** Removal and replacement of a damaged base (cleave the glycosidic bond).
4. **Mismatch repair:** A process which detects when DNA has been mismatched and corrects the error.
5. **Daughter-strand gap repair:** The parent strand is used to repair a damaged daughter strand in a process called genetic recombination.
6. **Transletion synthesis:** Damaged DNA polymerases are switched out with specialised transletion polymerases on replication.
7. **Double-strand break repair:** Two severed ends of a duplex are joined together again.

### 3.3.2 | Defending against pH effects

Organisms can handle the effects of pH via 'passive' or 'active' methods designed to maintain a consistent internal pH. An example of an active method for alkaliphiles is the development of **antiporters**<sup>7</sup> which exchange  $\text{Na}^+$  or  $\text{K}^+$  (from inside the cell) for  $\text{H}^+$  (from outside the cell). Similarly, an active methods for acidophiles is to pump out  $\text{H}^+$  as part of the respiratory chain [46]. In *E. Coli*,  $\text{Na}^+/\text{H}^+$  antiporter activity is up to  $10^5$  exchanges per minute. This increases by three orders of magnitude between pH 6.5–8.5. Passive methods tend to include membranes which are more robust to the adverse pH conditions. These can be quantified with the pI value of the membrane proteins. The pI, or isoelectric point, is the pH at which the protein has a net charge of zero. Krulwhich (2011) [46] summarises some passive methods, which include:

---

<sup>7</sup>An antiporter is a protein in a cell's membrane which mediates transfer of material into or out of the cell.



- Surface proteins of acidophiles usually have high pI values, making them more positively charged. This would act as a H<sup>+</sup> repellent.
- Similarly, surface proteins with low pI values are typical of alkaliphiles as they contribute to better H<sup>+</sup> capture.
- Leakage of protons into the cell can be reduced by thicker and unsaturated fat rich membrane lipids.
- Acidic secondary cell wall polymers can help H<sup>+</sup> intake for alkaliphiles. It has been shown that removing this helps cells grow at neutral pH, suggesting that building these cell walls increases  $E_{\text{syn}}$ .
- Acidophiles may also make use of periplastic pH homeostasis. In this, there is a periplasm between outer and inner membranes which acts as a buffer solution.

The power demand posed by pH homeostasis has yet to be quantified due to the complexity in the adaptations outlined above. We can make a first approximation of it if we know the rate at which protons leak through the membrane after considering the effect of the passive methods. Then, we also need to know the energetic cost of pumping those protons back in (or out) of the cell as needed. The Gibbs free energy of pumping a proton across a membrane can be written:

$$\Delta G_H = -2.3RT\Delta\text{pH} \quad (3.26)$$

$$\Delta G_{OH} = -2.3RT\Delta\text{pOH} \quad (3.27)$$

where  $\Delta\text{pH}$  is the pH difference across the membrane  $\text{pH}_{\text{int}} - \text{pH}_{\text{ext}}$ . [10, 28]. This can be derived by considering the Gibbs free energy changes of membrane diffusion (Box 3.4).

The key sticking point is the calculation of the rate at which protons need to be pumped,  $r_H$ . Nagle (1987) [145] proposed some mechanisms for H<sup>+</sup> transport across membranes. Using a transient hydrocarbon chain (tTHC), protons can be transported across ‘water bridges’ which offer much higher permeability to protons than for other ions [146]. However, this has been reported to be difficult to verify empirically [147]. Further, while it was once thought that this is not a feasible transfer method because the lifetime of water bridges is too small (<50ps) [148], studies in recent years show that they can stabilise for up to ‘hundreds’ of ps [149].

Here we present a first approximation to this flux inspired by historic estimates [145, 150, 151]. Begin with the Goldman-Hodgkin-Katz flux equation [152]:

$$I_{Ai} = \bar{P}_i z_i^2 \frac{\Delta\Psi F^2}{RT} \left( \frac{c_{\text{int}} - c_{\text{ext}} e^{-z_i(\Delta\Psi F/RT)}}{1 - e^{-z_i(\Delta\Psi F/RT)}} \right) \quad (3.28)$$

**Box 3.4: Free energy of membrane diffusion**

In a system with species A, B, C ... with molar content a, b, c ..., the total Gibbs free energy in the system  $G$  is:

$$G = a\bar{G}_A + b\bar{G}_B + c\bar{G}_C + \dots \quad (3.29)$$

where  $\bar{G}_X$  [J mol<sup>-1</sup>] is the partial molar Gibbs free energy (also known as chemical potential with symbol  $\mu$ ; but in this thesis  $\mu$  refers to microbial growth rate) of species  $X$ . For a dilute solution these can be approximated as:

$$\bar{G}_X = G_X^\circ + RT \ln a_X$$

Here,  $G_X^\circ$  is the standard state chemical potential (also referred to in the literature as  $\mu_X^\circ$ ). Then, for some change in a system, the Gibbs free energy change is:

$$\Delta G = G_{\text{Final}} - G_{\text{Initial}}$$

Now consider two regions, inside and outside the membrane, with H<sup>+</sup> concentrations of [H<sub>in</sub><sup>+</sup>] and [H<sub>out</sub><sup>+</sup>] respectively. The free energy difference between these two sides of the membrane is given by:

$$\Delta G = G_{H_{\text{in}}} - G_{H_{\text{out}}}$$

Incorporating this into the expression above:

$$\begin{aligned} \Delta G &= (G_H^\circ + RT \ln a_{H_{\text{in}}}) - (G_H^\circ + RT \ln a_{H_{\text{out}}}) \\ &= RT \ln \left( \frac{a_{H_{\text{in}}}}{a_{H_{\text{out}}}} \right) \\ &\approx RT \ln \left( \frac{[H_{\text{in}}^+]}{[H_{\text{out}}^+]} \right) = -2.3RT \Delta \text{pH} \end{aligned}$$

where  $\Delta \text{pH} = \text{pH}_{\text{in}} - \text{pH}_{\text{out}}$ . This tells us that if the pH inside is smaller than the pH outside,  $\Delta G$  is negative, meaning it is energetically favourable for protons to travel from the outside of the cell to the inside.

In Equation 3.28,  $I_{Ai}$  is the current of ions  $i$  [A m<sup>-2</sup>],  $\bar{P}_i$  is the **permeability coefficient** of the membrane to the ion [m s<sup>-1</sup>],  $c_{\text{int}}$  and  $c_{\text{ext}}$  [mol L<sup>-1</sup>] are the concentrations of the ion on each side of the membrane,  $\Delta \Psi$  [V] is the **total potential across the membrane**  $\Psi_{\text{int}} - \Psi_{\text{ext}}$ ,  $z_i$  is the valency of the ion (equivalent to its unit charge), and  $F$ ,  $R$ , and  $T$  are the Faraday constant, gas constant and temperature. Use of the Goldman-Hodgkin-Katz flux equation requires a number of assumptions [152]:

- The membrane is a homogeneous substance with a constant electrical field across it.
- Ions interact with the membrane surface instantaneously. This can be alleviated as long as the concentrations used are those suitably close to the membrane.
- The ions do not interact with each other during the flow. For example the ions flowing in do not interact with the flow outwards of the same species, nor does it interact with other species traversing the membrane.

Let us substitute a dimensionless constant  $\Lambda = \Delta\Psi F/RT$  into Equation 3.28:

$$I_{Ai} = \bar{P}_i z_i^2 F \left( \frac{c_{int} - c_{ext} e^{-z_i \Lambda}}{1 - e^{-z_i \Lambda}} \right) \quad (3.30)$$

We need this in terms of ion flux  $J_{Ai}$  [mol s<sup>-1</sup> m<sup>-2</sup>]. This can be achieved formally via unit conversion:

$$I_{Ai} = \frac{1}{A} \frac{Q_i}{t} = \frac{1}{A} \frac{N_i}{t} q_i \quad (3.31)$$

$$J_{Ai} = \frac{1}{A} \frac{n_i}{t} = \frac{1}{A} \frac{N_i}{N_A t} \quad \longrightarrow \quad N_i = A N_A t J_{Ai} \quad (3.32)$$

$$I_{Ai} = J_{Ai} N_A q_i \quad (3.33)$$

where  $n_i$  [mol] is the number of moles of ions transferred,  $q_i$  [C] is the charge of each ion passing through in coulombs ( $z_i q_H$  where  $q_H \approx 1.6 \times 10^{-19}$ ),  $N_i$  is the number of ions transferred,  $A$  [m<sup>2</sup>] is the surface area,  $t$  is time, and  $N_A$  is Avogadro's constant. We arrive at the expression:

$$J_{Ai} = \bar{P}_i z_i^2 \frac{F}{N_A q_H z_i} \left( \frac{c_{int} - c_{ext} e^{-z_i \Lambda}}{1 - e^{-z_i \Lambda}} \right) \quad (3.34)$$

$$J_{Ai} = \bar{P}_i z_i \left( \frac{c_{int} - c_{ext} e^{-z_i \Lambda}}{1 - e^{-z_i \Lambda}} \right) \quad (3.35)$$

because  $F = N_A q_H$ . This is the flux of a given ion  $i$  across a membrane with permeability coefficient  $\bar{P}_i$ , between two concentrations,  $c_{int}$  and  $c_{ext}$  per unit surface area. It would be useful to express this as a flux per unit cell  $J_i$  [mol (s cell)<sup>-1</sup>] so multiply by  $A_{cell}$  the surface area of the cell:

$$J_{Ai} = \bar{P}_i z_i \left( \frac{c_{int} - c_{ext} e^{-z_i \Lambda}}{1 - e^{-z_i \Lambda}} \right) A_{cell} \quad (3.36)$$

It is important we express caution with units here. A such, we introduce a factor of  $10^3$  to the equation to convert the concentrations from mol L<sup>-1</sup> to mol m<sup>-3</sup>. Then, its requirements are the permeability coefficient in m s<sup>-1</sup>, the surface area in m<sup>2</sup>

and the calculated flux will be  $\text{mol (s cell)}^{-1}$ . Finally then, we can write the flux of protons and hydroxide into or out of a cell as:

$$J_H = \bar{P}_H \left( \frac{10^{-\text{pH}_{\text{int}}} - 10^{-\text{pH}_{\text{ext}}} e^{-\Lambda}}{1 - e^{-\Lambda}} \right) A_{\text{cell}} 10^3 \quad (3.37)$$

$$J_{OH} = -\bar{P}_{OH} \left( \frac{10^{[\text{pH}_{\text{int}} - \text{p}K_w]} - 10^{[\text{pH}_{\text{ext}} - \text{p}K_w]} e^{\Lambda}}{1 - e^{\Lambda}} \right) A_{\text{cell}} 10^3 \quad (3.38)$$

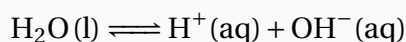
where  $\text{p}K_w$  is equivalent to  $-\log_{10} K_w$  and  $K_w$  is the **auto-dissociation constant of water**, which changes with temperature and pressure and can be computed with thermodynamic databases. This variation is the root cause to the ‘neutral’ pH varying from 7 with temperature and pressure (Box 3.5). Overall, quantifying the flux via this method requires knowing  $\Delta\Psi$ ,  $\bar{P}_H$  (and/or  $\bar{P}_{OH}$ ),  $\text{pH}_{\text{int}}$ ,  $\text{pH}_{\text{ext}}$ ,  $A_{\text{cell}}$  as well as the temperature (and pressure for  $\bar{P}_{OH}$ , though this is a minor contributor in comparison to temperature (Box 3.5)). Furthermore,  $\bar{P}_i$  is temperature dependent. An alternative derivation of the expressions above (Appendix A.3) suggests a temperature dependency of at least  $\bar{P}_i \propto T$ , other authors suggest it is exponential [153].

3\_Theory/figs/fluxplot.pdf

**Figure 3.5** The absolute flux of protons and hydroxide ions across the cell membrane and the corresponding power demand required to pump them back at varying membrane potentials, permeability coefficients and cell sizes. Solid lines show fluxes of protons, and dashed lines show the flux of hydroxide ions. Code to recreate data: Appendix B.3.

**Box 3.5: The ‘neutral’ pH varies with temperature and pressure**

Many think of the de-facto ‘neutral’ pH to be 7. In fact, this is only strictly the case in standard conditions, that is at temperature of 298 K (25 °C) and a pressure of 1 bar (0.987 atm). The reason that the ‘neutral’ pH changes owes to the definition of pH as  $-\log_{10} [\text{H}^+]$ . The dissociation of water occurs like so:



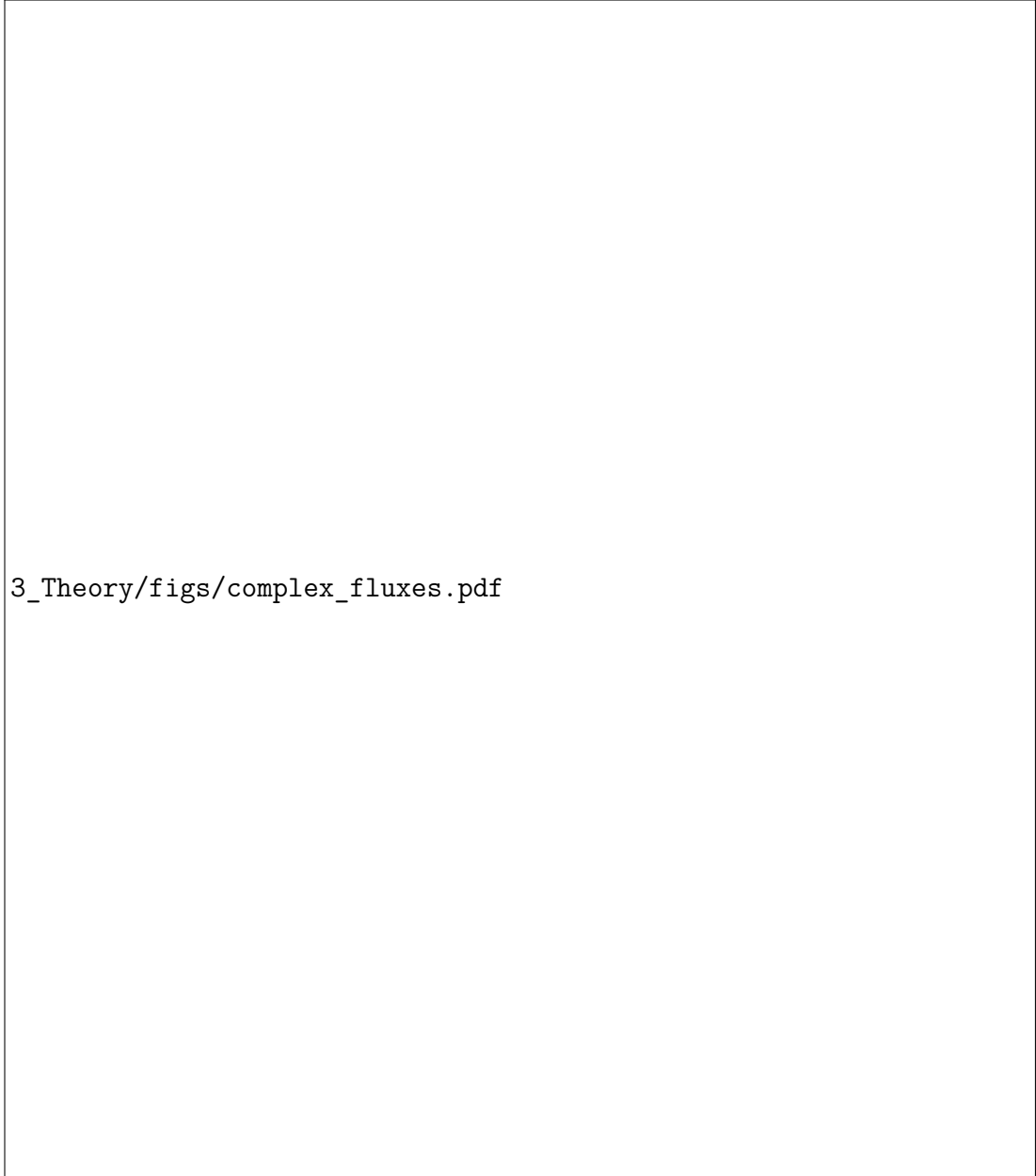
The equilibrium constant of this equation  $K_w$  changes with temperature and pressure, just like any other chemical reaction. By Le Chatelier’s principle, the reagent concentrations shift to oppose the change, here a higher pH at low temperatures and a lower pH at higher temperatures and a lower pH at higher pressures as there is higher entropy in the products of the reaction above. This change can be computed using SUPCRT92 and the reagent class of the NutMEG model, introduced in Chapter 4. The figure below shows the variation in the neutral (equilibrium) pH of pure water at various temperatures and pressures. Code to recreate: Appendix B.1.

3\_Theory/figs/pH\_with\_T.pdf

Figure 3.5 shows the absolute value of the flux of  $H^+$  and  $OH^-$  across a membrane and the effect of changing the parameters above when  $pH_{int} = 7$  and  $T = 298$  K. The solid lines show the flux of  $H^+$  ions into the cell (when  $pH_{ext} < 7$ ) and out of the cell when  $pH_{ext} > 7$ . The dashed lines show the same for  $OH^-$  ions. As seen in Equations 3.37 and 3.38, varying  $\bar{P}_H$ ,  $\bar{P}_{OH}$  or  $A_{cell}$  result in a simple y-axis translation. To illustrate the effect of these parameters, the ‘default’ case has values of  $10^{-10} \text{ m s}^{-1}$  for  $\bar{P}_H$  and  $\bar{P}_{OH}$ . This is broadly representative of membrane proton permeability coefficients which have been reported to be between  $10^{-6}$ – $10^{-11} \text{ m s}^{-1}$  [153, 154]. Membrane hydroxide permeability coefficients may be much smaller and are discussed further below. The proton permeability  $\hat{P}_H$  of mesophiles and psychrophiles generally falls within the narrow range of  $10^{-1.33}$ – $10^{-1.6} \text{ s}^{-1}$  regardless of temperature. The relationship between the permeability and the permeability coefficient is simply  $\hat{P}_H = \bar{P}_H/d$  where  $d$  is the thickness of the membrane. This implies that active mechanisms are usually in place to maintain the pmf, such as adapting the lipid concentration in the membrane [153, 155]. The default membrane potential difference here was arbitrarily chosen as -1 mV, and the cell surface area used was  $\sim 1.1 \times 10^{-11} \text{ m}^2$ , corresponding to the average methanogen size defined from the data collected and discussed in Chapter 5.

The key parameters which add complexity to these flux values are the external pH, the membrane potential  $\Delta\Psi$  (recall that  $\Lambda \propto \Delta\Psi$ ), and the internal pH. The effect of changing these on the default case in Figure 3.5 is shown in Figure 3.6. At membrane potentials close to zero, the minimum flux is close to the internal pH, but as it becomes larger than  $\pm 1$  mV the minimum moves. For  $H^+$ , this is to higher pH values at more positive  $\Delta\Psi$  and lower values at more negative  $\Delta\Psi$ . As  $\Delta\Psi$  becomes more negative,  $e^\Lambda \rightarrow 0$  and there ceases to be a minimum for  $OH^-$  as shown by the red dashed line in Figure 3.6(a). However when it becomes more positive  $e^\Lambda \rightarrow \infty$  and Equation 3.38 reduces to a linear relationship in  $10^{-pH_{ext}}$ , shown by the blue dashed line. The inverse is true for  $H^+$ , whose flux flat-lines at significantly positive  $\Delta\Psi$  (blue line) and becomes linear in  $10^{-pH_{ext}}$  at more negative  $\Delta\Psi$  (red line).

Varying  $pH_{int}$  shifts the minimum flux to that external pH value as would be expected, but also introduces disparity between the flux of  $H^+$  and  $OH^-$  even when the membrane permeability to each ion is identical because varying  $pH_{int}$  affects when on the exponential the fluxes flat-line (as discussed above). In real systems, the membrane potential and  $pH_{int}$  will be co-variant so Figure 3.6(b) does not tell the whole story, but together with Figures 3.5 and 3.6(a) is illustrative of the effect of key parameters in Equations 3.37 and 3.38.



3\_Theory/figs/complex\_fluxes.pdf

**Figure 3.6 The flux of protons and hydroxide ions across the cell membrane and the corresponding power demand required to pump them back at varying membrane potentials and internal pH values.** Panels (a) and (b) show the flux of ions in the default case:  $\bar{P}_H = 10^{-10}$ ,  $\bar{P}_{OH} = 10^{-10}$ ,  $\Delta\Psi = 10^{-5}$ ,  $\nu = 3.44 \times 10^{-18}$ , when varying membrane potential and internal pH. Solid lines represent fluxes for  $H^+$ , and dashed lines are for  $OH^-$ . Panels (c) and (d) show the corresponding power demand. Panels (e) and (f) show the power demand in identical conditions, with a reduced membrane permeability to  $OH^-$ . Code to recreate datais available in Appendix B.3.

To calculate the power required to counter this proton and hydroxide leakage is a simple case of multiplying together the energetic cost of pumping the ions out (Equations 3.26, 3.27) and the flux at which they leak in (Equations 3.37, 3.38):

$$P_{\text{pH}} = |J_H|\Delta G_H + |J_{OH}|\Delta G_{OH} \quad (3.39)$$

$$= (|J_H| + |J_{OH}|)\Delta G_H \quad (3.40)$$

because  $\Delta \text{pH} = \Delta \text{pOH}$  when the internal and external pressure and temperature are equal. The absolute value of the fluxes is taken such that the power can account for the energetic cost of leakage *into* the cell and leakage *out of* the cell. Figures 3.6(c) and 3.6(d) show this calculated power demand posed by the fluxes in the panels above them. The dependence of  $P_{\text{pH}}$  on  $\Delta \text{pH}$  enforces that the power demand  $\rightarrow 0$  when there is no proton or hydroxide gradient across the membrane. More positive  $\Delta \Psi$  values appear to yield a smaller power demand than negative potentials at low external pH values, but not when  $\Delta \text{pH}$  is smaller. Hyperacidophiles which grow at pH values of  $< 2$  can exhibit ‘reversed’ or positive  $\Delta \Psi$  [46]. By this power demand model, this makes sense as it reduces the power demand due to proton leakage (Figure 3.6(c)). However, typical alkaliphiles do not appear to do this. Because the  $\text{OH}^-$  ion is significantly larger than  $\text{H}^+$  one could assume that membranes are likely to be significantly less permeable to  $\text{OH}^-$ . Figures 3.6(e) and 3.6(f) replots the panels above with a trans-membrane  $\text{OH}^-$  permeability coefficient of  $10^{-13} \text{ m s}^{-1}$  (a value for  $\text{Cl}^-$ , which is expected to be similar to  $\text{OH}^-$  [146]). This significantly reduces the power demand at high pH values, such that a positive  $\Delta \Psi$  may not be required, or the benefits of a negative  $\Delta \Psi$  for energy acquisition outweigh a comparatively minor increase in power demand. However, Deamer (1987) [154] notes that an effective larger hydroxide permeability coefficient than this could be expected due to proton translocation interactions in the cell. Indeed, this entire discussion is only part of the story as each of these parameters also affects the energy uptake of the organism (Section 3.1.3). Krulwich (2011) [46] summarises this best, quoted in the paper excerpt box overleaf.

In any case, the analysis in this section puts forward a simple model for estimating the power demand associated with  $\text{H}^+$  and  $\text{OH}^-$  leakage. The disparity in organism-specific parameters, such as permeability coefficients the trans-membrane potential and the internal pH makes agnosticising such defences difficult. At the same time, it is difficult to characterise this power demand for a *single species*! Nonetheless, we can explore how the combination of pH and temperature can affect the overall power demand an organism could face when dropped into demanding conditions.



**Excerpt from Krulwich (2011) [46]**

Much has been learned about individual strategies for bacterial pH homeostasis and the molecules that are involved, but bacterial pH homeostasis is a cell-wide physiological process that deploys and integrates these strategies differently depending on other environmental factors (for example, oxygen availability and salinity). The development of systems-level models will depend on further efforts to gather broad-based, quantitative ‘omics’ information as a function of pH under different conditions. Such models will also require detailed molecular information about the stoichiometry of the reactions and about the kinetic and mechanistic properties of key transporters, as has been obtained for *E. coli* NhaA. Data of both types are particularly scarce for extremophiles, but such systems models would enhance our understanding of extremophile adaptations and facilitate the application of that understanding to ecological settings (for example, for bioleaching and bioremediation).

### 3.3.3 | Combining temperature and pH adaptations

The derived power demand of homeostasis is dependent on temperature at a number of steps, specifically in the expressions for  $\bar{P}_i$ ,  $\Lambda$ ,  $pK_w$  and  $\Delta G_H$ . However, the impact of this dependency on the power demand is minor in comparison to other key parameters. Figure 3.7 shows the power demand computed using Equation 3.40. The polygon on the left shows the range of proton permeability coefficients which are representative of typical membranes ( $10^{-11} < \bar{P}_i < 10^{-6} \text{ m s}^{-1}$  (at 298 K) [153–155]) and the two polygons on the right show how that power demand changes between 298 K and 400 K for permeabilities of  $10^{-11}$  and  $10^{-6} \text{ m s}^{-1}$ . Furthermore, this temperature dependence on  $P_{\text{pH}}$  is overshadowed by the power cost of defending against temperature itself (Subchapter 3.2, Figure 3.4).

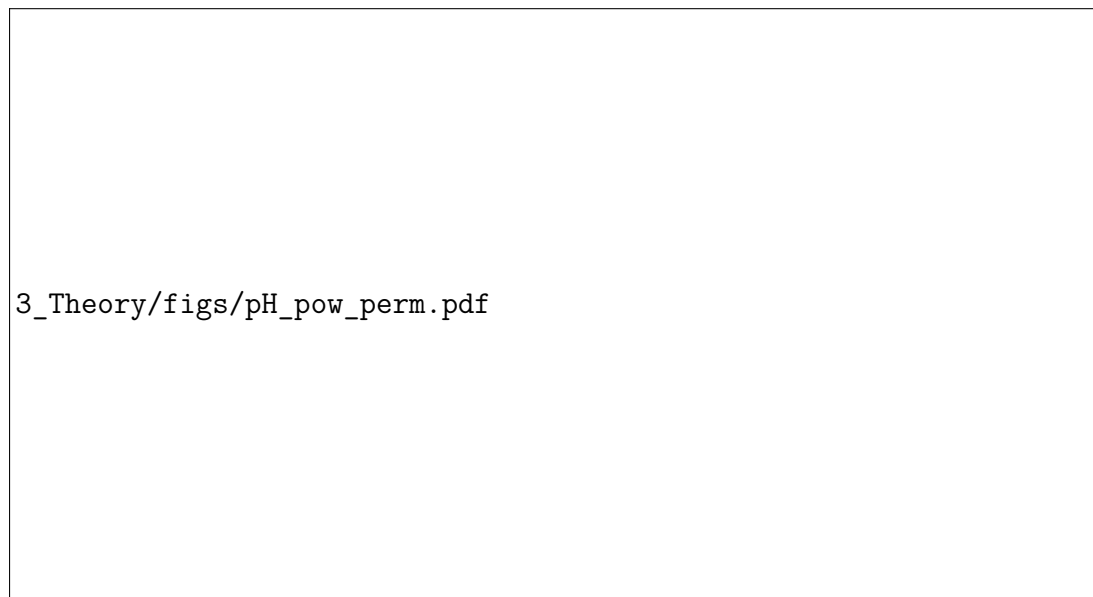


**Figure 3.7 The power demand required to pump unwanted protons and hydroxide ions back across a cell membrane** at two different permeabilities,  $10^{-11}$  and  $10^{-6} \text{ m s}^{-1}$  and at two different temperatures, 298 K and 400 K. Also shown is the demand of pumping them back at varying membrane potentials, and internal pH values. Code to recreate data is available in Appendix B.3.

The total power demand of temperature and pH can be calculated via:

$$P_M = P_T + P_{\text{pH}} \quad (3.41)$$

and visualised on a map of temperature and pressure. Figure 3.8 shows this, for combinations of  $\bar{P}_H = \bar{P}_{OH} = 10^{-6}, 10^{-9}, 10^{-12} \text{ m s}^{-1}$  and three temperature costs from Figure 3.4. Other pH demand parameters are fixed at their ‘default’ values as defined above. Between 273 K and 400 K and the three permeability options, the power demand could vary by up to 12 orders of magnitude.



**Figure 3.8 Heatmaps of the combined maintenance power owing to temperature and pressure** using the measures outlined in this chapter.

## 3.4 Summary and outlook

---

In this chapter we have identified methods to estimate:

1. The Gibbs free **energy available** from a chemical interaction.
2. How life **extracts this energy** from the environment.
3. The **rate** at which it is thermodynamically reasonable to **extract** this energy.
4. How much **energy** is required to **build new biomass**.
5. The **power required** to cope with the unavoidable **effects of temperature**.
6. The **power required** to pump in or out unwanted protons and hydroxide ions under **pH stress**.

Each of these methods has unique shortcomings. In this subchapter we will briefly discuss some of them and describe how these ideas are implemented for the remainder of this thesis.

There are a number of ways to compute the Gibbs free energy of a chemical reaction. Each method presented in Subchapter 3.1 and Appendix A.1 are valid, provided due diligence is taken when selecting the standard thermodynamic parameters and ensuring they are corrected for the desired environmental conditions. Nowadays, the availability of thermodynamic databases and code which implements the relevant equations makes this a simple endeavour.

The most likely place for problems to emerge here is in the calculation of the reaction quotient  $Q$ , which requires the activities of all reagents in the chemical reaction. Often, the activity of a substance can be approximated as equal to its molality or molarity. However, as these parameters increase, this ceases to be the case. In Appendix A.1 some theory is outlined for calculating this relationship. This extra theory is also built into the NutMEG code, and could be used for future analysis. However, because the work in this thesis considers low concentrations of substrates, this theory is not utilised for Chapters 4–7, and the assumption above is maintained unless specified otherwise. A notable exception is in the Enceladus geochemical model we develop in Chapters 6 & 7 to provide initial values of the chemical activities of dissolved gases in the icy moon's ocean.

Another example of caution being needed when calculating the quotient comes when using empirical data as an input. Methanogens consume  $\text{CO}_2$  and  $\text{H}_2$  to produce  $\text{CH}_4$  and  $\text{H}_2\text{O}$ , but when grown in culture usually authors report the gas overhead e.g. 80:20  $\text{H}_2$ : $\text{CO}_2$  and pressure. If we wanted to calculate the energy

available to methanogens in this scenario, we would have to calculate how much of the gas is dissolved in the culture media. This is what needed to be done for our Venusian habitability analysis (Section 4.4.2) and when using our model to characterise laboratory methanogens (Chapter 5). The technique we used to do so can be found in Appendix A.4.

ATP is the universal energy currency of life and the theory of chemiosmosis (electron transport chain) is widely accepted as a first approximation of how life extracts its energy. However, the ambiguity in Subchapter 3.1, of the electrons passing through ‘a series of proteins’ will need to be maintained if this theory is to be agnosticised to ‘all life’, because individual species will use different — very complex and often not fully understood — metabolic pathways to extract ATP. This is where the notion of a biological energy quantum can come in useful. While it is impossible to know the intricacies of metabolism for any arbitrary organism, we can estimate how many protons it enables to be pushed across the membrane, and how much ATP can be produced as a byproduct of its other metabolic processes. This total number of ATP would be a collection of  $\Delta G_{ATP}$  joules of energy, which must be less than the energy available from the metabolism  $\Delta G_{cat}$ . Provided we can make assumptions about the ATP efficiency of the overall metabolism, we can yield free energies in such a way that is conducive with the kinetic theory introduced in Section 3.1.4.

However, ATP is not a typical way for energy to be stored due to its instability. When energy is stored away in other molecules such as lipids there must be some form of energy loss to the environment each time they are formed and broken up into ATP again. However, if organisms use their ATP continually e.g. for maintenance processes or growing new biomass this issue would be alleviated. Owing to the range of ways energy could be stored, and the unknown energetic cost doing so would have, we do not consider such effects throughout this thesis.

The rate of a biochemical reaction can be estimated if we know the energy being released by the metabolism  $\Delta G_{cat}$ , the energy that yields for the organism  $\Delta G_{ATP}$ , the rate constant for the metabolic pathway and the concentration of the chemical species required for the reaction. The new parameter required here is the rate constant. In Chapter 5 we calculate the rate constant of biologically-mediated methanogenesis using data on methanogenic growth from the literature. By considering a large number of species with a variety of optimum conditions, this conveniently provides a pressure and temperature dependent rate constant for us to satisfy these requirements. A downfall in these methods however is a lack of empirical testing for their validity. In Chapter 5 we fit the model to empirical data, but analysis of changing environmental landscapes — such as energy limitation — needs to be done further in the laboratory to confirm this. These ideas are explored further in the discussion section of Chapter 5.

Another important constraint on metabolic rates and hence microbial power supplies is the biomass concentration itself. Throughout this thesis, we focus on the cell-specific metabolic rate and power supply, such that we can make transparent comparisons to cell-specific power demands and growth requirements. The problem here is that the chemical input into these models is defined in a volumetric style, for example chemical concentrations in  $\text{mol L}^{-1}$  or rates in  $\text{mol (L s)}^{-1}$ . One can deduce qualitatively that for a suitably dense microbial population, different microbes within that volume may experience different chemical availability. The origins of such heterogeneity could arise owing to differences in biomass concentration across that volume — such as some locations of high cell density becoming depleted in substrate faster than others, or each cell in such regions having lower cell-specific power supply due to the local competition. Similarly, at very low biomass concentrations it seems tenuous to assume that a cell with a diameter on the order of microns can access all the free energy in a litre of solvent. As such, there is clearly a nuance to asserting the reliability of cell-specific rates and power supplies. Whenever the theory outlined in Section 3.1.4 is used in this thesis, rate constants are computed from empirical data sets such that the cell-specific power supply and energy uptake rates reflect those in such settings. Aside from Chapter 7, which is speculative analysis, the biomass concentrations that we consider are similar to these empirical conditions.

We introduced a group contribution algorithm for estimating how much energy is required to build a cell. Standard Gibbs free energies are not available for large biomolecules, but they can be estimated as the sum of their smaller parts. We showed an example of this using a paper excerpt where proteins were broken down into peptide links and the R groups of their constituent amino acids which offers a minor improvement over existing models which only considered the ‘mean’ R group without special consideration for glycine. This technique is not perfect, and some studies have demonstrated that the energy put into forming peptide links decreases with chain length, but it is the most accepted method of estimating the energetics of cell synthesis in the literature.

Key to this estimate is the concentration of biomolecules and their constituents inside the cell. This is of course hugely dependent on the species, their environmental conditions, their growth states, even *where* in the cell the molecule is being formed. We use the rather limited approach of tabulated *E. coli* amino acid abundances (unless otherwise specified) and a protein concentration of  $10^{-12}$  M, which is consistent with the current literature. We further discuss the effects of this approach in Chapter 5 as part of a published manuscript. In that example, the synthesis energy only needs to vary within an order of magnitude at temperatures less than  $\sim 320$  K to reduce the estimated maintenance costs to near-zero. This highlights the importance of accuracy in our estimates of synthesis energy, which

calls into question not only these concentration values, but also the assumption that the energetics cost is similar for all biomolecules. It is typical in the literature to use the cost of protein synthesis to represent the entire cell mass by scaling it up accordingly. Even if a typical cell is 55% proteins, that means it is 45% *not proteins*. To complete this method requires considering the energetic cost of building the other biomolecules in cells, like DNA, RNA and lipids. We have developed a similar group combination approach to the one shown in Subchapter 3.2 for these molecules as part of a separate project. A manuscript presenting this results is currently in preparation [8].

Finally, we introduced some methods to estimate the energetic cost of survival against temperature and pH effects. For the temperature effects we examined a technique which estimated the maintenance power from empirical data, and another which quantified the rate of thermodynamically unavoidable amino acid racemization. At any given temperature they vary by approximately 3–5 orders of magnitude. It is probable that the *true* maintenance cost due to temperature effects lies somewhere between these values, because the racemization estimate acts a fundamental minimum and the empirical estimate was computed in ideal conditions and represents a maximum. These estimates are used as a benchmark for the maintenance requirement due to temperature for the remainder of this thesis. In Chapter 5 the empirical estimate is specified for methanogens using literature data on their optimum growth conditions. Then in Chapter 6 these three estimates, along with an estimate of Earth subsurface habitable power supplies, are used to assess the balance between power supply and demand in Enceladus' subsurface ocean.

The empirical estimates, including those made in Chapter 5, are limited by their data set. The Tijhuis et al. (1993) [60] data is limited to temperatures between 5–57°C and the data set used in Chapter 5 is at 20–98°C. Estimates outwith these ranges are hence extrapolations and may not be accurate. Our results in Chapter 5 appear to show that the maintenance power required by thermophiles may be considerably higher than the estimates shown in this chapter. The racemization estimate scales linearly with the energetic cost of protein synthesis, adding another critical element for its reliable quantification to those already outlined above.

There is less information available on the maintenance costs owing to adverse pH, and it is yet to be quantified formally in terms of power. We attempted to make a first estimate of this by combining the energy required to pump protons and hydroxide ions across a cell membrane and the rate at which they would need to be pumped to offset natural diffusion. The power demand requires knowledge of the potential difference across the membrane, the permeability of it to each ion considered and the internal pH. Uncertainty in each of these result in power demands that can vary

by more than 5 orders of magnitude for any combination of internal and external pH. Owing to the variation, lack of empirical validation, and organism specificity that this technique requires it is not used for the simulations performed Chapters 5–7 unless as part of their discussion sections. However, it is built into the code (Chapter 4) such that in the future it will be easily accessible for other researchers to build upon and/or test against empirical data.

In summary, this chapter has outlined the theory which we used to calculate the key parameters for the agnostic growth models proposed in Chapter 2. While each requires unique assumptions, collecting these together allows us to build a microbial model which is flexible to different conditions. Moreover, the calculations introduced here will offer realistic values to use when assessing the energetic habitability of extraterrestrial environments.



# CHAPTER 4

---

## NutMEG: an energetic habitability model

---

The theory and ideas presented in Chapters 2 & 3 are wide ranging but have been constrained to the same few microbial parameters. To properly predict microbial behaviour, they all need to be accounted for which can be a daunting task. To realise this we created NutMEG, a python package to make it easier for the wider scientific community to predict microbial growth, survival and biomass as well as environmental habitability and biosignatures.

In this chapter we introduce the model concept and the basics of its computational design. We outline how NutMEG predicts microbial growth and behaviour and summarise some published examples of it being used to solve astrobiological problems.

### Subchapters

4.1	Nutrients, maintenance, energy and growth ...	78
4.2	Computational design .....	81
4.3	Implementing a growth simulation .....	102
4.4	Example applications .....	106
4.5	Summary .....	116

## 4.1 Nutrients, maintenance, energy and growth

NutMEG [Nutrients, Maintenance, Energy and Growth] is an open-source python package for astrobiology which, through bioenergetic considerations, enables the user to assess the habitability, biomass and biosignature production of poorly characterised environments. With only basic information about the local environment, such as its composition, temperature and pressure the model can begin making predictions about the suitability of an organism with a known overall metabolic reaction. It can also calculate a number of secondary and tertiary parameters such as microbial adaptation and nutrient fluxes. This subchapter provides a broad overview of how NutMEG simulates organisms, and how it can be used for habitability assessments, microbial growth predictions and biomass estimates.

### 4.1.1 | The core concept

An environment is energetically habitable if the amount of energy available to life outweighs the energetic costs of surviving there. This means that the habitability of an environment can be quantified by assessing the energy fluxes available to and required by microorganisms — power supply and demand [e.g. 10, 40]. Put simply, this is because the amount of power (energy/time) associated with biological functions is a mathematical function of the physico-chemical characteristics of the surrounding environment, most importantly its temperature, pressure and composition (Chapters 2 & 3). NutMEG estimates microbial growth via an approach where efficiencies are applied to the energetic input from metabolism ( $P_S$  [W cell<sup>-1</sup>]) corresponding to microbial maintenance ( $\mathcal{E}_M$ ), and nutrient uptake ( $\mathcal{E}_{UT}$ ). Any leftover energy can be directed into biomass synthesis ( $P_G$  [W cell<sup>-1</sup>]):

$$P_G = \mathcal{E}_{UT} \mathcal{E}_M P_S \quad (4.1)$$

Assuming for a moment that  $\mathcal{E}_{UT} = 1$  such that nutrients are not limiting growth, the expression above resembles a more self-evident form of quantifying power requirements:

$$P_G = P_S - P_M \quad (4.2)$$

$$\therefore \mathcal{E}_M = 1 - \frac{P_M}{P_S} \Leftrightarrow \mathcal{E}_{UT} = 1 \quad (4.3)$$

Where  $P_M$  is the total maintenance power. This is the sum of the power demand made by microbial survival processes which do not directly contribute to growth. These could include maintaining a specific internal pH ( $P_{pH}$  [W cell<sup>-1</sup>]), repairing biomacromolecules as they break down with temperature ( $P_T$  [W cell<sup>-1</sup>]) and defending against adverse salinity ( $P_{SAL}$  W cell<sup>-1</sup>) to give a few examples:

$$P_M = P_{pH} + P_T + P_{SAL} + \dots \quad (4.4)$$

$P_M$  can be estimated a number of ways, from theoretical basal maintenance estimates [e.g. 37, 45], to empirical estimates based on laboratory or in-situ analyses [e.g. 1, 39, 60]. More information on maintenance powers and how to quantify them can be found in Chapter 3. In a way, at its base the model works as if everything is well and good at some thermodynamic minimum maintenance power, and we slowly add perturbations to it in the form of these energetic costs. This enables us to push the limits of the possible boundaries of habitability.

To calculate the possible rate of nutrient uptake, NutMEG requires the concentration of each nutrient  $\nu$  in mol L<sup>-1</sup> in the local environment, and the associated pseudo first-order rate constant for its uptake,  $k_\nu$  [s<sup>-1</sup> cell<sup>-1</sup>]. Further information on how this works can be found in Box 4.1 later in this chapter. We should note that this nutrient inclusion needs further improvements based on laboratory data or enhanced theory. We examine this in Subchapter 4.5 and Chapter 5.

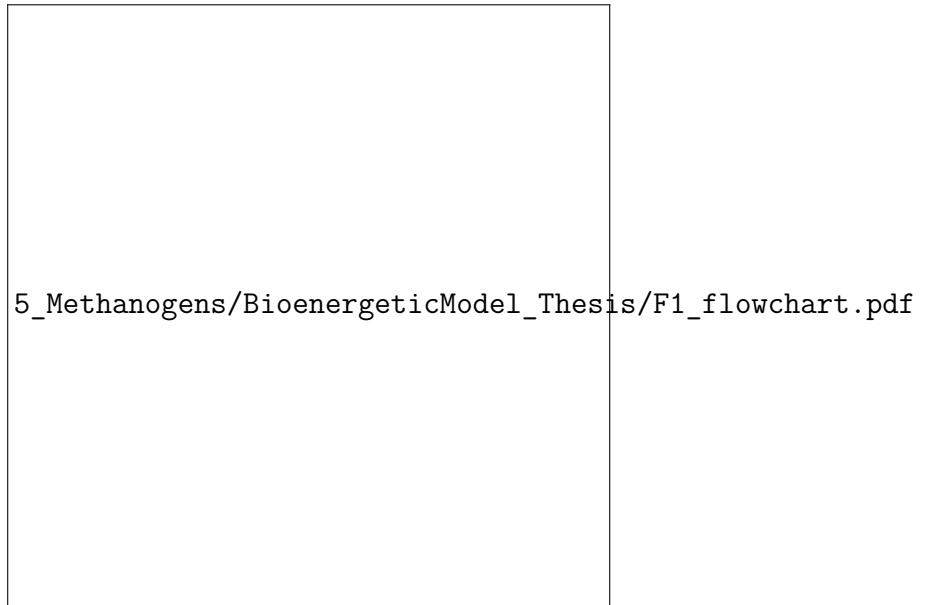


**Figure 4.1** Flowchart to demonstrate the concept behind NutMEG.  $\mathcal{E}_M$  and  $\mathcal{E}_{UT}$  are the energetic efficiencies of maintenance and nutrient uptake respectively. From [1].

NutMEG uses a modular system to calculate  $P_S$ ,  $\mathcal{E}_M$  and  $\mathcal{E}_{UT}$  to predict  $P_G$ ; this is visualised in Figure 4.1. Efficiencies  $\mathcal{E}_{UT}$  and  $\mathcal{E}_M$  are separated such that they can be estimated using the methods outlined above. This necessitates the assumption that the nutrient uptake has no bearing on the success of any maintenance processes. Examples of where this may be an issue include in repair of biomacromolecules which need specific nutrients or salt-out pH defences. Be that as it may, this means there will always be a limit to microbial growth in a closed system, as there should be. A microbial community will run down the energetic and nutrient availability with time and invariantly will reach an unsustainable level.

### 4.1.2 | Habitability assessments

As shown above, NutMEG requires estimates of  $P_S$ ,  $\mathcal{E}_M$  and  $\mathcal{E}_{UT}$  to predict  $P_G$ . It is noteworthy that if any of these input variables are 0, the growth power will also be 0, meaning the environment is expected to be uninhabitable.

The cell-specific power supply  $P_S$  is estimated using a combination of the Gibbs free energy of a given metabolism provided by the local environment  $\Delta G_{cat}$  [J mol<sup>-1</sup>], the Gibbs free energy yield of ATP production inside the cell  $\Delta G_{ATP}$  [J (mol cat.)<sup>-1</sup>], and the rate at which this process can occur,  $r_{cat}$  [mol (L cell s)<sup>-1</sup>]. The Gibbs free energies can be estimated with knowledge of the local composition (both inside and outside the cell) and relevant readily accessible thermodynamic data (Subchapter 3.1).  $r_{cat}$  can be estimated by comparison to empirical data [1] and/or thermodynamically limited biochemical kinetics (Section 3.1.4). For the latter, a rate constant for the metabolic pathway is required and the relevant rate law applied. This rate constant can also be estimated from empirical data, provided the relevant parameters are reported. In Chapter 5 we perform such a fit to empirical data.

### 4.1.3 | Growth rates and biomass estimates

If  $P_G > 0$ , power and nutrients are available for growth. To convert this growth power into new biomass, one must know the energy required to synthesise each cell from the nutrients available  $E_{syn}$  [J cell<sup>-1</sup>] (Subchapter 3.2). Then, if either the energy or nutrient supply is the limiting factor in growth and not the rate of biomass production, following a suitably small time step  $dt$  [s], the total biomass  $B(t + dt)$  [cells] is:

$$B(t + dt) = B(t) \left( 1 + \frac{E_G(t, dt)}{E_{syn}} \right) \quad (4.5)$$

where  $E_G(t, dt) = P_G(t)dt$  [J (cell s)<sup>-1</sup>] is the total energy each cell can contribute to growth per time step.

## 4.2 Computational design

---

This subchapter provides a primer for how the theory and ideas outlined in Chapters 2 & 3 fit into the computational design of NutMEG. The actual implementations and thorough explanations of scientific methods it utilises have been covered elsewhere in this thesis and are referred to accordingly.

### 4.2.1 | Overall structure

NutMEG has an object-oriented design, and is structured much like a natural system. A flowchart of the how various objects communicate with each other is shown in Figure 4.2. Reagents sit inside a reactor with common temperature and pressure and can make up various chemical reactions within that reactor. A community of organisms can be placed in that reactor and make use of some of the available reactions — those which represent their metabolic pathways. Multiple types of organism form a culture and overall we have an ecosystem. More information on these objects including selected attributes is detailed below.

The object-oriented design allows for constant communication between classes and the ability to include specific organisms and reactions through inheritance. For example, hypothetical Methanogen and SulfateReducer classes could inherit characteristics of a base\_organism and be placed in the same culture but any species-specific characteristics will be maintained through the chain of objects.

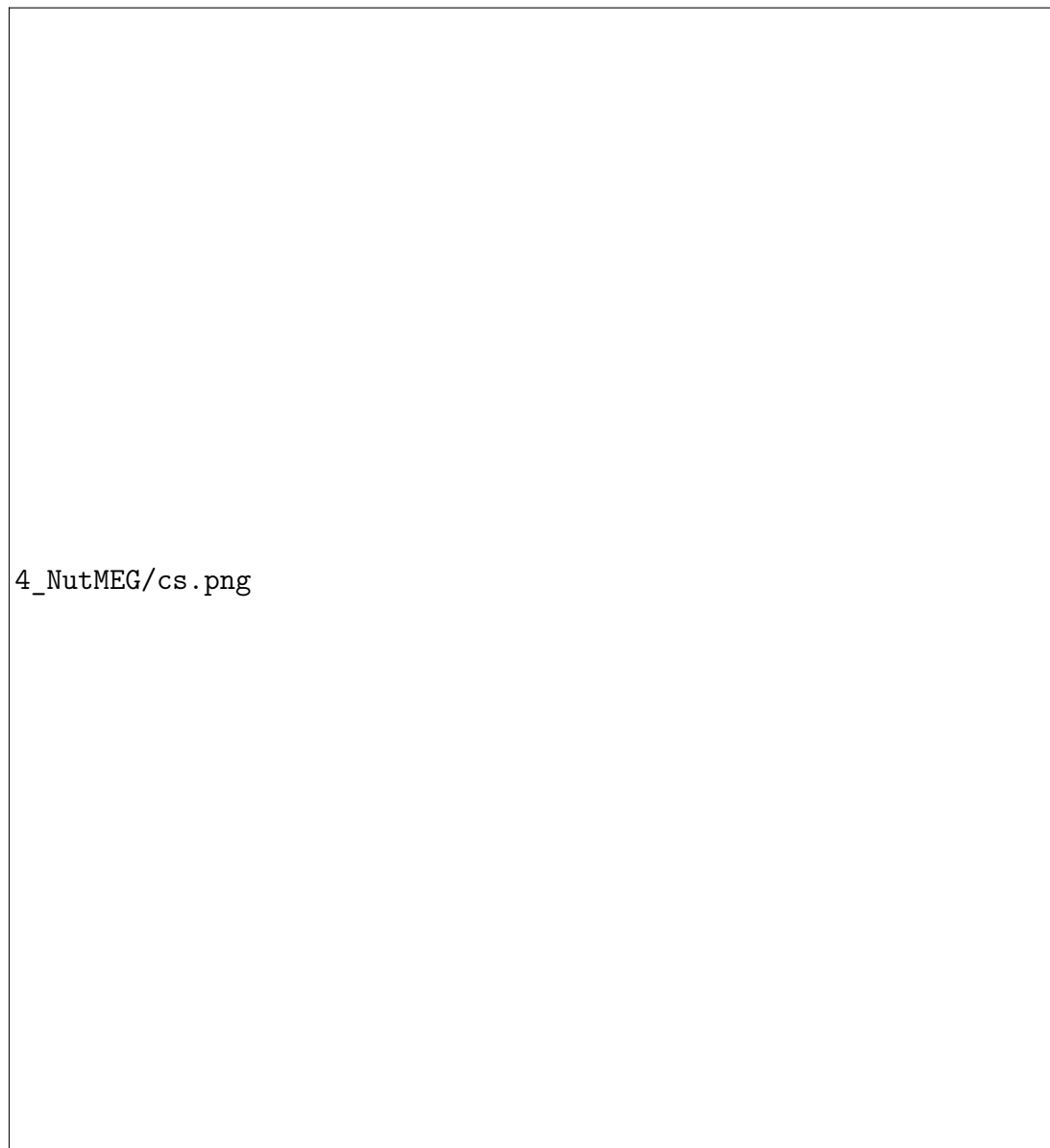


**Figure 4.2 Simplified class diagram to show how the major objects in NutMEG interact and depend on each other** for a simple microbial growth simulation. Solid arrows imply dependencies on only one incidence or specific instances, dashed lines show objects that can contain multiple incidences, and dotted lines indicate inheritance. For example a reactor can only have one environment (it cannot have multiple temperatures), but can contain multiple reagent objects.

## 4.2.2 | The environment

The environment is the simplest and lowest level module used by NutMEG<sup>1</sup>. It contains the core physical variables (e.g. temperature, pressure) of the world enclosed by its volume. The environment also contains placeholders for the temperature, pressure and volume in standard conditions. As shown in Figure 4.2 all objects in NutMEG ultimately depend on a single environment instance — a change in  $T$  or  $P$  will have a ripple effect throughout the model.

## 4.2.3 | The reaction module

NutMEG contains its own rudimentary chemical reaction system, which uses a more powerful chemical (dis)equilibrium model, `reaktoro` [58], to calculate relevant parameters for energetic calculations such as standard enthalpies, entropies, and free energies (Chapter 3, Appendix A). At the most basic level, NutMEG's system has reagent and reaction objects.

### 4.2.3.1 | reagent objects

The reagent class represents individual chemical species in molar and molal terms. For instance, an object `S04` representing  $\text{SO}_4^{2-}$  has properties which could include `S04.charge = -2`, `S04.phase = "aq"` and `S04.conc = 0.001` (in M). reagent objects also contain thermodynamic properties including standard formation enthalpies, entropies and free energies ( $\Delta H_f^\circ$ ,  $\Delta G_f^\circ$  and  $\Delta S_f^\circ$ ) and specific heat capacities  $C_p$ . For each, values are stored for both RTP and in the current environment. These can be updated for changing environmental conditions with the `update_reagent()` function, which uses an SUPCRT model and the HKF equations (Chapter 3, Appendix A).

While molar/molal concentrations are often used in chemical calculations, they are in fact an approximation of that reagent's activity. Concentrations are related to chemical activity via the expression  $a = \gamma_M M = \gamma_m m$ , where  $\gamma$  is known as the activity coefficient (with respective subscripts for molarity and molality). In suitably dilute solutions  $\gamma \approx 1$ . Calculations using reagent objects make use of

<sup>1</sup>In hindsight, this was an unfortunate choice in variable name and is not to be confused with the python environment (e.g `venv` or `conda`). It is a hangover from the early days of development and most users will not need to interact with it, instead calling properties of `reactor`.

```

1  import NutMEG as nm
2  import NutMEG.reaction as rxn
3
4  E = nm.environment(T=298., P=1e5) # temperature in K, pressure in Pa
5
6  # set up reagents
7  H2aq = rxn.reagent("H2(aq)", E, phase="aq")
8  SO4 = rxn.reagent("SO4--", E, phase="aq", charge=-2)
9  H = rxn.reagent("H+", E, phase='aq', charge=1)
10 HS = rxn.reagent("HS-", E, phase='aq', charge=-1)
11 H2O = rxn.reagent("H2O(l)", E, phase='l')
12
13 # put reagents into a reaction.
14 # Dictionary values are the molar ratios.
15 SulfateReduction = rxn.reaction(
16     {H2aq:4, SO4:1, H:1}, {HS:1, H2O:4}, E)

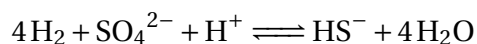
```

Listing 4.1 *Initialising a reaction object.*

their activity attributes and their gamma attribute can be updated when needed, either manually or through methods in specialist subclasses such as electrolyte, introduced in Section 4.2.3.3.

#### 4.2.3.2 | reaction objects

The reaction class collects reagent objects in the form of a chemical reaction from which free energies and other parameters can be extracted. It does so via two key attributes: reactants and products; each of these are dictionary objects in the form {reagent1 : MR1, reagent2 : MR2, ...} where MR is a float referring to the molar ratio of the reagent key. A reaction also requires a reference to the environment to extract key physical parameters such as temperature and pressure. As an example of creating a reaction, consider sulfate reduction:



The code in Listing 4.1 will build a reaction object to represent sulfate reduction.

Standard thermodynamic parameters can be computed in two ways: i) use the standard formation parameters of the reagents and apply Equation 3.7 or ii) natively calculate  $\Delta H_r^\circ$ ,  $\Delta G_r^\circ$  and  $\Delta S_r^\circ$  using reaktoro. Ultimately, both techniques are equivalent and relevant methods can be found in NutMEG's documentation [3]. To compute the molar Gibbs free energy of reaction also requires the quotient  $Q$ , which can be calculated with the `update_quotient()` function. reaction objects



also have a `react(n)` function, which converts  $n$  moles of reactants into products. For example, the command `SulfateReduction.react(0.001)` would consume 4 mM of  $\text{H}_2$  and 1 mM each of  $\text{H}^+$  and  $\text{SO}_4^{2-}$ , then add 1 mM of  $\text{HS}^-$  and 4 mM of  $\text{H}_2\text{O}$ .

### 4.2.3.3 | Subclasses of reaction

The reaction class implements core thermodynamic calculations which are usually sufficient in dilute solutions or for ideal gases, and accurate for deviations with temperature and pressure. However, as the system diverges from other chemical standards (e.g. towards high ionic strength or low water activity) estimates of reagent activities which are important for computing the molar Gibbs free energy become less reliable.

Calculations made throughout this thesis (Chapters 5–7) are generally dilute and the reaction module is used. However, NutMEG includes some methods for more complex solutions chemistry which can be used in future studies. These implement the theory outlined in Appendix A in a series of reaction subclasses. These were implemented into NutMEG before the introduction of reactor objects and hence some of them stretch the definition of ‘reaction-like’ objects as discussed in this work.

#### i) `reaction.neutralsol`

This is a class for neutral solutes in neutral solutions. The total activity of dissolved solutes can be calculated from the osmotic coefficient  $\phi$  [phi], which requires the activity of the solvent to be known (Appendix A.1.2.1).

#### ii) `reaction.electrolyte`

This is a class for fully dissociated salts in pH neutral solutions. It acts as a precursor to its subclasses, `redox_half` and `redox`. It calculates the activity coefficients of the reactants from Debye-Hückel Theory ( $M < 0.05 \text{ mol L}^{-1}$ ), and the mean activity coefficients of the electrolytes in solution from the Mean Spherical Approximation ( $M < 1.0 \text{ mol L}^{-1}$ ) using theory described in Appendix A.1.2.2. The latter requires that we know the radius of all electrolytes in the solution but is more accurate. The former can be used for order-of-magnitude activity coefficients of electrolytes in solution [59].

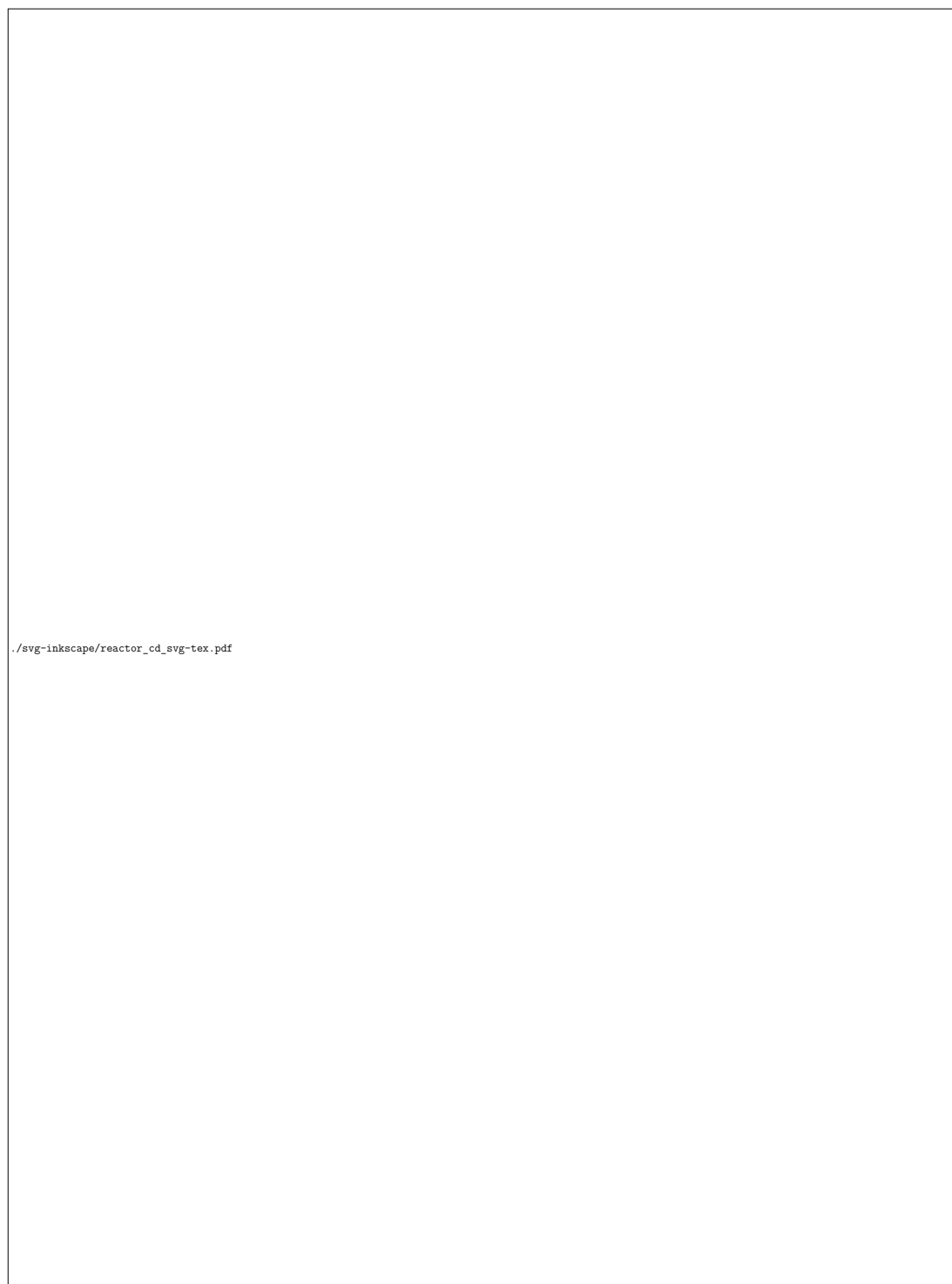


**Figure 4.3** Class diagram of the reaction module and how it relates to the reactor module. Coloured boxes indicate different namespaces. Filled diamonds indicate dependence on a single incidence, unfilled diamonds indicate dependence on multiple incidences, and an arrow indicates inheritance.

In order to calculate  $\gamma_{\pm}$  (the mean activity coefficient for a dissociated salt, c.f. Appendix A.1.2.2) using molal properties, it is necessary to know the volume ratio ( $V_{RTP}/V$ ) of the solution for conversion reasons. These two numbers are attributes of the environment, and if they are not known NutMEG assumes the ratio is 1.

There are a number of ways that these calculations could be extended in the future, and there is a vast chemical literature on them. In general, however, special parameters and/or experimental values are typically required for each reagent. In future iterations of NutMEG, such parameters and calculations could be integrated into subclasses of reagent and acted upon in subclasses of reactor.

### iii) `reaction.redox_half`

This class is designed to host redox half equations, two of which can be used to build a complete redox reaction (introduced below). It inherits methods to properly estimate dissolved ion activities from the `reaction.electrolyte` class. To initiate a `redox_half` object some extra arguments are required, specifically the number of electrons transferred [ $n$ ], and the standard electrode potential of the half reaction [ $\text{stdE}$ ]. Optional arguments include the first and second derivatives of the potential with respect to temperature and the change in specific isobaric heat capacity (which can be used to calculate the second order derivative if it is unknown). The theory for these calculations is summarised in Appendix A.1.3. The class includes methods such as `update_E()` to update the electrode potential with changing temperature or pressure and a unique implementation of `update_std_molar_gibbs()` to update the free energy of the half reaction.

### iv) `reaction.redox`

This class applies the equations in Appendix A.1.3 to calculate non-standard electrode potentials for a redox couple, and update the non standard molar Gibbs free energy. It takes the forward and reverse reactions as `reaction.redox_half` objects. It will also accept electrolyte reactions which include the non-interacting ion(s) instead of electrons, which are important for calculating non-ideality in the reactants based on their surroundings (Appendix A). It also takes the overall cell reaction as a standard reaction-like object. The only other necessary attribute is the number of moles of electrons transferred in the cell reaction for the production of 1 mole of product  $n$ , along with any other keyword arguments from the `reaction` class. This method of passing necessitates repeating the reagents occasionally, so they must always point to the same location in memory taking care not to initiate the same reagent more than once. If this reaction is created inside a reactor this will not be an issue thanks to methods therein to prevent duplicate reagent objects.

The choice of standard is also important when using `redox_half` and `redox` objects. Standard electrode potentials are not just at defined standard temperatures and pressures, but also at a defined standard pH. For chemists this is typically 0, and for biologists/biochemists it is usually 7. To add to the frustration, the standards used when reporting values are not always defined. These classes do not contain methods of changing  $E$  with pH so values of  $E^\circ$  and  $\Delta E^\circ$  are only valid at the pH standard used. Typically, the  $^\circ$  notation is used to indicate the chemical standard, and  $^{\circ'}$  notation is used to indicate the biological standard. It is possible to convert between these standards for Gibbs free energies in some circumstances (Appendix A.2).

Another issue with using redox equilibria is that there is not always a clear redox pathway used by an organism, especially when considering overall metabolisms or poorly understood ones. As a result, the default for NutMEG is to use the standard thermodynamic method and this has been adopted throughout this work. The choice of reaction sub-class to use depends on the specific location one wants to simulate. Some examples are listed overleaf:

- **Hydrothermal vents:** There is usually substantial amounts of mixing, meaning redox behaviour cannot be reliably predicted and the reaction kinetics will be dominated by conventional thermodynamics [156]. Hence, `reaction.redox` should not be used and instead the base reaction class with free energies corrected for temperature and pressure should be used.
- **Saline settings:** NutMEG can deal with saline environments in the general case provided  $M < 0.1$  in line with the Debye Hückel theory. NutMEG will print a warning if salinities higher than this are given, but will still return some numbers (they should just be taken with a pinch of salt<sup>2</sup>).
- **Non-neutral pH:** It can be demonstrated that the Gibbs free energy of a reaction which does not depend on  $H^+$  is independent of pH, provided the activities of all reagents is known (Appendix A.2). If this is the case for your metabolism, the base reaction class should be used. If not, a `reaction.redox` with careful consideration of standards should be used. If  $E^\circ$  is not known at the required pH, it will not be accurate.

### 4.2.4 | The reactor and saved\_systems

The reactor class defines the chemically reactive environment. It collects together all the reaction objects of interest in a system along with all of the relevant reagent objects, unifying them in a single environment. A default reactor

---

<sup>2</sup>Pun intended.

only works in well-mixed near-equilibrium conditions where the composition does not appreciably change unless something which disrupts the system such as an organism is introduced. In other words, there is no active chemistry element to it. Some kind of environmental maintained disequilibrium can be introduced such as a constant fresh supply of one or more reagents using the `composition_inputs` attribute.

reactor objects specifically contain `reactionlist` and `composition` attributes. Both are dictionaries which reference all of the reaction and reagent objects in its volume space. When new reaction or reagent objects are added to the reactor it ensures that there are no duplicates and that all references to the `composition` and `reactionlist` point to the correct space in memory. This allows for multiple chemical interactions to occur which feature the same species — an example could be a reactor in which hydrogenotrophic methanogenesis and sulfate reduction could take place. Both of these reactions depend on dissolved  $H_2$  as a reactant. If the `react()` method is called on either reaction (or alternatively `perform_reaction(re_eq, n)` directly from the reactor), the concentration of  $H_2$  in the reactor will decrease, affecting the free energy yield of both metabolisms and the bioavailability of  $H_2$  to any organism in the reactor.

Specific environments require specific considerations, so in practicality reactor is used as a superclass for a chemically reactive system. Subclasses have been made for two environments important to astrobiologists, `VenusDrop` and `Enceladus`. These are important in different ways. Modern Venus is a sterile world and widely expected to be uninhabitable [e.g. 4], whereas Enceladus is one of the prime candidates for extraterrestrial habitability in the solar system [e.g. 2].

#### i) `saved_systems.VenusDrop`

A `VenusDrop` object has the major parameters and chemical makeup of a droplet in the Venusian cloud layer. It contains methods to convert atmospheric concentrations (in ppm) into dissolved gas concentrations for locations within the Venusian cloud layer, using observational data from space missions. It is populated with reagent objects representing the expected composition in a droplet in the temperate region of the atmosphere. `VenusDrop` was used to estimate the molar free energy available in these droplets in a study published in *Astrobiology* [4]. More information on this study can be found in Subchapter 4.4.

#### ii) `saved_systems.Enceladus`

An `Enceladus` object represents a slice of the parameter space of Enceladus' wider subsurface ocean. It uses Cassini data on gas mixing ratios from the spacecraft's

flybys of the satellites' surface geysers to estimate the internal composition. By default, the mixing ratios used are those from Waite et al. (2017) [15]. These are matched to a calculated dissolved CO<sub>2</sub> concentration, estimated by either:

1. The oceanic pH (default 8.5 [15, 86, 87]).
2. The temperature of the 'tiger stripes' on Enceladus' surface (default  $192 \pm 20$  K [86, 96]).
3. Tabulated results from a carbonate speciation model (developed in Chapter 6).

The Enceladus class also contains some static methods to calculate the maximum temperature at the bottom of the ocean [85, 94]. Owing to the large uncertainties associated with Enceladus environments, this `saved_system` makes use of the `uncertainties` package to handle variables and their uncertainties together. To use floating point numbers representing nominal values instead, the user can pass the keyword argument `nominals = True`. The Enceladus object is used extensively in this thesis, throughout Chapters 6 & 7 to constrain the habitability, plausible biomass levels and suitability of proposed biosignatures on Enceladus.

### 4.2.5 | A culture of organisms

Organism behaviour is managed within a culture object. A culture contains a list of horde objects and/or a list of colony objects, each of these are ultimately based on `base_organism` objects. horde objects directly inherit their behaviours from `base_organism` and act as if the colony of that species is 'one giant organism'. colony objects instead contain a numpy array of organism objects (which also inherit from `base_organism` objects) such that each individual can be simulated independently. Figure 4.4 shows a class diagram of some key attributes and methods of the culture class. For numerical methods implemented by the `ecosystem`, culture has functions to identify the best time-steps for simulations. For instance, `getmin_timestep()` computes suitable time-steps for growth simulations of all present colony and horde objects, and selects the minimum of them for analysis. It can also calculate total organism populations and biomasses. A helper class, `culture_output` manages output of information about the culture to the terminal and to the database.

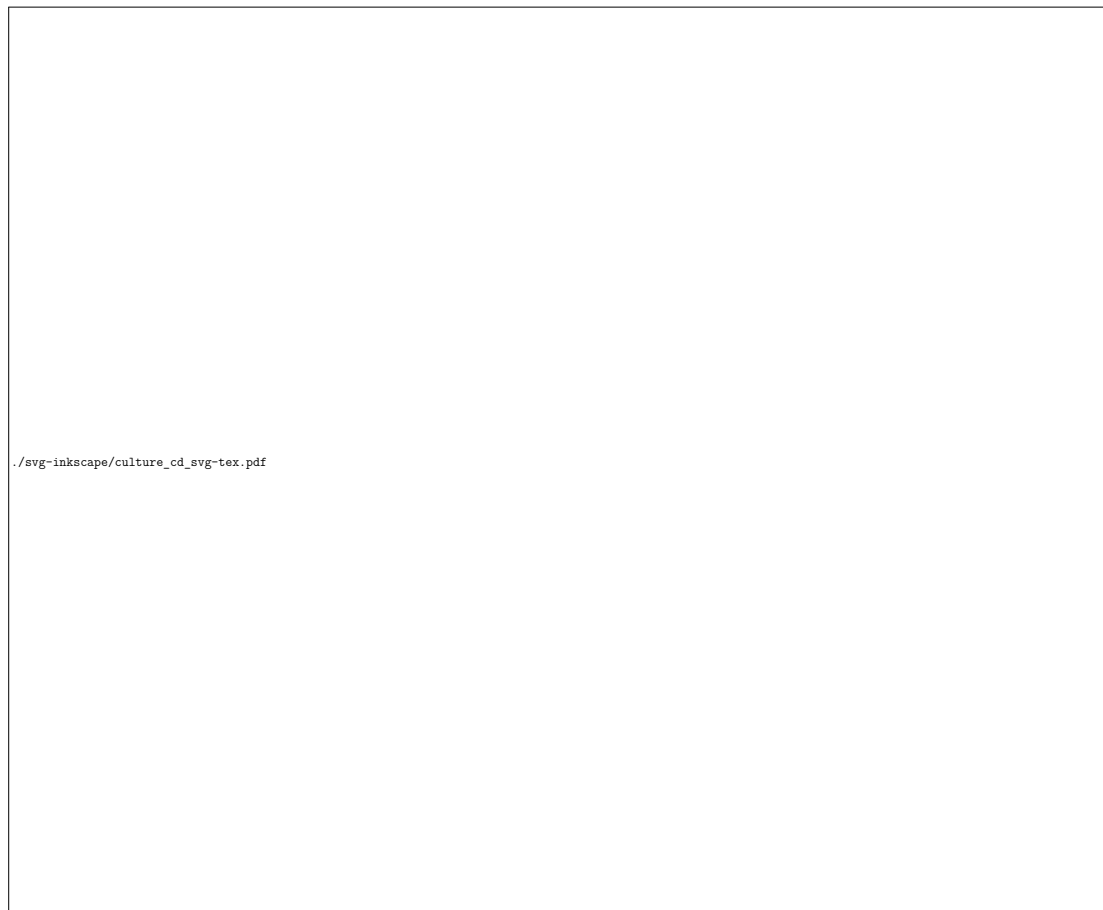


**Figure 4.4 Class diagram of the culture module.** Coloured boxes indicate different namespaces. Filled diamonds indicate dependence on a single incidence, unfilled diamonds indicate dependence on multiple incidences, and an arrow indicates inheritance.

#### 4.2.5.1 | `base_organism` objects

A `base_organism` object describes an individual simple organism attempting to survive in a reactor. It has several parameters such as the obvious — mass, volume etc. — and some less intuitive such as death rates and maximum metabolic rates (some listed in Figure 4.5). There are other NutMEG-specific objects which `base_organisms` take as attributes: `respirator`, `maintainer`, `CHNOPSexchanger`, and `cell_synthesis` as well as an `adaptations` submodule. All of these help compute various aspects of the organism's chance of survival, using the theory outlined in Chapter 3. The `base_organism` also contains the crucial `take_step()` method, where the metabolism is performed with the reactor and survival/growth is predicted for NutMEG's growth algorithm.

##### i) `maintainer`

The `maintainer` attribute of a `base_organism`-like object computes the power costs of microbial maintenance processes. It can implement various theories described in Subchapter 3.3, methods for which are stored in the `NutMEG.applications` module.



**ii) respirator**

The respirator attribute of a `base_organism`-like object manages its catabolic behaviour. Gibbs free energies of the `net_pathway` and `ATP_production` (which are reaction objects) are used to implement Jin-Bethke kinetics (Section 3.1.4). A key organism parameter for this is the rate constant of metabolism  $k$ , which is pressure and temperature dependent. If known in the desired conditions, this can be passed as-is with the keyword argument `k_env`. Alternatively it can be passed as the rate constant at RTP  $k_{RTP}$  and *estimated* at elevated temperatures by passing the keyword argument `k_RTP`. This estimate uses the expression:

$$k = k_{RTP} \times 2^{\frac{(T-298)}{10}} \quad (4.6)$$

This is a typical first approximation of biologically mediated reaction rates, doubling every 10 K [59]. Where rate constants are required in this thesis (e.g. when computing biologically conservable power supply), specific values at  $T$  and  $P$  are used based on empirical values so this approximation is not needed. We also derive these for methanogens in Chapter 5.

**iii) CHNOPSexchanger**

The `CHNOPSexchanger` object manages the exchange of CHNOPS (Carbon, Hydrogen, Nitrogen, Oxygen, Phosphorus and Sulfur) elements between the reactor and a `base_organism`-like object. Each instance includes a dictionary called `nutrients` which contains information about the key nutrients in the locale, in the format:

```

1 {key : value} = { 'C' : [
2     [
3         0.0, # rate of consumption in mol/s,
4         0.50/12.0, # moles required per dry gram of cells in mol / (g cell),
5         0.0, # concentration in reactor in mol/L,
6         self.uptake_consts['C'] # max rate of uptake in /s
7     ],
8     [r1, r2 ...]]
9 }
```

where `[r1, r2, ...]` is a list of the reagents in the reactor which contain this nutrient. The indices are updated internally and the default nutrient requirements are as listed in Table 4.1. The method `find_nutrients()` unifies the `nutrients` with chemicals in `host.locale.composition`. Finally, the method `grow_with_nutrients(E_synth, t)` extracts the relevant nutrients used for growth from the `host.locale.composition`. The way in which this fits into a growth simulation is summarised in Box 4.1.

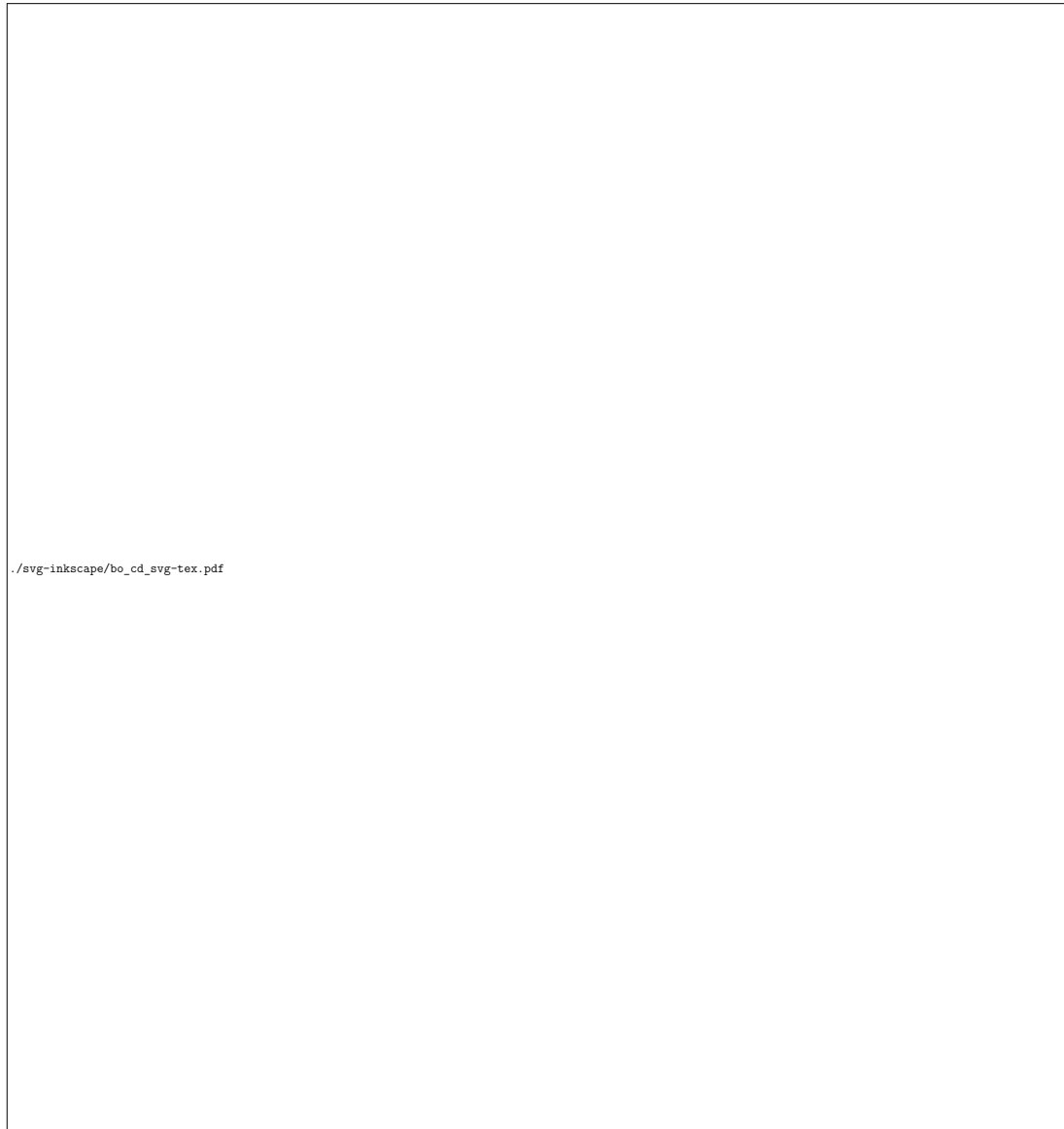


**Figure 4.5 Class diagram of the `base_organism` namespace.** Filled diamonds indicate dependence on a single incidence, unfilled diamonds indicate dependence on multiple incidences, and an arrow indicates inheritance.

**Table 4.1 Average CHNOPS makeup of a microbe** compiled in [157], adapted slightly to 100% as there are other contributions from non-CHNOPS elements. From Higgins & Cockell (2020) [1].

Element	Actual average % dry wt	Used average % dry wt	corresponding mol per dry gram
C	50	50	0.4167
H	8	9	0.09
N	14	15	0.0107
O	20	20	0.0125
P	3	4	0.0013
S	1	2	0.0006

#### iv) adaptations

The adaptations submodule contains static classes to compute various power demands for adaptation to extremes. For example, `Tadaptations` contains a `getLeverME()` and a `getTijhuisME()` method to compute power costs using the methods of Lever et al. (2015) [37] and fits of Tijhuis et al. (1993) [60] respectively. Both of these use the parameters of the host `base_organism` to tune their estimates dependent on its size, mass and protein content. Similar methods exist in `pHadaptations` for pH adaptation. The theory for all methods in this submodule is presented in Chapter 3 and figures therein were plotted using this submodule and the `NutMEG.applications` module (Appendix B.2 & B.3).

#### v) synthesis

The synthesis submodule contains methods to calculate the energetic cost of amino acid production from  $\text{HCO}_3^-$ ,  $\text{H}^+$ ,  $\text{NH}_4^+$ ,  $\text{H}_2\text{S}$  and  $\text{H}_2\text{O}$  as described in McCollom and Amend (2004) [138], and the energetic cost of protein synthesis from these amino acids using a group contribution algorithm (Subchapter 3.2). The submodule also contains a `BioMolecule` class. It is distinct from reagent objects as this module was originally developed separately from NutMEG. It has some unique attributes used by `cell_synthesis`, such as `frequency`, which represents the molar percentage of one essential amino acid relative to the other 19.

**Box 4.1: How CHNOPSexchanger estimates nutrient limitation**

The `update_nutrient_yield()` function computes the maximum rate of uptake for each nutrient (i.e. if there were an unlimited supply of energy), and puts them in another dictionary called `MaxMolOrg`:

```
MaxMolOrg = {}
for key, value in self.nutrients.items():
    MaxMolOrg[key] = value[0][2]*value[0][3]/value[0][1]
```

which has units [dry gram of cells (L s)<sup>-1</sup>]. The smallest entry in `MaxMolOrg` is the limiting nutrient, as it can produce the fewest cells per second. The `nutrients` entry regarding the rate of consumption for each nutrient is then normalised to reflect how many moles of each the organism will actually need to uptake — for all of these apart from the limiter, this will be smaller than its respective value in `MaxMolOrg`. This is then multiplied by the volume of the locale resulting in the unit mol s<sup>-1</sup>:

```
sublimiter = min(MaxMolOrg, key=MaxMolOrg.get)
factor = MaxMolOrg[sublimiter]
for key, value in self.nutrients.items():
    value[0][0] = factor*value[0][1]*(
        self.host.locale.volume*1000)
```

Finally, `grow_with_nutrients(E_synth, t)` computes how much biomass can be made given the limitations computed above in time  $t$  in kg:  $g_{UT}(t)$ . This is compared to the amount of biomass the energy yielded by the respirator can produce,  $g_E(t)$ , to calculate  $\mathcal{E}_{UT}$ :

$$\mathcal{E}_{UT}(t) = \begin{cases} 1, & g_E(t) < g_{UT}(t) \\ \frac{g_{UT}(t)}{g_E(t)}, & g_E(t) > g_{UT}(t) \end{cases}$$

If  $\mathcal{E}_{UT} = 1$ , `value[0][0]` is revised again, to reflect how many nutrients to uptake us use all of the energy available for growth to synthesise biomass. If  $\mathcal{E}_{UT} < 1$ , not all of the energy available for growth can be used as nutrient uptake is not fast enough. `value[0][0]` is not revised and the organism extracts as many nutrients as possible in  $t$  from the reactor. Energy which is not used is returned to the host.

### 4.2.5.2 | colony objects

If modelling each organism individually is required, they can be placed into a colony by species. A colony is at its core a collection of `base_organism`-like objects to ease numerical modelling. Its attributes include `collection`: a numpy array of the active `base_organism`-like objects, and `inactive`: a numpy array of inactive `base_organism`-like objects, representing those in stasis or dead. It also utilises a `colony_output` class to manage saving data and printing to the terminal.

The issue with using colony objects is that when they contain a large number of organisms they make NutMEG simulations become very computationally expensive very quickly, so this method is best left for smaller or extremely energy/nutrient limited systems. In most cases, it would be best to use a horde.

### 4.2.5.3 | horde objects

A horde object is a child class of `base_organism` and simulates a large number of organisms as one, though its attributes remain defined in units of ‘per cell’. This significantly improves computation speed but there is less fidelity when considering individual organisms, for example if one were to monitor minor discrepancies or directed evolution within a community. For the majority of NutMEG applications and the timescales considered however, using horde objects over colony objects is preferred. Unique attributes include `num`: the total number of individuals the horde represents, and `deathnum` the number of inactive or dead organisms in the horde (as these still contribute to total biomass).

The horde class overwrites a number of `base_organism` functions to work for a `num` of organisms rather than just one. As such it overwrites `take_step(t)`, `get_mass()`, `get_volume` *etc.* It contains unique functions such as `update_num(t)` to calculate the population from the new biomass being created in time `t`. Like colony, there is also a `horde_output` helper class to aid in outputting and saving data.

#### 4.2.5.4 | saved\_organism classes

Similar to `saved_systems`, species can inherit their general behaviour from a `horde` or `base_organism` and have their own individual attributes and functions as necessary. At present there is only one `saved_organism`, the `TypicalOptimalMethanogen`, which is a child class of `horde`. This represents a hydrogenotrophic methanogen which adapts its behaviour, including the rate constant of methanogenesis and its maintenance power, to grow optimally at the local temperature of its reactor. It contains unique functions: `setup_methanogenesis()` to add methanogenesis to the reactor's `reactionlst` if necessary, and `avg_org_params()` to setup its behaviour for a changing reactor. Properties of a `TypicalOptimalMethanogen` are discussed fully in Chapter 5, in which it was used to explore the effects of energy and nutrient limitation on biomass and biosignature production. We go on to use the `TypicalOptimalMethanogen` to assess the habitability, possible biomass turnover and resulting biosignature production on Enceladus in Chapters 6 & 7.

#### 4.2.6 | Altogether, an ecosystem

Quite simply, an `ecosystem` collects a culture and reactor and manages its behaviour with time. The class may be expanded in the future as further applications for NutMEG are developed, but at present its core function is to facilitate microbial growth simulations, and save the output for further analysis (Section 4.2.8). This all managed within a large method `predict_growth()`, which implements the algorithm outlined in Subchapter 4.3.

#### 4.2.7 | The applications module

Extended applications of NutMEG which may be of use for future work — and to ease the replicability of Chapters 5–7 — are included in the `NutMEG.applications` module. At present it contains three submodules but could expand in the future should NutMEG be used for more diverse projects.

### 4.2.7.1 | NutMEmatcher — maintenance power from empirical data

The NutMEmatcher is a class for matching the outputs of an ecosystem simulation to empirical data by iterating over unknown organismic or environmental parameters. We use this in Chapter 5 to isolate the maintenance power experienced by hydrogenotrophic methanogens growing optimally in laboratory settings. Because each set of data tells us the composition, growth rate, organism mass, size, methane evolution rate *etc.*, we could iterate over different maintenance power values to see which ones reliably replicate the empirical results. At present, NutMEmatcher can only iterate over maintenance powers, as thus far this is the only application we have used it for. However, it is designed in such a way that new parameters to be iterated over can be included.

NutMEmatcher is initialised with a `base_organism`-like object and a reactor-like object. Then, the function `match(level, paramsdict, target)` performs the iteration for the passed dictionary of iterables `paramsdict`, and the dictionary of target parameters `target`. Variables are identified as the same strings that are allocated to them in NutMEG's databases (Section 4.2.8), so for maintenance power this is `'MaintenanceFrac'`, for growth rate it is `'GrowthRate'` *etc.* These attributes are dictionary objects in case future versions of NutMEmatcher are used to fit multiple variables to multiple criteria. The `'level'` argument is a string determining the complexity of the output to the terminal.

### 4.2.7.2 | theoryestimates — for easy comparisons of maintenance estimates

This application provides easy access to the maintenance power estimates introduced in Chapter 3, to save users who are not interested in a time-dependent simulation from navigating the culture namespace, and help those who are more concerned with seeing what maintenance powers an organism could face by different measures. It is initialised with a `base_organism`-like object and a reactor-like object, and methods including `temperature_defences(T)` and `pH_defences(pH)` will return dictionaries of all NutMEG-native maintenance powers associated with those extremes. For temperatures these are: `'Lever10pc'`, `'Lever2pc'`, `'Lever1/250'`, `'Tijhuis'`, `'TijhuisAerobe'` and `'TijhuisAnaerobe'` corresponding to Lever et al. (2015) [37] racemization maintenance costs at 10%,

2% and 0.4% thresholds for protein replacement, and the Tijhuis et al. (1993) [60] average, aerobic and anaerobic results respectively. Subchapter 3.3 contains more information on how these are calculated.

### 4.2.7.3 | `steady_state_1org` — for steady states with one species

The typical growth curves observed in microbiology (e.g. Figure 2.1) are not actually representative of life's long-term behaviour in the environment. While it may reflect what happens upon inoculation of a new species, an established biosphere will maintain a status-quo with its environment on long timescales, less there are any external forces. This is particularly true if, like most habitats on Earth, that environment has low energy availability [35, 38]. The `steady_state_1org` class utilises user-defined bounding parameters to determine whether a steady state can be achieved between life and the environment by the end of a NutMEG simulation. This is not necessarily one in which the total microbial population is static. Similar to `NutMEmatcher`, `steady_state_1org` has been written in such a way that more bounding parameters can be added in the future. At present, a steady state can be defined by either the 'Quotient' or 'Composition'. If the chosen bounding parameter moves beyond the user-defined limits by the end of a growth simulation, the system is not a steady state because it has changed too significantly from the introduction of this organism. In Chapter 7 we use `steady_state_1org` to isolate regions of Enceladus' ocean which could host a steady state methanogenic biosphere which does not significantly alter the composition from values which can be inferred from Cassini observations.

## 4.2.8 | Data Management

Raw output from NutMEG is stored in SQL-formatted databases which can become large in size and contain time-series information of all chemical and organismic data for any number of simulations. They also store information about specific incidences of organisms and environments such that there is no need to accidentally repeat simulations. These are multidimensional tables whose size can vary dependent on the number of simulations performed; publishable databases average approximately 1–5 GB. These files are largely managed within the `ecosystem_dbhelper` class, and data on reactor-like and `base_organism`-like instances is managed using `reactor_dbhelper` and `base_organism_dbhelper` respectively. Each time step, the variables listed in Table 4.2 are recorded, and every



**Table 4.2 The variables which are recorded in the NutMEG database at each time step.** Column names with a +n indicate that there is one of each of these for each organism species in the reactor. This example table is the output for a horde, there are fewer outputs for a colony.

SQL column name	Description
'time'	Total time elapsed for this simulation [s]
'Composition'	A dictionary of the total composition of the reactor in the format {'name' : activity}.
'totBM_cells'	The total biomass (sum of all organisms, regardless of metabolism) in terms of number of cells.
'totBM_vol'	The total volumetric biomass (sum of all organisms, regardless of metabolism) in m <sup>3</sup> .
'totBM_kg'	The total biomass (sum of all organisms, regardless of metabolism) in kg.
'no_alive_'+n	The number of active cells of species n.
'EnergyAvailable_'+n	The molar Gibbs free energy $\Delta G$ of the metabolic pathway of species n [J mol <sup>-1</sup> ]
'EnergyConservable_'+n	The molar Gibbs free energy yielded via ATP phosphorylation per unit metabolic pathway $\Delta G_{ATP} \times n_{ATP}$ for species n [J mol <sup>-1</sup> ]
'CatabolicRate_'+n	The rate at which the metabolism of species n is proceeding [mol (L s) <sup>-1</sup> ]
'MaintenanceFrac_'+n	The fractional cost of maintenance for species n. Equivalent to the ratio of maintenance power to power supply, $P_M/P_S$ .
'PowerSupply_'+n	The overall available power uptake per cell of species n [W cell <sup>-1</sup> ]. May not reflect actual power uptake in nutrient limited conditions.
'GrowthPower_'+n	The total amount of power per cell going into growth processes for species n [W cell <sup>-1</sup> ]. Unlike the above, this is computed after considering nutrient limitation.
'GrowthRate_'+n	The growth rate $\mu$ of species n [s <sup>-1</sup> ].
'CHNOPSUptakes_'+n	A dictionary indicating the rate of uptake for each CHNOPS element, in the format {'Name' : rate} for species n. Rates are in mol (L s cell) <sup>-1</sup> .
'tot_no_cells_'+n	The total number of cells of species n. This is different to 'no_alive_'+n because it includes inactive (dead) cells.
'Volume_tot_'+n	The total volumetric biomass representing species n [m <sup>3</sup> ]. Represents all biomass, active and inactive.

100 time steps these are saved into a table for that simulation, which is named automatically. The values are also saved when the simulation is ended. This way, even if an error occurs, there will still be output to analyse and/or debug.

The default NutMEG database contains tables with names 'Reactor', 'Organism', 'Reactions', 'Composition', and 'Summary' as well as a unique table for each growth simulation. The named tables have primary keys 'LocID', 'OrgID', 'ReactID', 'CompID', and 'SimID' respectively. These are properties of specific incidences of the various NutMEG objects introduced in this chapter. When initiated, unless the keyword argument `workoutID` is passed as `False` an entry is made in the relevant table, saving the objects attributes for future use if desired. For example, say you performed a simulation some time ago with `SimID='Sim1'`. From this you can use the static method `ecosystem_dbhelper.findOrgIDsLocID(SimID)` to find out the IDs of the organisms and reactor in that simulation. You could then examine the attributes of each instance used for that simulation, or even regenerate them as objects (using their `from_db()` constructor methods) and run a new simulation with minor changes.

## 4.3 Implementing a growth simulation

---

Growth simulations are performed by calling the `predict_growth()` method of an `ecosystem`. An example of setting up such a simulation up is introduced in Section 4.4.1. But first, it is important to understand exactly what is happening under-the-hood each time step and how NutMEG decides to stop a simulation.

### 4.3.1 | Walk-through of a simulation step

Overleaf is an excerpt from Higgins & Cockell (2020) [1], the remainder of which is presented in Chapter 5. This walk-through is accurate for all versions of NutMEG used in this thesis, versions 0.9.0–1.0.1. Most characters referred to in the excerpt below are customisable.

**Excerpt from Higgins & Cockell (2020) [1]**

If a time step  $dt$  [s] is not manually input, it is determined by the model as the amount of time it would take for the slowest growing microbial community to increase by 0.1%. Then, each time step consists of the following:

- Increase age of all cells by  $dt$
- Update local composition data if there is an inflow/outflow included.
- Update the reaction quotient for the catabolic reaction using local composition data, and calculate its free energy (Sec 5.5.2).
- Use thermodynamically limited biochemical kinetics to calculate the conservable power supply  $P_S(t)$  (Sec 5.5.3).
- Maintenance contributions
  - Calculate (where necessary) and sum the contributions to maintenance power  $P_{M,i}(t)$ . In this work, the maintenance power was entered explicitly as the temperature-dependent values inferred from the growth rates of methanogens in optimal conditions (Sec 5.2.2, Fig 5.2). The actual power organisms use for maintenance varies with growth phase, substrate availability and other environmental parameters [23], though this was not included in this analysis.
  - The maintenance efficiency is then  $\mathcal{E}_M = 1 - \sum P_{M,i}(t)/P_S(t)$
- Nutrient contributions
  - From maintenance calculations, we have the total instantaneous power available for growth,  $\mathcal{E}_M P_S(t)$
  - Using their activity and uptake rate constants, work out which of the CHNOPS elements would be limiting (i.e. the limiting contribution to making cells per unit time — we could have enough C for 6 cells  $\text{hr}^{-1}$  but only enough phosphorus for 2 cells  $\text{hr}^{-1}$  for example.)
  - Set the uptake rate for all of the elements such that they would match that production rate.
  - Given the total quantity of nutrients that could be collected in  $dt$ , compute the biomass this could correspond to:  $g_{UT}(t)$ .
  - Using this and the biomass which the energy can create  $g_E(t)$ , compute  $\mathcal{E}_{UT}$ :

$$\mathcal{E}_{UT}(t) = \begin{cases} 1, & g_E(t) < g_{UT}(t) \\ \frac{g_{UT}(t)}{g_E(t)}, & g_E(t) > g_{UT}(t) \end{cases} \quad (4.7)$$

- Perform the metabolic reaction with the local environment.

- If  $\mathcal{E}_{UT} = 1$ , all of the available power supply is being utilised for maintenance and growth, and the molar concentration of reagents for each organism to react in the catabolism  $[\text{M cell}^{-1}]$  is simply  $r_{cat}(t)dt$ , where  $r_{cat}(t)$   $[\text{M substrate s}^{-1}]$  is the thermodynamically limited rate of the catabolic reaction (Sec 5.5.3).
- However, if  $\mathcal{E}_{UT} < 1$ , growth is also restricted by the availability of nutrients (i.e. nutrient uptake is the growth rate-determining step). This means the organism need not collect all of the power available, as it cannot be used for growth and would otherwise be wasted. The power supply needed in this scenario is then  $(1 - (1 - \mathcal{E}_{UT})\mathcal{E}_M)P_S$ .
- In either of the cases above, the total molar concentration of reagents to react in the catabolism  $[\text{M}]$  can be expressed as:

$$(1 - (1 - \mathcal{E}_{UT})\mathcal{E}_M) \times N(t) \times r(t) \times dt \quad (4.8)$$

- Increase the biomass volume, mass and cell count by the number of new cells created:  $(P_G(t) \times dt)/E_{syn}$
- If the organism has a set life span, deactivate all cells that have exceeded it.

```

1 ecosystem.stoppingdict = {
2     'Volume_Fraction' : {
3         'Max':0.99, 'Min':0., 'Consistency':0, 'Count':0},
4     'Maintenance_Fraction' : {
5         'Max':1.0, 'Min':-0.1, 'Consistency':10, 'Count':0},
6     'Metabolic_Rate' : {
7         'Max':float('inf'), 'Min':1e-40, 'Consistency':10, 'Count':0},
8     'Growth_Rate' : {
9         'Max':float('inf'), 'Min':-0.5, 'Consistency':50, 'Count':0},
10    'Population' : {
11        'Max':float('inf'), 'Min':0, 'Consistency':10, 'Count':0}
12 }
```

**Listing 4.2** Dictionary showing criteria for ending a NutMEG simulation. The NutMEG ecosystem default `stoppingdict`, which defined the criteria which needs to be met for NutMEG to end a microbial growth simulation.

### 4.3.2 | Stopping a simulation

A number of criteria can cause a simulation to end, sometimes abruptly. `ecosystem` objects have an attribute called `stoppingdict` which is a dictionary of dictionaries, and has the default structure presented in Listing 4.2. For each, the keys `'Max'` and `'Min'` represent the maximum and minimum values an organism attribute can reach respectively. In the case of `'Volume Fraction'` this is the total organismic volume fraction of the reactor. The `'Consistency'` key is the number of steps that need to have been taken with the parameter outside the limits before the simulation ends. The `'Count'` key keeps count of how many steps have passed for this purpose. The user can change these dictionary entries to their desired simulation endgames. For example, if one is looking for a steady state they may want to increase the `'Consistency'` or `'Max'` keys of `'Maintenance_Fraction'` to better accommodate brief correctional periods (e.g. this is needed in Chapter 7, see Figures 7.11 & 7.12).

## 4.4 Example applications

---

NutMEG has the potential to be a useful tool for many astrobiological studies. Owing to its modular design we can use different aspects of it for different problems. Here we will give an overview of some example NutMEG applications, presenting how the model was used and how we can interpret its results. In the first example, we present a simple microbial growth simulation which predicts the competition between two fictional methanogenic and sulfate reducing organisms. In the second, we show how NutMEG was used to estimate the energy available to life in Venus' temperate (but uninhabitable) clouds. In the third, we discuss how NutMEG was used in a novel 'bottom-up' approach for predicting biosignature levels and observations on a hypothetical exoplanet. The second and third examples are from articles which have been submitted for publication [4, 5]. We do not discuss the results of these in depth; we merely explain how NutMEG was utilised and summarise the key findings related to that application. For full discussion, the reader is referred to those stand-alone publications [4, 5].

### 4.4.1 | Microbial competition

We put together a simple example of a NutMEG microbial growth simulation for the package's documentation [3]. We explored how different environmental and microbial parameters can affect competition between some methanogens and sulfate reducers using arbitrary values. Listing 4.3 defines a method `simulate_competition` which performs a NutMEG growth simulation between a methanogen and a sulfate reducer, returning a `SimID` to access their results in the database. Listing 4.4 summarises 5 implementations of this method, with one control and the four others altering i) the methanogen maintenance power, ii) ATP yield of the sulfate reducer, iii) chemical inflow of  $H^+$ , and iv) giving both horde objects a life span which their constituent organisms cannot exceed. These results are plotted in Figure 4.6. It should be stressed that this example is fictional, and none of these parameters are intended to be reflective of real methanogens, sulfate reducers, or their natural environment, but it does provide a useful example of how NutMEG can be used to simulate competition between organisms which may behave differently. An extended walk-through of this example along with the complete source code is available in NutMEG's documentation [3].

Despite this example's lack of realistic input values we can show qualitatively that NutMEG is working as intended. In Figure 4.6 the top left panel shows a control case from which we will deviate. Solid lines represent the sulfate reducer horde

and dashed lines represent the methanogen horde. The top right panel shows the composition throughout the control case. It is clear that  $\text{CH}_4$  is produced at an increasing rate as the methanogens grow. Meanwhile  $\text{SO}_4^{2-}$ ,  $\text{H}^+$ ,  $\text{CO}_2$  and  $\text{H}_2$  are consumed, with  $\text{H}_2$  consumed the most due to its relative importance in both metabolisms. The sulfate reducers grow much less than the methanogens because they are energy limited due to the low  $\text{H}^+$  concentration. The rest of the panels demonstrate how the growth curves would change if the control case organism(s) or environments were changed slightly. Lighter colours indicate increased deviation from the control case, and correspond to the values in Listing 4.4. The left-middle panel alters the maintenance power of the methanogens only. This clearly slows down their growth, as more of the energy they uptake is required for survival processes. Interestingly this also affects the sulfate reducers — when the methanogens grow more slowly they are able to process a larger share of the available energy before the metabolisms become non-viable. The right-middle panel shows what happens if the sulfate reducer has a higher ATP yield per mole of  $\text{SO}_4^{2-}$ . This means the sulfate reducers can access more energy for an equivalent metabolite uptake resulting in faster growth for the sulfate reducers. The bottom-left panel shows the growth curves in response to an inflow of  $\text{H}^+$ . Because only the sulfate reduction metabolism strictly depends on this, and from the top-right panel  $\text{H}^+$  is clearly the energy-limiting reagent, this results in faster growth for the sulfate reducers without significantly affecting the methanogens. In the bottom-right panel we introduce a lifespan for both species whereby cells become inactive once that amount time as elapsed since their creation. For each of these changes, the cultures do not recover. This is because by the end of their growth curves it is not energetically viable in the environment to kick-start growth again.

**Figure 4.6 (opposite)** Plots of some output from Listings 4.3 & 4.4. Dashed lines in shades of red-to-yellow characterise a horde of methanogens and solid lines in shades of blue-to-green characterise hordes of sulfate reducers. The top left plot shows growth curves in the control case, and the top right plot shows the change in composition with time in that control case. Time is measured in seconds within NutMEG, but to add context to these plots  $10^5$  seconds is approximately 1.15 days or 27.8 hours. The remaining panels show the growth curves when microbial or environmental conditions deviate from the control case. As lines get lighter in hue, e.g. towards yellow and green, the conditions or microbial parameters are increasingly different as compared to the control case. These are discussed in detail in the main text. The centre-left plot shows the effect of increasing the maintenance power required by the methanogens. The centre-right plot shows the effect of increasing the ATP yield of the sulfate reducer. The bottom-left plot shows the effect of an inflow of  $\text{H}^+$  into the system, which the sulfate reduction metabolism depends upon. The bottom-right plot shows the effect of introducing a lifespan for both hordes.



**Figure 4.6** Simple example results showing microbial competition. See caption opposite.



```

1 import NutMEG as nm
2
3 def simulate_competition(comp={}, k=[0.001,5000], inflow={'H+':0},
4     methanogen_changes={}, SR_changes={}, reactor_changes={},
5     dbpath='NutMEG_db'):
6
7     # passing workoutID=False means it doesn't save parameters to the
8     # database yet. We'll make some changes and do so later.
9     R = nm.reactor('reactor1',
10         workoutID=False, pH=7.0, dbpath=dbpath, **reactor_changes)
11
12     initial_conditions(R, comp=comp) # sets up the composition.
13
14     # create a horde of 10 methanogens, and give it any unique parameters.
15     H = nm.horde('Methanogen', R, setup_methanogenesis(R, k_RTP=k[0]), 10,
16         Tdef='None', dbpath=dbpath, **methanogen_changes)
17     # Tdef shows which adaptations against temperature to use, here we'll
18     # ignore it and put in our own maintenance powers.
19
20     # similarly, create a horde of 10 sulfate reducers.
21     H2 = nm.horde('SulfateReducer', R, setup_sulfatereduction(R, k_RTP=k[1]),
22         10, Tdef='None', dbpath=dbpath, **SR_changes)
23
24     # Organism set-up adds their metabolisms to R so it is ready to save!
25     R.dbh.workoutID()
26
27     # put both hordes in a culture object, which keeps organisms together.
28     Cu = nm.culture(hordes=[H2, H])
29
30     # put the culture and the reactor together. Now we have an ecosystem
31     # ready to go!
32     ES = nm.ecosystem(R, Cu, dbpath=dbpath)
33
34     # this runs a growth prediction with the two hordes together in the
35     # reactor with initial conditions as defined and saves the output
36     # in the database. Various criteria cause the simulation to stop.
37     # We'll add a maximum time (equivalent to ~6yrs).
38     ES.predict_growth(tmax=2e8)
39
40     # return the simulation ID, which can be used to extract the data.
41     return ES.dbh.SimID

```

**Listing 4.3** *Example of running a simulation with two organisms.* Complete code including the methods referenced in this snippet and further methods for data extraction and plotting can be found in the NutMEG-applications repository [3]. Implementation and output (as a plot) are in Listing 4.4 and Figure 4.6.

```

1  import matplotlib.pyplot as plt
2  import numpy as np
3
4  fig, axs = plt.subplots(3, 2, figsize=(6,8))
5  orgfig = nutplt.growthparams(fig=fig)
6
7  ControlSim = simulate_competition(
8      methanogen_changes={'Basal':1e-15}, SR_changes={'Basal':1e-15})
9  # orgcurves and comcurves are methods we prepared to plot the growth
10 # and composition output of a passed simulation.
11 orgcurves(orgfig, [ControlSim], ax=axs[0][0])
12 compcurves(orgfig, [ControlSim], ax=axs[0][1])
13
14 # Now change some model parameters to show how it can change the
15 # growth curves.
16
17 # First increase the maintenance power of the methanogen, making
18 # survival harder
19 for MP in [2e-15, 5e-15, 1e-14, 5e-14]:
20     _Sim = simulate_competition(
21         methanogen_changes={'Basal':MP}, SR_changes={'Basal':1e-15})
22     orgcurves(orgfig, [_Sim], ax=axs[1][0], ls='--')
23
24 # change the yield of ATP per mol metabolism - for the sulfate reducer
25 for n in np.linspace(0.5,1.5, num=5):
26     _Sim = simulate_competition(
27         methanogen_changes={'Basal':1e-15},
28         SR_changes={'Basal':1e-15, 'n_ATP':n})
29     orgcurves(orgfig, [_Sim], ax=axs[1][1], ls='--')
30
31 # Add an inflow of H+, required for sulfate reduction but does not
32 # affect methanogenesis
33 for h in np.logspace(-16,-12, num=5):
34     _Sim = simulate_competition(
35         methanogen_changes={'Basal':1e-15}, SR_changes={'Basal':1e-15},
36         reactor_changes={'composition_inputs':{'H+':h}})
37     orgcurves(orgfig, [_Sim], ax=axs[2][0], ls='--')
38
39 # give both organisms a life span which they can't exceed.
40 for l in [1e3, 1e4, 5e4]:
41     _Sim = simulate_competition(methanogen_changes={'Basal':1e-15,
42         'base_life_span':l}, SR_changes={'Basal':1e-15, 'base_life_span':l})
43     orgcurves(orgfig, [_Sim], ax=axs[2][1], ls='--')

```

**Listing 4.4** *Implementation of the `simulate_competition` method from Listing 4.3 to generate data plotted in Figure 4.6. Complete source code with plotting routines can be found in the NutMEG-applications repository [3].*

### 4.4.2 | Biologically available energy in the Venusian clouds

A substantive application of NutMEG arose in a project elucidating the uninhabitability of the Venusian clouds which resulted in a successful publication in a special edition of the journal *Astrobiology* [4]. Led by C. S. Cockell, this broad review quantified the available CHNOPS elements, redox couples, and energetic availability to life in the planet's 'temperate' cloud layer. Although as far as we know Venus is a sterile world, constraining why the clouds are uninhabitable may prove a useful analogue for models on what could happen to Earth in a runaway greenhouse scenario.

For an undergraduate project, A. A. Johnstone reviewed the literature of historic missions to Venus and collected atmospheric measurements of species which could constitute biologically useful redox couples and/or CHNOPS elements and heavy

```

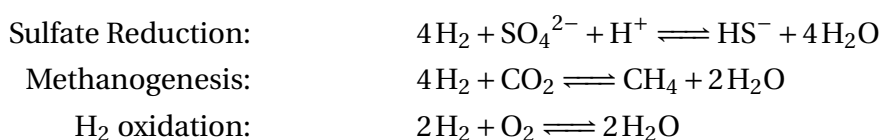
1  import NutMEG as nm
2  from NutMEG.reactor.saved_systems.VenusDrop import VenusDrop
3
4  V = VenusDrop(H2ppm=25) # use a VenusDrop object
5  # Computes the dissolved conc. from the atmospheric ppm
6  update_all_comp_ppm(V)
7
8  # create a base_organism with Sulfate Reduction as the net_pathway
9  # setup_SulfateReduction(V) places a sulfate reduction reaction in V.
10 # Generating one is similar to Listing 4.1
11 SRorg = nm.base_organism('Sulfate Reducer', V, setup_SulfateReduction(V))
12
13 # loop through nominal and endmember H2 ppms
14 for H2ppm in [15,25,35]:
15     V.update_reagent('H2(aq)', H2ppm)
16     # unify_reaction ensures the organism and environment reactions point
17     # to the same space in memory.
18     V.unify_reaction(SR.respiration.net_pathway, overwrite=False)
19
20     # this method updates the quotient, standard gibbs, and molar gibbs
21     # in the current environment.
22     SRorg.respiration.net_pathway.update_molar_gibbs_from_quotient()
23
24     print(SRorg.respiration.net_pathway.molar_gibbs)

```

**Listing 4.5** *Example of extracting the free energy of sulfate reduction in a Venusian cloud droplet*, continuing from Listing 4.1. This type of application was repeated for different temperatures and metabolisms to generate results including Figure 4.7. Complete code including the methods referenced in this snippet can be found in the NutMEG-Implementations repository [3]

metals. He also used NutMEG to investigate quantitatively the available Gibbs free energy for metabolisms compatible with the composition of the droplets. To do this he used the `base_organism` and `reactor` modules, with different reaction objects representing different metabolisms. Dissolved gas concentrations in cloud droplets were estimated from the atmospheric concentration in parts per million [ppm] (Appendix A.4), but otherwise the reaction objects were initialised in similar vein to Listing 4.1. Then, the free energies were extracted as presented in Listing 4.5, which extends the sulfate reduction example.

We examined three metabolisms, sulfate reduction, methanogenesis and  $\text{H}_2$  oxidation, which have the following overall reactions:



4\_NutMEG/VenusSummary.pdf

**Figure 4.7 Molar free energies of metabolic pathways that could be feasible in the Venusian clouds.** Molar Gibbs free energy of sulfate reduction, methanogenesis, and  $\text{H}_2$  oxidation at their nominal dissolved concentrations and the variation in value with reaction quotient caused by varying the atmospheric parts per million. Also shown is  $\text{H}_2$  oxidation at 3 ppm  $\text{O}_2$ , an edge-case. From [4].

There is variability in each of these Gibbs free energies caused by the uncertainty in ppm measurements. Figure 4.7 shows the molar free energy available from each of these metabolisms between 273 K and 373 K. While one could draw the conclusion that there is energy available for life in part of this temperature range (and all of it for H<sub>2</sub> oxidation) there are many other qualities of Venus' clouds which render it uninhabitable, as well as limitations in the analysis to arrive at these values. One core problem is the water activity, which may be <0.1, far below the lower known limit for life of ~0.6 [4]. One example of a limitation is that the dissolved gas model (Appendix A.4) assumes the solvent is approximately pure water, whereas in Venusian cloud droplets the solvent is sulfuric acid, making up over 80% of the molar content [4]. A sense of scale is also important when thinking about these droplets and the Gibbs free energies. While there appears to be energy available per mole of species, the dissolved concentration of said species can be incredibly tiny. For example, all of the metabolisms we quantified depend on H<sub>2</sub>, but at a temperature of 314 K, a droplet with diameter 10 µm would only contain *one molecule* of H<sub>2</sub>. Even though the rate of diffusion from the atmosphere into the droplet is unknown, such low quantities of metabolite availability renders cloud droplets unsustainable habitats [4].

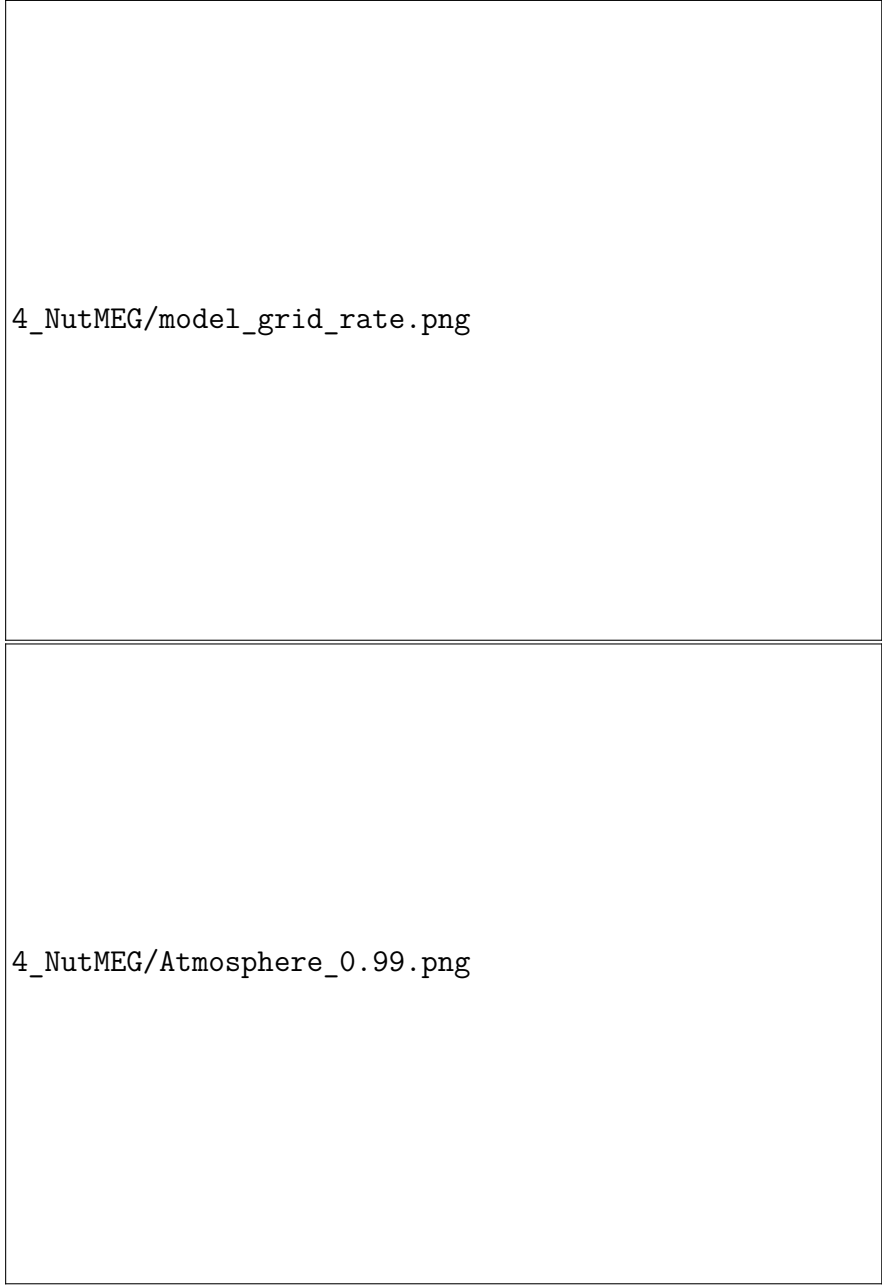
#### 4.4.3 | Exoplanets and biosignature detection

Another application of NutMEG arose in a summer project undertaken by L. M. R. Seeburger, resulting in a manuscript under review for the journal *Astrobiology* [5]. The idea was to explore what is needed to bridge the gap between microbial modelling and observations of exoplanet atmospheres. A flash-point of discussion in exoplanet science for many years has been the promise of biosignature detection by future instruments. Biosignatures are observables which are indicative of life's presence. Arriving at a consensus on the most useful biosignatures has proven difficult because while life can produce an abundance of chemical indicators [125], oftentimes very similar (or identical) chemical species can be produced by abiotic means such as water-rock reactions. An excellent example of this is methane [CH<sub>4</sub>] which on Earth can be produced by an array of organisms (e.g. methanogens, cows) but also in hydrothermal vents at the bottom of the ocean through a process known as serpentinisation [158]. In this project we coupled a microbial model (NutMEG) to NASA's planetary spectrum generator (PSG)<sup>3</sup>, presenting a 'bottom-up' approach to biosignature detection. In summary, we modelled putative methanogens on an Archean-Earth-like planet and computed the scale of biological activity which would actually be needed for a confident detection of biogenic CH<sub>4</sub>. It should be

<sup>3</sup><https://psg.gsfc.nasa.gov>

stressed this was a first approximation and lacks proper ocean and atmospheric modelling, but the core intention was to draw the link — and map out the path — between biological activity on a hypothetical exoplanet and its detection.

For this example we will not present the code used, as it is a more complex implementation of the Listings in Section 4.4.1. A `TypicalOptimalMethanogen` was used as the horde in a series of environments representative of Earth-like hydrothermal vents. These were fluids at 300 K (for the most accurate microbial parameters) with different inflow rates of  $\text{H}_2$  and  $\text{CO}_2$  to constrain  $\text{CH}_4$  production (Figure 4.8, top). We then extrapolated these  $\text{CH}_4$  production rates to an atmospheric methane concentration using a simple percentage-based estimate of how much  $\text{CH}_4$  completes the trip to the top of the atmosphere (Figure 4.8, bottom. This shows the most pessimistic case of 1% success). We then used this updated atmospheric concentration to generate spectra as if the planet were seen from next-generation space telescopes including: i) the James Webb Space Telescope [JWST], ii) the Large Ultraviolet Optical Infrared [LUVOIR] Surveyor, and iii) the Habitable Exoplanet Observatory [HabEx]. In the literature, a 1% atmospheric methane concentration on an Earth-like planet is considered ‘probably biogenic’, but our results suggest it is very difficult to resolve between 0.1%, 1% and 10% levels unless awarded unprecedented observing time for all instruments, though HabEx and LUVOIR perform notably better than JWST. This work highlights the need for (exo)planetary scientists, astrobiologists and observational astrophysicists to work together such that biological activity can be confidently linked to atmospheric compositions, and we demonstrate that models such as NutMEG could play a part in these studies.



4\_NutMEG/model\_grid\_rate.png

4\_NutMEG/Atmosphere\_0.99.png

**Figure 4.8 Methane production and detectability on an Earth-like exoplanet.** Selected results from Seeburger et al. (in rev.) [5]. Top: The rate of methane production from a community of methanogens at different inflow rates of  $\text{H}_2$  and  $\text{CO}_2$ , constrained via estimates of this production at hydrothermal vents [HV] on Earth. Bottom: The atmospheric concentration of methane this results in if we assume the most pessimistic case where only 1% of HV methane production completes the trip to the top of the atmosphere. This is shown for different fractional HT coverages (the fraction of the ocean floor that contain HVs.) Also noted for interest are comparisons to modern Earth.

## 4.5 Summary

---

While it remains a work-in-progress, NutMEG has promise as a very useful python package for astrobiological problems. Owing to its modular design, users can create their own unique organisms and environments to examine habitability, biomass levels, biosignature production, competition, energy and nutrient limited growth, and more. The computational design is intuitive, following the structure of a natural system. Reactants which make up reactions are placed in a reactor. A culture of different organisms makes use of that reactor and its contents within an ecosystem. Because of this arrangement, the chemical aspect of NutMEG sees life as a chemical ‘black box’ which exchanges energy and nutrients with it, and the biological aspect sees the chemical environment through the bioenergetic lens. Chemical reactions can behave as a standard thermodynamic reaction or as a redox couple, reagent activities can be estimated from Debye-Hückel theory and/or the mean spherical approximation, and reaction energetics can be quantified by the Helgeson-Kirkham-Flowers equations of state. Organism catalysed energy uptake is estimated using thermodynamically limited biochemical kinetics. Microbial growth is predicted using the energetic requirements of maintenance and synthesis in terms of the power available per organism.

Some of NutMEG’s limiting aspects are discussed in Chapter 5. As it is based on theory developed in Chapter 3, the limitations therein also extend to NutMEG simulations. In Chapters 6 & 7 NutMEG is applied to more specific problems regarding Saturn’s moon Enceladus. The discussion sections of those chapters cover other limiting aspects in the model from the theory employed. There still remain a number of additions that could be made to future versions of NutMEG to enhance its viability even further. Some particular examples of these are:

- **Cell lysis and disintegration.** `base_organism`-like objects can become inactive via their `lifespan` or `deathrate` attributes but the model does not account for the disintegration of that biomass. Doing so could release reactants into the reactor, providing metabolites for other species, for example fermentative species.
- **Dormancy.** Similarly, there is currently no implementation within ecosystem to reactivate dormant `base_organism`-like objects during a growth simulation. In natural systems, some species can remain dormant or minimally-metabolising for extended periods of time, waiting to make the most of erratic energy/nutrient availability [35].



- **Time-variable or context-variable attributes.** Extending the point above, many organism attributes are not varied throughout a simulation. The dormancy problem above could be solved by including time or context-variable death rates and maintenance powers.
- **Predation.** For simulations of more complex life, some form of predation could be included, where some organisms can consume others.
- **Improvements to nutrient uptake** While this is discussed extensively in Chapter 5, it also merits mention here. Nutrient availability is a cornerstone of habitability as we understand it. However, unlike energy uptake and survival, little attention has been paid to generalising how organisms uptake and process nutrients. NutMEG includes a rudimentary method using pseudo first-order rate constants but to be reliably employed requires matching to empirical data which we do not have yet. Laboratory studies focusing on the uptake of specific CHNOPS elements is required to test this methodology. We explore nutrient limitation in Chapter 5 by changing parameters in the CHNOPSexchanger, but cannot consider nutrient limitation in Chapters 6 & 7 due to this lack of a known reliable input and theory.
- **Enhancements to NutMEG's native (geo)chemical modelling.** Chemistry in these versions of NutMEG is static, in that the chemical system is defined at initialisation and utilised by biology. Chemical inflows and outflows can be included, but there is no specific modelling of the chemical implications these have. Future versions of NutMEG should make further use of existing chemical models such as reaktoro or PHREEQPy to improve how it handles nonequilibrium environments. Native consideration of geochemical reactions, for example at rock-water interfaces will also significantly improve estimates in locations of interest to astrobiologists.
- **More pre-built instances of organisms and reactors.** More and more child classes stored in the saved\_systems and saved\_organisms modules can continue to be added to NutMEG as we develop its applicability to different species and environments.
- **Enhanced accessibility for users.** The ecosystem module attempts to streamline simulations as much as possible, but it could be made easier for users to interpret the output data. NutMEG does contain a nutfig module, designed to help users plot growth curves and plot habitability maps (see Chapters 6 & 7) using only a SimID, OrgID and/or LocID, but this could be enhanced for more complex applications.
- **More applications modules.** With each publication featuring NutMEG as the focus (Chapters 5–7) we have created a new applications submodule to make the analysis easily repeatable for other systems and organisms. The hope is that as more applications for NutMEG are established, the more

the applications submodule can flourish. Good examples could include introducing methods for the analysis of biosignature production or time-variability in organism behaviour.

Nonetheless, NutMEG has been successfully applied to several projects. Beyond the Venusian clouds [4] and exoplanet methanogenesis [5] examples presented in this chapter, NutMEG was used to parameterise an optimal Earth-like methanogen, assess the habitability of Enceladus' subsurface ocean, and predict its potential for biomass and biosignature production. These three applications are the focus of Chapters 5, 6 and 7.

# CHAPTER 5

---

## A typical optimal methanogen

---

Hydrogenotrophic methanogens are organisms of particular interest in astrobiology. They have an ancient, simple metabolism whose basic ingredients can be found across the universe.

In this chapter, which contains an article published in the **Journal of the Royal Society: Interface**, we parameterise hydrogenotrophic methanogens using data from laboratory studies on Earth for use with NutMEG. Then, we examine what our model predicts for their growth behaviour in energy- or nutrient-limited conditions. We also explore some further properties of the calculated rate constant.

### Subchapters

5.1	Introduction .....	122
5.2	Methods .....	124
5.3	Results .....	131
5.4	Discussion and conclusions .....	140
5.5	Extended methods .....	144
5.6	Remarks on the rate constant .....	147

**Box 5.1: Declaration**

Subchapters 5.1–5.5 make up a manuscript which has been published in **Journal of the Royal Society: Interface** following peer review [1]. Some minor formatting edits have been made to match the rest of this thesis, and what were supplementary figures have either been included in this chapter or others for the benefit of the reader. One figure and one table from this article have been relocated to elsewhere in this thesis and are referenced accordingly. Parts of the extended methods have also been moved to other parts of this thesis as indicated. They can be found in ‘paper excerpt’ boxes.

## A bioenergetic model to predict habitability, biomass and biosignatures in astrobiology and extreme conditions

P. M. Higgins and C. S. Cockell

2020

Please cite this work as:

Higgins P. M. and Cockell C. S. “A bioenergetic model to predict habitability, biomass and biosignatures in astrobiology and extreme conditions” *J. R. Soc. Interface*. **17**.171 (2020), p. 20200588 DOI: 10.1098/rsif.2020.0588

---

## Abstract

---

In order to grow, reproduce and evolve life requires a supply of energy and nutrients. Astrobiology has the challenge of studying life on Earth in environments which are poorly characterised or extreme, usually both, and predicting the habitability of extraterrestrial environments. We have developed a general astrobiological model for assessing the energetic and nutrient availability of poorly characterised environments to predict their potential biological productivity. NutMEG [Nutrients, Maintenance, Energy and Growth] can be used to estimate how much biomass an environment could host, and how that life might affect the local chemistry. It requires only an overall catabolic reaction and some knowledge of the local environment to begin making estimations, with many more customisable parameters, such as microbial adaptation. In this study, the model was configured to replicate laboratory data on the growth of methanogens. It was used to predict the effect of temperature and energy/nutrient limitation on their microbial growth rates, total biomass levels, and total biosignature production in laboratory-like conditions to explore how it could be applied to astrobiological problems. As temperature rises from 280 to 330 K, NutMEG predicts exponential drops in final biomass ( $10^9$ — $10^6$  cells L<sup>-1</sup>) and total methane production<sup>1</sup> (62—3  $\mu$ M) despite an increase in peak growth rates (0.007—0.14 hr<sup>-1</sup>) for a typical methanogen in ideal conditions. This is caused by the increasing cost of microbial maintenance diverting energy away from growth processes. Restricting energy and nutrients exacerbates this trend. With minimal assumptions NutMEG can reliably replicate microbial growth behaviour, but better understanding of the synthesis and maintenance costs life must overcome in different extremes is required to improve its results further. NutMEG can help us assess the theoretical habitability of extraterrestrial environments and predict potential biomass and biosignature production, for example on exoplanets using minimum input parameters to guide observations.

---

<sup>1</sup>The total methane production here refers to the total amount produced per litre in one full growth cycle.

## 5.1 Introduction

---

Astrobiology has the challenge of studying life on Earth in environments which are poorly characterised or extreme, usually both, and predicting the habitability of extraterrestrial environments. A habitable environment can allow an organism to undergo metabolic activity and hence maintain itself and grow or reproduce [22]. Locations of interest across the field vary: from extreme conditions on Earth [61], to the Martian surface [159] and subsurface [67, 68, 160, 161], icy moons (e.g. Enceladus [15]) and even exoplanets [71]. The extreme conditions expected in these targets are typically under-studied and often difficult to replicate in the laboratory. We set out to create a computational model which can help take steps towards answering three key questions in astrobiology using a minimal number of input assumptions:

- **How much biomass can we expect in a given environment?** If the availability of energy and nutrients is known, what biomass could theoretically be sustained and would it reach detectable levels? Where, in the myriad of astrobiological targets is the best place to look for it?
- **What are life's minimum requirements?** Beyond water, life also needs a supply of energy and nutrients in order to grow and reproduce [10, 12], but what is the minimum supply of these required to remain viable?
- **What markers could extraterrestrial life be leaving for us to search for, and will they be in detectable quantities?** If the minimum requirements are met and we can expect some biomass, what signatures could life be leaving? Biosignatures can take many forms, and regardless of whether we look to the solar system or beyond to exoplanets [125], we must focus on those which are most likely to be above detection limits.

Biogeochemical modelling has been used extensively in an attempt to understand regions of the Earth that are not easily accessible, such as hydrothermal vents [e.g. 108–110, 162], the marine subsurface [e.g. 39, 41, 111], drylands [e.g. 112], and the atmosphere [e.g. 113]. These modern ecological models can provide very effective results, but have high specificity and still require a large number of potentially complex input parameters and knowledge of the systems they aim to replicate.

Alternatively, there are many routes to estimating biomass yields from a more theoretical basis [e.g. 78, 79, 160], but often little attention is paid to differing environments and the effect of extremes such as temperature and salinity. In geomicrobiology and environmental microbiology, many of these extremes are more commonplace. A comprehensive method of modelling growth energetically

in these natural settings is described by LaRowe and Amend [39, 40], in which the rate of change in total biomass is calculated by considering the balance between energetic supply and demand. Such a general approach is required for astrobiology, albeit more agnostic and requiring fewer known variables because often little is known about astrobiological targets. Furthermore, extraterrestrial life, if it exists at all, may not necessarily behave in the same way as Earth life. Nonetheless, it must be bound by the laws of thermodynamics and we could reasonably take this as a starting point to assess the biological potential of any extraterrestrial environment.

This study focuses on assessing habitability using an energetic and kinetic approach. The energetic approach to habitability [10, 11] parameterises the way in which biology interacts with its environment in terms of energy, based on the notion that an appropriate supply of energy and nutrients is necessary for life to synthesise the complex structures required for metabolism, growth and reproduction. A multitude of energy sources are possible, but when one thinks of energy as a fuel for life the most common method of uptake is through chemical pathways featuring redox couples, occasionally involving the absorption of radiation [10]. This energetic uptake can be quantified by calculating the free energy  $\Delta G$  [J mol<sup>-1</sup>] of the relevant process(es).  $\Delta G$  is a measure of the spontaneity of a chemical reaction, demonstrating whether it is a net source or sink of energy. A negative  $\Delta G$  describes a spontaneous process — one in which energy is released — such as in the break down of polymers or simple metabolisms, and a positive  $\Delta G$  requires net energetic input, such as building new biomacromolecules. Free energies vary with the local composition, temperature and pressure [131].

Organisms grow and reproduce by using overall energy-yielding reactions with negative  $\Delta G$  to drive energy-consuming reactions with positive  $\Delta G$  [10]. More important, however, is the rate at which the organisms can access this energy — the available power  $P$  [W] [12]. To calculate this one must also be aware of the kinetics of these biologically-mediated interactions, which are strongly dependent on the energetic availability and physicochemical environment [135]. Principally, the metabolic reaction must provide enough power to overcome the energetic costs of survival [12] (for example, overcoming rates of amino acid racemization with temperature [37]).

A simple organism can direct its energy supply into either growth or maintenance processes [40]. For this work, growth processes are those concerning the energetic cost of biosynthesis (i.e. building new biomass), and all other mechanisms of energetic loss are considered maintenance processes. In reality, the computation of both these contributions is complex, with the compounding effects of temperature [e.g. 24, 25], pressure [e.g. 26], salinity [e.g. 27], pH [e.g. 28], nutrient availability [e.g.

29] *etc.* each contributing to the organism's ultimate fate [9, 10, 163]. The actual power organisms use for maintenance also varies with growth phase and substrate availability [23].

We present a novel computational model which can estimate maintenance costs in extreme and/or nutrient limited environments from theory or empirical data. It can predict theoretical biomass levels and rates of biosignature production from as little as an overall catabolic reaction in poorly characterised, extreme (extra)terrestrial environments and other locations of astrobiological interest. A collection of organisms and their local environment are considered as self-contained objects communicating only via energy and nutrient exchange. The notion of modelling certain bioenergetic processes such as metabolism in a modular fashion has been suggested before [164] although it has also been recognised that modelling life in extreme environments, for which there is little information, is difficult [10]. The model's simplicity does come with some caveats and these will be discussed.

## 5.2 Methods

---

### 5.2.1 | An efficiency based model for microbial growth

For any given organism, the power going into growth processes must be a fraction of the power supply from metabolism, as other energetic processes necessary for maintenance must take precedence [10, 135]. Beyond this primary limitation due to maintenance, the ability of an organism to grow new biomass can also be restricted by the availability of key nutrients. The majority of biological matter is made up of six elements: carbon, hydrogen, nitrogen, oxygen, phosphorus and sulphur, hitherto referred to as 'CHNOPS' elements [9].

We have developed Nutrients, Maintenance, Energy, and Growth [NutMEG], an open source Python module for predicting growth behaviour of life in poorly characterised environments [3]. To do so, it estimates the free energy  $\Delta G$  of internal cellular processes corresponding to: metabolism (Section 5.5.2); growth (Section 5.5.4) and optionally maintenance, and the rate of these processes (Section 5.5.3). This novel schema offers several benefits. The use of kinetics allows for more realistic consideration of the thermodynamics at play governing metabolic rates [135] rather than simply using static total energetic availability to predict biomass. By monitoring metabolic rates and nutrient uptake,  $\Delta G$  is dynamically corrected



as the organism(s) interact with the environment (via Equation 5.4, Sec. 5.5.2). This allows us to also consider external effects on the metabolic energy yield with time, such as an abiotic source or sink of substrate. The minimum required input parameters for a growth prediction are shown in Table 5.1.

NutMEG considers cells as small engines whose growth is throttled by a maintenance efficiency  $\mathcal{E}_M \in [0, 1]$  (equivalent to  $1 -$  the fractional energetic cost of maintenance vs. the energetic supply). Hence, with an instantaneous power supply  $P_S(t)$  and maintenance cost  $P_M(t)$ , both in  $\text{W cell}^{-1}$ , the net power available as fuel for growth,  $P_F(t)$  [ $\text{W cell}^{-1}$ ] is:

$$P_F = P_S - P_M = \mathcal{E}_M P_S \quad (5.1)$$

Growth also necessitates the availability of nutrients to build the new biomass. If nutrient uptake can also be characterised as an efficiency  $\mathcal{E}_{UT} \in [0, 1]$  then the final power which can be used for biomass production,  $P_G(t)$  [ $\text{W cell}^{-1}$ ], is:

$$P_G(t) = \mathcal{E}_{UT} [\mathcal{E}_M [P_S(t)]] \quad (5.2)$$

Further details on how these efficiencies are parameterised and calculated can be found in Subchapter 5.5. This schema is shown in Figure 4.1.

To convert this growth power into new biomass, one must know the energy required to synthesise each cell from the nutrients available  $E_{\text{syn}}$  [ $\text{J cell}^{-1}$ ] (Section 5.5.4). Then, if either the energy or nutrient supply is the limiting factor in growth and not the rate of biomass production, for a suitably small time step  $dt$  [s], the total biomass  $B(t)$  [cells] is:

$$B(t + dt) = B(t) \left( 1 + \frac{E_G(t, dt)}{E_{\text{syn}}} \right) \quad (5.3)$$

where  $E_G(t, dt) = P_G(t) dt$  [ $\text{J (cell s)}^{-1}$ ] is the total energy each cell can contribute to growth per time step.

At first glance the simplicity of this model may give the impression of limited applicability. We argue that sorting processes into groups concerning supply, maintenance, nutrient uptake and growth is useful for determining how these factors could affect habitability. One can introduce unique traits of organisms without compromising computational efficiency (allowing for trivial inclusion of: life spans; unique rates for nutrient uptake, growth, metabolism; competition between organisms *etc.* (Section 5.4, 5.5)). At the same time, NutMEG allows flexibility in input for conditions which have limited data or large uncertainties (e.g. extraterrestrial environments), and can highlight areas in which a given

**Table 5.1 Minimal organism and environment parameters required to initialise a growth prediction and default parameters for NutMEG to output in time series.**

There are many more parameters included in the model for organisms which allow for fine tuning of a well-characterised species or an exploration of possible parameter spaces for others. Further information on what can be changed can be found in NutMEG's documentation. By default, *E. coli*-like parameters are chosen unless otherwise specified. Where these are unavailable, other model organisms are used and these are noted in the documentation. Using inheritance, one can increase specificity for organisms or environments allowing new parameters or adaptations to be introduced. The order of the catabolic reaction is given by  $z$ .

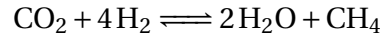
Organism parameter	Symbol	Unit
Rate constant of catabolism	$k_M$	$M^{(1-z)} s^{-1}$
Rate constants of nutrient uptake	$k_x$	$s^{-1}$
Catabolic reaction	–	–
Environment parameter	Symbol	Unit
Composition activities or molarities	$[x]$	– or M
Temperature	$T$	K
Pressure	$p$	Pa
Volume	$V$	$m^3$
pH	pH	–
NutMEG output	Symbol	Unit
Population	$B$	cells
Population volume	$V_{BM}$	$m^3$
Free energy of catabolism	$-\Delta G_A$	$J (mol CO_2)^{-1}$
Free energy of ATP production	$\Delta G_C$	$J (mol CO_2)^{-1}$
Rate of catabolism	$r_{cat}$	$(M CO_2) s^{-1}$
Available power supply	$P_S$	$W cell^{-1}$
Maintenance as a fraction of supply	$1 - \mathcal{E}_M$	–
Power available for growth	$P_G$	$W cell^{-1}$
Growth rate	$\mu$	$s^{-1}$
Composition activities or molarities	$[x]$	– or M
Rates of nutrient uptake	$r_x$	$M s^{-1}$

environment or organism requires better understanding. For example, in-keeping with the concepts outlined above, one could define upper and lower efficiencies required for life in various environments, i.e. best-case and worst-case habitability assessments.

### 5.2.2 | Configuration against empirical methanogenic growth data

By either calculating or estimating the total efficiency ( $\mathcal{E}_{UT}\mathcal{E}_M$ ), NutMEG can be used to simulate both extreme environments in which specific maintenance calculations need to be performed, and those which have limited data sets. This flexibility makes NutMEG an appropriate model for examining the habitability of extraterrestrial and extreme environments.

To demonstrate the model concept and explore how restricting the availability of energy or nutrients can affect microbial growth behaviour, a simple model of methanogens growing in both optimal and energy/nutrient limited environments was produced. Hydrogenotrophic methanogens were selected because their metabolism is thought to be ancient, and their use of hydrogen and carbon dioxide has made them of interest in astrobiology. Methanogens could use these primordial gases on other planetary bodies as a redox couple:



Methanogens can grow in numerous extreme environments, including at a wide range of temperatures, pH extremes, pressures and salinities [165]. There are multiple locations in the solar system whose physicochemical environments are known or suspected to overlap with those habitable to methanogens on Earth, including Mars [161] and Enceladus [15].

First, an organism is selected and parameterised in its optimum environment for use with NutMEG, then energy and nutrient limitation is simulated to demonstrate how that affects growth rates, biomass levels, and biosignature (methane) production.

### 5.2.2.1 | Modelling empirical methanogens

To ensure simulation results were realistic reflections of biological behaviour, we matched NutMEG's results to empirical data for methanogens. NutMEG was used to reparameterise data from hydrotrophic methanogen growth experiments into the required format and find  $P_M$  in optimal conditions for a variety of temperatures. To achieve this, growth prediction simulations (Section 5.5.1) were performed on methanogens for which data on: cell volume, optimal growth rate, optimal temperature, optimal pH, optimal pressure, substrate headspace composition, and growth rate calculation methods were available from the phymet2 database [166]. The growth rate calculation methods were found in the publications referring to specific species. Substrate concentrations were inferred from the headspace composition [4], which for all methanogens was  $H_2:CO_2 = 80:20$ .

The reaction quotient and rate constant of methanogenesis are also necessary for the growth prediction (Section 5.5.2, 5.5.3). Computing the quotient requires the concentration of  $CH_4$ , and the rate constant can be estimated from its rate of change. Of the methanogens in the database, 40% of growth rates were calculated using Powell (1983)'s method [167], which uses  $CH_4$  rates of change, with the remainder being from OD measurements or cell counts. Powell's technique was used in reverse to estimate the rate of change of  $[CH_4]$  for each empirical methanogen. The methane concentration was set at  $3 \times 10^{-8}$  M, as this corresponds to a maintenance power equivalent to Tijhuis et al. (1993)'s prediction [60] at 300 K. We chose to match to this value as Tijhuis et al. (1993)'s maintenance costs are based on empirical data, the majority of which are around this temperature. It was used as a conservative benchmark; recent analyses suggest it may be an overestimate of maintenance [23].

As this data pertains to methanogens growing optimally in growth media, it is assumed that they are not nutrient limited e.g.  $\mathcal{E}_{UT} \sim 1$ . It follows that in optimum conditions the difference between  $P_G$  and  $P_S$  for these organisms is the maintenance power  $P_M$  [W cell $^{-1}$ ].

### 5.2.2.2 | A typical optimal methanogen [TOM]

When outside their optimal growth temperature range, each of the methanogens would be affected in different ways depending on their unique physiology. This is due to differences between the methanogens themselves (e.g. their size, adaptations for maintenance, synthesis energy (Section 5.5.4) *etc.*), and uncertainty in the

empirical data. The data used originates from a variety of experimental procedures performed at various times over the past 50 years, many of which without reported confidence values [166]. Some of the methanogens in the database were also noted as requiring extra nutrients than standard media (15%), formate or acetate as additional substrates (8%), or were also observed reducing sulphur (6%).

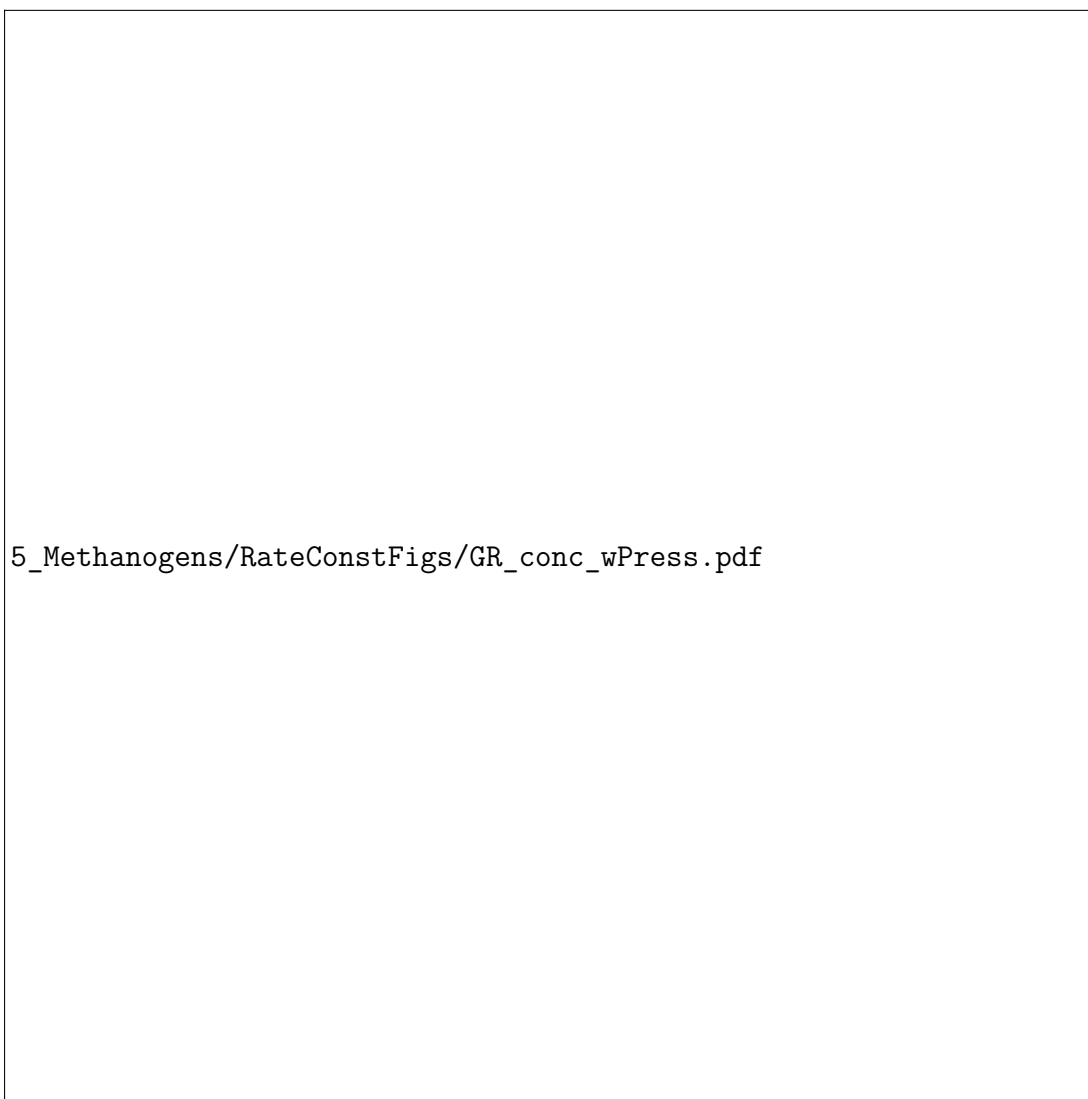


**Figure 5.1** The rate of CH<sub>4</sub> consumption and growth rate of real methanogens in optimal settings, with those of the typical optimal methanogen for comparison. Linear regression of the rate of CH<sub>4</sub> consumption [mol (cell s)<sup>-1</sup>] and growth rate [s<sup>-1</sup>] for the typical optimal methanogen (black line) with the equivalent for the empirical methanogens (blue). In the published article, this was supplemental figure S2. This has been updated since then to also show the optimal pressure of the methanogens, discussed in Subchapter 5.6.

To isolate the effect of temperature on energy and nutrient limitation, a **typical optimal methanogen** [TOM] was created. The TOM is an artificial methanogen, designed to behave as if any given temperature were its optimum by mimicking the growth behaviour of a real methanogen which is well-adapted to said temperature. It had the mean of each of: cell volume ( $3.44 \mu\text{m}^3$ ), optimal pH (6.9), and optimal local pressure (182 kPa) of the database methanogens as described above. Maintenance powers were estimated using an identical procedure to the empirical methanogens; the calculated  $P_M$  for the TOM is the reduction in  $P_S$  required to match its growth rate. This growth rate is estimated from a linear regression of the database methanogens' optimal growth rates with temperature (Figure 5.1).

## 5.3 Results

### 5.3.1 | Maintenance costs of methanogens

Values of  $P_M$  were selected which yielded the empirical growth rates for each empirical methanogen (Figure 5.2, blue crosses). While the different methanogen species clearly have different maintenance powers, an exponential trend upwards with increasing temperature can be seen, consistent with previous studies [60]. The maintenance power of the TOM follows a similar trend (Figure 5.2, orange bar).

Below temperatures of 280 K, one bound of the TOM's maintenance power range (corresponding to an ATP yield of 0.5 mol per mol  $\text{CO}_2$ ) drops significantly (i.e.  $\mathcal{E}_M \rightarrow 1$ ,  $P_M \rightarrow 0$ ). A  $P_M$  of 0 is nonphysical, and this reflects a scenario in which NutMEG predicts that the  $P_S$  is less than the  $P_G$  required to match the target growth rate. This suggests that methanogens at low temperatures must be metabolically efficient and able to metabolise more moles of ATP per mole of  $\text{CO}_2$  or have lower energies of cell synthesis. It should be noted however that this occurs outwith the temperature range for which methanogen data was available (288–371 K) [166] and our logarithmic extrapolation of target growth rates (Figure 5.1) could be unreliable.

These maintenance power predictions can be compared with previous theoretical and empirical estimations. Tijhuis et al. (1993) [60] used empirical data to estimate the maintenance power requirement with temperature for *E. coli*. Shown in black in Figure 5.2 is the Tijhuis prediction for a cell with the same size as the TOM. Also shown in Figure 5.2 are theoretical estimates generated using Lever et al. (2015)'s method whereby minimum thermodynamic maintenance predictions are based on



**Figure 5.2 Predicted maintenance power required for the empirical methanogens and typical optimal methanogen [TOM]** . This shows the required maintenance cost [ $\text{W cell}^{-1}$ ] for the TOM (orange line) and empirical methanogens (blue crosses) to grow optimally at various temperatures. For both, error bounds indicate possible variations in power supply due to variation in ATP yield per  $\text{CO}_2$  metabolised; between 0.5 and 1.5 [168, 169]. Initial  $[\text{CH}_4]$  was unknown in the data, so a value which yielded a maintenance cost equivalent to Tijhuis et al. (1993) [60] at 300 K for the TOM was used. The red vertical line shows the limit of our confidence in TOM maintenance powers when the ATP yield is 0.5 because at temperatures below this they converge to zero, which is nonphysical.



protein replacement after racemization [37]. The lines on Figure 5.2 represent the cost of protein replacement to the TOM after 2% or 10% racemization of the amino acids in an average protein.

### 5.3.2 | Energy and nutrient limitation of the TOM

NutMEG was used to artificially limit the availability of energy and nutrients to explore the effect they would have on the predicted growth rates, biomass levels, and total  $\text{CH}_4$  produced by the TOM. Figure 5.3 shows growth curves for the TOM with its calculated maintenance cost at 280 K, 300 K and 330 K. Figure 5.4 shows the peak growth rate, final biomass, and total  $\text{CH}_4$  production for temperatures between 280 K and 330 K. For both figures, each column represents the effect of a specific limiting factor on the organism. These include reducing the initial concentration of dissolved metabolic substrates  $\text{CO}_2$  and  $\text{H}_2$ , or nutrient sources P (the sole phosphorus source), or limiting the rate constant with which the organism can access phosphorus (Section 5.5.5). All simulations were performed in 1 L ‘vessels’ saturated in nutrients apart from the phosphorus limiting simulations.

#### 5.3.2.1 | Growth curves

When the concentration of either  $\text{CO}_2$  or  $\text{H}_2$  is restricted with no other changes to the organism or environment, growth curves become more characteristic of inhibited microbial growth as shown in Figure 5.3. For higher temperatures, the effect of limiting  $\text{CO}_2$  and  $\text{H}_2$  becomes more pronounced, with little to no growth at 90% optimal  $[\text{CO}_2]$  at 330 K compared to almost optimum growth at 280 K. This is due to the higher maintenance power at higher temperatures (Figure 5.2).

Limiting the concentration of available nutrients places a cap on the growth curves when all of the available phosphorus is locked in biomass for the cooler environments with slower growth (Figure 5.3 centre-right, top & middle). This demonstrates that the rate of uptake of phosphorus is not the key limiting factor until there is too little remaining to sustain exponential growth of a large culture. At 330 K, the growth rate is also limited by a lower  $[\text{P}]$ , due to the overall uptake rate (below, Section 5.5.5) running slower than the metabolism.

If instead of changing the concentration of available phosphorus the uptake rate constant  $k_P$  was changed (parameterising phosphorus' bioavailability and microbial adaptation to its uptake), the growth rate slows but there is little impact on biomass levels. This is because the growth rate becomes nutrient limited i.e. phosphorus uptake rather than the metabolism is determining the rate of biomass production, but there remains enough phosphorus to continue building large cultures. The final biomass is still lower than the optimal alternative because the methanogens are surviving for a longer period of time and hence more of the available energy in the system has been diverted to maintenance costs before reaching the limit of microbial growth. Specific characteristics of the growth curves and how they change with temperatures can be examined in further detail.

### 5.3.2.2 | Growth rates

There is an exponential increase in peak growth rate with temperature for the TOM in its optimal conditions (Figure 5.4, top row). When restricting substrate concentration to a fraction of the optimal dissolved amount, the effect on growth rate becomes more pronounced at higher temperatures. This is due to the higher maintenance power predicted for the TOM at higher temperatures (Figure 5.2). The initial  $\mathcal{E}_M$  value decreases with increasing temperature because maintenance costs become a larger fraction of power supply. As  $\mathcal{E}_M \rightarrow 0$  the TOM can tolerate smaller deviations in substrate concentration before maintenance power exceeds power supply and the growth rate  $\rightarrow 0$ .

With limiting nutrients, different effects are seen depending on the extent to which we restrict [P]. For this example, when restricted to  $10^{-8}$  M there is no slow down in growth rate meaning the TOM remains energy limited at all temperatures while in its exponential phase. When restricted instead to  $10^{-10}$  M the growth is nutrient limited for temperatures  $> 300$  K meaning the rate of uptake of phosphorus cannot meet the demands for biosynthesis made by  $P_F$  (Section 5.5.1). For all temperatures above 300 K the growth rate is then restricted by this uptake rate. Changing the phosphorus uptake rate constant more explicitly limits the nutrient availability for reasons discussed above.



**Figure 5.3 Growth curves of simulated typical optimal methanogens [TOM] under energy or nutrient limitation.** The TOM, methanogens which exhibit maximum growth rates across given temperatures, are shown growing in their optimal conditions in each subplot and growing in energy or nutrient limited conditions at various temperatures. Columns from left to right show the effect of  $[\text{CO}_2]$ ,  $[\text{H}_2]$ ,  $[\text{P}]$ , and  $k_P$ , the latter the rate constant of phosphorus uptake. Each row shows the same changes at different temperatures. The optimal dissolved  $[\text{CO}_2]$  and  $[\text{H}_2]$  vary with temperature (Figure 5.5) so changes are shown with a % change on the optimal concentration at that temperature. The filled-in segments show variation in growth curves at various yields of ATP per mol  $\text{CO}_2$  — between 0.5 and 1.5. Where the dark blue curve appears absent it is obstructed by the light blue curve; for these cases  $\mathcal{E}_{UT} = 1$  and energy is the main limiting factor, as increasing nutrient availability does not increase growth rates.



5\_Methanogens/BioenergeticModel\_Thesis/F4\_temperaturecurves.pdf

**Figure 5.4 Peak growth rates, final biomass values and total CH<sub>4</sub> production of the simulated typical optimal methanogens [TOM], growing under energy or nutrient limitation.**

The TOM, methanogens which exhibit maximum growth rates across given temperatures, growing in their optimal conditions are shown by the dark blue line in each subplot and growing in energy or nutrient limited conditions at various temperatures. For the TOM in energy and nutrient saturated conditions, as temperature rises from 280 to 330 K NutMEG predicts exponential drops in final biomass ( $10^9$ — $10^6$  cells L<sup>-1</sup>) and total methane production (62—3  $\mu$ M) despite an increase in peak growth rates (0.007—0.14 hr<sup>-1</sup>). Equivalent doubling times are ~100—5 hr. Columns from left to right show the effect of [CO<sub>2</sub>], [H<sub>2</sub>], [P], and  $k_P$ , the latter the rate constant of phosphorus uptake. The optimal dissolved CO<sub>2</sub> and H<sub>2</sub> vary with temperature (Figure 5.5) so changes are shown with a % change on the optimal concentration at that temperature. The filled-in segments show variation in growth curves at various yields of ATP per mol CO<sub>2</sub> — between 0.5 and 1.5. Where the dark blue curve appears absent it is obstructed by the light blue curve; for these cases  $\mathcal{E}_{UT} = 1$  and energy is the main limiting factor, as increasing nutrient availability does not increase growth rates.

### 5.3.2.3 | Biomass levels

With increasing temperature the final expected biomass in the vessel decreases exponentially. This is due to the effects on  $\mathcal{E}_M$  described above. Reducing substrate availability exacerbates this by decreasing net power supply while maintenance power remains constant, decreasing  $\mathcal{E}_M$  further until the energy limitation renders the environment uninhabitable to the TOM at these maintenance powers. It has been postulated, however, that in extreme energy-limited systems some organisms focus on other processes at the expense of repairing non-fatal protein degradation, reducing the maintenance by up to 95% [23, 37].

The availability of phosphorus also affects the final biomass levels. When  $[P] = 10^{-8}$  M, while growth rates in the exponential phase are the same as the optimum, growth arrest begins sooner, but not until phosphorus is completely exhausted at lower temperatures (Figure 5.3 centre-right top). At temperatures  $>315$  K, growth stops before all of the phosphorus has been consumed, hence there is only energy limitation in this scenario. When  $[P] = 10^{-10}$  M, there is a gentle increase in final biomass with temperature because at lower temperatures there is slower growth and more energy overall is used for maintenance before nutrient limitation becomes important. However, there is a peak in biomass at  $\sim 310$  K after which the energy limitation also becomes important, as above for the  $10^{-8}$  simulation. When decreasing  $k_p$  the final biomass falls with temperature at an increased rate due to a larger amount of energy being used for maintenance in total throughout the lifetime of the simulation.

### 5.3.2.4 | CH<sub>4</sub> production

The total CH<sub>4</sub> production has a qualitatively similar trend to total biomass production with temperature: at increased temperature the final methane concentration decreases exponentially. This suggests that net biosignature production of thermophilic methanogens in closed systems could be lower than their psychrophilic counterparts. It is important to note though that the faster metabolism and growth rate with temperature means that the rate of CH<sub>4</sub> production is higher at higher temperatures but growth arrest occurs sooner leading to this lower overall CH<sub>4</sub> production. In natural systems with substrate replenishment this may not be the case (e.g. hydrothermal vents).

Restricting  $[P]$  reduces total  $\text{CH}_4$  production at lower temperatures (Figure 5.4, centre-right bottom). At the lower  $P_M$  at these temperatures, the organism is nutrient limited because less energy is required for maintenance. The  $\text{CH}_4$  production increases for these nutrient limited organisms with temperature until energy becomes limiting (at 285–295 K for  $[P] = 10^{-8}$  M and 300–305 K for  $[P] = 10^{-10}$  M) and total  $\text{CH}_4$  production begins to decrease again, for reasons discussed above. These results show that as extreme environments require more energy to survive, biosignatures produced by the overall metabolism (methane in this case), will be produced at a higher rate per unit biomass.



**Figure 5.5 Concentration of dissolved  $\text{CO}_2$  and  $\text{H}_2$  at different temperatures from a typical laboratory setup for methanogens.** This is the ‘optimal’ concentration of  $\text{CO}_2$  and  $\text{H}_2$  at different temperatures. Dissolved gas concentrations were calculated using a headspace gas composition of  $\text{H}_2:\text{CO}_2 = 80:20$  at 182 kPa and the method described in [4].  $[\text{CH}_4]$  was kept constant at  $3 \times 10^{-8}$  M. In the published article, this was supplemental figure S3.

### 5.3.3 | Alternative explanation: synthesis energy

One input variable to NutMEG which is difficult to estimate is the energy required to synthesise a cell  $E_{\text{syn}}$ . For this study it was estimated by combining the energetic cost of amino acid synthesis [138] in anoxic environments and the cost of protein synthesis from these amino acids (Section 5.5.4; [136, 137], and increases with the local temperature (Figure 3.3). Were  $E_{\text{syn}}$  larger, a lower maintenance power would be required for NutMEG's output to match the empirical growth data (Section 5.3.1). Figure 5.6 shows the proportion with which  $E_{\text{syn}}$  needs to be increased such that the maintenance power required to match empirical growth rates would be zero — a scenario classically considered by Monod kinetics [73], though thermodynamically unrealistic [10]. At temperatures exceeding 320 K  $E_{\text{syn}}$  would need to be corrected by an order of magnitude or more to minimise  $P_M$ , but in these conditions the maintenance cost would be non-zero [10, 37, 45, 60]. At less extreme temperatures,

5\_Methanogens/BioenergeticModel\_Thesis/F5\_Esynthmesh.pdf

**Figure 5.6** Factor by which the synthesis energy of the typical optimal methanogen needs to be increased for the optimal maintenance power to be zero. The correction to the  $E_{\text{syn}}$  needed for the maintenance to be zero while still returning empirical growth rates. More realistic  $E_{\text{syn}}$  values could be between the values used for this study and the values on this contour.

such as 300 K, a correction of less than 10x would minimize the maintenance contribution required. Even if this were the case, one would expect that the growth curves and biosignatures in Figures 5.3 and 5.4 would be similar — perhaps with more  $\text{CH}_4$  production if  $\mathcal{E}_M \rightarrow 0$  after more substrate usage due to the lower maintenance power.

## 5.4 Discussion and conclusions

---

A common problem for astrobiologists is investigating the habitability of extreme environments on Earth or extraterrestrial environments for which we have very little information. We have developed a simple bioenergetic model for the dynamic monitoring of both organism and environment as they interact with one another, allowing for the study of growth rates, biomass production, biosignature (e.g. gas) production and other parameters. By matching the model predictions to laboratory observations we have investigated how placing a theoretical methanogen under either energy or nutrient limitation can affect the rates of microbial growth, total biomass production, and total  $\text{CH}_4$  production in closed, well-mixed systems. Increased energy and nutrient limitation restrict the total biomass expected — an important measure of habitability — increasingly at higher temperatures owing to the low energy yield of the methanogenesis metabolism and higher maintenance power. They also limit the total  $\text{CH}_4$  production, which would be an important biosignature for detecting methanogens on other planets, such as on exoplanets. The model's simplicity does mean that these results come with some caveats.

First, our results rely on the assumption that in optimal conditions the uptake of  $\text{CO}_2$  and  $\text{H}_2$  is the rate-determining step in the metabolism; a reasonable assumption for such a low-energy reaction. When calculating the effects of energy limitation there are two major effects on the simulation parameters. First is the free energy yield of the metabolism (Equation 5.4), second is the rate of the metabolism  $r_{cat} = r_+ F_T$  where  $r_+$  is the forwards rate of the metabolic pathway's rate-determining step, and  $F_T$  is a thermodynamic scaling factor [135, Sec. 5.5.3]. Here we assume that the rate-determining step is the uptake of  $\text{H}_2$  or  $\text{CO}_2$ , e.g.  $r_+ = k_M [\text{CO}_2] [\text{H}_2]^4$  where  $k_M$  is the rate constant of methanogenesis, but it could be from another step in the metabolism such as the phosphorylation of ATP or an enzyme-controlled interaction in the pathway [135]. If this were the case, and in our optimal conditions  $[\text{CO}_2]$  and/or  $[\text{H}_2]$  were well above the value at which their uptake would be the rate-limiting step, they could be lowered without effect until this were reached and energy limitation becomes important. From that point



on, one would achieve results qualitatively similar to those reported in this paper. Further laboratory experiments are required to help better understand at which  $[\text{CO}_2]$  and  $[\text{H}_2]$  accessing these substrates will become the rate-determining step, but in the meantime our results provide a qualitative view of what will happen at that stage.

The maintenance power was used as a single temperature dependent value, whereas in reality it would reflect the energy change from a series of chemical transactions the organism has made. For extreme conditions, the maintenance power should be computed explicitly for each adaptation to every given extreme [10] and NutMEG does allow for this. For example, the energetic cost of maintaining cellular pH against a gradient  $\Delta\text{pH}$  could be estimated as  $\Delta G = -2.3RT\Delta\text{pH}$  where  $R$  is the universal gas constant [10, 28]. The power cost can then be computed, if the rate of the mechanism is known. This knowledge is not available for many extremes, and different organisms will use different pathways with varying efficiencies. As a result, further understanding of microbial adaptations to extremes is required — either by predicting such pathways or finding their net minimum thermodynamically viable energetic cost [10, 163].

The maintenance power can also vary with the organism's growth phase and the local energetic availability [e.g. 23]. Most empirical data, including that used in this study, is based on measurements made in the exponential phase which are not representative of life in natural systems. In energy-limited systems, maintenance costs could be substantially lower than those calculated here [23], for example a recent study suggests that in Earth's deep subsurface most methanogens could be surviving on energy fluxes between  $\sim 10^{-19}$  and  $10^{-21}$  W cell $^{-1}$  [42]. For NutMEG to successfully simulate natural systems, better understanding of how organisms can survive on such low energy fluxes is required.

The synthesis energy was calculated by combining the cost of amino acid and protein synthesis, but our analyses would benefit from a more comprehensive complement of biomacromolecules. Proteins account for approximately 55% the dry mass content of *E. coli* in the exponential growth phase [137, 170], and the inclusion of other biomolecules such as RNA and lipids will improve the quality of this estimation. Similarly, protein repair is a key factor in maintenance costs but the cost of RNA repair becomes more important with increasing cell size [45]. Biomolecular content also varies significantly between species and growth phase and this should also be accounted for [170, 171].

NutMEG primarily predicts growth arrest when the maintenance power exceeds the supply power among other criteria, but there are other explanations of what could cause growth to stop. An example is the potential role of quorum sensing in some

bacteria [e.g 172], which means that some microbes will not grow until a critical cell density is achieved, even though theoretically the energy and substrates for growth are available. The problem with the specifics of growth arrest is that it is often tied to the specific physiology of particular species. NutMEG's philosophy in part relies on having minimal ties to the peculiarities of particular terrestrial organisms and instead opts for a general approach. Nevertheless, these specific behaviours could be included if one was modelling organisms in which one wished to investigate the influence of such characteristics on biomass or biosignature production.

While the simulations we performed did predict growth, none reached a steady state with the environment. This is because there was no cell death or net inflow of substrates to sustain the methanogen population after  $\mathcal{E}_M \rightarrow 0$ . This would, inevitably, lead to the death of all of the organisms. This issue is mitigated in this study, as we explicitly considered laboratory-like 'vessels' as well-mixed closed systems for analysis. Mixing and diffusion effects will also need to be considered in wider astrobiological applications which would aim to achieve a steady state, such as the simulation of hot springs or oceans. Some small steps can be made with NutMEG to mitigate these issues, such as including net inflows or outflows of substrates. Omission of a cell death rate is common in simulations of cell dynamics, but it has been shown to be an important factor in maintenance considerations. Characterising its effects along with other kinetic factors such as growth rate are some of the major problems in the current understanding of maintenance requirements [163].

Other parameters within NutMEG can be altered and have a significant effect on growth rates, biomass, and biosignature production. To explore them we also trialled some simulations including: varying the maintenance power to see how less well-adapted organisms could be quantified or to what extent a new extreme could be tolerated; including a life span for the methanogens after which they become inactive; and including net sources/sinks of  $\text{CO}_2$  and  $\text{H}_2$  to dynamically change the energetic availability with time (Supplemental Animation). Increasing the maintenance power by up to 20% has a similar effect to the energy limitation across different temperatures. Inclusion of a lifespan reduces peak biomass values (and final active biomass falls to zero) but it did not significantly affect  $\text{CH}_4$  production.

Adding a net inflow of  $\text{CO}_2$  or  $\text{H}_2$  increased all three of the peak growth rates, biomass levels, and biosignature production as this is fundamentally the opposite of energy limitation. However, reservations must be made when considering these predictions, as the growth of real methanogens is likely limited by the rate-determining step, such that decreasing the availability of nutrients may slow growth down, but increasing nutrients will not necessarily enhance growth any further. Adding a sink of  $\text{CO}_2$  or  $\text{H}_2$ , for example by abiotic processes or a competing organ-

ism, has a similar effect to energy limitation. There are examples of natural systems exhibiting higher cell concentrations than those achievable in the laboratory [e.g. 173]. Properly including sources and sinks of potential substrates and nutrients could help explain these observations; our results suggest that sometimes slower peak growth rates could produce higher concentrations of biomass given enough time.

As some of the results presented in Section 5.3.2 predict growth on the scale of years, resupply of substrates will be of particular importance when estimating how much biomass such an environment could sustain for these long periods of time. There could also be a significant influence from other CHNOPS elements, nutrients and micro-nutrients, which should be included if they act as a significant limiting factor. For example, observations from the Cassini spacecraft suggest Enceladus' subsurface ocean may contain the major ingredients of methanogenesis in an energy-yielding configuration [e.g. 15]. Phosphorus is the only CHNOPS element yet to be directly detected [13, 15], but a recent study suggests it could be as low as  $\sim 10^{-10}$  M [106], a level at which our results suggest nutrient limitation could be important. This tenuous energetic and nutrient landscape provides a salient example of how NutMEG could be applied to astrobiological problems.

When attempting to model extraterrestrial environments, existing studies generally infer possible energetic habitability from the free energy values alone [e.g. 15], or predict maximum biomass values from the total free energy available [e.g. 161]. NutMEG can offer valuable additions to such calculations by dynamically calculating the kinetics of metabolism, maintenance costs, and variation in free energy yield as the local composition changes with time. Monitoring of the organisms and environment also allows us to see the trends in biomass and biosignatures with time.

In conclusion, NutMEG offers a new computational technique to investigate habitability and potential growth, biomass and biosignature production in little understood terrestrial and extraterrestrial environments. It was used to predict that in energy and nutrient saturated conditions, there is an exponential drop in final biomass ( $10^9$ — $10^6$  cells  $L^{-1}$ ) and total methane production ( $62$ — $3$   $\mu$ M) despite an increase in peak growth rates ( $0.007$ — $0.14$   $hr^{-1}$ ) as temperature rises from 280 to 330 K for methanogens in ideal conditions. When placed in energy or nutrient limiting environments, all three parameters are further reduced.

In the future, NutMEG's credibility can be bolstered by comparing its first order predictions with empirical evidence from real extreme environments on the Earth. In extraterrestrial environments it can provide a basis for prioritising locations to be studied. Example applications could be to explore energy and nutrient availability

on Saturn's moon Enceladus or in the subsurface of Mars. Given the minimal observations and inferences available from exoplanets, NutMEG can also be used to explore the possible parameter space for expected biomass and gas production which can impact, and therefore be used to explain, exoplanetary spectra.

## 5.5 Extended methods

---

NutMEG has been developed as a wide ranging model to assess the key requirements of energetic habitability and a full complement of its applicability with further examples is available in its documentation. Here, we will summarise the key calculations performed for the results in this work.

### 5.5.1 | Implementation of growth prediction

To contextualise the calculations presented here, the reader may wish to first review NutMEG's most basic overall function — to predict growth curves. The overview of this process has been moved to Subchapter 4.3

The simulation can be ended when either user-defined criteria are met, or alternatively upon the death of all organisms or sufficiently low growth rate variability. For this work, the simulation ends when  $\mathcal{E}_M = 0$  for more than 10 steps, the metabolic rate drops below  $10^{-40}$  M CO<sub>2</sub> (cell s)<sup>-1</sup> for 50 steps, or the cell population reaches 0.

### 5.5.2 | Free energy availability in natural systems

The free energy of a chemical interaction can be expressed as:

$$\Delta G = \Delta G^\circ + RT \ln Q \quad (5.4)$$

where  $\Delta G^\circ$  [J mol<sup>-1</sup>] is the standard free energy of the interaction,  $R$  [J (mol K)<sup>-1</sup>] is the universal gas constant, and  $Q$  the reaction quotient all at temperature  $T$  [K]. Standard free energies of metabolisms are calculated using an SUPCRT92

database [132] and the reaktoro package for chemical systems<sup>2</sup>, which implements the revised HKF equations [34]. The free energy changes dynamically with the composition, so as the composition is updated in the implementation (Section 5.5.1) the available free energy per mole of substrate changes over time.

### 5.5.3 | Thermodynamically limited biochemical kinetics

This section has been moved to Section 3.1.4

### 5.5.4 | The energetic cost of cell synthesis

This section has been moved to Subchapter 3.2

### 5.5.5 | Nutrient limitation

In order to successfully build or repair a cell, an influx of CHNOPS elements is required. To calculate the possible rate of nutrient uptake, NutMEG requires the concentration of each nutrient  $\nu$  [mol L<sup>-1</sup>] in the local environment, and the associated rate constant for its uptake,  $k_\nu$  [s<sup>-1</sup>]. This rate constant could be extracted from empirical data using a similar technique to that used to extract the rate constant of methanogenesis (Section 5.2.2) if such data is available, though for this analysis an artificially high rate constant was used for each CHNOPS element as to separate it from other limiting factors (apart from when it was deliberately lowered e.g. Figures 5.3 and 5.4).

The uptake rate required to reach maximum efficiency for each CHNOPS element varies depending on how much is required in the cell itself. Table 4.1 summarises the standard dry weight percentage population by element for bacteria, slightly adapted to remove the 4% population of other elements. This composition was assumed for the simulated methanogens.

<sup>2</sup><https://reaktoro.org/index.html>

### **Acknowledgements**

This work was supported through the Science and Technology Facilities Council (STFC) grant ST/R000875/1 and an STFC studentship to PMH. We thank three reviewers for their detailed and constructive comments.

### **Author contributions**

PMH and CSC conceived the core concepts of the model. PMH developed the methodology and code, performed the simulations and analysis, and drafted the manuscript. CSC offered astrobiology and microbiology insight and guidance throughout the study and helped with the structure and editing of the manuscript.

### **Data accessibility**

All of the code required to replicate these results, as well as data files containing the data plotted in all figures are available in the NutMEG-Implementations GitHub repository, in the TOM directory:

<https://github.com/pmhiggins/NutMEG-Implementations>

NutMEG itself is available in the NutMEG public GitHub repository:

<https://github.com/pmhiggins/NutMEG>

## 5.6 Remarks on the rate constant

Further information can be extracted about the rate constant of methanogenesis than was when originally creating the TOM (Section 5.2.2). As defined, the TOM is only designed to change its behaviour with temperature and composition and otherwise behaves as the average methanogen in the database. This includes some environmental parameters: optimal pH (6.9) and optimal local pressure (182 kPa).

The rate constant of methanogenesis  $k_M$  was evaluated with the following expression:

$$k_M = \frac{r_{\text{CH}_4}}{[\text{CO}_2][\text{H}_2]^4} \quad (5.5)$$

where  $[\text{CO}_2]$  and  $[\text{H}_2]$  were calculated using the theory outlined in Appendix A.4 and depend on the temperature, pressure of the headspace and salinity of the media (the latter considered to be 0).

NutMEG's `base_organism.respirator` attribute uses the rate constant of reaction at 298 K as the default and corrects to the local temperature (Section 4.2.5.1). To do so it assumes the rate constant doubles for every increase by 10 K:

$$k_T = k_{298} \times 2^{\frac{(T-298)}{10}} \quad (4.6 \text{ revisited})$$

This is convenient when  $k(T)$  is only available for some values and it is necessary to extrapolate it out to some more, but in the case of the TOM there are range of temperatures available to fit so this estimation is not necessary.

When building the `TypicalOptimalMethanogen` for this publication, a computed  $k_M(298 \text{ K})$  was saved (at various T, and pressure 182 kPa) as input for its `respirator`. In other words, somewhat confusingly the  $k_M(298)$  values saved for the TOM vary with temperature  $T$  and are specifically for a methanogen adapted to temperature  $T$ , adjusted to 298 K and at 182 kPa. However, from Equation 5.5, the rate constant varies with pressure as well as temperature — because so too do the rate and dissolved gas composition — and hence it will need to be corrected accordingly. By considering the rate constants as dependent on temperature and pressure, the

following can be written:

$$\text{let } D(T_i) = 2^{\frac{(T_i-298)}{10}} \quad (5.6)$$

$$\frac{k_{298}(T_1, P_1)}{k_{298}(T_2, P_2)} = \frac{D(T_2) k_T(T_1, P_1)}{D(T_1) k_T(T_2, P_2)} \quad (5.7)$$

$$\text{and } \frac{k_T(T_1, P_1)}{k_T(T_2, P_2)} = \frac{r_{\text{CH}_4}(T_1, P_1) [\text{CO}_2]_{(T_2, P_2)} [\text{H}_2]_{(T_2, P_2)}^4}{r_{\text{CH}_4}(T_2, P_2) [\text{CO}_2]_{(T_1, P_1)} [\text{H}_2]_{(T_1, P_1)}^4} \quad (5.8)$$

$$\therefore \frac{k_{298}(T_1, P_1)}{k_{298}(T_2, P_2)} = \left( \frac{D(T_2)}{D(T_1)} \right) \left( \frac{r_{\text{CH}_4}(T_2, P_2)}{r_{\text{CH}_4}(T_1, P_1)} \right) \left( \frac{[\text{CO}_2]_{(T_2, P_2)} [\text{H}_2]_{(T_2, P_2)}^4}{[\text{CO}_2]_{(T_1, P_1)} [\text{H}_2]_{(T_1, P_1)}^4} \right)$$

This can be simplified. If  $T_1 = T_2$  then  $\left( \frac{D(T_2)}{D(T_1)} \right) = 1$  because  $D(T_i)$  is independent of pressure. We can approximate that  $\left( \frac{r_{\text{CH}_4}(T_2, P_2)}{r_{\text{CH}_4}(T_1, P_1)} \right)$  is dominated by the  $T_i$  contribution using the colourbar of Figure 5.8, meaning this term is also  $\approx 1$ . The  $k_{298}$  which is saved is for  $T = 298$  K and  $P = 182000$  Pa. Hence,  $k_{298}$  at pressure P can be written:

$$k_{298}(298, P) = k_{298}(298, 182000) \left( \frac{[\text{CO}_2]_{(298, 182000)} [\text{H}_2]_{(298, 182000)}^4}{[\text{CO}_2]_{(298, P)} [\text{H}_2]_{(298, P)}^4} \right) \quad (5.9)$$

This can be performed for each TOM at the relevant temperatures of this work. It adjusts the curve to match the empirical values at similar pressures more closely (Figure 5.7). Another method of accounting for the clear uncertainty of  $k$  invariant of pressure is employed in Chapters 6 & 7, we simply consider the full range of values from the parameter space (Figure 5.8).





**Figure 5.7 The methanogenesis rate constant of simulated and empirical methanogens.** The rate constant of the empirical methanogens' metabolism are shown as data points, and those for the typical optimal methanogen's metabolism are shown by lines, varying with temperature and pressure as outlined in the text.



**Figure 5.8 How variable rate constants can be used to cover the entire range of methanogenic growth behaviour** . This shows the total CH<sub>4</sub> production of methanogens considered in Higgins & Cockell (2020) [1] along with the equivalent value drawn from the typical optimal methanogen in that work (solid line, at 182 kPa). The dashed lines show the effect of changing the rate constant of methanogenesis ( $k_M$ ) by  $\pm 1$  order of magnitude. This is from Higgins et al. (2021) (ref. [2], Chapter 6), where it was Supplemental Figure S5.

# CHAPTER 6

---

## Habitable windows for methanogens on Enceladus

---

A potentially habitable world beckons as Enceladus, a tiny moon of Saturn, is one of the most exciting bodies for 21<sup>st</sup> century solar system astrobiology. Under its icy shell lies an ocean of weakly alkaline salty seawater which contains the ingredients of one of the earliest metabolisms to appear on Earth.

In this chapter, which is an insert of a manuscript published in the **Journal of Geophysical Research: Planets**, we examine the ‘snap-shot’ of Enceladus’ ocean observed by the Cassini spacecraft. We determine what combinations of its proposed global parameter space could yield habitable conditions.

### Subchapters

6.1	Introduction .....	155
6.2	Methods .....	156
6.3	Parameter space selection .....	160
6.4	Results .....	164
6.5	Discussion .....	176
6.6	Summary .....	183

**Box 6.1: Declaration**

This chapter is an insert of a manuscript which has been published in the **Journal of Geophysical Research: Planets** following peer review. Some minor formatting changes have been made to match the rest of this thesis, and supplemental information can be found in Appendix C.

In this chapter we regularly refer to ‘instantaneous power supply’, and ‘instantaneous habitability’. Often, a more suitable term would be to use ‘spontaneous’ in place of ‘instantaneous’, which is adopted in Chapter 7. However, to stay true to the original paper this terminology has been left as it was when published.

## Instantaneous habitable windows in the parameter space of Enceladus’ ocean

P. M. Higgins, C. R. Glein and C. S. Cockell

2021

Please cite this work as:

Higgins P. M., Glein C. R. and Cockell C. S. “Instantaneous habitable windows in the parameter space of Enceladus’ ocean” *Journal of Geophysical Research: Planets* **126.11** (2021), e2021JE006951. DOI: 10.1029/2021JE006951

---

## Key points

---

1. Key known drivers of the Enceladus ocean's habitability with respect to methanogens are identified and their uncertainties accounted for.
2. There is energy available for methanogens in most cases if the pH of the bulk ocean is less than 10.
3. Instantaneous microbial power supplies imply both habitable and uninhabitable conditions are possible.

## Plain Language Summary

---

Observations of Enceladus in recent years have revealed tantalising details of its potentially habitable subsurface ocean, allowing its conditions to be resolved in unprecedented detail compared to other icy moons. Still, the variation in possible parameters below its icy shell is huge, ranging from the cold bulk ocean with a pH similar to seawater on Earth to potentially scalding alkaline fluids at its depths. The ocean contains the ingredients of an ancient metabolism which is used by life on Earth by organisms known as methanogens. In this work, we explore the instantaneous habitability of Enceladus' subsurface ocean to methanogens using a range of environmental parameters informed by data from the Cassini mission and modelling. In other words, we ask: if Cassini's observations offered a 'snapshot' view of the ocean, does a habitable window exist within the uncertainty of the data, without considering as-yet unconstrained (but still important) variables such as a supply of nutrients? Some parameter combinations appear habitable, but not all the combinations are suitable for methanogens as we know them on Earth. We identify the most important drivers of habitability in Enceladus' ocean and explain how they can be better constrained by future research or space missions.

## Abstract

---

In recent years, Enceladus' subsurface ocean has become a tantalising case-study for potentially habitable conditions in an extraterrestrial ocean world. However, we still know very little about its subsurface conditions. Its oceanic composition is difficult to characterise with current data and estimates are highly dependent on model-based interpretations which are also not yet tightly constrained. In light of these uncertainties, we consider a wide selection of the inferred parameter spaces to quantify the energy available to putative hydrogenotrophic methanogens on Enceladus in the bulk ocean at cool and elevated temperatures. We estimate the instantaneous power supply their metabolism could provide in these conditions and compare it to expected power demands of life on Earth. To be habitable for methanogens a 273 K ocean with relatively high salt content must have  $\text{pH} < 10$ , and a relatively low salt ocean must have  $\text{pH} < 8$  at 273 K, or  $\text{pH} < 9$  when heated to  $> 360$  K. Some combinations meet the power demands of exponential growth, but large swathes of the parameter space appear energetically uninhabitable. The habitability of the Enceladus ocean for methanogens appears to be a delicate balance between its temperature, pH, salinity and concentrations of carbonates, nutrients and dissolved gases (particularly  $\text{H}_2$ ). Many of these parameters are co-dependent; variation in any one of them could tip the balance into uninhabitable conditions. Further constraining these variables should be a priority for future missions to ocean worlds in order to enable definitive assessments of their habitability.

## 6.1 Introduction

---

Enceladus is a unique and important target for astrobiology in the solar system. The icy moon has a large subsurface ocean [93, 174], and analysis of measurements by the Cassini mission show the existence of  $\text{CO}_2$ ,  $\text{H}_2$ , and  $\text{CH}_4$  — the reactants and products of the hydrogenotrophic methanogenesis metabolism — as well as salts, silica and organics [e.g. 13–15, 85, 100, 104]. These species were detected in plumes of gases and ice grains which erupt from Enceladus' south polar region. Determining the exact oceanic composition of these species from plume data has proven difficult. Estimates extend over many orders of magnitude and are strongly coupled to pH [15, 87], which is not well-constrained itself. Estimates of oceanic pH range between 8–13.5 with most studies settling on the weakly-alkaline end of this scale [e.g. 14, 85–87].

From the Cassini data there is limited information about the icy moon's subsurface ocean, but comparisons have been drawn to inhabited Earth systems such as sub-glacial lakes and alkaline hydrothermal vents [e.g. 43]. There is overlap in Enceladus' possible parameter space with those environments in which methanogens are known to grow and reproduce on Earth [165]. Enceladus' subsurface ocean has hence become a compelling target for geochemical and astrobiological modelling analyses [e.g. 15, 16, 19–21, 86, 87, 175].

Estimates of the icy moon's composition have been used to explore whether there is sufficient energy available to sustain life [e.g. 15, 19, 20]. This is achieved by estimating the Gibbs free energy  $\Delta G$  [ $\text{J mol}^{-1}$ ] of potential metabolic pathways, a measure of the energy that life can extract from chemical disequilibrium in an environment. These assessments are limited however because they depend upon the weakly constrained physico-chemical conditions in the ocean [18]. Waite et al. (2017) [15] identified that in the bulk ocean there is Gibbs free energy available through hydrogenotrophic methanogenesis and since then it has widely been assumed that there is energy for life on Enceladus. However, this is not conclusive evidence that the subsurface ocean is habitable. A more comprehensive picture requires 1) a wider parameter space, accounting for various expected temperatures, pressures, salinities, pH values and other relevant physico-chemical parameters; and 2) consideration of the thermodynamics and kinetics of microbial metabolism to assert whether the available energy could be biologically useful in those settings.

One way to assess habitability quantitatively is by computing the energy fluxes available to life (power supply) and comparing them to the energetic demands posed by its environment (maintenance, or power demand) [10]. The power

supply can be determined from a combination of the available  $\Delta G$  from a potential metabolic pathway — which is determined by the temperature, pressure and chemical composition — and kinetic factors related to the organism and its environment [1]. The power demand reflects the energetic cost of processes necessary for survival but not strictly related to growth. These could include the burdens of biomass degradation at elevated temperatures and pressures, or the toll of maintaining a consistent internal pH and cell composition at adverse pH and salinity, for example [10]. The maintenance power also varies with the growth state of the organism [23].

In this work, we examine the instantaneous habitability of Enceladus' subsurface ocean to hydrogenotrophic methanogens using a wide parameter space informed by Cassini data and modelling. This allows us to initially assess whether the ocean could be habitable based on observed parameters, at an instant in time, without requiring energy and nutrient inflows. We use a geochemical model coupled to a bioenergetic model to predict how the ranges of temperature, pressure, pH, salt content, and dissolved gas composition affect the ocean's habitability to Earth-like methanogens. This assessment is performed by first calculating the free energy yield of hydrogenotrophic methanogenesis, converting it to a microbially accessible power supply and comparing that to 1) typical maintenance powers and 2) known power supplies and demands associated with methanogens and other anaerobes on Earth.

## 6.2 Methods

---

The bioavailable power supply is determined by both the degree of energy availability in a system and an organism's ability to utilize that energy. These are governed by a combination of environmental (e.g. composition, temperature) and organismic (e.g. kinetics and energetic yield of metabolism) variables. For this work, a geochemical speciation model was used to estimate the dissolved gas composition and pH of the ocean under a variety of conditions. This was then used as an input to a bioenergetic model to compute the energetic availability and possible power supplies to hydrogenotrophic methanogens.



### 6.2.1 | Geochemical model

The thermodynamic drive for hydrogenotrophic methanogenesis depends on the activities of  $\text{CO}_2$ ,  $\text{H}_2$ ,  $\text{CH}_4$ , and  $\text{H}_2\text{O}$ . The activity can be thought of as an effective concentration that is used to quantify relative stability under non-standard conditions. Aqueous species' activities are based on the 1 molal (mole of solute per kg of water) standard state that is referenced to infinite dilution at any pressure and temperature, and the activity of  $\text{H}_2\text{O}$  is relative to the pure solvent.

The activity of  $\text{CO}_2$  in Enceladus' ocean was previously estimated by calculating the carbonate speciation at 0 °C [15], using the composition of major identified salts ( $\text{NaCl}$ ,  $\text{NaHCO}_3$  and/or  $\text{Na}_2\text{CO}_3$ ) in plume ice grains [14] and a suggested pH range of ~9–11 [88]. The activities of  $\text{H}_2$  and  $\text{CH}_4$  in Enceladus' ocean were estimated by assuming that the number ratios of these species relative to  $\text{CO}_2$  in the ocean are similar to those in the plume gas, and also assuming that the activities of neutral species can be approximated by their molal concentrations [15]. The activity of  $\text{H}_2\text{O}$  was set to unity, as is typical in fluids that are not highly concentrated in salts.

Here, we extend the dissolved gas model of Waite et al. (2017) [15] to elevated temperatures, motivated by the significant interest in hydrothermal environments on Enceladus [85, 94, 176]. Such systems (or parts of them) could serve as habitable zones inside Enceladus, so it is important to understand how the thermodynamics of methanogenesis would change at temperatures higher than that of the bulk ocean. To estimate the activities of methanogenesis reaction species above 273 K, we take the inferred ocean composition from Waite et al. (2017) [15] and respeciate the ocean water at different temperatures. This 'heated seawater' approach does not consider that chemical processes in hydrothermal environments such as water-rock interaction will increasingly contribute to the ocean composition in regions of elevated temperature. We do not include an estimate of the hydrothermal fluid composition on Enceladus beyond such heated seawater. However, it is a useful first step and may be relevant to possible Enceladean seawater aquifers and warmer regions of the ocean which are dominated by seawater, discussed further in Section 6.5. It also allows us to explore what happens in the hypothetical scenario where Enceladus' bulk ocean is heated up, and how this affects its habitability to methanogens.

The respeciation calculations are performed using the SpecE8 app in The Geochemist's Workbench 15, with the thermo.com.V8.R6+ database. This program calculates chemical equilibrium by simultaneously solving all of the equilibrium constant and mass balance relationships among aqueous species [177] in the simplified Enceladus ocean system of  $\text{Na}-\text{Cl}-\text{CO}_2-\text{O}-\text{H}$ . We represent the composition

of dissolved salts in the same way as done by Glein & Waite (2020) [87]. The two key model input parameters for the detected salts are the total concentration of chloride [Cl], and the concentration of dissolved inorganic carbon [DIC] (sum of the molalities of  $\text{CO}_2(\text{aq})$ ,  $\text{HCO}_3^- (\text{aq})$  and  $\text{CO}_3^{2-} (\text{aq})$ ). Postberg et al. (2009) [14] provide constraints on [Cl] ( $0.05\text{--}0.2 \text{ mol kg}^{-1}$ ) but only the sum of bicarbonate and carbonate ( $0.02\text{--}0.1 \text{ mol kg}^{-1}$ ). Because of this, we had to first find the corresponding [DIC] as a function of ocean pH. Once that value was obtained, SpecE8 was used to compute the concentration of Na via charge balance, and this value was then used to evaluate the pH at elevated temperatures.

At elevated temperatures, the activities of  $\text{H}_2$  and  $\text{CH}_4$  stay fixed at ocean values in our model because there are no alternative forms of these species (for simplicity, we do not consider redox reactions during the cooling trajectory, but these could be ongoing (discussed in Section 6.5.2)). In contrast, the activity of  $\text{CO}_2$  is allowed to vary because the carbonate speciation changes with temperature. This occurs because the equilibrium constants between carbonate species (e.g.,  $\text{CO}_2$ ,  $\text{HCO}_3^-$ ,  $\text{CO}_3^{2-}$ ) are temperature dependent, and the fluid pH co-evolves with the carbonate speciation. The activity of  $\text{H}_2\text{O}$  is also obtained as an output of these calculations.

### 6.2.2 | Bioenergetic model

The bioenergetic model NutMEG [1, 3] was used to compute Gibbs free energies of methanogenesis, ATP production and the power supply available for methanogens across the Enceladus ocean's parameter space. NutMEG is a Python package for predicting habitability and biomass in environments relevant to astrobiology. It casts microbial behavior in a quantitative framework and considers the power supply available for life in a given environment, the power demands associated with living in such settings, and the availability of key nutrients. In this work NutMEG was used to calculate the instantaneous bioavailable power supplies provided by the parameter space and compare them to the power demands experienced by life on Earth.

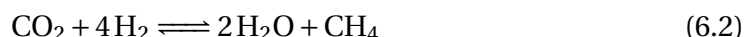
In order to compute the available Gibbs free energy, NutMEG requires the environmental temperature  $T$ , pressure  $P$ , and activities of all metabolic reagents. In addition to these, computing the bioavailable power supply requires a number of organism-specific parameters. These include: the rate constant of the metabolism  $k$  at  $T$  and  $P$ ; the net ATP yield  $n_{\text{ATP}}$  (the number of moles of ATP formed per mole of  $\text{CO}_2$  consumed); and the cell composition. These latter variables have been constrained previously for hydrogenotrophic methanogens (Section 6.3.3, Supplemental Figures S1, S4, S5, Higgins & Cockell (2020) [1]). NutMEG calculates the

bioavailable power supply using thermodynamically limited biochemical kinetics, in which the power conserved by life is dependent on both the Gibbs free energy of the overall metabolic reaction and the amount of energy the organism can preserve via ATP production [1, 135].

For a chemical reaction, the Gibbs free energy  $\Delta G$  is given by:

$$\Delta G = \Delta G^\circ + RT \ln Q \quad (6.1)$$

where  $\Delta G^\circ$  [ $\text{J mol}^{-1}$ ] is the standard Gibbs free energy of the reaction,  $R$  [ $\text{J (mol K)}^{-1}$ ] is the universal gas constant, and  $Q$  the reaction quotient, all at temperature  $T$  [K] and pressure  $P$  [Pa].  $Q$  is calculated from the activities of the reaction species and stoichiometry of the reaction and  $\Delta G^\circ$  is computed using SUPCRT92 [132] with the slop07 database. This software calculates thermodynamic parameters at a wide range of temperatures and pressures, and slop07 includes many useful biomolecules such as ATP and ADP [178]. Thermodynamic data for the other chemical species used in this work originates from Shock et al. (1989) [179] and Plyasunov & Shock [180]. NutMEG computes the Gibbs free energy using equation 6.1 for both the overall metabolism ( $\Delta G_M$ ):



and for ATP production  $\Delta G_{\text{ATP}}$ :



where  $\text{P}_i$  represents an orthophosphate ion. To carry out these calculations requires the activities of all constituents. We used NutMEG's default configuration for calculating  $\Delta G_{\text{ATP}}$  using values for [ADP], [ATP] and  $[\text{P}_i]$  which aim to be broadly representative of life on Earth: 0.1, 5 and 4  $\text{mmol L}^{-1}$  respectively [133]. These concentrations vary significantly between organisms and their metabolic states, but for this work we address this issue by considering a broad range of  $n_{\text{ATP}}$  values which offer comprehensive coverage of energetic uptake (Section 6.3.3, Supplemental Figure S4). The temperature dependence of  $\Delta G_{\text{ATP}}$  owes mainly to the temperature dependence of  $\Delta G^\circ_{\text{ATP}}$  (Supplemental Figures S1, S4). Further information on the specific methods employed by the model and the code prepared for this work are summarised in the Supplemental Material, NutMEG's documentation (Data Availability; Higgins 2021) [3]), and by Higgins & Cockell (2020) [1].

## 6.3 Parameter space selection

---

We have deliberately chosen a wide range of parameter values to encompass the uncertainties in the Cassini observational data and current interpretations of these data. This allows us to explore as broad a range of possible values that might exist in Enceladus' ocean, and to take into account the range of environmental parameters under which methanogenesis can occur on Earth. The energetic and power availability in the ocean was computed over a grid of possible temperature and pH values. The chemical composition and microbial parameters were constrained to within expected uncertainties and the total parameter space considered for this analysis is shown in Table 6.1.

### 6.3.1 | Temperature and pressure

Enceladus' ocean is thought to have a temperature minimum  $\approx 272$  K at the water-ice interface increasing to  $\approx 363$  K or a maximum possible  $\approx 563$  K at the ocean floor (the boiling limit) [85, 88]. Improved constraints on the hydrothermal temperatures within the core are required to specify the temperatures at which the hydrothermal fluid meets the bulk ocean [e.g. 15, 85, 88, 94], but the temperature difference between the water-ice and water-core boundaries must be at least 90 K [16, 85, 181]. The temperatures of putative hydrothermal systems in the core have been inferred from their expected mineralogy and the pH of the ocean as those required to satisfy Cassini observations of silica and  $H_2$  [e.g. 15, 85, 88, 94]. For this study, a temperature distribution between 273–473 K was adopted. While this does not increase to the highest suggested temperatures, the current maximum temperature limit observed for life is 395 K [52]. Also, our heated seawater approach becomes increasingly less accurate at elevated temperatures due to the likely contribution of hydrothermal fluid to the overall composition (discussed in Section 6.5.2).

The pressure of the ocean is dependent on its depth and the thickness of the surface ice shell. Current estimates suggest the differentiated hydrosphere to have an average thickness of 21 km and 37 km for the shell and the ocean respectively [95]. If at the ocean's deepest point the ice shell is only a few kilometers thick, a widest pressure variability of between  $\sim 1$  and  $\sim 100$  bar can be expected. This pressure choice has a minimal effect ( $\ll 1$  kJ mol $^{-1}$ ) on  $\Delta G^\circ$  compared to temperature for both methanogenesis and ATP production (Supplemental Figure S1), and the pressure effects on life are poorly understood [182, 183]. We expect any changes in composition caused by pressure to be insignificant in comparison to those

Table 6.1 Parameter range of Enceladus' ocean and hydrogenotrophic methanogens considered for this study.

Environmental parameter	Symbol	Proposed range	Reference(s)	Range used	Dependencies
Temperature	$T$	272–563 K	Section 6.3.1	273–473 <sup>a</sup> K	–
Pressure	$P$	1–100 bar	Section 6.3.1	1 bar <sup>f</sup>	–
Bulk ocean pH	$\text{pH}_{bo}$	8–13.5	various <sup>b</sup>	7–12	–
Speciated pH <sup>c</sup>	pH	–	various <sup>c</sup>	6.77–12	$T$ , $a_{\text{CO}_2}$
Activity of $\text{CO}_2$ <sup>c</sup>	$a_{\text{CO}_2}$	–	various <sup>c</sup>	$10^{-10}$ – $10^{-2}$	$T$ , $\text{pH}_{bo}$
Plume vol. mixing ratio of $\text{CH}_4$	–	$0.2\% \pm 0.1$	Waite+ 2017	$0.2\% \pm 0.1$	–
Plume vol. mixing ratio of $\text{H}_2$	–	$0.9\% \pm 0.5$	Waite+ 2017	$0.9\% \pm 0.5$	–
Dissolved inorganic carbon	[DIC]	$0.01$ – $0.1 \text{ mol kg}^{-1}$	Section 6.2.1	$0.01$ – $0.1 \text{ mol kg}^{-1}$	–
Concentration of Cl	[Cl]	$0.05$ – $0.2 \text{ mol kg}^{-1}$	Postberg + 2009	$0.05$ – $0.2 \text{ mol kg}^{-1}$	–
Organism parameter	Symbol	Proposed range	Reference	Range used	Dependencies
ATP yield per mol $\text{CO}_2$	$n_{\text{ATP}}$	$\leq 2.0$	Section 6.3.3	$0.25$ – $2.0$	–
$\log_{10}$ methanogenesis rate const. <sup>d</sup>	$\log_{10}(k)$ <sup>d</sup>	$(-7)$ – $0 \pm 1$ <sup>d</sup>	Higgins+ 2020	$(-7)$ – $0 \text{ s}^{-1} \pm 1$ <sup>d</sup>	$T$ , $n_{\text{ATP}}$
Energy of protein synthesis	$E_{pro}$	–	Higgins+ 2020	$790$ – $2750 \text{ J (dry g)}^{-1}$	$T$ , organism makeup
Methanogen power demand <sup>e</sup>	–	–	Higgins+ 2020	$\sim 10^{-15}$ – $10^{-9} \text{ W cell}^{-1}$	$T$ , $k$
Anaerobe power demand <sup>e</sup>	–	–	Tijhuis+ 1993	$\sim 10^{-14}$ – $10^{-10} \text{ W cell}^{-1}$	$T$ , cell mass
Minimal power demand <sup>e</sup>	–	–	Lever+ 2015	$\sim 10^{-20}$ – $10^{-12} \text{ W cell}^{-1}$	$T$ , $E_{pro}$
Minimum Earth power supplies	–	–	Bradley+ 2020	$\sim 10^{-21}$ – $10^{-18} \text{ W cell}^{-1}$	–

<sup>a</sup> This maximum is variable depending on the geochemistry of rock-water reactions at the bottom of the ocean. The upper temperature limit could be much higher, but 473 K is already well above the known maximum temperature limit for life. See main text for details.

<sup>b</sup> We consider a wider range than recent studies which have constrained the oceans' pH values to 8–10 (see main text).

<sup>c</sup> By the carbonate speciation model used, the activity of  $\text{CO}_2$  is estimated from the pH at 273 K. Upon increasing the temperature, the model was internally respecified to acquire new values of  $\text{CO}_2$  activity and pH. These rows do not contain entries for 'expected range' because they were computed for the parameter space as summarized in Section 6.2.1.

<sup>d</sup> Rate constants calculated in Higgins & Cockell (2020) were based on hydrogenotrophic methanogens in the exponential phase under optimal conditions and vary with temperature as shown in Supplemental Figure C.5.

<sup>e</sup> The ranges for the power demands correspond to their values at temperatures between 273 and 400 K rather than the full temperature range of the parameter space. This is because 400 K is an approximate maximum temperature limit for life.

<sup>f</sup> Higher pressures are not considered for reasons outlined in the main text. Differences in output between 1–100 bar are expected to be small in comparison to the effects of other variables in the parameter space (section 6.3.1, Supplemental Figure C.3).

caused by other variables in the parameter space. By computing the equilibrium constants of the carbonate system at 1 and 100 bar, we can expect the activity of  $\text{CO}_2$  ( $a_{\text{CO}_2}$ ) to vary by 7–25% (Supplemental Figure S3). This variation is negligible when compared to that due to salt content and pH which affect  $a_{\text{CO}_2}$  by orders of magnitude (discussed below). To avoid complications with temperature, depth and the software used for chemical speciation, pressure effects are not considered in this analysis and all calculations were performed at the default value of The Geochemist's Workbench and SUPCRT92 which is 1 bar between 273–373 K and the saturation pressure of  $\text{H}_2\text{O}$  at temperatures higher than this.

### 6.3.2 | Chemical composition and pH

A number of studies have estimated the pH of Enceladus' ocean and largely agree that it is likely to be weakly to strongly alkaline with  $\text{pH} > 8$  [14, 85–87, 101]. In this study, a range of “bulk ocean pH” values (defined as the pH of the ocean at 273 K) between 7 and 12 were used, encompassing most of these estimates. The carbonate speciation model outlined in Section 6.2.1 was used to compute the activity of  $\text{CO}_2$  ( $a_{\text{CO}_2}$ ) at 273 K and the specified ocean pH in three scenarios: a high salt, high carbonates case ( $[\text{Cl}] = 0.2 \text{ mol kg}^{-1}$ ,  $[\text{DIC}] = 0.1 \text{ mol kg}^{-1}$ ), a low salt, low carbonate case ( $[\text{Cl}] = 0.05 \text{ mol kg}^{-1}$ ,  $[\text{DIC}] = 0.01 \text{ mol kg}^{-1}$ ) and a nominal case ( $[\text{Cl}] = 0.1 \text{ mol kg}^{-1}$ ,  $[\text{DIC}] = 0.03 \text{ mol kg}^{-1}$ ). These maximise, minimise and provide the geometric mean for  $a_{\text{CO}_2}$  respectively which are consistent with Cassini data (Supplemental Table S1, Supplemental Dataset; [87]).

To account for the changing pH and  $a_{\text{CO}_2}$  with seawater temperature, the speciation was performed on the ocean solution again after heating the fluid by intervals of 10 K. In other words, the simulated solution was warmed and its pH, water activity ( $a_{\text{H}_2\text{O}}$ ) and  $a_{\text{CO}_2}$  were self-consistently recalculated at the new temperature. The effect this has on the pH is shown by the dashed lines in Figure 6.1. Its uncertainty and effect on  $a_{\text{CO}_2}$  can be found in the Supplemental Dataset and is visualized in Supplemental Figure S2.

The activities of  $\text{H}_2$  ( $a_{\text{H}_2}$ ) and  $\text{CH}_4$  ( $a_{\text{CH}_4}$ ) and their uncertainties were calculated by comparison between their volume mixing ratios reported by Cassini (Table 6.1, Waite et al. (2017) [15]) and that of  $\text{CO}_2$  which is  $0.55 \% \pm 0.25$  using the  $\text{CO}_2$  activity calculated at 273 K. It was assumed that  $a_{\text{H}_2}$  and  $a_{\text{CH}_4}$  are unaffected by the ion speciation, and do not significantly change with increasing seawater temperature. Other elements of the ocean composition important to habitability, such as concentrations of CHNOPS elements used in biomass construction were

assumed to be non-limiting and nutrients were not considered here as our goal is to calculate the instantaneous power available to life. The importance of nutrients is discussed in Section 6.5.

### 6.3.3 | Methanogen parameter space

Methanogenic power supply calculations were performed using NutMEG [1, 3], which contains a ‘typical optimal methanogen’ class exhibiting typical behaviour of an exponentially growing hydrogenotrophic methanogen based on data from the literature. It has a cell volume of  $3.44 \mu\text{m}^3$  and a dry mass of 1 pg. The default number of moles of ATP produced per mole of  $\text{CO}_2$  metabolised in the code is between 0.5 and 1.5 [168, 169], but for this study it was extended down to 0.25 and up to 2.0. This allows for effective energetic yields between  $14 \text{ kJ (mol CO}_2\text{)}^{-1}$  and  $130 \text{ kJ (mol CO}_2\text{)}^{-1}$  (Supplemental Figure S4), the lower limit approaching minimum free energies that methanogens subsist on in natural settings [184].

The rate constant of microbial methanogenesis has been constrained as a function of temperature by a comparison to the growth rates and  $\text{CH}_4$  evolution rates of methanogens in empirical studies [1]. This was independent of pressure, though the pressure range that was probed in the laboratory data was only 0.8–3 bar (Supplemental Figure S5). Uncertainty in the rate constant is taken in the decimal logarithm-space as  $\pm 1$  encompassing the majority of empirical methanogenic growth data. These rate constants were computed based on data from optimal energy and nutrient saturated conditions and hence present a conservative lower limit.

NutMEG was also used to calculate the power demand associated with the various temperatures in the parameter space, and does so using methods from the literature. We used three temperature-dependent power demands: i) derived directly from optimal growth of methanogens in the laboratory [1] ii) derived from the growth of anaerobic bacteria [60] and iii) a theoretical minimum tied to the rate of amino acid racemization [37]. The Higgins & Cockell (2020) [1] power demand was calculated using NutMEG and the ‘typical optimal methanogen’ class so only requires temperature as an input. The Tijhuis et al. (1993) [60] and Lever et al. (2015) [37] power demands additionally require the dry mass of the organism and the energetic cost associated with protein synthesis respectively. The latter is computed internally in NutMEG [1] to between  $790$  and  $2750 \text{ J (dry g)}^{-1}$  between temperatures of  $273$ – $400 \text{ K}$ . This calculation is inclusive of amino acid synthesis and protein polymerization. We selected these three measures because it seemed appropriate to assume that the true maintenance cost experienced by putative microbes on



Enceladus lies somewhere between these values. The racemization estimate acts as a fundamental thermodynamic minimum and the empirical estimates are based on the most favourable conditions and represent a maximum. Finally, to complement this analysis with an absolute minimum, we also examined whether power supplies on Enceladus can exceed the approximate minimum power supplies available to methanogens in Earth's marine subsurface (between  $10^{-18}$  and  $10^{-21}$  W cell<sup>-1</sup> [42]).

## 6.4 Results

---

### 6.4.1 | Free energy availability

Figure 6.1 shows the nominal free energy of methanogenesis at various seawater temperatures and ocean pH values. As temperature increases, the free energy becomes less negative owing to a combination of the decreasing CO<sub>2</sub> activity (Supplemental Figure S2), increasing  $\Delta G^\circ_M$  (Supplemental Figure S1) and the  $T$  contribution in equation 6.1 which offsets the decrease in  $\ln Q$ . More free energy is available at lower pH, which is also a result of higher CO<sub>2</sub> activity in less alkaline conditions. Figure 6.1 also shows how the pH is affected by increasing temperature from 273 K in the nominal case. High bulk ocean pH values may be decreased by over two units at 475 K, whereas pH values of 7, 8 and 9 decrease when warmed to ~325 K, then invert and increase. Supplemental Figure S2 shows the pH values with increasing temperature, with the change in pH of pure water for comparison.

The Gibbs free energy of methanogenesis changes significantly within the chemical parameter space. The dotted contour lines in Figure 6.1 show how the free energy would be different in the best-case and worst-case scenarios for life offered by the parameter space. Here, the best-case scenario is a high salt ocean (maximising  $a_{\text{CO}_2}$ ) with maximised  $a_{\text{H}_2}$  and minimised  $a_{\text{CH}_4}$  and the worst-case scenario is a low salt ocean (minimising  $a_{\text{CO}_2}$ ) with minimised  $a_{\text{H}_2}$  and maximised  $a_{\text{CH}_4}$ . The endmembers of the chemical speciation can have an equivalent effect to a shift by  $\pm 0.5$  bulk ocean pH units or  $\pm 50$  K in temperature. The CO<sub>2</sub> activity (dependent on the salt level via the mole ratio of carbonates/chloride determined by Postberg et al. (2009) [14]) is the dominant contributor to this uncertainty as it also contributes to the determination of other key species' activities in the dissolved gas model that is adopted here [15]. Supplemental Figure S6 shows some further contours, in the limiting case of each salt choice.





**Figure 6.1 The Gibbs free energy of methanogenesis in seawater throughout the Enceladus ocean parameter space** . Blue regions indicate those combinations of parameters where energy is available and red where it is not for a dissolved gas composition determined by the nominal salt case as described in the main text. The solid contour line also reflects this nominal free energy. The dotted contour lines show the total variation given by the chemical parameter space (salt endmember,  $a_{\text{H}_2}$  and  $a_{\text{CH}_4}$ ) with respect to the closest solid line. The dashed lines reflect the nominal salt case pH variation with temperature.

The Gibbs free energy of ATP production also varies with temperature and similarly to methanogenesis it is dominated by the  $T$  term in equation 6.1 at low temperatures, but these changes are minor in comparison to variation in  $n_{\text{ATP}}$  (Supplemental Figure S4). At  $T > 400$  K, the Gibbs free energy yield per mole of ATP begins to decrease owing to contributions from  $\Delta G^\circ_{\text{ATP}}$  (Supplemental Figures S1 and S4). As the internal composition of the methanogens considered was fixed,  $\Delta G_{\text{ATP}}$  does not vary with environmental pH here. This is not strictly representative of all thermoalkaliphiles on Earth, whose adaptations vary between maintaining a trans-membrane pH gradient (i.e. changing internal pH with external pH) to maintaining their internal pH when faced with varying environmental pH stresses [185]. As our  $\Delta G_{\text{ATP}}$  does not vary with environmental pH, it yields an energetically similar effect to preserving the trans-membrane pH gradient (a consistent proton-motive force).

### 6.4.2 | Net power supply

The power supply available to an organism is determined by both its microbial machinery and the free energy available from the environment. The nominal instantaneous power supply for a typical methanogen was calculated at intervals of seawater temperature and a bulk ocean pH value of 10 K and 0.5 units respectively and is shown in Figure 6.2. This uses the  $\Delta G_{\text{M}}$  plotted in Figure 6.1, an  $n_{\text{ATP}}$  of 1 mole per mole of  $\text{CO}_2$  and the nominal rate constant of methanogenesis at the selected temperature. Figure 6.3 shows endmember values of this power supply given by the parameter space when  $n_{\text{ATP}} = 1$  and other variables in Table 6.1 are either minimised or maximised. Also noted on Figures 6.2 and 6.3 is a maximum temperature limit for life at approximately 400 K. This reflects the highest temperatures observed for survival and growth of life on Earth, though it has been hypothesised that a true upper limit may be as high as  $\sim 425$  K [24]. It is possible that this limit at 400 K could also decrease with increasing pH, as thermoalkaliphiles appear to be rare on Earth [61]. This could be explained by the difficulty in accessing Earth's scarce quantity of high-pH high-temperature environments, or signal that the combined extremes of temperature and high pH are particularly difficult to overcome (for example by promoting the cleavage of biomolecules [10]).



**Figure 6.2 Power supply available to a hydrogenotrophic methanogen in the nominal case of the parameter space at various seawater temperatures and bulk ocean pH values.** The nominal case refers to an ATP yield per mole  $\text{CO}_2$  of 1.0, NutMEG default methanogenesis rate constant, and a dissolved gas composition determined by the nominal salt case as described in the main text. Also noted at 400 K is an approximate maximum temperature limit for life and dotted lines reflect the nominal salt case pH variation with seawater temperature.

The amount of ATP that a methanogen attempts to produce per mole of  $\text{CO}_2$  defines a minimum amount of available Gibbs free energy for the metabolism to run efficiently. This means that while a larger  $n_{\text{ATP}}$  allows for more efficient energy extraction when  $\Delta G_{\text{M}}$  is highly negative, it relies on high energy yields being available in perpetuity. Similarly, a low  $n_{\text{ATP}}$  allows for a methanogenesis-driven power supply to low energy yields, but is less versatile to extract more power in higher energy environments. This is demonstrated in Supplemental Figures S7 and S8 which present variants of Figure 6.3 with different  $n_{\text{ATP}}$  values.

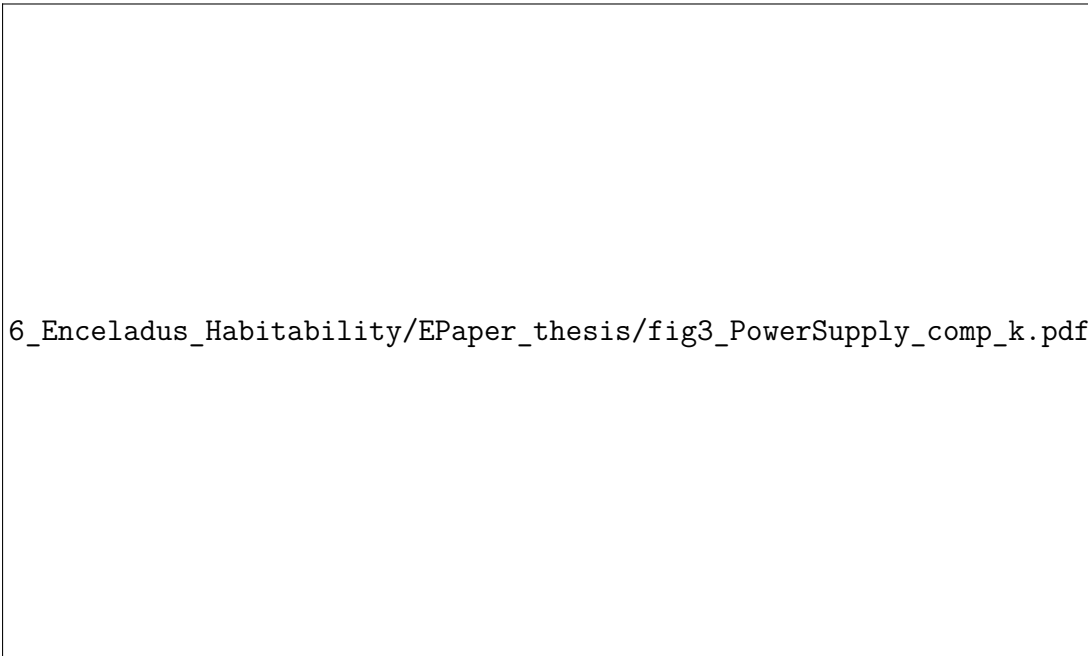


**Figure 6.3 Limiting bounds of power supply for a methanogen on Enceladus.**

Power supply available to a methanogen at the limiting cases of the parameter space at various seawater temperatures and bulk ocean pH values. Left: low salt endmember, minimised  $a_{\text{H}_2}$  and  $k$ , maximised  $a_{\text{CH}_4}$ . Right: high salt endmember, maximised  $a_{\text{H}_2}$  and  $k$ , minimised  $a_{\text{CH}_4}$ . Both at  $n_{\text{ATP}} = 1.0$ , limiting cases of  $n_{\text{ATP}}$  are shown in Supplemental Figure C.7 and C.8.

### 6.4.3 | Variance in power supply from the parameter space

The endmembers of power supply presented above give some insight into how wide ranging these values could be in the ocean's parameter space. To elucidate how each parameter contributes to this variation, samples were taken across their possible values (Table 6.1). Figure 6.4 shows the total variance for a random uniform sampling of  $n_{\text{ATP}}$ ,  $k$ ,  $a_{\text{H}_2}$  and  $a_{\text{CH}_4}$  across bulk ocean pH values of 8, 9, 10, and in the nominal and limiting cases of ocean salt content. Each plot contains a sample of 2000 cases. In general, the variance caused by this parameter space is approximately (+2)–(–3) orders of magnitude regardless of temperature or pH choice. In some limiting cases, such as the top-left and center-left plots of Figure 6.4, the bounds of variance decrease. This is because the NutMEG model prevents the simulated methanogens from consuming  $\text{CO}_2$  at a faster rate than has been observed in its input database [1]. The upper bounds in the center-left plot approach this maximum metabolic rate with increasing  $T$ . In the top-left plot, the nominal case is already above the maximum metabolic rate and many combinations of the parameter space are restricted to a smaller variance.

In some cases, the expanded parameter combination can provide power when the nominal case cannot. These are characterised in Figure 6.4 by red bins. The key driver of this is low  $n_{\text{ATP}}$  values decreasing the free energy requirement for microbial methanogenesis to operate, as discussed above.



**Figure 6.4 Variance in power supply for methanogens on Enceladus.** Total variance within the parameter space from the nominal power supply at various combinations of seawater temperature, bulk ocean pH and level of salt in log10 space. Parameter spaces within these plots are between endmembers of  $a_{\text{CH}_4}$ ,  $a_{\text{H}_2}$ ,  $n_{\text{ATP}}$  and  $k$  and  $T$  range 273–400 K. The nominal case refers to an ATP yield per mole  $\text{CO}_2$  of 1.0, NutMEG default methanogenesis rate constant, and a composition determined by the nominal salt case as described in the main text, plotted in Figure 6.2. Samples were taken from a flat distribution in each parameter. Sample size was 2000 per plot. The individual contribution of each of these is summarised in Table 6.2 and in the Supplemental Data. The blue shades show the total variance from the nominal power supply in log10 space and the red shades show areas where the wider parameter space provided power supplies when the nominal case could not.

The contributions of the individual parameters to this variance were explored and are summarised in Table 6.2. Random uniform samples were drawn between the endmembers of  $\log_{10}(k)$ ,  $n_{\text{ATP}}$ ,  $a_{\text{H}_2}$  and  $a_{\text{CH}_4}$  (Table 6.1) with all other parameters taken at their nominal values. As with the overall variance, there is no variation with temperature, pH choice or salt level unless the maximum metabolic rate is approached. This maximum metabolic rate represents the apparent limit of Earth methanogens so could potentially be exceeded by hypothetical Enceladus methanogens. The largest contribution is from  $a_{\text{H}_2}$ , due to the large range of values of volume mixing ratio and its conversion to the concentration of dissolved  $\text{H}_2$  exacerbating its uncertainty, and the rate of metabolism being dependent on  $(a_{\text{H}_2})^4$ , along with contributions of its effect on the available Gibbs free energy of reaction via the reaction quotient (Equation 6.1). In contrast, the contribution of  $a_{\text{CH}_4}$  is much smaller as it is not a variable in the rate calculations, only the Gibbs free energy. The variance contribution of  $k$  is uniformly distributed between  $\pm 1$  order of magnitude, reflecting its contribution to the microbial kinetics (Supplemental Figure S5; Higgins & Cockell (2020) [1]). The variance contribution of  $n_{\text{ATP}}$  is minor in comparison to  $k$  and  $a_{\text{H}_2}$ , but as discussed above the choice of  $n_{\text{ATP}}$  can extend the availability of power supplies to higher temperatures and higher bulk ocean pH values. These contributions are plotted at various temperatures, pH and salt concentration values in the Supplemental Dataset.

**Table 6.2 Variance contribution of the parameter space to the methanogenic power supply in log10 space.** These contributions are independent of bulk ocean pH, seawater temperature, and ocean salt content. Plots of the complete contributions for 20 combinations of  $\text{pH}_{bo}$  and  $T$  are available in the Supplemental Dataset.

Parameter	Best-case variation for life	Worst-case variation for life
$a_{\text{CH}_4}$	+ 0.1	– 0.1
$a_{\text{H}_2}$	+ 1.0	– 2.0
$n_{\text{ATP}}$	+ 0.5	– 0.5
$k$	+ 1.0	– 1.0

### 6.4.4 | Energetic habitability of the parameter space

To be habitable, an environment must provide enough power to meet the demands of survival imposed by its physico-chemical settings. The power supplies computed from the parameter space were compared against characteristic power demands in various metabolic states from the literature, corrected for the size of the methanogen. The latter powers are shown by the solid bars in Figure 6.5. The Higgins & Cockell (2020) [1] ‘maintenance’ powers are derived from methanogenic growth data in optimal conditions; the Tijhuis et al. (1993) [60] maintenance powers are from a more general case for anaerobic bacteria; the Lever et al. (2015) [37] maintenance powers characterise the cost of protein repair whereby proteins are replaced after between 2% and 10% of their constituent amino acids are racemized; and the Bradley et al. (2020) [42] power range is the approximate minimum power supply available to (and possibly survived by) methanogens in Earth’s subseafloor sediments. The three maintenance power models are temperature dependent and do not account for the environmental pH, hence the horizontal bars on the left hand side of Figure 6.5. As pH deviates from neutrality, it is expected that the power demand will increase [10]. Similarly, the minimum power supplies are shown as a horizontal bar on the right hand side of Figure 6.5. This range represents Earth’s subseafloor sediments, and were calculated at  $T = 278$  K and  $P = 100$  bar [42] so a true minimum is likely to be higher than this at elevated temperatures.

**Figure 6.5 (overleaf)** Power supply available in select bulk ocean pH and seawater temperature  $T$  combinations, with representative estimates of power demands due to temperature in those settings. The left hand column is at fixed  $T$  and changing bulk ocean pH, the right hand column is at fixed bulk ocean pH and changing  $T$ . Power supplies plotted are the nominal case (solid line), nominal high- and low-salt cases (dashed lines) and the endmembers that the composition may allow in those cases (dotted lines). The coloured bars represent the power demands expected in the given conditions. The Higgins & Cockell (2020) [1] bar only partially covers temperature and bulk ocean pH values as these were the limits of the data input to their model. This figure is for  $n_{\text{ATP}} = 1.0$ , identical graphs for  $n_{\text{ATP}} = 0.25$  and  $n_{\text{ATP}} = 2.0$  are available in Supplemental Figure C.9 and C.10 respectively.



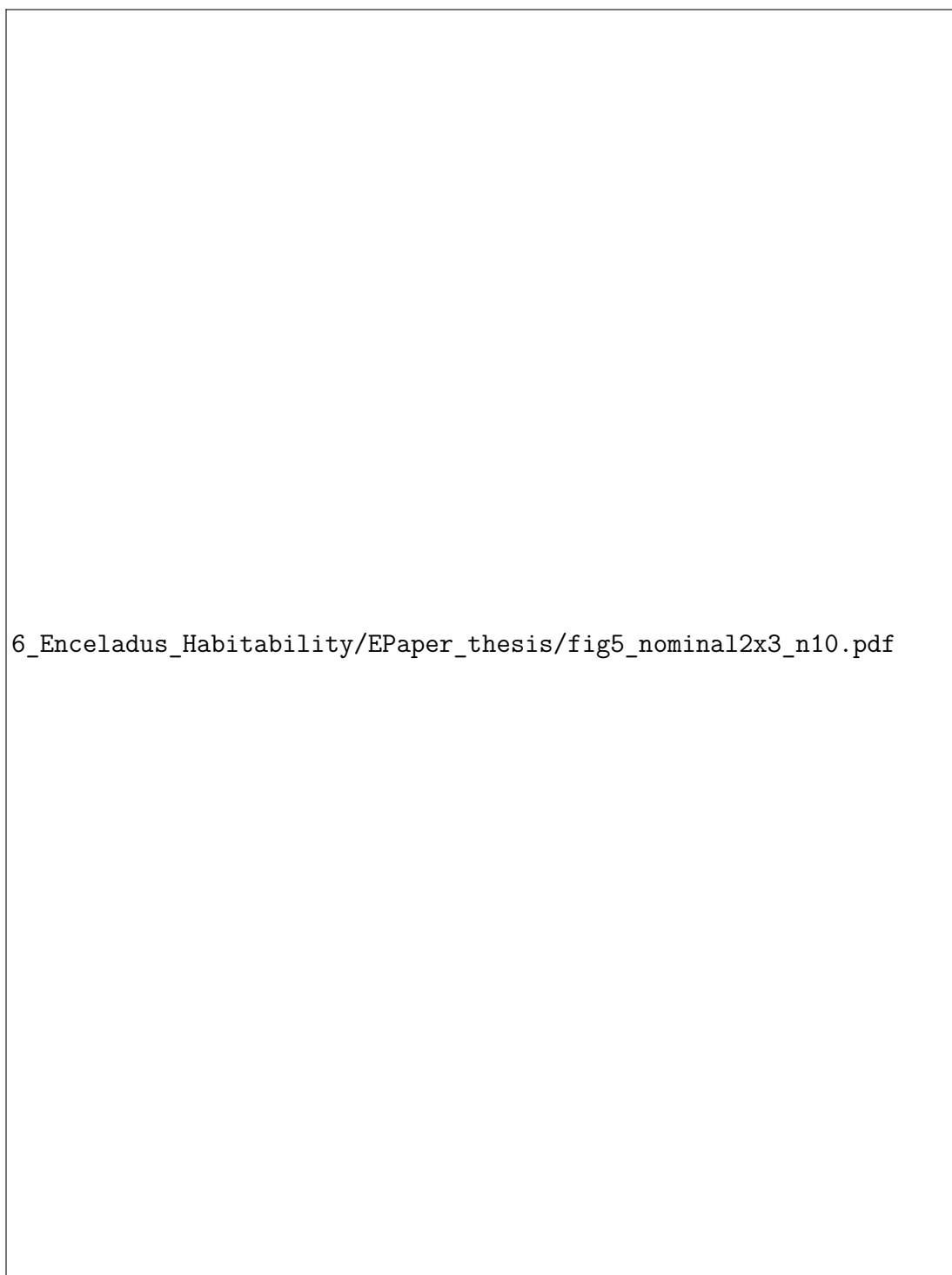


**Figure 6.5** Representative instantaneous power supplies and demands in the Enceladus ocean . See caption overleaf.

The characteristic power supplies in Figure 6.5 are the nominal values at 275 K, 300 K and 325 K changing with bulk ocean pH on the left and at bulk ocean pH 8, 9, and 10 changing with seawater temperature on the right (solid lines), alongside high salt and low salt nominal values (dashed lines), and the best-case and worst-case scenarios offered by the parameter space (dotted lines). From this figure it is clear that some configurations of the parameter space offer power supplies which exceed the various power demands in the literature and some do not — typically those at higher bulk ocean pH and lower seawater temperature. The configurations that meet the thresholds of the four habitability measures are shown in Figure 6.6 for  $n_{\text{ATP}} = 1$ . The lighter shaded segments can be exceeded by more of the parameter space than the darker shaded segments, which are only ‘habitable’ to the cases with higher power supply yields. Much of the parameter space with a bulk ocean pH of less than 10 exceeds the expected minimum power supply available to methanogens on Earth, taken as a conservative  $10^{-18}$  W/cell, the upper limit of such predictions [42]. Similarly, there could be a large enough instantaneous power supply to exceed minimal maintenance estimates [37] at bulk ocean pH values of less than 9.5.

Some cases of the parameter space suggest that the chemical disequilibrium may be large enough to host optimal methanogenic growth (Figure 6.6, top row), similar to that observed in laboratory experiments. However, this would only be the case if the ocean has a pH of 8.5 or less and the ocean has a high salt content. Variation in  $n_{\text{ATP}}$  cannot increase this to higher pH values (cases for  $n_{\text{ATP}} = 0.25$  and  $n_{\text{ATP}} = 2.0$  are shown in Supplemental Figures S11 and S12). Because we do not consider hydrothermal fluid as a contributor to the chemical composition, at elevated temperatures we present a conservative bioenergetic scenario. As such, that even some of the seawater parameter space can host optimal methanogen growth brings tantalising possibilities for the habitability of putative hydrothermal systems with higher activities of methanogenesis ingredients, particularly  $\text{H}_2$ . Alternatively, highly alkaline hydrothermal fluids could shift the carbonate speciation and decrease  $a_{\text{CO}_2}$  compared to seawater. Abiotic reactions and/or microbial competition could also create significantly different conditions in these systems. Some of these possibilities are explored in Sections 6.5.2 and 6.5.3 but to confidently quantify these effects requires more information on the nature of Enceladus’ hydrothermal fluids.

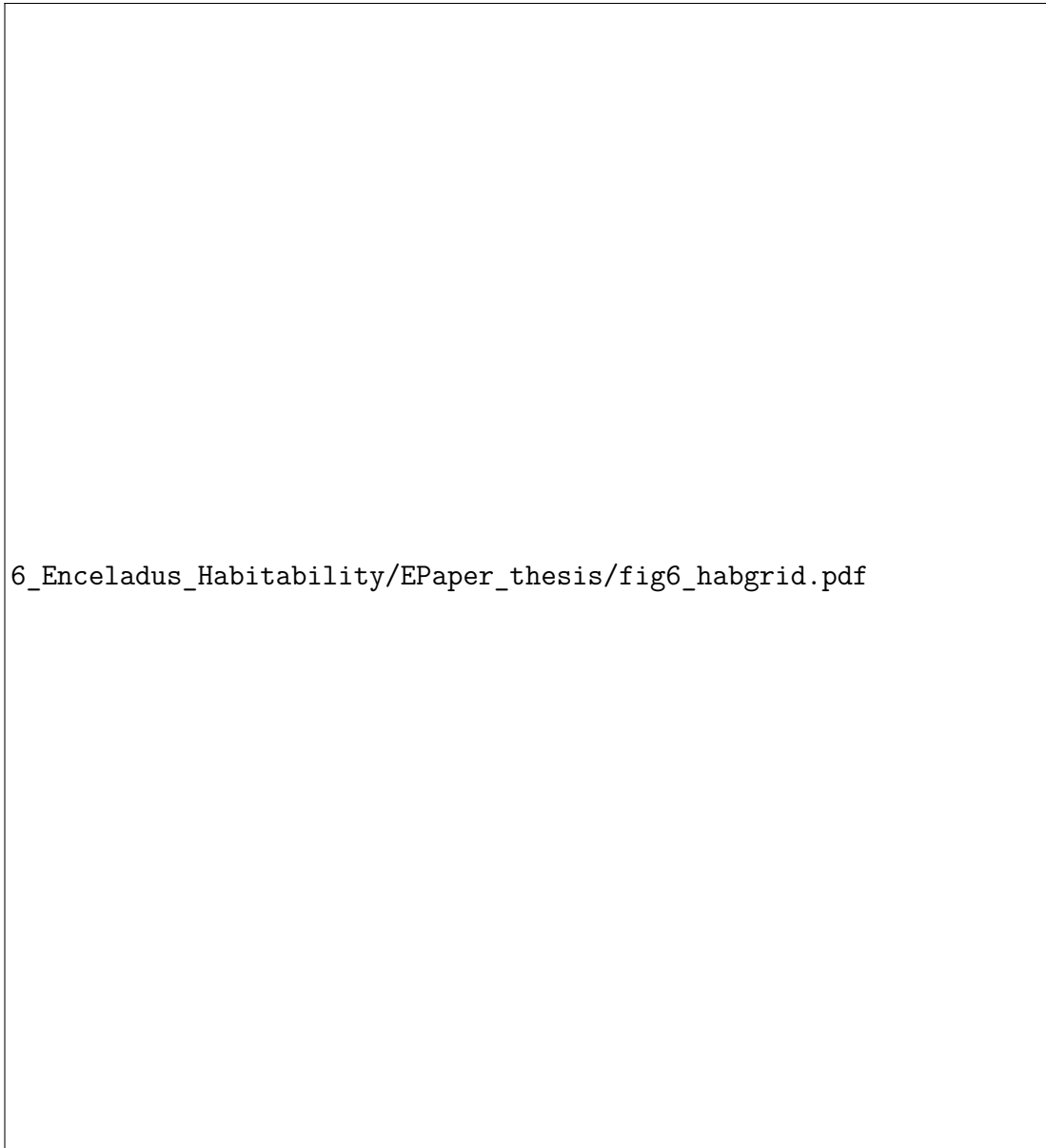


**Figure 6.6 Areas of the Enceladus ocean parameter space which meet various criteria for habitability.** Segments are filled when part of the parameter space's predicted power supply exceeds the power demand posed by one of four scenarios: top-left) exponential growth of methanogens; top-right) exponential growth of anaerobes; bottom-left) cost of protein repair after amino acid racemization; bottom-right) minimal power supplies to methanogens in Earth's deep marine subsurface. These cases are for  $n_{\text{ATP}} = 1.0$ , companion graphs for  $n_{\text{ATP}} = 0.25$  and  $n_{\text{ATP}} = 2.0$  are available in Supplemental Figures C.11 and C.12 respectively.

## 6.5 Discussion

---

Despite the optimism about the habitability of icy moons, and particularly Saturn's moon Enceladus, we still do not have sufficiently precise observational constraints on the parameters necessary to assess the habitability of such environments in the context of the currently known limits to life. In this work, we have sought to address this by quantifying the energy and power available to hydrogenotrophic methanogens under a range of possible parameter values in the Enceladus bulk ocean to both identify what factors might determine the habitability of the seawater and illuminate which parameters might be a priority for improved measurements in future missions.

### 6.5.1 | Implications for Enceladus' habitability

Observations of Enceladus in recent decades have revealed tantalising details of its subsurface ocean, allowing it to be resolved in unprecedented detail in comparison to other icy moons. Still, the breadth of parameter spaces that the Enceladus ocean may possess is significantly larger than one might expect. We have stripped back models of the icy moon's subsurface to focus on its ocean — considering Enceladus seawater at both cold and elevated temperatures — as derived from Cassini's measurements in an attempt to find out where in its observable parameter space conditions would permit the persistence of Earth-like methanogens. This has allowed us to identify the most important drivers of habitability for methanogens in our model as being the pH and salt/carbonate content, because they are linked to the activities of  $H_2$  and  $CO_2$ .

Our results show that both energetically habitable and uninhabitable environments within the possible parameter space of Enceladus' subsurface ocean may exist and we have been able to quantify where the energetic thresholds for habitability may lie for methanogens. To provide useful energy to methanogens, a 273 K ocean that is relatively high in salts and carbonates must have a  $pH \leq 10$ . If the ocean has a relatively low concentration of salts and carbonates, the pH needs to be 8 or lower to meet the minimum power supplies required by methanogens on Earth, with this value increasing to pH 9 or lower at temperatures above 360 K. We stress that these are only energetic thresholds for habitability which do not consider other important measures such as nutrient content and the potential for increased energy availability in hydrothermal fluid (see below). As such, these results should be

considered conservatively optimistic when suggesting low temperature habitable regions, and somewhat pessimistic when higher temperatures and pH values appear uninhabitable.

For highly efficient metabolisms, some regions of the parameter space may be able to meet the maintenance requirements of exponential growth, for example in a high salt case at pH 8.5 or lower, and in a low salt case at pH 7. Because exponential growth would not be sustainable for geological timescales, if future observations determined that such conditions existed in perpetuity on Enceladus with no further evidence of life they could be interpreted as an uninhabited (or vacant) habitat [186]. Alternatively, if such conditions were fleeting and Enceladus inhabited, methanogens in non-growing states could be poised to take advantage of the short-lived energy availability as life does in low-energy environments on Earth [35]. One interesting example of this could be variability in Enceladus' geological activity owing to irregular tidal heat generation or transport processes [187] causing 'waves' of energy for life. Another more speculative idea could be that if Enceladus is young ( $\sim 100$  Myr) [107] and life was only recently established, it may not have yet reached a steady state with the environment. In any case, if Enceladus is  $\sim 100$  Myr old, material exchange with the inner solar system is a low probability event and so it would be likely that, if inhabited, such life would have emerged independently from Earth [16]. As we do not know the probability of life emerging on Enceladus, a vacant habitat or uncertainties in our model could yet be the simplest explanations.

### 6.5.2 | Uncertainties in composition owing to hydrothermal activity

A remaining question is the influence of hydrothermal activity on the oceanic composition at elevated temperatures. The chemical makeup of these warmer regions on Enceladus is likely to be significantly affected by interactions at the rock-water boundary, including  $a_{\text{H}_2}$ ,  $a_{\text{CO}_2}$ ,  $a_{\text{CH}_4}$  and nutrient content. If Enceladus' hydrothermal systems are similar to those on Earth, we would expect significant chemical differences compared to the ocean above. This includes the potential for different activities of methanogenesis ingredients, particularly increased  $a_{\text{H}_2}$  and possibly  $a_{\text{CO}_2}$ . This could yield higher instantaneous power supplies for life, perhaps such that systems with lower salt content and/or higher pH could appear more habitable than our results suggest. Alternatively, the system could become depleted of one or more key energy/nutrient sources for methanogens from abiotic reactions or competition, discussed below. Furthermore, the discharge of these species from the plume will generate a chemical gradient in the ocean which could affect their abundances throughout it, even at low temperatures. Including such

influences could provide more habitable niches with  $H_2$  and  $CO_2$  concentrations exceeding the ones used here, but would vastly complexify the parameter space as presented in this work. Future work which explores the scope of hydrothermal activity on Enceladus coupled with the models we have developed here would be valuable for more conclusively assessing its habitability in these critical regions.

Our results above 273 K could still be useful for some environments which may exist on Enceladus. One example could be seawater in an aquifer with minimal localised hydrothermal activity. On Earth, cool basaltic ridge-flank hydrothermal systems ( $\leq 293$  K) have very similar compositions to seawater at the ocean floor [188]. Similar settings could exist on Enceladus in water-rock systems which are already close to non-redox equilibrium aside from a small change in temperature. The composition would be most seawater-like in a significantly carbonated sub-seafloor layer which could be present in a heterogeneous structure of Enceladus' rocky core [87]. At temperatures of tens of degrees Celsius, element exchange between water and rock could also be kinetically inhibited if the residence times of the aquifer fluids are sufficiently short. Seawater could seep into these systems and be gently warmed along the conductive geothermal gradient, with composition and habitability similar to that of our heated seawater.

Our results can also approximate the heated seawater contribution to relatively low-temperature mixed fluids near hydrothermal systems on Enceladus. The composition of these tentative habitable zones would be determined from both that of the heated seawater and hydrothermal fluid. On the one hand, if the water-rock temperature is very high ( $\gg 400$  K), then mixtures at temperatures well into our parameter space could be dominated by seawater. On the other hand, if the water-rock temperature is much lower, then most elevated temperatures of our parameter space will be dominated by the hydrothermal contribution. Ultimately, we need to know the temperature of the hydrothermal systems and degree of mixing with seawater to determine the extent to which our results at elevated temperatures may contribute to mixed hydrothermal fluids on Enceladus. The scale and nature of water-rock interaction on Enceladus remains an open question, but our heated seawater approximation can act as a starting point for the chemical composition and habitability of systems which are dominated by seawater.

### 6.5.3 | Other limitations of the parameter space and model

This study necessarily involved other simplifications and assumptions and here we elaborate what these are. One limitation is in the establishment of a sufficient power supply for habitability. Both the rate of microbial energy uptake and maintenance powers are difficult to determine empirically. The maintenance power of organisms can vary significantly depending on environmental conditions and their growth state (e.g. between lag, growth and stationary phases) [23]. Four characteristic maintenance powers were used here, covering the minimum energy fluxes available to methanogens in Earth's subsurface, up to the expected cost when exponentially growing in the laboratory. Three of these maintenance power models use temperature as their defining variable but none of them account for the effects of pH. It is expected that maintenance power increases as the pH deviates from neutrality, but while energetic costs at different pH values can be estimated, to our knowledge no empirical quantification has been published yet [10].

Limitations in the datasets for these maintenance power models should also be highlighted. The Higgins & Cockell (2020) [1] dataset covers optimal methanogen growth between 288–371 K and pH values of 6–9.1. The Tjihuis et al. (1993) [60] dataset covers microbial growth temperatures between 280 and 330 K. As their results were resolved to an expression in  $T$ , we tentatively extended them to 400 K for our analysis. Better constraints on the power demands owing to various physico-chemical parameters including temperature, pH, pressure, salinity etc. are needed to further improve our assertions of (unin)habitability.

Beyond the local energetic availability, the choice of  $n_{\text{ATP}}$  highlights the efficiency of the microbial machinery towards the rate of energy uptake. While a low  $n_{\text{ATP}}$  allows energy extraction at low energetic availability, this hinders the power supply when there is more energy available per mole of  $\text{CO}_2$ . Similarly, a high  $n_{\text{ATP}}$  allows a large fraction of the available free energy to be extracted when it is plentiful, but makes the metabolism thermodynamically unfavorable in periods of low energy availability. If versatility in the number of ATPs produced per mole of  $\text{CO}_2$  with a changing environment were introduced to the model, the methanogens would be able to 'adapt' to their settings allowing for different behaviour in low-energy and high-energy environments as described above. Similarly, alternative sources of energy to ATP could be considered such as pyrophosphate, acetyl phosphate or thioesters. This would lead to an alternative amount of Gibbs free energy conserved by the organism (in this work,  $\Delta G_{\text{ATP}}$ ). We would expect similar results to this work, provided such alternative Gibbs free energies fell within the broad scope considered

here (Supplemental Figure S4). Furthermore, as we have shown in this work, the changes in energy availability often come with significant changes in temperature and pH, variation toward which organisms typically have a low tolerance.

Our results can be compared to the limits of methanogens on Earth. Methanogen species are known that grow optimally at salinities of up to 9–12 % [27], and many can tolerate salinities higher than this [189, 190]. The highest salinities from this work (pH 12 in the high salt case) are  $\approx 4$  % so the salinity of the ocean from our model should fall well within these limits. However recent modelling studies suggest the salinity could be significantly higher deeper in the ocean [70]. Methanogens have not yet been observed to grow at pH values higher than  $\approx 10$  [165], but their presence has been indicated at locations such as Lost City which contains fluids at higher pH than this [191], so methanogenesis above pH 10 should not be ruled out. Our results indicate that methanogenesis becomes severely energetically limited when the Enceladus bulk ocean pH approaches these values, so survival would require extra adaptation such as  $\text{CO}_2$  concentrating mechanisms. However, there are significant chemical differences such as increased  $\text{H}_2$  activity that could be expected between hydrothermal fluid and our heated seawater model, as discussed above. In alkaline settings on Earth, methanogens are typically outcompeted for  $\text{H}_2$  by sulfate reducers [190]. Ray et al. (2021) [19] computed that the dissolved  $\text{SO}_4^{2-}$  concentration could be up to  $\sim 1 \text{ mmol (kg H}_2\text{O)}^{-1}$  so such competition on Enceladus is worth consideration. In a mixed fluid, abiotic reactions between  $\text{H}_2$  and  $\text{SO}_4^{2-}$  could deplete these species limiting their availability for both methanogens and sulfate reducers, but such reactions are thought to be kinetically inhibited at Enceladus' expected alkaline pH [192]. Even so, the possibility of abiotic  $\text{H}_2$  sinks at high temperatures should not be ruled out; such processes are common in hydrothermal systems on Earth [e.g. 193, 194].

Further to the points above, hydrogenotrophic methanogenesis may not be the only metabolism that Enceladus' subsurface ocean can host. While  $\text{CO}_2$  is the most biologically useful oxidant directly observed [17], mechanisms of delivery for other oxidants such as  $\text{O}_2$  and  $\text{H}_2\text{O}_2$  have been proposed which allow for a variety of possible metabolisms to be considered [19]. Still, despite these alternatives methanogenesis appears to have the highest energy yield and biomass potential for a weakly-alkaline ocean owing to large dissolved  $\text{CO}_2$  and  $\text{H}_2$  activities in comparison to other biologically useful chemical species [19]. Enceladus' surface radiation flux is much less than that of Europa, making radiolytic processing of the surface ice provide a smaller input of oxidants. This may restrict Enceladus' inventory of biologically available oxidants [17, 195]; alternative sources could include radioactive decay within the ocean or in the deeper interior [19, 196].



Nutrient availability is another cornerstone of an environment's habitability. Enceladus' nutrient inventory is not yet completely known and neither iron, phosphorus nor sulfur — key elements required by life on Earth — have been confidently detected, only modelled [6, 19, 90, 106], but they are widely expected to be present. While a detection of  $\text{H}_2\text{S}$  has been reported [13], subsequent analyses suggest ambiguity in its identification [90]. A possible nitrogen source for life is available in the form of ammonia [15, 197], or ammonium if the ocean pH is below  $\sim 10$ . Carbon sources other than  $\text{CO}_2$  and  $\text{CH}_4$  have also been reported in the form of diverse types of organic compounds that span a spectrum from simple to complex [13, 104, 105]. While the results presented here identify some power supplies which can overcome maintenance costs, nutrients such as these are required not only for synthesising new biomass, but also for cell repair [10]. This means that our results indicating habitability are optimistically conservative. A low availability or lack of any of these unconstrained nutrients will foster more challenging conditions for any form of life, restricting the ease at which it can survive, grow and evolve [1]. Consequently, the parameter space could be less habitable than we have presented it here.

This study focused on the instantaneous habitability of the ocean using the chemical disequilibrium indicated by geochemical modelling and Cassini observations. To be habitable on longer timescales requires substrate and nutrient resupply. Rates of serpentinization and other rock alteration processes have been proposed [15, 16, 20, 87, 198, 199] as a way to supply further  $\text{CO}_2$  and  $\text{H}_2$  on geological timescales, but these predictions vary over several orders of magnitude. Methane may be continuously removed from the ocean by plume outgassing activity. In order to confidently estimate the sustainable levels of biomass in the habitable regions of this parameter space, more information on the nutrient content of the ocean is needed, along with the rate of supply of such nutrients and the methanogenesis reactants [16].

Finally, as a natural system, Enceladus' ocean is not homogeneous, and there cannot be a one-size-fits-all equation for its composition in any given place. While we attempted to span as wide a possible parameter space as practical for this study, a conclusion that oases of habitable niches exist (such as Figures 6.2–6.6 at pH 7–8.5) cannot be confirmed until the exact nature of the ocean is resolved further. On the other hand, conditions on Enceladus not included in this parameter space such as more complex hydrothermal systems in the rocky core or a possible highly saline deep-ocean could well provide far more diverse and lucrative redox energy sources.

### 6.5.4 | Recommendations for future work and missions

Our results complement recent studies which aim to elucidate whether Enceladus could — or has ever been — habitable or inhabited using an array of innovative techniques [e.g. 15, 19–21]. It is encouraging that such analyses rarely suggest that Enceladus is completely uninhabitable, but each model (including our own) has unique limitations. By continuing to explore icy moon habitability and determine detectable biosignatures using new techniques we can inform future missions on the critical variables to measure when they next visit [200, 201].

This work also highlights some key goals to pursue by either modelling analyses, laboratory experiments or future observations to further constrain the habitability of Enceladus' ocean, including:

1. **Determine whether the ocean composition can be directly quantified from the salty plume ice composition.** For instance, can the extent of fractionation and/or concentration processes between leaving the ocean and entering the plume be determined for each species? This would allow us to better constrain the geochemistry of the ocean.
2. **Further our understanding of the relationship between the dissolved H<sub>2</sub> concentration and the measured H<sub>2</sub> mixing ratio in the plume.** This may be complicated from the present model by different outgassing rates of H<sub>2</sub> and CO<sub>2</sub>, as well as heterogeneity with ocean depth [15, 88].
3. **More tightly constrain the ocean pH and temperature** at its floor. This could be accomplished using geochemical indicator species/ratios in the plume, or via direct measurement of pH in a melted sample of collected plume ice grains or plume “snowfall” on the surface.
4. **Improve the precision of the concentration of carbonates in the ocean,** which will be supported by point 1) above. Further analysis of Cassini CDA data may provide new insights. Future measurements of anions in plume ice grains (Cassini CDA could only detect cations), or other approaches to determine carbonate alkalinity would enable a significant advancement.
5. **Add more concrete constraints to the Enceladus ocean's possible nutrient inventory.** Ideally this would come from direct measurements of species that contain sulfur or phosphorus. Alternatively this could be achieved indirectly from observations or experimental work that better constrain geochemical processes that deliver these elements to the ocean [16].
6. **Improve our understanding and inventory of thermoalkaliphiles on Earth** and how they might fare in Enceladus-like conditions. At present, there are no perfect analogue environments of Enceladus' ocean as we understand it [88].

Culture experiments which are representative of the ocean's geochemistry as predicted by models such as ours would help determine whether these conditions can be habitable for known life.

7. **Constrain the nature of Enceladus' hydrothermal systems.** These are arguably some of the most promising known potentially habitable zones beyond Earth. Confidence in their physico-chemical nature, including for instance their composition, temperature and interactions with seawater is tantamount to deducing whether they are habitable or not.

Continuing avenues of research such as these will not only elucidate more information on the Enceladus ocean, but will further its applicability as a stepping stone for studies of other extraterrestrial liquid water environments, such as those on Mars, Ceres, Europa, Ganymede, Titan, and possibly Pluto and Triton.

## 6.6 Summary

---

We have used coupled geochemical and microbial metabolic models (The Geochemist's Workbench and NutMEG) to explore the possible physical and chemical parameter space of the Enceladus ocean to identify where thresholds between habitable and uninhabitable conditions could lie for hydrogenotrophic methanogens. Our results emphasise the importance of pH and the concentration of carbonates in determining these thresholds with current models — with implications for mission measurement priorities — and they show how, with respect to this metabolism, a non-homogeneous Enceladus could possess pockets of habitability. This work has also shown how microbial metabolic models can be used to explore the diverse physical and chemical combinations in extraterrestrial environments to 'map' their habitable and uninhabitable spaces. Beyond the example of Enceladus, similar approaches can be applied to other astrobiology targets in the solar system, for example on jovian moons using results from the Europa Clipper and JUICE missions.

### Data availability

The source code for NutMEG and links to its documentation are available in the NutMEG github repository: <https://github.com/pmhiggins/NutMEG>, and archived in Zenodo [3]. For this work, version 1.0.0 was used (doi: 10.5281/zenodo.4746807). All of the code required to replicate these results, as well as data files containing the data plotted in all figures are available in the NutMEG-Implementations GitHub repository, in the Enceladus2021\_ParameterSpace directory: <https://github.com/pmhiggins/NutMEG-Implementations> (archived in Zenodo, doi: 10.5281/zenodo.4746637). Supplementary datasets are available on figshare (doi: 10.6084/m9.figshare.14562144) and summarised in the Supporting Information document. Supplementary Text, Tables and Figures are available in the Supporting Information document<sup>1</sup>.

### Acknowledgments

This work was supported through the Science and Technology Facilities Council (STFC) grant ST/R000875/1 and an STFC studentship to PMH. CRG acknowledges support from NASA through the astrobiology project Habitability of Hydrocarbon Worlds: Titan and Beyond. We thank two anonymous reviewers for their detailed and constructive comments.

---

<sup>1</sup>The supporting information document is included in this thesis as Appendix C.

# CHAPTER 7

---

## Enceladus' biomass and biosignatures

---

So, it appears that some pockets of the Enceladus ocean's parameter space could be habitable to Earth-like methanogens. This is particularly the case at low temperature and near-neutral pH. But could methanogens fit into a steady state system on Enceladus that still looks like the one Cassini observed? If so, how many of them could there be? Could they be leaving markers for us to look for in future missions?

In this more speculative chapter, we estimate the amount of biomass that the habitable regions could sustain and make some first estimates as to how long related biosignatures could be preserved in the ocean. To do this, we build different schemes by which life could be surviving in a steady-state ocean that does not significantly deviate from the geochemical configuration we computed in Chapter 6.

### Subchapters

7.1	Introduction .....	186
7.2	Methods .....	187
7.3	Results .....	201
7.4	Discussion and conclusions .....	221

## 7.1 Introduction

---

Numerous claims have been made about the habitability of Enceladus in recent years with varying degrees of optimism [e.g 2, 15–21]. There is broad consensus that Enceladus is likely to possess habitable regions, but the scale of them is still unknown. In Chapter 6, we assessed the spontaneous habitability of the Enceladus bulk ocean at various temperatures and pH values expected from observations and modelling. Our conclusions were conservatively optimistic, in that much of the near-neutral pH parameter space appeared to be habitable for hydrogenotrophic methanogens. Notably, however, they were somewhat *less* optimistic compared to some of the other studies referenced above; but indicate habitability nonetheless. Our work also did not consider the significantly different compositions which would be expected near high temperature water-rock activity which could make such environments more habitable.

Consensus on habitable settings is a useful first step, but leaves many open questions. Indeed, we expect ‘habitable’ environments to be pervasive throughout the universe [6]. The real prize, particularly for solar system astrobiology, is in the detection of life. There is understandable difficulty in sending a spacecraft to Enceladus and scooping up some microbes — or finding there are none to scoop up — particularly as the consensus is that the most habitable regions are at the *bottom* of the ocean, some ~40 km below the surface. Instead, the pathway to life detection is through observable biosignatures, markers which can only be produced by biological activity. One such option is the chiral properties of amino acids. Most life on Earth is selective in the chirality of amino acids it uses, but over time these decay and become indistinguishable from those produced naturally in the environment [20].

To estimate plausible biosignature production rates, typically one also need to know the scale of the biosphere producing them. For non-racemic mixtures of amino acids as a biosignature, the waste production of the biosphere is also needed. In Chapters 4–5 we introduced NutMEG, a python package for predicting microbial growth, biomass and biosignature production, and built a Typical Optimal Methanogen [TOM] which behaves as a well-adapted Earth-like methanogen for any specified chemical environment. In this chapter, we apply NutMEG to combine ideas and results from Chapters 3–6 and estimate, for a variety of plausible Enceladean conditions:

1. The **inflow** of methanogenesis ingredients into the ocean from water-rock interaction.
2. The **amount of biomass** such inflow can support.
3. The biological and environmental **requirements** which must be met for a **sustainable Enceladus methanogen biosphere**.
4. The **rate** at which detritus from such a biosphere will become **racemized**, with implications for biosignature detection.

## 7.2 Methods

---

### 7.2.1 | Refining the parameter space

The parameter space we resolved in Chapter 6 is useful for constraining the scope of plausible conditions on Enceladus, but performing growth simulations on every possible combination of organismic and environmental parameter would not be computationally feasible. Consider the full instantaneous parameter space and resultant habitability maps defined in Chapter 6. They varied as outlined in Table 7.1, where we have also defined a reduced parameter space which factors out the conditions we determined as uninhabitable in all cases. If growth simulations were to be performed on all of these, including an extra variable quantifying chemical inflow and outflow  $j$ , 36,960  $j$  sets of results would be produced. This is neither computationally nor analytically feasible. We can reduce the parameter space slightly such that it still captures the range of spontaneously habitable conditions found in Chapter 6. For example, the temperature range can be reduced from 273–473 K to 273–373 K, and the bulk ocean pH from 7–12 to 7–10. The salt content and  $n_{\text{ATP}}$  can be reduced to the ‘nominal’, ‘minimal’ and ‘maximal’ conditions, and the maintenance power can be reduced to an ‘exponential growth’ estimate [1] (Chapter 5) and a ‘basal’ estimate [37] (Chapter 3). This results in 1,386  $j$  simulations in total. This number of simulations is more manageable, but remains cumbersome to work with, so as a compromise to streamline the analysis within this chapter, we eliminated the variance in  $n_{\text{ATP}}$  by introducing a ‘best  $n_{\text{ATP}}$ ’ for a given parameter set. This allows for 462  $j$  combinations.

**Table 7.1** A refined parameter space for the 'habitable' regions of Enceladus' ocean.

This is the parameter space as outlined in Chapter 6, with the total number of values for each variable considered such that we can work out the total number of dimensions required to consider all possible combinations.

Parameter	Values	Intervals	Total values	Values of interest
Temperature	273–473 K	10 K	21	11
pH	7–12	0.5	11	7
Relative salt content	n/a*	n/a*	5	3
ATP Yield [ $n_{\text{ATP}}$ ] <sup>†</sup>	0.25–2.0	0.25	8	1
Maintenance power	n/a*	n/a*	4	2
			36,960	462

\* The salt content and maintenance power values are codependent on other variables. The total values of 5 and 4 refer to those used in Figures 6.5 and 6.6.

<sup>†</sup> In Chapter 6 the ATP yield was used at 3 values, but up to 8 are available in the code. As is discussed in the main text, here we reduce  $n_{\text{ATP}}$  to a single value of interest.

### 7.2.1.1 | The 'best' ATP yield

In Chapter 6 we computed the bioavailable power supply under various combinations of the Enceladus parameter space. The environmental dependencies were the temperature, pH and salt content, where a carbonate speciation was performed given these three inputs to yield the chemical composition. The conservable power supply for the organism varied under the biological constraints of the methanogenesis rate constant  $k_M$  and ATP yield  $n_{\text{ATP}}$  (Chapters 3, 5 & 6). The rate constant was selected as the value for the closest corresponding  $n_{\text{ATP}}$  value used in Chapter 5, so in effect the key variable driving the methanogens' kinetic behaviour was their ATP yield.

To reduce the parameter space further, we selected only the best values of  $n_{\text{ATP}}$  for a given set of environmental conditions. In other words, this assumes that any methanogens are perfectly adapted to the instantaneous environment as modelled to extract the most energy possible. For example, say that at a given temperature each ATP phosphorylation requires  $100 \text{ kJ mol}^{-1}$ . If the free energy of methanogenesis were  $-130 \text{ kJ mol}^{-1}$  in these conditions, the organism could extract between 0.25–1.25 mol ATP per mol  $\text{CO}_2$  (constrained to the 8 values in Table 7.1), but



not 1.5 or above because there would be no thermodynamic drive. One of these suitable values would produce the highest possible power supply, determined by the thermodynamically limited biochemical kinetic algorithm used (Chapter 3) and that is selected as the ‘best  $n_{\text{ATP}}$ ’. Figure 7.1 shows the best  $n_{\text{ATP}}$  values for the full parameter space. This reduces the total parameter product to 462j.



**Figure 7.1 The optimum ATP yield for methanogens throughout Enceladus' ocean.**

Maps showing the ‘best  $n_{\text{ATP}}$ ’ values for methanogens in Enceladus’ ocean at various temperatures, pH values, salt content and methanogenesis energy yield. These represent the  $n_{\text{ATP}}$  values which yield the maximum possible power supply in such conditions.

### 7.2.1.2 | Constraining chemical inflow and outflow

One major limitation of the results presented in Chapter 6 is that they do not consider the inflow and outflow of energy and nutrients. Properly doing so is a crucial step in constraining the possible levels of biomass and biosignatures over useful — i.e. geological and evolutionary — timescales. Here we outline a first approximation of the overall outflow and inflow of methanogenesis ingredients using Cassini observations and models of serpentinisation and rock alteration in the core.

The chemical outflow of the ocean can be inferred from Cassini's measurements. Consider the range of molar mixing ratios observed for  $\text{H}_2$ ,  $\text{CO}_2$  and  $\text{CH}_4$  summarised in Table 2.3 for a collection of Cassini flybys. The plume appears to have an outflow rate which averages between  $100\text{--}1000 \text{ kg s}^{-1}$  [16]. If the total molar content of 1 kg is 55.5 moles — similar to pure water, as  $\text{H}_2\text{O}$  makes up  $\sim 96\%$  of the molar content (Table 2.3) — then this can be converted to the total molar output of each species. The total outflow of the entire ocean alone is not immediately useful. To convert this into a mean outflow per unit volume, we divide through by the volume of the ocean. As there remains no consensus on the oceans' scale, this volume alone has an uncertainty. Using the mean ocean depth of 37 km and an ice shell thickness of 21 km used in Chapter 6 we arrive at a total ocean volume of  $2.1 \times 10^{16} \text{ m}^3$ . In contrast, Steel et al (2017) [20] used an ocean volume of  $2.7 \times 10^{16} \text{ m}^3$ . We take these uncertainties into account to predict the minimum and maximum mean molar outflows per unit volume in Table 7.2.

The total molar inflow of  $\text{H}_2$ ,  $J_{\text{H}_2}^{\text{in}}$ , has been estimated by multiple studies with little consensus at present. Typical estimates vary as  $J_{\text{H}_2}^{\text{in}} \in [10^{-3}, 10^2] \text{ mol s}^{-1}$  [16, 20, 198, 202], though often these conflate Enceladean and European hydrothermal conditions. Using these as minimum and maximum values of  $\text{H}_2$  inflow, we can compute the mean ocean inflow per unit volume as for the outflow above. However, this is limited as we know such processes are occurring at the rock-water boundary and not throughout the ocean. So instead, we could consider a shell of 1 L vessels at the rock-water boundary (Figure 7.2). This would correspond to  $\approx 5 \times 10^{14} \text{ L}$ . If each of these received all of the hydrothermal input, they would be 5–6 orders of magnitude larger than the mean ocean inflow (Table 7.2). To select a maximum inflow, we also consider the scenario where only 1% of the rock-water interface is experiencing such activity. This can increase the maximum  $J_{\text{H}_2}^{\text{in}}$  to up to  $10^{-10} \text{ mol (L s)}^{-1}$ .

It is important to note that some of these values do not add up, particularly the ocean mean inflow vs outflow. If hydrothermal activity and rock alteration processes are the only source of  $H_2$ , then there are regions of this uncertainty which are unphysical, e.g. more material outflow than is produced, or high inflow with no outflow. The degree of this discrepancy is visualised in Figure 7.3.

The rate of hydrothermal/oceanic  $CO_2$  and  $CH_4$  production on Enceladus is unknown, but it can be demonstrated that they are not required to build a steady state model provided that we assume life is present and acts as an intermediary, with no other chemical processes at play (Figure 7.3). For a given molar inflow and outflow to an inhabited volume, life must be consuming the difference if it is not zero:

$$J_{H_2} = J_{H_2}^{in} - J_{H_2}^{out} \quad (7.1)$$

$$J_{CO_2} = J_{CO_2}^{in} - J_{CO_2}^{out} = \frac{1}{4} J_{H_2} \quad (7.2)$$

$$-J_{CH_4} = J_{CH_4}^{in} - J_{CH_4}^{out} = \frac{1}{4} J_{H_2} \quad (7.3)$$

where the factors of  $\frac{1}{4}$  represent the molar ratios between  $CO_2$  and  $CH_4$  with  $H_2$  in methanogenesis. For the steady state NutMEG simulations in this chapter, the net inflow to an Enceladus object of each of these species is included in this way.



**Figure 7.2** Schematic of the simple inflow and outflow model for Enceladus' ocean **used here** , and how it is reflected in a NutMEG simulation. For a steady state the net input must match the production of the organism while the system remains within the uncertainty of inflows and outflows and the instantaneous composition.

**Table 7.2 Steps to compute the mean molar inflow and outflow of H<sub>2</sub>, CO<sub>2</sub> and CH<sub>4</sub> in Enceladus' ocean.** For CO<sub>2</sub> and CH<sub>4</sub> inflow remains unconstrained so we approximate these by assuming they are produced in quantities representative of methanogenesis and serpentinisation (Figure 7.2).

	H <sub>2</sub>		CO <sub>2</sub>		CH <sub>4</sub>	
	min	max	min	max	min	max
mixing ratio (%)	0.4	1.4	0.3	0.8	0.1	0.3
total molar outflow [mol s <sup>-1</sup> ]	22.2	777	16.7	444	5.55	167
mean molar outflow [mol (L s) <sup>-1</sup> ]	$8 \times 10^{-19}$	$4 \times 10^{-17}$	$6 \times 10^{-19}$	$2 \times 10^{-17}$	$2 \times 10^{-19}$	$8 \times 10^{-18}$
total ocean inflow [mol s <sup>-1</sup> ]	$10^{-3}$	$10^2$	-	-	-	-
mean ocean inflow [mol (L s) <sup>-1</sup> ]	$4 \times 10^{-23}$	$5 \times 10^{-18}$	-	-	-	-
rock-water shell [mol (L s) <sup>-1</sup> ]	$10^{-17}$	$10^{-12}$	-	-	-	-
localised rock-water shell [mol (L s) <sup>-1</sup> ]	$10^{-15}$	$10^{-10}$	-	-	-	-

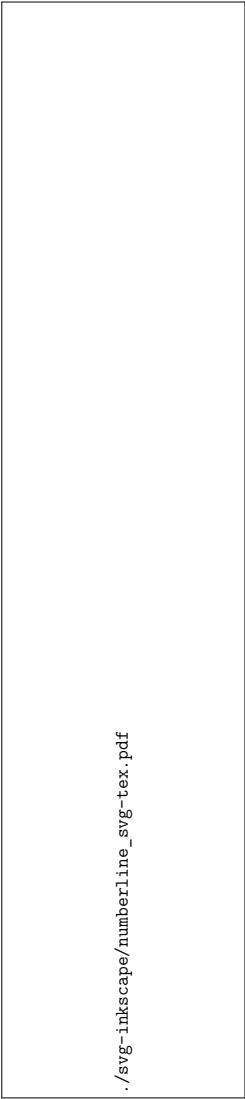


**Figure 7.3 Feasibility of different chemical inflows and outflows on Enceladus.** The number line shows the endmembers of mean H<sub>2</sub> inflow and outflow in Enceladus' ocean in mol (L s)<sup>-1</sup> in log<sub>10</sub> space, with inflow on the top and outflow on the bottom. Only a fraction of the proposed values are consistent with each other, but this simple comparison ignores other sources and sinks of H<sub>2</sub> in the ocean, including life.

## 7.2.2 | Towards a steady state

If there are methanogens in habitable niches on Enceladus, one would expect that they have reached a steady state with their environment. As the icy moon appears to have a persistent supply and release of material, it would be a useful endeavour to see whether life can exist within the flow of such a system — while remaining within the uncertainties of our observations and models derived from them. Here, we examine three case studies to identify suitable initial conditions for NutMEG simulations over long timescales to determine the ranges of biomass turnover and biosignature production which are consistent with what we know so far about Enceladus.

### 7.2.2.1 | Case study 1: maximum sustainable death rate

A methanogen death rate is required lest the population increase in perpetuity. The death rate of Earth methanogens is unknown, and in previous studies known death rates of other organisms have been used, such as algae [21]. We can find a crude upper limit for this by working out the maximum possible growth rate in a set of conditions and using this as the death rate. Then, as many cells are dying as are being produced per unit time and the population stays fixed because other variables such as the available energy and nutrients do not appreciably change if they are appropriately resupplied. This can be calculated for one such sustained disequilibrium using:

$$\mu(t) = \frac{dB}{dt} \frac{1}{B(t)} = \frac{1}{E_{syn}} \left( P_S(t) - P_M(t) \right) \quad (2.15 \text{ revisited})$$

At steady state,  $\mu(t) = \delta(t)$ , where  $\delta(t)$  is the death rate in  $s^{-1}$ . In the limit  $P_S^{deq} \gg P_M$  where  $P_S^{deq}$  is the power supply at the sustained disequilibrium, the maximum death rate can be expressed as:

$$\delta_{max} = \frac{P_S^{deq}}{E_{syn}} \quad (7.4)$$

If the ocean disequilibrium is sustained at the compositions inferred in Chapter 6,  $P_S^{deq}$  is equivalent to the microbially accessible power supplies derived in that work.

### 7.2.2.2 | Case study 2: 'new' sustainable biomass

Another simple model of a steady state can be made by assuming that the net incoming power supply from  $H_2$  and  $CO_2$  production in the core is being consumed by methanogens at some stage, leaving the system in the disequilibrium characterised in Chapter 6 overall. Assuming that the power made available is instantaneously taken up by life (and so not significantly affecting  $Q$ ), we can estimate the incoming power supply per unit volume as:

$$P_S^{\text{in}} \approx \Delta G^{\text{deq}} \frac{J_{H_2}}{4} \quad (7.5)$$

We can then estimate an upper bound on the number of cells that incoming power supply can sustain,  $B_{\text{new}} = P_S^{\text{in}} / P_M$  in cells  $L^{-1}$ . This is not ideal, because it: i) does not include the energy required to build that biomass in the first place; ii) assumes all of the incoming energy can be accessed by pre-existing organisms; and iii) does not constrain pre-existing biomass. However, this is the method that has been used in previous studies to estimate the possible biomass levels on Enceladus [16, 19, 20]. Immediately we can extend such estimates using our broad parameter space (from Chapter 6) and maintenance powers (from Chapters 3 & 5).

We also use this technique to examine whether the inflow could make regions of the parameter space which appear uninhabitable in Chapter 6 habitable. Because in that snapshot, these must have a zero-inflow biomass of 0 ( $P_S^{\text{deq}} < P_M$ ) we can calculate a range of possible biomasses in this scenario, which is between:

$$B_{\text{max}} = \frac{P_S^{\text{in}}}{P_M - P_S^{\text{deq}}} \quad (7.6)$$

$$B_{\text{min}} = \frac{P_S^{\text{in}}}{2P_M - P_S^{\text{deq}}} \quad (7.7)$$

The former assumes that all that is needed is for the total bioavailable power supply be brought up to  $P_M$  (e.g. an upper limit), the latter assumes that needs to happen and then the sustainable biomass is calculated on top of it (e.g. a lower limit, similar to the new sustainable biomasses above).

To work out the  $H_2$  flux required to make these regions habitable for a single cell per litre, we used the relation:

$$P_M - P_S - P_S^{\text{in}} = 0 \quad (7.8)$$

$$J_{H_2} = \frac{4P_S^{\text{in}}}{\Delta G} = -\frac{4(P_M - P_S^{\text{deq}})}{\Delta G} \quad (7.9)$$

### 7.2.2.3 | Case study 3: sustainable biomass by preserving the reaction quotient

An alternative way to determine how much biomass could be sustained in the ocean is to assume that putative life is preserving the reaction quotient as we observe it. The idea here is that if the ocean is inhabited, and has a constant supply of  $H_2$  and  $CO_2$ , life must be consuming it in such a way that our observations are consistent with the overall status quo of the ocean. Algebraically,  $J_{H_2}$  [ $\text{mol (L s)}^{-1}$ ] must be equivalent to the net consumed  $H_2$ :

$$4Br_{cat} = J_{H_2} \quad (7.10)$$

where the factor of 4 corrects for the fact that 4 moles of  $H_2$  are consumed per mole of the methanogenesis reaction. Then, we can write:

$$B = \frac{J_{H_2}}{4r_{cat}} = \frac{J_{H_2}}{4k_M[CO_2][H_2]^4} \quad (7.11)$$

$$= \frac{J_{H_2}}{4P_S^{\text{deq}}/\Delta G^{\text{deq}}} = \frac{J_{H_2}\Delta G^{\text{deq}}}{4} \frac{1}{P_S^{\text{deq}}} \quad (7.12)$$

$$= \frac{P_S^{\text{in}}}{P_S^{\text{deq}}} \quad (7.13)$$

Note that this is only an approximation, as it does not include a contribution from  $\Delta G_{ATP}$ . It appears that when there is a lower spontaneous power supply, we need a higher density of cells for a constant incoming power. This runs the risk that very low (i.e. energetically uninhabitable) spontaneous power supplies will demand very large biomasses to be viable — which of course is improbable. We rectify this with the conservative assumption that the Cassini-derived conditions are actually habitable, i.e.  $P_M \leq P_S^{\text{deq}}$ . In environments where this was not already the case, e.g. the uninhabitable regions defined in Chapter 6, we do not use this method.



Case study 3 appears a more pessimistic approach than case study 2 and relies on the assumption that the Cassini-derived ocean is habitable, e.g. the inflow cannot make up for any cases where the steady-state is energetically uninhabitable. However, it is more realistic in the sense that it does not assume anything about the growth of the colonies where case study 2 yields the total biomass that could be supported, neglecting how much energy is required to build it in the first place. Case study 3 fits organisms into observable data, whereas case study 2 ‘forces’ organisms into observable data. A superior approach to both of these would be to run a time dependent NutMEG simulation and find out what ecosystems can coexist with our constrained parameter spaces and inflows.

#### 7.2.2.4 | NutMEG implementation

The considerations above were used as an input for an application of NutMEG’s `steady_state_1org` class (Section 4.2.7). This allows the user to define maximum and minimum parameters for variables of the reactor and resident hordes to monitor. It performs a growth simulation, and tells the user whether or not the final state is within this defined parameter space and — if it isn’t — outputs what was violated, or what failed (e.g. all organisms have died, or the composition no longer reflects that which was constrained in Chapter 6).

The goal here was to extend the case studies above to constrain, for a given set of conditions, the *ranges* of biomass that could be sustained *without* perturbing the Cassini-derived conditions so much that the system wanders outside the parameter space from Chapter 6. The key unknown variable which affects the TOM’s (Typical Optimal Methanogen, Chapter 5) behaviour is its death rate,  $\delta$ . To achieve this, we assigned initial conditions which must be a steady state for a given  $J_{H_2}$ , temperature, bulk ocean pH, and ocean salt level (Chapter 6), which were a biomass given by case study 3:

$$B = \frac{J_{H_2}}{4r_{cat}} \quad (7.14)$$

which is a simple calculation as  $r_{cat}$  is computed upon initialisation of a horde object. To choose an initial death rate, one time step was taken in the chosen conditions with  $\delta = 0$ .  $\delta$  was then set to the resultant growth rate from that step. This conveniently allows for  $\delta$  to account for the `maximum_metabolic_rate` property of the TOM, an improvement over case study 1, and together with  $B$  defines conditions under which a microbial population could coexist under such inflow with no change in any other conditions.

Owing to the breadth of the parameter spaces we identified in Chapter 6, there must be a variety of populations which could be supported while keeping the composition within those bounds. To try and compute them, we varied the death rate of the TOM to see if a new steady state could be achieved over a computationally reasonable timescale in which the final composition is within the error bounds identified in Chapter 6. As one might expect, increasing the death rate inevitably leads to the demise of the culture — they simply die faster than they can grow — so for this analysis, death rates were only reduced. To ease computation time, the reduction in  $\delta$ ,  $\delta_{\%}$  [%] was first attempted at:

$$\delta_{\%} = 1 - \frac{\log_{10} B}{100} \quad (7.15)$$

If that could not result in a steady state,  $\delta_{\%} = 0.99$  was attempted. When a steady state was found, the new death rate was reduced again by the same percentage until the population becomes unsustainable. We chose to cap  $\delta_{\%}$  at 0.99 because: i) higher values would become computationally prohibitive; and ii) an environment which is not resilient to an unconstrained organismic variable changing by less than 1% is unlikely to be tenable for long-term habitability.

The hypothesis here is that this will allow for larger biomasses in some parameter combinations up to a point at which either: i) the growth becomes unsustainable for the environment; or ii) the environment becomes so far removed from our constrained parameter space that it cannot be explained by Cassini observations and existing models. To perform this analysis, a new helper class `NMsteadystate` was created which builds grids of the steady state values with temperature and pH, using the `NutMEG.steady_state_1org` class with a TOM and Enceladus, over the parameter space defined in Section 7.1.1.

From these growth simulations, we extract the range of possible steady state biomasses and death rates ( $B_{ss}$  and  $\delta_{ss}$ ). Immediately, this can be converted to biomass turnover  $B_{to}$  in cells (L s)<sup>-1</sup>:

$$B_{to} = \delta_{ss} B_{ss} \quad (7.16)$$

This tells us the number of dead cells per second per litre which are being produced by the system. We can use the rate of deterioration of this matter to assert whether it could be a valid (and detectable) biosignature by the time it reaches the top of the ocean.

### 7.2.3 | Biomass turnover and racemization

Life is selective in chirality, and so is inherently not racemic. However, chiral species naturally degrade into racemic mixtures with time when there are no selective (bio)chemical processes (Subchapter 3.3 & Box 3.3). Chirality has been touted as a possible biosignature, as it distinguishes between organic species which can be formed through both biological and abiological processes [20]. If we can constrain the rate at which amino acids racemize, we can estimate how long it takes the detritus produced by putative life on Enceladus to appear indistinguishable from abiologically produced organic matter (e.g. from hydrothermal activity).

A standard way to characterise a mixture containing chiral species is the  $D/L$  ratio. This is the ratio between the dextrorotatory  $D$  and levorotatory  $L$  isomers — the two enantiomers — respectively. Life on Earth mostly utilises amino acids in the  $L$ -form. The change in the ratio with time (e.g. as it approaches a racemic mixture ( $D/L = 1$ )) has been resolved using forward modelling [203]:

$$\left(\frac{D}{L}\right)_{t+dt} = \frac{e^{2k_{rmz}(t+dt)}R_t - 1}{e^{2k_{rmz}(t+dt)}R_t + 1} \quad (7.17)$$

$$R_t = \left[ \frac{(1 + D/L)}{(1 - D/L)} \right]_t \quad (7.18)$$

using a suitable time step  $dt$  and the first order rate constant of racemization for the species in question,  $k_{rmz}$  [ $s^{-1}$ ]. For our analysis, in which the amino acid content produced by life is chirally selective, the initial  $D/L$  ratio is 0. Figure 7.4 shows values of  $k_{rmz}$  constrained by Cohen and Chyba (2000) [203], with the ‘average’ racemization rate constant used by Lever et al. (2015) [37]<sup>1</sup>. These rate constants were constrained at pH 7–7.6 and ionic strength 0.01–0.5 M. These are representative of ‘inside the cell’ pH and ionic strength values (Chapter 3), but not necessarily the wider Enceladus environment (Chapter 6).

We present results in terms of the  $L$ -form %  $L_{\%}$  of the system, equivalent to  $100 - (50 \times D/L)$ . For example, a fully racemic mixture has an  $L_{\%}$  of 50%.  $L$ -form percentages of >60% are generally considered likely to be biogenic, so we use 60% as the lower acceptable limit for a ‘biosignature’ by the  $L_{\%}$  of the system. Equation 7.17 resolves the  $D/L$  ratio for a fixed initial concentration, we instead have a constant input of detritus  $B_{to}$  assuming the biosphere has settled into a steady state. Because the route to  $L_{\%} = 60\%$  is exponential, there will still come a point at which even the

<sup>1</sup>This is the racemization rate constant used for their maintenance power due to amino acid racemization in the cell. It is interesting that their values, particularly at low temperatures, are much higher than those reported by Cohen and Chyba (2000) [203]. This means minimal maintenance powers could be substantially lower below ~300 K.

7\_Enceladus\_Biomass\_sig/figs/k\_rmz.pdf

**Figure 7.4 Rate constants of amino acid racemization** at temperatures between 270 and 400 K. Individual amino acid racemization rate constants are from Cohen and Chyba (2000) [203], also plotted is the Lever et al. (2015) [37] average rate constant inside the cell.

constant chirally selective input is overshadowed by the overwhelmingly racemic surroundings. We find this critical time,  $t_{60}$  [s], as the time when the mean  $L_{\%}$  of the time steps leading up to it is 60. We can then also immediately find the concentration of dead cells which have been produced up to the point at which the composition has been racemized beyond being clearly biogenic:

$$B_{d60} = t_{60} B_{to} \quad (7.19)$$

## 7.3 Results

### 7.3.1 | Steady state case studies

First let us examine the case studies for determining a suitable steady state input for our NutMEG simulations. In case study 1, we estimate the maximum possible death rate of methanogens. In case studies 2 & 3 we use different methods to estimate how much biomass is needed to utilise the incoming energy.

#### 7.3.1.1 | Case study 1

Figure 7.5 shows the growth/death rates required for a steady state according to Equation 7.4 at the temperatures, pH values and salt levels outlined in Table 7.1, constrained to the corresponding ‘best’  $n_{\text{ATP}}$  value (Figure 7.1). It also shows these growth rates as constrained by initialising a TOM object which reduces the maximum metabolic rate to match that of an Earth-like methanogen — operating with the TOM or minimal maintenance powers (Chapters 3 and 5). These latter two are also restricted via the `max_metabolic_rate` parameter of the TOM. Where a segment is coloured black, there is not sufficient power available for growth e.g.  $P_S^{\text{deq}} < P_M$ . In one segment of Figure 7.5 — at pH 10 373 K in a low salt ocean — the ‘maximum’ growth rate is also coloured black. In this set of conditions there is no free energy available so the ocean is uninhabitable. Calculating a maximal death rate in this way is rather limited, because:

1. Many of the high-end of the growth/death rates predicted by Equation 7.4 are above maximum recorded growth rates for methanogens.
2. Many of the low-end of the growth/death rates are immeasurably small —  $3 \times 10^{15}$  s is 100 Myr, the lower limit of Enceladus’ age [107]!
3. The maintenance power is a significant contributor in all cases for empirical estimates, and in many cases for the minimal maintenance estimates (Chapter 6), so the assumption that  $P_S^{\text{deq}} \gg P_M$  is not valid for all conditions. This is reflected in the NutMEG growth rates of Figure 7.5.

On point 3 above, including the relevant maintenance powers in the calculation above returns values very similar to the growth rates predicted by Equation 7.4 when the power supply is at least double the power demand, unless the maximum metabolic rate is reached. This means that NutMEG’s numerical solution is ap-

proximately equivalent to Equation 7.4 in such conditions. In others, the NutMEG extracted peak growth rates are either: i) slightly lower than this owing to the  $P_M$  contribution or ii) zero because  $P_S^{\text{deq}} < P_M$ .

These growth rates can be used as the maximum 'death rate' required to sustain a population which is in an enforced equilibrium as defined in Chapter 6. What this does not tell us, however, is the level of biomass that exists in these conditions.



**Figure 7.5** Maps of the death rate required for a steady state on Enceladus at various temperatures, bulk ocean pH values, salt-content and maintenance power costs. At each entry for pH, the left-hand wedge corresponds to a maintenance power of zero and the right hand wedge is segmented into TOM and minimal maintenance powers. Black wedges represent conditions which are uninhabitable.

### 7.3.1.2 | Case study 2

For case study 2, we introduce a simple inflow and outflow of methanogenesis ingredients controlled by models of rock-water activity and plume outgassing respectively. We use this to approximate the average incoming power supply and how much biomass this could sustain.

Figure 7.6 shows the total power supply a given net  $H_2$  inflow,  $J_{H_2}$ , would provide to the parameter space (Equation 7.5). The net inflow of  $CO_2$  and  $CH_4$  is calculated from  $J_{H_2}$  as outlined in Equations 7.2–7.3. The results shown are for  $J_{H_2} = 10^{-10} \text{ mol (L s)}^{-1}$  but by Equation 7.5, changing  $J_{H_2}$  simply results in a translation in the  $y$  axis in the  $\log_{10}$  scale. Interestingly, the inflow is less useful for methanogens at elevated temperatures and pH values. This owes to the less negative  $\Delta G^{\text{deq}}$  values in these conditions (Figure 6.1). Furthermore, for pH values  $\geq 10$ , sharp drops in incoming power supply emerge as  $\Delta G^{\text{deq}} \rightarrow 0$ .



**Figure 7.6 The incoming power supply to Enceladus at different temperatures, bulk ocean pH, salt-level and rates of  $H_2$  inflow.** Dashed lines indicate the nominal salt case, and shaded regions show the variability between high- and low-salt cases. Changing the  $H_2$  inflow rate is equivalent to a  $y$  axis translation in  $\log_{10}$  space.

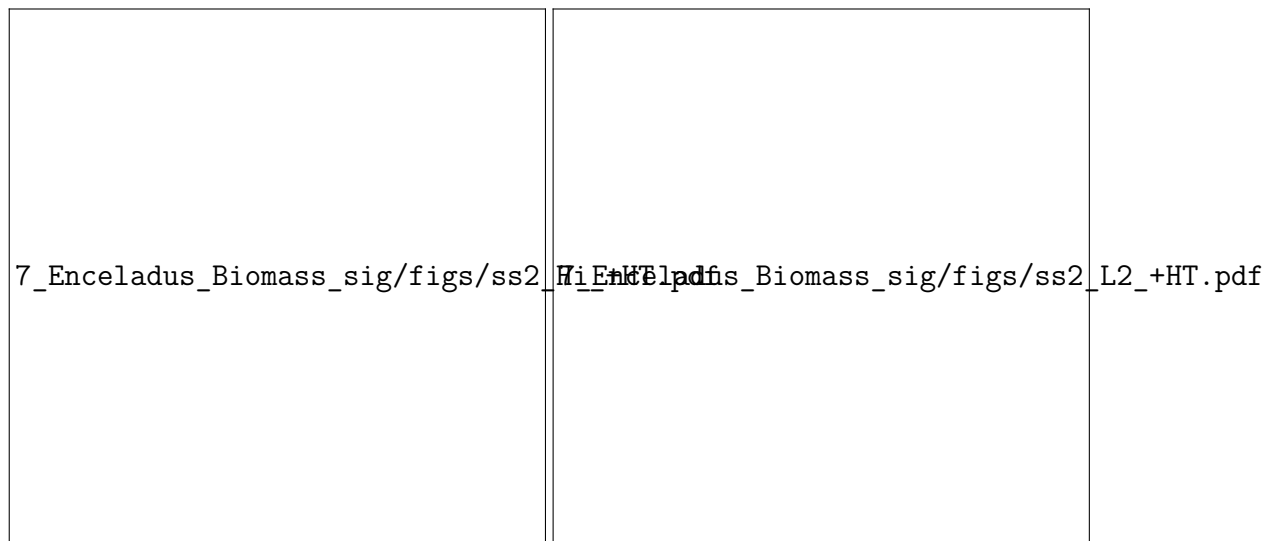


**Figure 7.7 New sustainable biomass predicted by case study 2** at different temperatures, bulk ocean pH, salt-level and rates of  $H_2$  inflow on Enceladus. The two panels represent different maintenance powers. The filled in areas show the difference between a low salt, low energy ocean and a high salt, high energy ocean, and colours denote pH as in Figure 7.6. The new sustainable cells do not vary significantly with pH unless that pH indicates uninhabitability. Changing the  $H_2$  inflow rate is equivalent to a  $y$  axis translation in  $\log_{10}$  space.

Figure 7.7 shows the ‘new’ sustainable biomass corresponding to the incoming power supplies shown in Figure 7.6 for four values of  $J_{H_2}$ :  $10^{-10}$ ,  $10^{-12}$ ,  $10^{-17}$  and  $10^{-23}$ , and at two characteristic maintenance powers. These are the default TOM maintenance power (Chapter 5) [1] and the Lever et al. (2015) [37]  $P_M$  with protein replacement after 2% racemization. As with the incoming power supply, changes in  $J_{H_2}$  are reflected in a simple  $y$  axis translation on a  $\log_{10}$  scale as all other variables are determined by the Cassini-derived conditions. Horizontal lines are drawn on Figure 7.7 at  $10^0$  — indicating the threshold at which the inflow is not even enough to sustain 1 cell per litre!

We can see that the minimum mean total ocean inflow from Table 7.2 of  $\sim 10^{-23}$  is not able to sustain more than 1 cell  $L^{-1}$  in any conditions under any maintenance powers. However, this is not useful as a mean inflow of  $\sim 10^{-23}$  mol  $(L\ s)^{-1}$  is unphysical with the plume output (Figure 7.3). The minimum mean inflow which is physical with the plume output,  $10^{-17}$  mol  $(L\ s)^{-1}$ , appears to be able to sustain organisms operating at minimal maintenance below 400 K but only very low populations  $\sim < 10^6$  cells  $L^{-1}$  and can sustain some ( $< 10^2$  cells  $L^{-1}$ ) operating with optimal growth maintenance powers at temperatures below 300 K. Because this technique is similar to methods used in previous work, we can compare the ‘new’ sustainable biomasses in Figure 7.7 to those calculated by others. Cable et



al. (2020) [16] combine some results from these studies under equivalent ocean assumptions (aside from  $J_{\text{H}_2}$ ) to derive cell abundances between  $10^{-3}$ – $10^{6.6}$  cells  $\text{L}^{-1}$  at 273 K [16, 20, 198]. The maximum here is similar to our estimate with  $J_{\text{H}_2} = 10^{-17}$  mol  $(\text{L s})^{-1}$  with minimal maintenance power. An important limitation with all of these low biomasses is the assumption that the organisms can access the incoming energy instantaneously —  $10^6$  organisms with a volume  $\sim 1 \mu\text{m}^{-3}$ , would only take up  $\sim 10^{-7}\%$  of one litre!

We also considered the ‘new’ sustainable biomass that could exist if *all* of the incoming  $\text{H}_2$  were consumed at the water-rock boundary, leaving only the amounts required in the bulk ocean to satisfy plume output. As we have shown algebraically and visually on Figure 7.7, increasing  $J_{\text{H}_2}$  on a  $\log_{10}$  scale results in an equivalent increase in the ‘new’ sustainable biomass. If the bulk of Enceladus’ putative biosphere is largely restricted to these regions — and consuming most of the  $\text{H}_2$  and  $\text{CO}_2$  there — we could expect biomasses up to 7 orders of magnitude higher than reported above. Coincidentally, as this significantly increases the microbe concentration the assumption that organisms can access the inflow instantaneously becomes less limiting, but we are now saddled with the new assumption that life is restricted to these regions and must endure higher temperatures.

Case study 2 also offers an enticing, albeit even more speculative, idea: that the influx of  $\text{H}_2$  and  $\text{CO}_2$  could tip the balance of uninhabitable conditions as characterised in Chapter 6 to habitable ones. Figure 7.8 shows the maximum and minimum biomasses that spontaneously uninhabitable conditions could support, calculated using Equations 7.6–7.7 across the parameter space for four values of  $J_{\text{H}_2}$ :  $10^{-10}$  and  $10^{-23}$ . Once again we use the TOM and Lever et al (2015) characteristic maintenance powers. As with all the other case study 2 results, changes in  $J_{\text{H}_2}$  are reflected in a simple  $y$  axis translation on a  $\log_{10}$  scale on the predicted biomass as all other variables are determined by the Cassini-derived conditions.

The biomasses which can be made in Cassini-derived uninhabitable conditions are strikingly similar to the ‘new’ sustainable biomasses of Cassini-derived habitable conditions, provided  $\Delta G^{\text{deq}}$  is negative. This is due to the nature of Equations 7.7–7.6, when  $P_S^{\text{deq}} \ll P_M$ ,  $P_M - P_S^{\text{deq}} \approx P_M$ , and the expression for biomass is reduced to the same as that used for Figure 7.7. This means that — tentatively — by this model, with a suitable chemical inflow *all* of the conditions which have a negative  $\Delta G^{\text{deq}}$  could be sustaining sizeable biospheres, reliant on that inflow. We will explore this further in the discussion, but this fuels the idea introduced in Chapter 6: if the Cassini-derived conditions have a large chemical disequilibrium with swathes of unused energy for life, this could be an antibiosignature. If instead they teeter on the balance of uninhabitability and have a large energy supply this could be indicative of a bustling biosphere which makes efficient use of everything made available to it.

The final application of this case study was to assess *how much*  $H_2$  inflow is required to make those 'uninhabitable' regions of the parameter space habitable. We applied Equation 7.9 to the parameter space and this plot is shown in Figure 7.9. When the area is spontaneously habitable, or  $\Delta G^{\text{deq}}$  is positive, this technique cannot be used; these regions are shown by the black and green blocks in the figure respectively. On the left hand side, representing the TOM maintenance power (Chapter 5), required fluxes are maximised above 373 K because this extends beyond Chapter 5's data set.



**Figure 7.8 Biomass which can be created in Cassini-derived uninhabitable conditions** via assumptions in case study 2, at two rates of  $H_2$  inflow. These are  $10^{-10}$  and  $10^{-23} \text{ mol (L s)}^{-1}$  appearing at the top and bottom of each plot respectively. The top row of plots are at TOM maintenance levels and the bottom row are at minimal maintenance levels. Coloured numbers on the plot indicate the pH values that the lines represent. The labels 'max', 'nom' and 'min' refer to maximum salt/energy, nominal salt/energy and minimum salt/energy yields respectively. Changing the  $H_2$  inflow rate is equivalent to a y axis translation in  $\log_{10}$  space.



**Figure 7.9** Maps of the  $\text{H}_2$  inflow required in  $\text{mol (L s)}^{-1}$  to make the uninhabitable regions of the Enceladus parameter space habitable. Plots on the left hand side represent TOM maintenance powers and those on the right hand side represent minimal maintenance powers. Green wedges are habitable in Cassini-derived conditions (so no  $\text{H}_2$  is required), and black wedges have a positive Gibbs free energy of methanogenesis, where this method cannot be used.

Figure 7.9 goes some way to help explain why the biomasses in Figure 7.8 are so similar to those in Figure 7.7, because large swathes of the parameter space, particularly at minimal maintenance, require  $<10^{-14} \text{ mol (L s)}^{-1}$  for  $P_S^{\text{deq}} + P_S^{\text{in}} > P_M$ . Even more encouraging is that regions of the ocean at 273 K unanimously require inflows which are less than  $10^{-17} \text{ mol (L s)}^{-1}$  — which is physical with the plume output — so it appears there could be a sustainable power supply available were methanogens to briefly foray into the cool ocean. But that depends also on their ability to tolerate a variety of temperatures. On the other hand, higher temperatures need higher inflows to become habitable — but it is important to remember that it is the regions at elevated temperature which are more likely to get the lion's share of this input. It should be stressed once again that these results are limited in the sense that the inflow is the required amount to support 1 cell per litre, and assumes that single cell can access the inflow instantaneously. Hence these are conservative estimates, and in reality a much larger inflow would be required for the environment to appear truly habitable.

### 7.3.1.3 | Case study 3

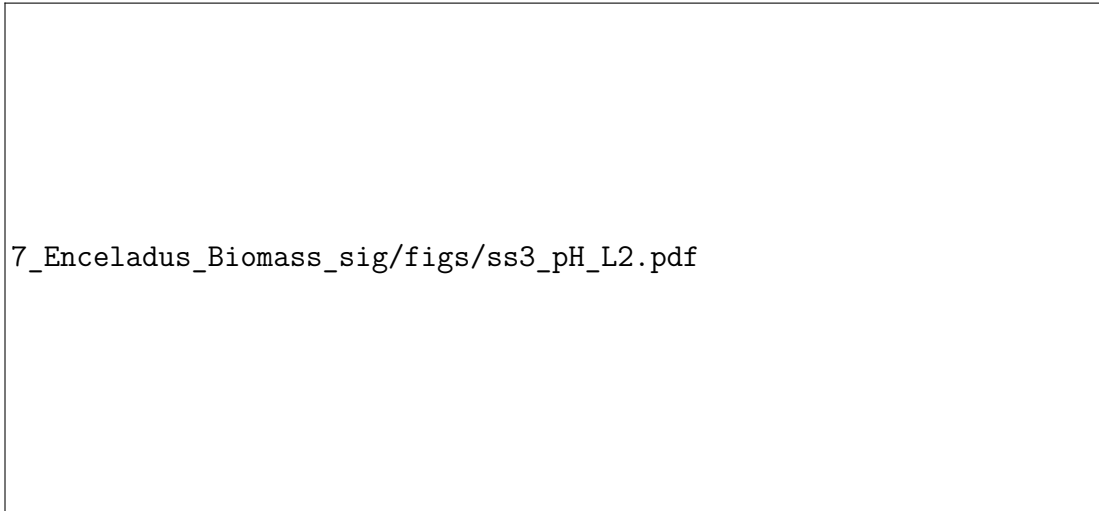
Case study 3 offers a more robust, conservative estimate of biomass than case study 2, because it is concerned with preserving the reaction quotient as we computed it in Chapter 6. It tells us how much biomass is *required* to account for a given  $\text{H}_2$  inflow, rather than how much biomass can *just about survive* on the same inflow.

Figure 7.10 shows the number of cells required to maintain the ocean in the state defined by the parameter space with the 2% racemization replacement maintenance costs at two endmember  $J_{\text{H}_2}$  values:  $10^{-23}$  and  $10^{-10}$ . Dashed, solid and dotted lines indicate a low, nominal and high salt level respectively. In this model, the biomass is a straight fraction between  $P_S^{\text{in}}$  and  $P_S^{\text{deq}}$  but only when  $P_S^{\text{deq}} > P_M^{\text{deq}}$ . The plot of biomass against temperature at varying pH and salt level thus appears the same for all maintenance powers but becomes truncated at different points. For example, on Figure 7.10, the black ticks highlight the lines at which the TOM maintenance power is no longer exceeded: only at pH 7 in nominal and high salt yield, and pH 8 at high yield. At pH 9 there is a truncated line in the nominal salt case at elevated temperature. This represents a small range where  $P_S^{\text{deq}} > P_M^{\text{deq}}$  at this maintenance estimate, but not at temperatures above or below this. Biomasses can be seen at a slightly higher precision of pH value in Figures 7.13–7.14 as part of the NutMEG initial conditions.

As with the case study 2 results, case study 3 biomasses change linearly with  $J_{H_2}$  in  $\log_{10}$  space. For equivalent, habitable conditions with identical  $J_{H_2}$  the ratio between sustainable biomasses is:

$$\frac{B_{cs2}}{B_{cs3}} = \frac{P_S^{\text{deq}}}{P_M} \quad (7.20)$$

From this we can immediately see that the biomass predicted by case study 2 will *always* be larger than that of case study 3, and that a larger spontaneous power supply exacerbates this trend. This is because if the spontaneous power supply is very large, there is unlikely to be a substantial biosphere making use of it — because if there were it would not be so high!



**Figure 7.10 The number of methanogens required to preserve the reaction quotient of methanogenesis in Enceladus conditions at different rates of  $H_2$  inflow.** In each plot, the top lines are for  $J_{H_2} = 10^{-10}$  and the bottom are for  $J_{H_2} = 10^{-23}$ . Changing  $J_{H_2}$  is equivalent to a translation of the y axis in  $\log_{10}$  space. The short black ticks indicate where lines would be truncated for an empirical maintenance power. A horizontal line is drawn at  $10^0$ , indicating only one cell per litre.

### 7.3.2 | Biomass turnover from a NutMEG-derived steady state

On long timescales, the biomass levels  $B_{ss}$  from case study 3 and the death rates of case study 1  $\delta_{max}$  lead to a long-term steady state via a NutMEG simulation (Figures 7.11–7.12). A `NutMEG.steady_state_1org` simulation was performed across a parameter space consisting of: 11 temperatures between 273 and 373 K, 7 bulk ocean pH values between 7 and 10, high-, low- and nominal-salt conditions, two net  $H_2$  inflow rates —  $10^{-12}$  and  $10^{-10}$  mol (L s) $^{-1}$ , and two maintenance powers — the TOM  $P_M$  and the Lever et al. (2015) [37] 2% racemization  $P_M$ . For each combination, the ‘best’  $n_{ATP}$  was used (Figure 7.1). The more conservative  $J_{H_2}$  values of  $10^{-23}$  and  $10^{-17}$  examined in the case studies all had steady state biomasses too small for a stable steady state. In consequence, our simple inflow model (Figures 7.3 & 7.2) suggests that if methanogenic life does exist on Enceladus, it is unlikely to prosper throughout the ocean.

We reduced the initial  $\delta$  to see whether a steady state can still be reached while the environment remains within the uncertainties of the parameter space as constrained by Cassini observations (Chapter 6). Figures 7.11 & 7.12 show some examples of the resulting growth curves, along with the growth rate, maintenance power as a fraction of supply, and composition of methanogenesis species throughout each simulation. Upon reduction of the death rate, broadly speaking one of four things happens:

1. A brief period of limit cycles begins until the culture settles into a new steady state with a composition which may or may not be within the error bounds of the composition (e.g. Figure 7.11)
2. The death rate has become too low, and exponential growth begins. The population reaches an unsustainable level at which the maintenance power is always larger than the power supply despite the inflow. This is not a steady state (e.g. Figure 7.12 LHS).
3. As scenario 2 above, but the peak biomass actually is sustainable with the inflow (e.g. maintenance fraction  $\sim 1$ ). As with scenario 1, the steady state may or may not be within the error bounds of the composition.
4. In some cases, the culture enters into permanent limit cycles in which the biomass regularly fluctuates by 1–2 orders of magnitude. In these scenarios the overall composition of methanogenesis ingredients may either stay within the expected parameter space or fluctuate in/out of it (e.g. Figure 7.12).

Throughout the parameter space, the most common outcome is scenario 2 above, even for changes in  $\delta$  of 1%.

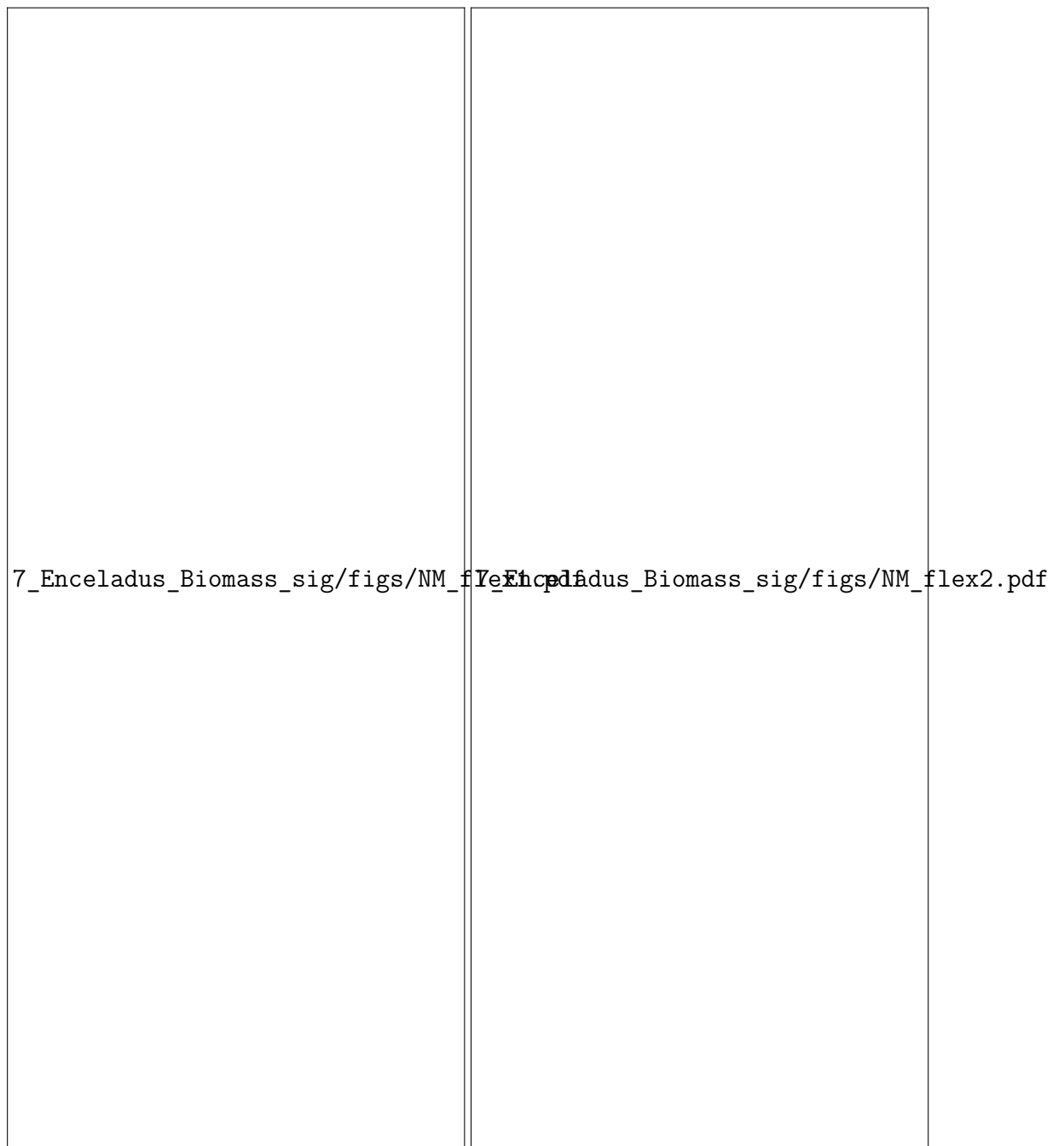


**Figure 7.11 Two characteristic NutMEG simulation results which were flexible in Enceladus-like conditions.** From top to bottom plots show the total biomass, maintenance power as a fraction of supply, growth rate, and composition. As the colour shifts from blue to magenta, the death rate is lowered. Approximately 1 in 5 simulation performed for each is plotted. After a brief correctional period, both of these plots are stable at their final values as seen on these plots for  $\sim 10^9$  s (approximately 100 years).

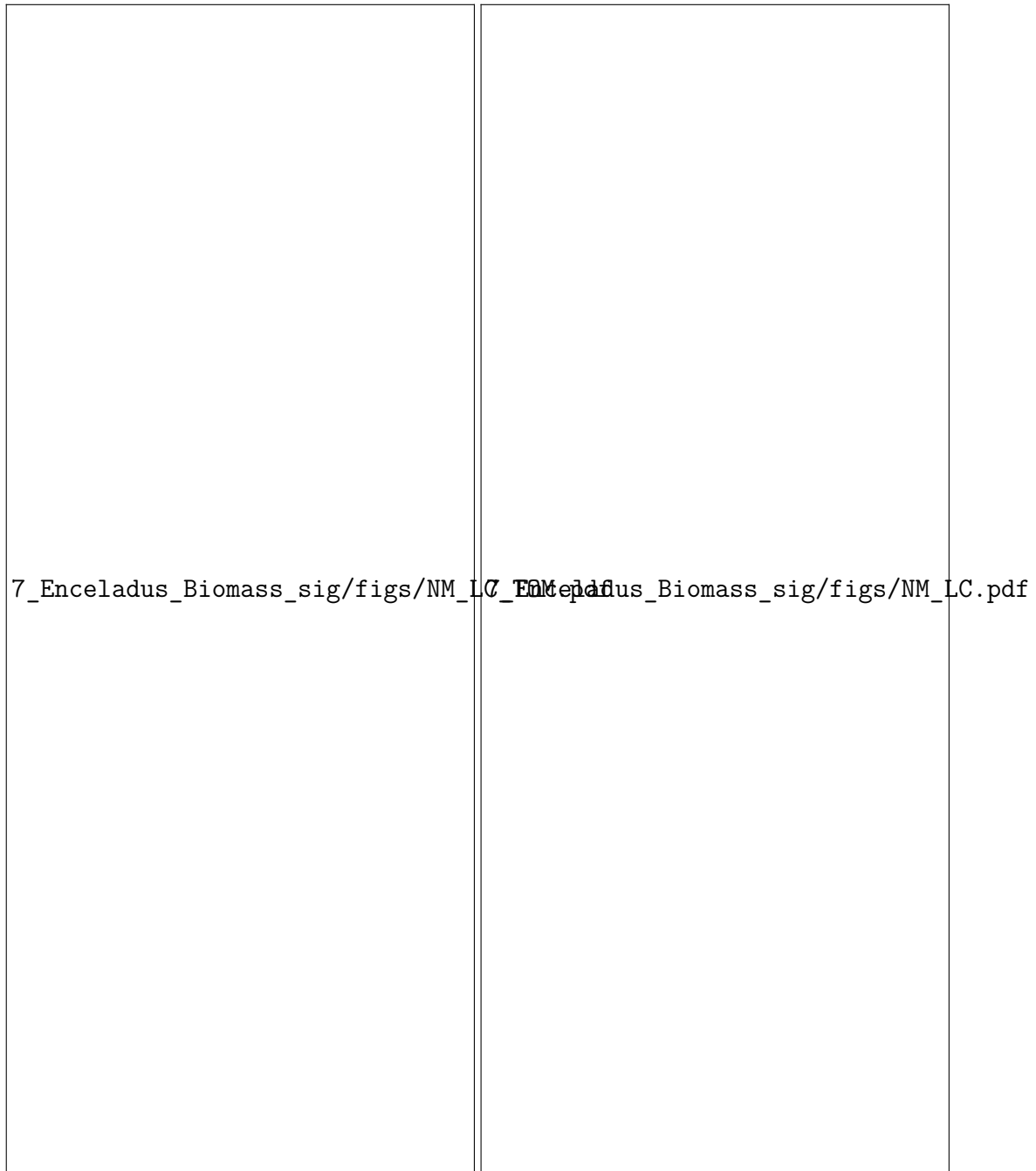


**Figure 7.12 Two characteristic NutMEG simulation results which ended in limit cycles.** From top to bottom plots show the total biomass, maintenance power as a fraction of supply, growth rate, and composition. As the colour shifts from blue to magenta, the death rate is lowered, and all simulations are plotted.



Regions of the parameter space which clearly have a large conservable power supply (traditionally thought of as the *most habitable*) struggle to stay as such when biological activity and chemical inflow is included. We can see this in Figures 7.13 and 7.14 which plot the steady state biomass, growth rates and biomass turnover rates in the parameter space. Wedges on the left-hand side of each pH entry are the input biomasses and growth rates, and wedges on the right-hand side are highest biomasses and lowest growth rates possible meeting the steady state criteria. An '=' symbol between them indicates no change in  $\delta$  could yield a steady state on long timescales, and they exist in abundance at the low end of the pH range and at high temperatures throughout the parameter space. Allowing  $\delta < \mu$  encourages organisms in these conditions to consume that excess energy while continuously growing. By the time that exponential period ends, the biomass is either i) too large to be supported by the chemical inflow — even at the highest  $J_{H_2}$  values, or ii) has altered the composition so much it is no longer reflective of Cassini observations. The 'knife-edge' steady state in these conditions is unlikely to be sustainable long-term, and adds credence to the 'uninhabited habitat' hypothesis if the ocean were indeed to be in such conditions.

The parameter space combinations most flexible to changes in  $\delta$  are those at higher pH values and lower temperatures, provided they are habitable to begin with. These are the combinations with the smallest habitable spontaneous  $P_S$ . Interestingly, this is the case despite these being the 'least habitable' conditions, because there is a lack of the excess power supply seen in other settings. Allowing growth to go ahead ( $\delta < \mu$ ) results in a much smaller change overall both in energy availability and biomass which is more easily balanced by the incoming  $CO_2$  and  $H_2$ . This allows for flexibility in steady state biomass of up to +2 orders of magnitude. Despite the fanfare of possible habitable niches on Enceladus, these results imply that the best case for flexible, long-term habitability is on these fringes at bulk ocean pH values of 8.5–9, *the most probable pH values of the ocean* [14, 87]. Unfortunately this is only the case *at elevated temperatures*, discounting the bulk ocean, and at *minimal maintenance requirements*; in no conditions, aside a few cases of limit cycles, are the empirical maintenance powers flexible to the parameter space.

Segments coloured yellow in Figures 7.13 and 7.14 are conditions which entered limit cycles, meaning a reliable biomass and growth rate could not be extracted. It is telling that these occur in settings which are close to those which were inflexible. Indeed, in some cases the limit cycles emerge between steady state biomasses and the breakdown of the colony.

As we saw in case study 3, the steady state biomass also increases as temperature is decreased and pH increases. Case study 1 showed us that the inverse is true for the initial  $\delta$ . Each of these are displayed on Figures 7.13 and 7.14. We can see from these figures that even though some conditions are very flexible to death rate, they do not often allow for significant differences in biomass when compared to a change in pH or temperature. This is reflected in the biomass turnover of each combination, indicated by the ★ colour on Figures 7.13 and 7.14. The rate of biomass turnover decreases with increasing temperature and increasing pH. In the cases where NutMEG was able to isolate larger steady state biomasses, their turnover actually decreases in comparison to the initial state, because the increase in biomass is more than offset by the decrease in death rate.

As with the biomasses in case study 2 and 3, the initial biomass here varies linearly in log10 space with  $J_{H_2}$ , but the initial  $\delta$  does not. This is reflected in the biomass turnover, the difference between  $J_{H_2} = 10^{-12}$  and  $J_{H_2} = 10^{-10}$  in most cases is equivalent to a factor of 100. This is reflected in Figures 7.13 and 7.14 by the different turnover colourmaps between them.

7\_Enceladus\_Biomass\_sig/figs/NMbig\_grid\_12.pdf

**Figure 7.13 The steady state biomass, death rates and biomass turnover rates in Enceladus' ocean with  $J_{\text{H}_2} = 1 \text{ pmol (L s)}^{-1}$ .** Wedges on the LHS of each pH entry reflect the input steady state, and wedges on the RHS reflect the highest biomass which still meets the steady state criteria. The background, ○, and ★ colours denote the biomass, death rate, and biomass turnover rate respectively. An '≡' symbol between wedges indicates no change in death rate could yield a steady state. Yellow wedges enter limit cycles.

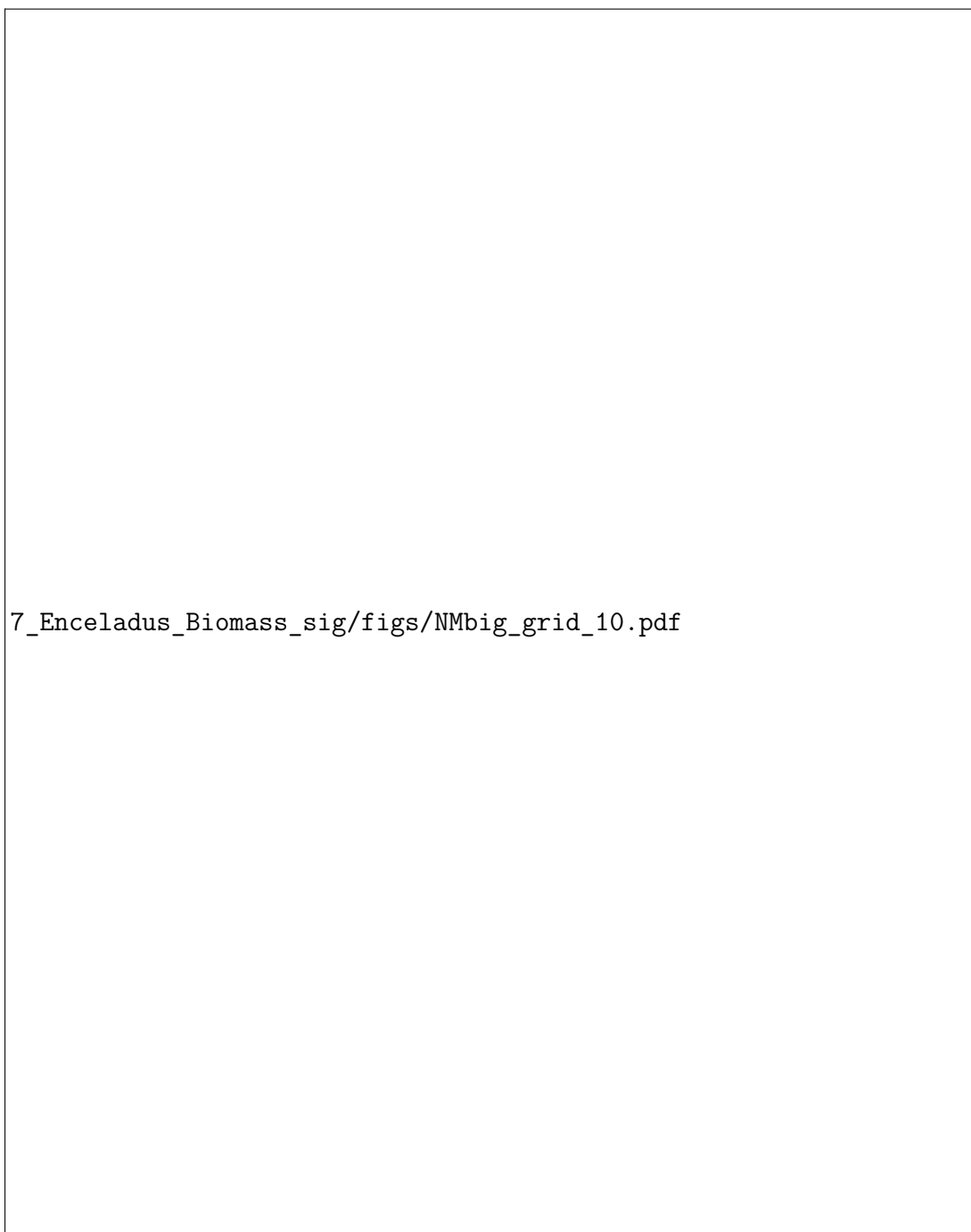


**Figure 7.14** The steady state biomass, death rates and biomass turnover rates in Enceladus' ocean with  $J_{H_2} = 100 \text{ pmol (L s)}^{-1}$ . Wedges on the LHS of each pH entry reflect the input steady state, and wedges on the RHS reflect the highest biomass which still meets the steady state criteria. The background, ○, and ★ colours denote the biomass, death rate, and biomass turnover rate respectively. An '=' symbol between wedges indicates no change in death rate could yield a steady state. Yellow wedges enter limit cycles.

### 7.3.3 | Racemization and biosignature detectability

Over time, a non-racemic mixture of chiral species will decay into a racemic mixture. This is equivalent to the  $D/L$  ratio moving from 1 to 0, and the  $L$ -form % moving towards 50% from 100%. Figure 7.15 shows this decay with time for Glutamic acid and the Lever et al. (2015) [37] mean at 273 K and 373 K. These values for  $k_{rmz}$  were chosen as Glutamic acid has the smallest  $k_{rmz}$  in all cases, and the Lever et al. (2015) average is the largest  $k_{rmz}$  in all cases (Figure 7.4). The dashed lines show the mean  $L_{\%}$  of all time steps, this characterises the  $L$ -form percentage of a mixture which has a constant inflow of 100% levorotatory amino acids. Noted on Figure 7.15 are the times at which the mean mixture has  $L_{\%} = 60\%$ ,  $t_{60}$ . Immediately we can see that the endmember estimates of  $k_{rmz}$  vary  $t_{60}$  by many orders of magnitude, and this is exacerbated further when we consider temperature differences.

Timescales to 60% racemic mixtures can range from months to millennia in the Enceladus parameter space. Figure 7.16 shows  $t_{60}$  values for a mixture with constant inflow of 100%  $L$ -form amino acids at different temperatures, between the same endmembers as above. In the cool bulk ocean, racemization timescales can be expected to be on the order of hundreds of thousands to hundreds of millions of years. At hydrothermal temperatures, this is reduced to as low as a few months to  $\sim 100$  years. Hence, the amount of time detritus is trapped in hydrothermal systems before mixing with the cool bulk ocean is likely to be the key driver of whether biological  $L$ -form percentages will persist to the top of the ocean.

This disparity in  $k_{rmz}$  also dominates the total amount of dead cells required for a closed system's amino acid content at fixed temperature to appear non-biogenic. This is visualised for the parameter space in Figures 7.17 & 7.18. All wedges use the maximum turnover from Figure 7.13 (for Figure 7.17) and 7.14 (for Figure 7.18). The left-hand side of each pH represents this turnover multiplied by the minimum  $t_{60}$  at this temperature, and the right-hand side represents this turnover multiplied by the maximum  $t_{60}$  at this temperature. We can see that the total cell production required decreases with increasing temperature, to the tune where  $< 10^{10}$  cells  $L^{-1}$  would need to be produced in most cases when  $T > 340$  K for  $L$ -form % to no longer be a detectable biosignature. This is a very simple analysis, however, and as discussed above the degree of racemization on Enceladus will be heavily dependent on ocean mixing. We discuss this and the other limitations of the speculative analysis in this chapter in the discussion subchapter.

7\_Enceladus\_Biomass\_sig/figs/DLratio.pdf

**Figure 7.15 Percentage of amino acids in L-form with time at different temperatures.** Dashed lines show a rolling mean of time steps, indicating the net L-form percentage of a mixture receiving constant input of 100% levorotatory isomers. The times at which a constant input of 100% levorotatory yields a mixture which persistently appears to have an *L*-form percentage of less than 60% is annotated for each line.

7\_Enceladus\_Biomass\_sig/figs/DLtime.pdf

**Figure 7.16 The time it takes for the buildup from a constant input of biological amino acids to appear indistinguishable from those with an abiotic origin with temperature.** Horizontal lines show characteristic timescales, which vary from months to millennia between 400 K and 273 K.

7\_Enceladus\_Biomass\_sig/figs/big\_cell\_grid\_12.pdf

**Figure 7.17 Total cell death required for the overall amino acid content to be indistinguishable from an abiotic mixture when  $\text{H}_2$  inflow is  $1 \text{ pmol (L s)}^{-1}$ .** Maps show the number of dead cells which will have been produced per liter at which time the amino acid content has been racemized beyond being clearly biogenic (60%) throughout the parameter space. At each pH value, the left hand side is the minimum estimate, and the right hand side the maximum estimate. Both of these were computed assuming maximal biomass turnover.

7\_Enceladus\_Biomass\_sig/figs/big\_cell\_grid\_10.pdf

**Figure 7.18 Total cell death required for the overall amino acid content to be indistinguishable from an abiotic mixture when  $H_2$  inflow is  $100 \text{ pmol (L s)}^{-1}$ .** Maps show the number of dead cells which will have been produced per liter at which time the amino acid content has been racemized beyond being clearly biogenic (60%) throughout the parameter space. At each pH value, the left hand side is the minimum estimate, and the right hand side the maximum estimate. Both of these were computed assuming maximal biomass turnover.



## 7.4 Discussion and conclusions

---

This chapter and the chapters leading up to it have brought us to the height of speculation about Enceladean habitability, crashed us back down to Earth again, and then offered a glimmer of hope — as it appears biology could play a role in a steady state Enceladus ocean as observed by Cassini. The assumptions made when modelling life in the icy moon's ocean can tip the balance between results that suggest it is teeming with life, those that indicate it is habitable but uninhabited, and it those that suggest it is completely devoid of life.

Using a reduced version of the parameter space introduced in Chapter 6, a simple model for chemical inflow and outflow, and three different methods, we estimated the amount of biomass the ocean could sustain in a steady state over long timescales. All methods predict that at the same rate of  $H_2$  inflow the total sustainable biomass is highest at the lowest temperatures. When using a traditional biomass estimate (case study 2), higher pH values (which have a lower spontaneous power supply) can support smaller steady state biomasses than lower pH values. However, a reaction quotient preservation estimate (case study 3, NutMEG initial conditions) suggests higher pH values mean a larger biosphere is needed to consume incoming  $H_2$ , provided conditions are not initially uninhabitable. A similar trend was observed with salt concentration's effect on the total biomass, in which high salt (more energy) conditions yielded higher biomass under case study 2, and low salt (less energy) conditions required higher biomass under case study 3. Most importantly, the more conservative case study 3 predicts lower biomass overall in almost all conditions. It is also defined by using life to preserve the state of the system, rather than inserting life into that system. In reality, biomass levels on an inhabited Enceladus would likely be somewhere between the values estimated by these methods, if life was to exist there.

Using NutMEG's microbial growth algorithm we explored how altering microbial behaviour affects the local environment and assessed whether different combinations of Enceladus' parameter space were flexible to a changing biosphere. In many cases, including almost all those with an empirical maintenance power, the ocean and/or Earth-like methanogens are inflexible to changes. The most flexible regions of the parameter space are those on the fringes of habitability with methanogens operating at minimal maintenance powers. These regions coincide with the current best estimate of the bulk ocean pH: 8.5–9, offering the tantalising prospect that methanogenic life could occupy niches in such an ocean without significantly affecting its chemistry as-observed. Importantly, uncertainties in the chemical inflow and scale of hydrothermal activity remain which could represent an abiotic

(habitable but uninhabited) ocean. Results from these simulations also indicate that if Enceladus is inhabited, the inflow of  $H_2$  proposed by current models is not enough for a large biosphere throughout the ocean, it must be limited to locations near the  $H_2$  source.

Ultimately, to separate the 'inhabited' and 'uninhabited' hypotheses regarding Enceladus' ocean requires the detection of biosignatures. Life as we know it is selective in the chirality of its amino acids, so a clearly biogenic *L*-form percentage would be indicative of (Earth-like) biological activity. We used the biomass turnover associated with life's modelled behaviour in the parameter space to explore how fast waste matter could become racemized and how much build-up would be required for the solution to appear indistinguishable from abiologically produced organic molecules. The time required for all biogenic amino acids to appear indistinguishable from abiogenic ones may be on the order of millions of years in the bulk ocean, but much lower (on the order of months) at elevated temperatures. At temperatures  $>340$  K the biomass build-up which will have occurred before this critical point is fewer than  $10^{10}$  dead cells per litre ( $10^7$  cells  $cm^{-3}$ ), but note from Chapter 6 that our speciated composition is probably increasingly unrepresentative at temperatures higher than  $\sim 300$  K. Crucially, to determine whether we can detect life using chirality on Enceladus requires better understanding of the degree of entrainment throughout the ocean. This is because at cool temperatures, with large  $H_2$  inflow ( $10^{-10}$  mol  $(L\ s)^{-1}$ ) — as unlikely as they may be — very large detritus build-ups (up to  $10^{20}$  dead cells per litre) are required to appear abiological. Assessing the flow of material throughout the ocean is essential for determining whether the racemization ratio of amino acids could feasibly be pursued as a useful biosignature on Enceladus.

To arrive at these conclusions required significant simplifications and assumptions, which compound those made in the work leading up to this. For the limitations in NutMEG and the typical optimal methanogen refer to Chapters 4 & 5, and discussion related to the Enceladus parameter space can be found in Chapter 6. Here we will focus on the extra assumptions made in this chapter, but first should acknowledge the most important limitations which carry-over from this other work:

- We continue to assume that the rate-determining step of the metabolism is in  $CO_2$  and  $H_2$  uptake and do not account for nutrient limitation. Alternative nutrient availabilities are introduced in Chapter 6. Ultimately, before this can be included we need to know more about both the effect of nutrient limitation on methanogens (Chapter 5), and the nutrient inventory of Enceladus (Chapter 6).

- While we aimed to use representative maintenance powers, as with Chapters 5 & 6 this only covers the effects of temperature and omits other important parameters on Enceladus such as pH and salinity. It also does not vary between microbial growth phases.
- Our estimates of the energetic cost of biomass synthesis  $E_{\text{syn}}$  retain the assumption that the organism must synthesise its own amino acids, and that proteins are representative of all biomacromolecules (Chapters 3 & 5). If there were substantial bioavailable amino acids on Enceladus (which there may be [104]), this energetic cost would be lower and the biospheres predicted here could be larger.
- We neglect other possible metabolisms which could be at play on Enceladus (discussed in Chapter 6).
- Plausible scenarios outwith the Enceladus parameter space have not been considered, for instance more complex hydrothermal systems or a highly saline deep ocean [70]. This is discussed at length in Chapter 6, hydrothermal systems on Enceladus may yet be the most habitable regions on the icy moon, but we need to first constrain the extent of their activity and local compositions.
- This work is also limited by the assumption that putative Enceladean life would be similar to Earth life, specifically hydrogenotrophic methanogens.

Significant uncertainties in this work arise from the limited understanding of Enceladus' physical oceanography and the modular nature of NutMEG reactors. Our simple chemical inflow/outflow model aimed to capture the scope of possibilities in Enceladus' ocean as we presently understand it, but leaves much to be desired. This is not in the raw numbers *per se*; it is more in the net chemical inflow which would be experienced by life at a given location in the ocean. For example, regions of the ocean close to hydrothermal vents will have much larger inflow than regions near the ice-water boundary, but they will also have much larger outflow. To constrain the scales of this outflow requires the local fluid velocity and chemical production rates, which is not uniform along the base of the ocean [94, 196]. Our simple model of reactors at the rock-water boundary is limited because a core assumption allowing  $J_{\text{H}_2}$  values of  $10^{-12}$ – $10^{-10}$  mol (L s) $^{-1}$  is that life in such a reactor can process *all* of that incoming energy. A spacially resolved model with chemical inputs moving through a mesh of populated reactors could be one possible solution to this, but is beyond the scope of this work and would require understanding of fluid velocities at the bottom of the Enceladus ocean. Still, this would not solve another problem caused by our 1 L reactor choice — that all the biomass in that body can instantaneously react with anything else in that volume which is difficult to justify with some of the very low biomasses predicted by our models.

This limitation feeds into the more general problems that our growth model's dependence on cell-specific properties present (discussed in Subchapter 3.4). The modelled methanogens have a metabolic rate constant indicative of those in empirical conditions, that is cell concentrations observed in the laboratory (above  $\sim 10^4$  cells  $L^{-1}$  by reading Figure 5.4). This introduces an implicit assumption that there is some pre-existing biomass in each reactor which may limit the rate constant or cause artificially high maintenance powers. Hence, an explanation for why so few of our parameter space combinations could achieve steady state lies in the fact that so few laboratory experiments on methanogens accurately reflect Enceladus-like conditions [e.g. 198].

We constrained the time required for Enceladus' biological detritus to appear indistinguishable from similar molecules of abiological origin as somewhere between months and millennia. A better understanding of the physical oceanography is also key to determining a better constrained timescale and unlocking whether chirality could be a valid biosignature on Enceladus. We would need to understand how quickly the detritus gets from the hydrothermal system to the plume, and what the temperature gradient it experiences is, neither of which is fully understood yet. If we only consider life at cool ( $< 300$  K) temperatures, such as in the bulk ocean or liquids in aquifers, then it will invariably take over 1000 years for complete racemization. This is encouraging for life detection should it be present in the cool bulk ocean, but in general our low temperature results appear inflexible to life. Additionally, the required death rates for habitability in such settings are the lowest of the parameter space. An interesting hypothesis could be that methanogenic life prospers in hydrothermal systems, and can minimally metabolise or enter stasis for a time when evicted into the cool bulk ocean. That way, it could take up to millions of years for these biological remnants to become undetectable.

It is important to discuss whether our methods are an attempt at 'forcing' life into Enceladus' ocean, or fitting it in gracefully with observations and models. While we have tried to use agnostic initial conditions and insert life as a missing-link in the disparity between expected chemical inflow and outflow, there are some aspects where we may have been overly optimistic. The standout assumption here is that the net inflow of  $CO_2$  and  $CH_4$  can be resolved using the ratios of methanogenesis. Clearly, this assumes that methanogens are the only things processing these chemical ingredients where in reality many other abiological (or biological) processes will also be at play, particularly given the apparent sustained chemical disequilibrium of the ocean. If future work were to constrain the hydrothermal and/or oceanic production of  $CO_2$  and  $CH_4$  these would make more agnostic inputs for our model.

Our results suggest that a large proportion of the most ‘habitable’ regions of the parameter space are not flexible to variable biological behaviour. We parameterised this variability using the death rate  $\delta$  of the TOM. We hypothesise that such inflexibility in locations with such apparent habitability could be explained by a ‘too-good-to-be-true’ fallacy. In other words, these high temperature and low pH possibilities having a consistently large amount of energy available for life — boosted by extra energy inflow — could simply be indicative of an uninhabited habitat. Moreover, such conditions also demand high values of  $\delta$  and low biomasses to ‘fit in’ to the system which seems counter-intuitive for settings with a large energy surplus. The reality is that it is incredibly difficult to *maintain* the reactor in such a state without triggering exponential growth that alters the composition beyond the one we constrained in Chapter 6. Of course, these results could also be explained by a myriad of other uncertainties in both NutMEG and our Enceladus parameter space that could restrict this apparent habitability, such as our choice of maintenance power, or that we know little of the nutrient content of the ocean. For instance, phosphorus could be significantly limiting [106], in the form of phosphate. Rock-alteration processes may only be sufficient to sustain  $10^7$  cells  $\text{L}^{-1}$  [16, 101]. On the other hand, regions closer to the limits of habitability (e.g pH 8.5–9) appear to be broadly flexible with  $\delta$ . This lies in tandem with the idea above, the fringes of habitability may be the best places to look for settings which could feasibly be inhabited — life is consuming most of the energy!



# CHAPTER 8

---

## Outlook

---

Now, how do we tie this all together? And what should astrobiological modellers focus on in the future? The NutMEG package provides some rudimentary tools to estimate habitability, biomass and biosignature levels, but there is still much to elucidate in this complex interdisciplinary field. To demonstrate how NutMEG can be useful, we have agnosticised Earth-like methanogen behaviour using empirical data, used that to predict the habitability of Enceladus' ocean, and from that estimated the biomass turnover we might expect there.

In this final chapter we collect our thoughts and briefly reflect on the main outcomes and implications of the work presented in this thesis.

Mirroring Chapter 1, we briefly summarise the key results of each chapter and pick out the most important avenues to explore next.

In this thesis we have brought together an overview of the energetics behind biological adaptation, survival and growth processes (Chapters 2 & 3) into one catch-all python package for quantitative habitability predictions (Chapter 4). In Chapter 5 we configured our model to predict methanogenic behaviour based on energetic and nutrient availability using data gathered on laboratories on Earth, and in Chapters 6 & 7 applied it to Enceladus' ocean to predict its habitability, possible biomass and biosignatures. Mirroring Chapter 1, let us reflect on the key steps we embarked upon in this thesis with an outward look for what future work should focus upon. For detailed discussion of the research involved in each chapter and their suggested next steps, refer to their 'Discussion' or 'Outlook' subchapters.

### i) Bioenergetics of adaptation, survival and growth

Chapter 2 included a broad overview of habitability, life in extremes and microbial growth models before introducing some of the environments relevant to astrobiology. We identified the energetic approach to habitability as a possible route towards building an agnostic habitability model. In Chapter 3 we explored some of the ways in which the relevant parameters can be quantified. In the context of the models we went on to work with, these parameters were:

1. **The power supply (rate of energetic uptake) of an organism,  $P_S$ .**
2. **The energetic cost of biomass synthesis,  $E_{\text{syn}}$ .**
3. **The power demands associated with temperature and pH,  $P_M$ .**

While each requires unique assumptions, collecting these together allowed us to build a microbial model which is flexible to different conditions. Key issues with computing these variables revolved around our attempts to remain 'agnostic' and provide catch-all predictions based predominantly on environmental variables, minimising assumptions about organismic variables (to simple ones, such as cell volume and internal pH). While this allows these ideas to be applied to a myriad of systems and species, the lack of specificity clearly decreases the accuracy of results from such methods. We relented on this somewhat in Chapter 4 allowing users the ability to create child classes reflecting specific environments and organisms. Future work could take this further, and we hope as NutMEG blossoms users will be able to create unique implementations for organisms we understand well and those we understand not-so-well.

Estimates of  $E_{\text{syn}}$  and  $P_M$  require further research to improve our confidence in these values. Our group contribution approach for  $E_{\text{syn}}$  assumes the energetic cost of building proteins is broadly representative of all biomacromolecules, but work in preparation indicates the cost of building the genome and transcriptome using a similar method is different [8]. We also found that while there have been empirical estimates of the power demand owing to temperature, there are none to our



---

knowledge which explicitly determine the power demand owing to pH. We created a rudimentary first-estimate of this but it requires some empirical determination, as we did for temperature effects in Chapter 5. On the whole, each of the parameters listed above require further empirical constraints, alongside experiments aimed squarely at resolving them.

## **ii) Nutrients, maintenance, energy and growth**

The python package NutMEG was built to help solve astrobiological problems. It casts habitability, biomass and biosignatures in the quantitative framework outlined in Chapters 2 & 3. If intuitive computational design allows it to be used by the wider scientific community with relative ease, and has been used by the author and collaborators for numerous projects [1, 2, 4, 5]. As an open source project it will always be available for the community to add improvements. Specifically we suggest it could be improved by considering cell lysis, dormancy, more time- or context-variable attributes, predation, and an improved nutrient uptake algorithm. More generally its accessibility could be improved further, and future work could include their methods and systems as new applications modules or child classes as we have done for the work in this thesis (Chapters 5–7).

## **iii) An empirical basis for Earth-like life**

In Chapter 5 we used NutMEG to match model predictions to laboratory data for hydrogenotrophic methanogens, then examined what could happen to microbial growth rates, biomass production and methane production in energy- or nutrient-limited settings. Increased energy and nutrient limitation restrict the total biomass expected — an important measure of habitability — increasingly at higher temperatures owing to the low energy yield of the methanogenesis metabolism and higher maintenance power. They also limit the total methane production, which would be an important biosignature for detecting methanogens on other planets.

This work acts as a proof-of-concept for similar future studies which parameterise organisms' growth behaviour by their metabolisms. We were able to optimise Earth-like methanogens and examine how they could behave in a variety of different environments (Chapters 6 & 7, [2, 4, 5]). Future work can repeat this process for other organisms relevant to astrobiology and extremes, such as sulfate reducers, iron oxidisers, or even phototrophs. To enhance the work we presented in Chapter 5, and improve the credibility of results further, its predictions should be compared to empirical evidence from real extreme environments on the Earth, for which we do not yet have the relevant parameters. This could provide an improved baseline for the conditions to focus on when considering extraterrestrial environments.

### **iv) Energetic habitability of Enceladus**

In Chapter 6 we used NutMEG and the methanogens derived above to examine the habitability of Enceladus' subsurface ocean. Despite the optimism rife throughout the literature, we do not have sufficient data to say once-and-for-all that the ocean is habitable to methanogens in the context of the currently known limits to life. This is because the ocean's habitability appears to be a delicate balance between its temperature, pH, salinity and concentrations of carbonates, nutrients and dissolved gases (particularly  $H_2$ ); many of which are co-dependent. Variation within the parameter space of any one of these could tip the balance from habitable to uninhabitable conditions and vice versa.

Our results were conservatively optimistic when suggesting low temperature habitable regions, and somewhat pessimistic when higher temperatures and pH values appear uninhabitable. While this interpretation appears esoteric, it is simply because of gaps in the available data. Low temperature regions appear habitable in our model; we do not know the extent of energy and nutrient inflow in the cool bulk ocean, so its longevity is unknown. Similarly, conditions at elevated temperatures and/or high pH will have increased energy and nutrient inflow and hence could be more habitable than our results suggested. Future work and missions need to constrain more information about the physical oceanography of Enceladus to tighten our understanding of its habitability.

### **v) Biomass and biosignatures on Enceladus**

The limitations above notwithstanding, in the more speculative Chapter 7 we attempted to extend this model to estimate the possible biomass and biosignature levels our proposed habitable regions could possess. The assumptions made when modelling life in the icy moon's ocean can tip the balance between results that suggest it is teeming with life, those that indicate it is habitable but uninhabited, and it those that cast is as completely devoid of life. We also tested how flexible parts of the Enceladus ocean's parameter space are to small differences in organism behaviour. The most flexible regions of the parameter space are those on the fringes of habitability with methanogens operating at minimal maintenance powers, and coincide with the current best estimate of the bulk ocean pH.

This result looks incredibly optimistic for a productive biosphere on Enceladus. However, uncertainties in the chemical inflow and scale of hydrothermal activity remain which could represent an abiotic (habitable but uninhabited) ocean. So, as with our recommendations above, better resolving Enceladus' physical oceanography is required to improve our habitability, biomass and biosignature predictions. Much of this can come from geochemical modelling, but the superior option is a return mission to Enceladus. Another significant complement to this work

---

could come from empirical work finding the death rate of methanogens. Whether biosignatures could be detectable via an amino acid racemization method depends on the temperature of the habitat and the flow of material through the ocean, neither of which are understood well enough to draw concrete conclusions yet. At hydrothermal temperatures  $>370$  K biosignatures decay within months, but in the cool bulk ocean they could be preserved for millennia. Further work is needed to resolve the temperature and flow of material within Enceladus. With that in hand, we will be able to determine whether it can feasibly host detectable biosignatures.

#### **vi) Final thoughts**

Beyond what we have discussed above, there is a broader context to the work presented in this thesis. NutMEG has the potential to be applied to countless systems, on both large and small scales. We have demonstrated this with our applications to laboratory vessels [1], micron-sized Venusian cloud droplets [4], the ocean floor of a hypothetical exoplanet [5], and the entire ocean of Enceladus [2]. No matter how much or how little we know of a system, NutMEG provides a means to make a first estimate of its habitability, biomass and possible biosignatures. However, users must be acutely aware of its limitations in the context of that system. In the future, NutMEG could be used extensively in exoplanet science with its more robust habitability estimates than simply ‘chasing the water’. It will also be of use for other solar system bodies such as Mars, or additional icy moons with subsurface oceans. The planned Europa Clipper mission should begin to resolve the composition its ocean, so similar modelling to what has been presented in this thesis could also be applied to the jovian icy moon.



# APPENDIX A

---

## Supplemental theory

---

This Appendix contains theory which compliments the main text of this thesis. In Appendix A.1 we introduce theory for computing the composition and Gibbs free energies in solutions. In Appendix A.2 we discuss how to relate biological and chemical standards. In Appendix A.3 we present an alternative method to compute the proton flux through a membrane, and in Appendix A.4 we outline methodology to compute the concentration of dissolved gases in solution.

### Sub-appendices

A.1	Calculating free energies .....	234
A.2	Relating biological and chemical standards ..	241
A.3	Alternative proton flux calculation .....	243
A.4	Dissolved gases in solution .....	245

## A.1 Calculating free energies

*Note: Any parts of this subappendix without clear citation represent information readily available in undergraduate textbooks [e.g. 59]. All terms in this subappendix are defined as in the main text and glossary.*

This subappendix acts as a whistle-stop tour of expressions that were considered while this research was underway and is not a thorough analysis of their applicability. However, many of them are implemented in NutMEG, ready to be examined in the future.

### A.1.1 | Temperature dependence of $\Delta H^\circ$ and $\Delta S^\circ$

Recall the expressions for the Gibbs free energy described in Chapter 3:

$$\Delta G_r = \Delta G_r^\circ + RT \ln Q \quad (\text{A.1})$$

$$\Delta G_r^\circ = \Delta H_r^\circ - T \Delta S_r^\circ \quad (\text{A.2})$$

$$\Delta G_r^\circ = -RT \ln K \quad (\text{A.3})$$

For an ideal gas (an aqueous solution in its standard state is assumed to be infinitely diluted and so can be treated as one), the deviation from the standard enthalpy and entropy change at RTP can be expressed as:

$$\Delta H^\circ(T_2) = \Delta H^\circ(T_1) + \int_{T_1}^{T_2} C_P(T) dT \quad (\text{A.4})$$

$$\Delta S^\circ = \int_{T_1}^{T_2} \frac{C_P(T)}{T} dT \quad (\text{A.5})$$

So, if the heat capacity  $C_P$  as a function of temperature is known for the solute, these can be accurately approximated at different temperatures. Often,  $C_P$  is a polynomial and relatively straight forward to integrate to some order. The equilibrium constant can be expressed as a function of temperature at constant pressure  $K_P$ . This is realised by using the Van't Hoff equation:

$$\ln K_P(T_2) = \ln K_P(T_1) + \int_{T_1}^{T_2} \frac{\Delta H_r^\circ(T)}{RT^2} dT \quad (\text{A.6})$$

However, these approximations can only realistically be used for ideal gases or near-infinitely diluted solutions. Readily available thermodynamic models such as SUPCRT92 implement more complex Helgeson-Kirkham-Flowers equations of state [34] to estimate  $C_p$ ,  $\Delta G^\circ$ ,  $\Delta H^\circ$ ,  $\Delta S^\circ$  and  $\ln K$  amongst other parameters. These models are implemented for the computational studies presented in the main text of this thesis.

## A.1.2 | Solutions

The major source of uncertainty in the Gibbs free energy calculations presented in Subchapter 3.1.3 come from the reaction quotient, and estimates of the activity of relevant reagents. Here we will present some methods to estimate the activity given the molarity and molality of species in solution. These methods are implemented in NutMEG's `reaction.special` submodule. Throughout this section we define any parameter with subscript-1 that of the solvent, and with subscript-2 the solute. Where a superscript \* appears, it means we are referring to the parameter pertaining to a 'pure' solvent, i.e. without solute. Further, let  $x_j$  be the molar fraction,  $a_j$  be the activity,  $P_j$  be the (vapour) pressure,  $\gamma_j$  the activity coefficient,  $\mu_j$  be the chemical affinity<sup>1</sup>,  $m_j$  be the molality and  $n_j$  the molarity. Activities are related to molalities using the activity coefficient:

$$a_j = \gamma_j m_j \quad (\text{A.7})$$

### A.1.2.1 | Neutral solutes

The activity of a neutral solute in solution, and that of the solvent can be defined as:

$$a_1 = \frac{P_1}{P_2^*} \quad a_{2x} = \frac{P_2}{k_{H,x}} \quad (\text{A.8})$$

where  $k_{H,x}$  is the Henry's law constant, which corresponds to  $P_2^*$  for an ideal (infinitely dilute) solution, and the subscript- $x$  means we are on a molar fraction scale. We can write that:

$$a_1 \rightarrow x_1 \quad \text{as} \quad x_1 \rightarrow 1 \quad (\text{A.9})$$

$$a_2 \rightarrow x_2 \quad \text{as} \quad x_2 \rightarrow 0 \quad (\text{A.10})$$

<sup>1</sup>Not to be confused with the microbial growth rates, which are represented by  $\mu$  elsewhere in this thesis

and hence for an ideal solution, the activity effectively becomes the molar fraction, and:

$$a_{2m} \rightarrow m \quad \text{as} \quad m \rightarrow 0 \quad (\text{A.11})$$

The same argument can be used for molarity. To correct for non-ideality (but still only valid for a dilute solution) use the following:

$$\ln a_1 = \frac{-m_2 \phi_2}{m_1^*} \quad (\text{A.12})$$

where  $\phi$  is the ‘osmotic coefficient’. To give perspective,  $m_1^*$  for water as a solvent is 55.506 mol kg<sup>-1</sup>. The osmotic coefficient can be related to the activity coefficient via the Gibbs-Duhem equation [59]:

$$\ln \gamma_2 = \phi - 1 + \int_0^{m_2} \left( \frac{\phi - 1}{m'} \right) dm' \quad (\text{A.13})$$

which has a polynomial solution.

### A.1.2.2 | Electrolytes

Solutions in which the solutes have charge require extra fine-tuning, because they are far more likely to interact with one-another (interactions vanishing as  $1/r$  instead of  $1/r^6$  if  $r$  is the distance between species). Let us now consider the dissociation reaction:



we write:

$$\mu_2 = \nu_+ \mu_+ + \nu_- \mu_- \quad (\text{A.15})$$

$$= \mu_2^\circ + RT \ln a_2 \quad (\text{A.16})$$

with

$$\mu_+ = \mu_+^\circ + RT \ln a_+ \quad (\text{A.17})$$

$$\mu_- = \mu_-^\circ + RT \ln a_- \quad (\text{A.18})$$

Hence, we can define:

$$a_2 = a_{\pm}^\nu = a_+^{\nu_+} a_-^{\nu_-} \quad (\text{A.19})$$



where  $a_{\pm}^v$  is referred to as the the mean ionic activity. Each ion also has their own activity coefficient:

$$a_+ = m_+ \gamma_+ \quad , \quad m_+ = v_+ m_2 \quad (\text{A.20})$$

$$a_- = m_- \gamma_- \quad , \quad m_- = v_- m_2 \quad (\text{A.21})$$

Hence:

$$a_{\pm} = a_{\pm}^v = m_{\pm}^v \gamma_{\pm}^v = m_+^{v_+} m_-^{v_-} \gamma_+^{v_+} \gamma_-^{v_-} \quad (\text{A.22})$$

Just like with neutral solutes, we can define an osmotic coefficient and hence calculate the mean activity coefficient:

$$\ln a_1 = \frac{-v m_2 \phi_2}{m_1} \quad (\text{A.23})$$

$$\Rightarrow \ln \gamma_{\pm} = \phi - 1 + \int_0^{m_2} \left( \frac{\phi - 1}{m'} \right) dm' \quad (\text{A.24})$$

For very dilute solutions ( $n_2^{1/2} < 0.05 \text{ mol L}^{-1}$ ),  $\ln \gamma_{\pm}$  can be estimated from Debye-Hückle theory:

$$\ln \gamma_j = \frac{-\kappa q_j^2}{8\pi\epsilon_0\epsilon_r k_B T} \quad (\text{A.25})$$

and

$$\ln \gamma_{\pm} = -|q_+ q_-| \frac{\kappa}{8\pi\epsilon_0\epsilon_r k_B T} \quad (\text{A.26})$$

where

$$\kappa^2 = \frac{2e^2 N_A \rho}{\epsilon_0 \epsilon_r k_B T} \cdot (I_n) \quad (\text{A.27})$$

Here,  $\kappa$  is “the thickness of the ionic atmosphere”, has units  $\text{m}^{-1}$  and can be generalised depending on the salt. For example, a 1:1 salt (e.g. NaCl) yields  $\kappa = \frac{m (\text{mol L}^{-1})}{304 \text{ pm}}$ .  $\rho$  is the density of the solvent (which increases with increasing electrolyte concentration),  $\epsilon_r$  is the permittivity of the solvent (which is temperature dependent [204]). It is also solute concentration dependent, but unfortunately there is no universal expression and its variation depends on the solute. Where this variation is available,  $\epsilon_r$  corrects the MSA (discussed later) to be in almost perfect agreement with experiment, see [66]. Recall that  $I_n$  is the ionic strength:

$$I_n = \frac{1}{2} \sum_{j=1}^s z_j^2 n_j \quad \text{or} \quad I_m = \frac{1}{2} \sum_{j=1}^s z_j^2 m_j \quad (\text{A.28})$$

where  $s$  is the total number of ionic species. Overall we see that at constant temperature and infinite dilution:

$$\ln \gamma_{\pm} \propto n^{1/2}, m^{1/2} \quad (\text{A.29})$$

A plot of these two variables will yield a unique gradient dependent on salt type (1:1, 2:3 etc.). Although this is only valid in very dilute conditions, its a useful check for our models in this range — as its developed from Debye-Hückle theory it *is* the limit as  $n, m \rightarrow 0$ . A further simplification is that at RTP:

$$\ln \gamma_{\pm} = -1.173 |z_+ z_-| \cdot (I_n)^{1/2} \quad (\text{A.30})$$

Over a large concentration range, the mean spherical approximation [MSA] is more accurate. It splits the mean activity coefficient into electrostatic and hard-sphere contributions:

$$\ln \gamma_{\pm} = \ln \gamma_{\pm}^{el} + \ln \gamma_{\pm}^{HS} \quad (\text{A.31})$$

with

$$\ln \gamma_{\pm}^{el} = \frac{h(1+2h)^{1/2} - h - h^2}{4\pi\rho d^3} \quad (\text{A.32})$$

$$\ln \gamma_{\pm}^{HS} = \frac{4y - \frac{9}{4}y^2 + \frac{3}{8}y^3}{(1 - y/2)^3} \quad (\text{A.33})$$

where  $y = \pi\rho_d d^3/6$ ,  $\rho_d$  is the number density of all ions,  $d$  is the sum of the radius of the cation and the radius of the anion, and  $h = \kappa d$ . When this activity coefficient has been found, it can be applied to the Nernst equation for electrochemical cells, which is discussed in the next section.

### A.1.3 | Redox

For an electrochemical cell the Gibbs free energy can be expressed as:

$$\Delta G_r = -n_e F E \quad (\text{A.34})$$

where  $n_e$  is the number of electrons in a the reaction per mole of product,  $F$  is Faraday's constant, and  $E$  is the standard electrode potential — however, if we know how  $E$  changes with temperature and pressure then we can also calculate  $\Delta G$  for this range. For constant pressure and changing temperature this can be implemented

via:

$$E_T^\circ = E_{298}^\circ + (T - 298.15) \left( \frac{dE}{dT} \right)_{298} \quad (\text{A.35})$$

with the assumption that  $\left( \frac{dE}{dT} \right)_{298}$  is approximately linear [65]. To correct slightly from the nonlinearity, we could include the second term of the expansion making it:

$$E_T^\circ = E_{298}^\circ + (T - 298.15) \left( \frac{dE}{dT} \right)_{298} + 0.5(T - 298.15)^2 \left( \frac{d^2E}{dT^2} \right)_{298} \quad (\text{A.36})$$

where the second derivative can be calculated using the standard heat capacity:

$$\left( \frac{d^2E}{dT^2} \right)_{298} = \Delta C_P^\circ / (298.15 n_e F) \quad (\text{A.37})$$

Often, this will bring about a 10% increase in accuracy, which is smaller than many of the uncertainties we have in measurements of  $E_{298}^\circ$  [65]. The first and second derivatives with  $T$  can also often be read from tables in the literature for common ions. Unless we have this derivative, we need to know the reaction quotient at the new temperature. To extrapolate to a nonstandard state:

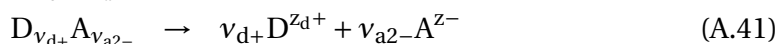
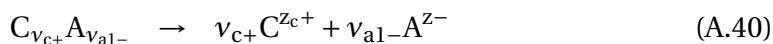
$$E_T = E_T^\circ - \frac{RT}{nF} \ln Q_T \quad (\text{A.38})$$

where  $Q_T$  can be calculated from the relevant activities and activity coefficients. For dilute solutions, the mean activity coefficient may also be found by rearranging the formula:

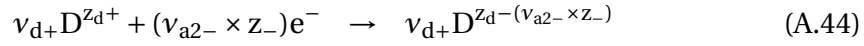
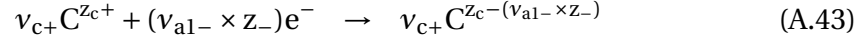
$$E = E^\circ - \frac{RT}{F} \ln(\gamma_\pm m)^{v_+ + v_-} \quad (\text{A.39})$$

### A.1.3.1 | Calculating the Quotient of a Chemical Cell

Consider the half equations (shown as dissociation reactions) and overall cell reaction below:



Equations A.40 and A.41 can be written in the more familiar form:



However, the previous formulation is more useful for us, as the choice of counter-ion has an effect on the reacting ion's activity, as we have seen in the previous section. Note that in this example the two solutions share the same anion, this is not necessary but is the norm in electrochemical experiments — a more general case with other anions can be derived. It is clear from the above expressions that Equation A.40 is the forwards reaction (confusingly, the dissociation running backwards), and Equation A.41 is the reverse reaction. The quotient can then be written:

$$Q = \frac{(a_{D^{z_{d+}}})^x a_C^y}{a_D^x (a_{C^{z_{c+}}})^y} = \frac{(a_{D_{\nu_{d+} A_{\nu_{a2-}}}})^x}{(a_{C_{\nu_{c+} A_{\nu_{a1-}}}})^y} \quad (A.45)$$

where C and D are taken to be in their standard states and have an activity of unity. These activities can be calculated from the expressions in Equation A.22:

$$(a_{C_{\nu_{c+} A_{\nu_{a1-}}}})^y = (a_{\pm}^{\nu_{c+} + \nu_{a1-}})^y = ((\gamma_{\pm}^{\nu_{c+} + \nu_{a1-}})(m_{C^{z_{c+}}}^{\nu_{c+}})(m_{A^{z_{a1-}}}^{\nu_{a1-}}))^y \quad (A.46)$$

$$(a_{D_{\nu_{d+} A_{\nu_{a2-}}}})^x = (a_{\pm}^{\nu_{d+} + \nu_{a2-}})^x = ((\gamma_{\pm}^{\nu_{d+} + \nu_{a2-}})(m_{D^{z_{d+}}}^{\nu_{d+}})(m_{A^{z_{a2-}}}^{\nu_{a2-}}))^x \quad (A.47)$$

So, if the molalities and mean activity coefficient at temperature  $T$  are known we can compute the reaction quotient of a chemical cell by inserting these two expressions into Equation A.45.

## A.2 Relating biological and chemical standards

The standard free energy  $\Delta G^\circ$  is the Gibbs free energy of a process in standard conditions at a given temperature and pressure. In chemistry and physics, these standard conditions are that everything has a concentration of 1 M. This means that in ‘standard conditions’, the concentration of  $H^+$  is 1 M, i.e. pH 0. This is not of much use in biology because many processes occur at or around pH 7 or at non-zero ionic strengths. So, there is also the ‘biological standard Gibbs free energy’  $\Delta G'^\circ$ , the biological part indicated by the apostrophe. This is the free energy at a given temperature, pressure, pH (usually 7), and ionic strength. There are problems with this though (listed in [131]). Adapting these standards for adverse temperatures and pressures is a complex problem, and as a result these can only be used accurately at RTP. To convert between the standard and biological standard free energies of formation for a given species, Alberty (1998) [205] gives this equation:

$$\Delta G'^\circ(pH, I) = \Delta G^\circ(I=0) - (2.91482z^2(I^{1/2})/(1 + (B(I^{1/2})))) - N[-2.91482(I^{1/2})/(1 + (BT^{1/2})) + RT \ln 10^{-pH}] \quad (A.48)$$

where  $I$  is the ionic strength,  $z$  is the charge of the species,  $B = 1.6 \text{ L}^{1/2} \text{ mol}^{-1/2}$ , and  $N$  is the number of H atoms in the species.  $R$  here is in  $\text{kJ} (\text{mol K})^{-1} = 0.00831$ . If the charge and/or ionic strength are zero, this is greatly simplified:

$$\Delta G'^\circ = \Delta G^\circ - NRT \ln 10^{-pH} \quad (A.49)$$

We can demonstrate that when constructing the free energy of a reaction that does not contain  $H^+$ , and has ionic strength of zero, the biological standard and chemical standards are the same at RTP. Consider the use of Hess’ law to compute the free energy of reaction using either of these free energies in identical conditions:

$$\Delta G^\circ = \sum \nu_i \Delta G^\circ_i - \sum \nu_j \Delta G^\circ_j \quad (A.50)$$

$$\Delta G'^\circ = \sum \nu_i \Delta G'^\circ_i - \sum \nu_j \Delta G'^\circ_j \quad (A.51)$$

for a reaction with products  $i$ , each having stoichiometric coefficient  $\nu_i$  and reactants  $j$  with stoichiometric coefficient  $\nu_j$ . From Equation A.51, we can write:

$$\Delta G'^\circ = \sum \nu_i (\Delta G^\circ_i - N_i \chi) - \sum \nu_j (\Delta G^\circ_j - N_j \chi) \quad (A.52)$$

$$\Delta G'^\circ = \sum \nu_i \Delta G^\circ_i - \sum \nu_j \Delta G^\circ_j - (\sum \nu_i N_i \chi) + (\sum \nu_j N_j \chi) \quad (A.53)$$

$$\Delta G'^\circ = \Delta G^\circ - (\sum \nu_i N_i \chi) + (\sum \nu_j N_j \chi) \quad (A.54)$$

where  $\chi = RT \ln 10^{-pH}$ . as the total number H in the products and reactants of a chemical expression must be conserved (e.g.  $\sum v_i N_i = \sum v_j N_j$ ), the second bracketed term above is zero.

## A.3 Alternative proton flux calculation

An alternative derivation of the flux equation for protons and hydroxide is possible using the Goldman equation for the current of a singly charged ion across a membrane per unit area [151]:

$$I_{Ai} = \frac{u_i F \Delta \Psi}{d} \frac{c_{ext} e^{-\Delta \Psi F / RT} - c_{int}}{e^{-\Delta \Psi F / RT} - 1} \quad (\text{A.55})$$

Here,  $I_{Ai}$  is the current of ions  $i$  [ $\text{A m}^{-2}$ ],  $u_i$  [ $\text{m}^2 (\text{V s})^{-1}$ ] is the ion's mobility,  $c_{int}$  and  $c_{ext}$  [ $\text{mol L}^{-1}$ ] are the concentrations of the ion on each side of the membrane,  $\Delta \Psi$  [V] is the total potential across the membrane  $\Psi_{int} - \Psi_{ext}$ , and  $d$  [m] is the membrane thickness. Let us substitute in a dimensionless constant  $\Lambda = \Delta \Psi F / RT$ :

$$I_{Ai} = \frac{u_i \Lambda RT}{d} \frac{c_{ext} e^{-\Lambda} - c_{int}}{e^{-\Lambda} - 1} \quad (\text{A.56})$$

We need this in terms of ion flux  $J_{Ai}$  [ $\text{mol s}^{-1} \text{m}^{-2}$ ]. This can be achieved via unit conversion:

$$I_{Ai} = \frac{1}{\text{A}} \frac{Q_i}{t} = \frac{1}{\text{A}} \frac{N_i}{t} q_i \quad (\text{A.57})$$

$$J_{Ai} = \frac{1}{\text{A}} \frac{n_i}{t} = \frac{1}{\text{A}} \frac{N_i}{N_A t} \quad \longrightarrow \quad N_i = A N_A t J_{Ai} \quad (\text{A.58})$$

$$I_{Ai} = J_{Ai} N_A q_i \quad (\text{A.59})$$

where  $n_i$  [mol] is the number of moles of ions transferred,  $q_i$  [C] is the charge of each ion passing through,  $N_i$  is the number of ions passing through per unit time, and  $A$  [ $\text{m}^2$ ] is the surface area. We arrive at the expression:

$$J_{Ai} = \left[ \frac{u_i RT \Lambda}{d N_A q_i} \right] \frac{c_{ext} e^{-\Lambda} - c_{int}}{e^{-\Lambda} - 1} \quad (\text{A.60})$$

This is equivalent to Equation 3.35 in the main text when  $z_i = \pm 1$  and we make the substitution:

$$\bar{P}_i = \left[ \frac{u_i RT}{d N_A q_i} \right] \quad (\text{A.61})$$

This can further be demonstrated by dimensional analysis:

$$\begin{aligned}
 \frac{u_i RT}{dN_A q_i} &\longrightarrow \frac{\frac{\text{m}^2}{\text{V s}} \frac{\text{J}}{\text{mol K}} \text{K}}{\text{m} \frac{1}{\text{mol}} \text{C}} \\
 &\longrightarrow \frac{\text{m J}}{\text{V s C}} \\
 &\longrightarrow \frac{\text{m}}{\text{s}}
 \end{aligned}$$



## A.4 Dissolved gases in solution

### Excerpt from Cockell et al. (2021) [4]

At equilibrium the volume of dissolved gas found per litre of liquid phase  $C_g$  is given by Weiss (1974) [206]:

$$C_g = \frac{V_g}{V_l} = P_g \beta P_{BAR} \quad (\text{A.62})$$

where  $P_g$  is the partial pressure of the gas, and  $P_{BAR}$  is the total barometric pressure, both in atm.  $\beta$  is the solubility coefficient in units of  $\text{L (L atm)}^{-1}$ . By Weiss' definition, this is the volume of gas at room temperature and pressure (RTP) dissolved in a unit volume of solution at temperature  $T$  when the total pressure and fugacity are both 1 atm. As such, functionally the equation above simply corrects the solubility coefficient for local pressure. Using the ideal gas law, the concentration of dissolved gas (moles per unit volume) can be approximated as:

$$\frac{n_g}{V_g} = \frac{P_g}{R_{atm} T} \quad (\text{A.63})$$

This can then be corrected to molarity by multiplying by  $C_g$ :

$$[g] = \frac{n_g}{V_l} = \frac{P_g^2 \beta P_{BAR}}{R_{atm} T} \quad (\text{A.64})$$

Barometric pressure in the cloud layer of interest is omitted in this equation as seen in the main text, as it is approximately 1 atm.

The solubility constant  $\beta$  was calculated with the following equation:

$$\ln \beta = A_1 + A_2(100/T) + A_3(\ln T)/100 + S[B_1 + B_2(T/100) + B_3(T/100)^2] \quad (\text{A.65})$$

The values of  $A$  and  $B$  unique to each molecule can be found in the literature.  $S$  is the salinity in parts per thousand.



# APPENDIX B

---

## Availability of code and data

---

This appendix contains code listings which accompany some of the figures and results presented in this thesis. They can be used to demonstrate how NutMEG can help solve various simple problems. Any code that is too long or complex to be digestible in this format has been uploaded to GitHub and will always be open access [3].

### Sub-appendices

B.1	pH variation with temperature (Box 3.5) ...	249
B.2	T adaptation calculations (Figure 3.4) .....	250
B.3	pH adaptation calculations (Figures 3.5–3.7)	251

## Appendix B. Availability of code and data

---

This Appendix contains snippets of python code for figures and results which appear in this thesis. In order to run, they assume that NutMEG and NutMEG-Implementations are either installed in your python environment or included as a sys path variable. The latter can be achieved by adding the below to the top of any source code presented here:

```
1 import sys, os
2 sys.path.append(os.path.dirname(__file__)+ 'NutMEG')
3 sys.path.append(os.path.dirname(__file__)+ 'NutMEG_Implementations')
```

If you are working in a directory which contains the NutMEG and NutMEG-Implementations directories, e.g. a structure that looks like this:

```
Project/
├── NutMEG/
├── NutMEG-Implementations/
└── YourCode.py
```

For Figures to have the same form-factor as in this document, include these settings to matplotlib at the top of your file too:

```
1 import matplotlib as mpl
2
3 mpl.rcParams['contour.negative_linestyle'] = 'solid'
4 mpl.rcParams['font.family'] = 'sans-serif'
5 mpl.rcParams['font.sans-serif'] = 'cmr10'
6 mpl.rcParams['font.serif'] = 'Times.tcc'
7 mpl.rcParams['axes.linewidth'] = 2
8 mpl.rcParams['lines.linewidth'] = 4
9 mpl.rcParams['mathtext.fontset'] = 'cm'
10 mpl.rcParams['xtick.labelsize'] = 12
11 mpl.rcParams['ytick.labelsize'] = 12
12 mpl.rc('axes', unicode_minus=False)
13 mpl.rcParams['hatch.linewidth'] = 2.0
14 mpl.rcParams['font.size'] = 12
```

Use the following link to access the code snippets from this appendix with full context, in the Thesis directory:

 <https://github.com/pmhiggins/NutMEG-Implementations>

## B.1 pH variation with temperature (Box 3.5)

```

1 import NutMEG as nm
2 import matplotlib.pyplot as plt
3 import numpy as np
4 import math
5
6 R = nm.environment() # default NutMEG environment. 1bar, 298 K
7
8 H2O = nm.reaction.reagent('H2O(l)', R, phase='l')
9 H = nm.reaction.reagent('H+', R, phase='aq')
10 OH = nm.reaction.reagent('OH-', R, phase='aq')
11 rxn = nm.reaction.reaction({H2O:1}, {H:1, OH:1}, R)
12
13 Ts = np.linspace(273,500, num=(500-273)*2) # temperature range
14 pHs_1b = []
15 pHs_100b = []
16 pHs_1000b = []
17
18 for T in Ts:
19     rxn.env.T = T
20     for P, pH in zip([1e5,1e7,1e8], [pHs_1b, pHs_100b, pHs_1000b]):
21         rxn.env.P = P # NutMEG stores Pressures in Pa, 1 bar = 105 Pa
22         rxn.rto_current_env() # updates std Gibbs and eq. constant
23         pH.append(-math.log10(math.sqrt(math.exp(rxn.lnK))))
24
25 fig, ax = plt.subplots(figsize=(6,4), constrained_layout=True)
26 ax.plot(Ts, pHs_1b, c='rebeccapurple', label='P = 1 bar')
27 ax.plot(Ts, pHs_100b, c='tab:orange', ls='dotted', label='P = 100 bar')
28 ax.plot(Ts, pHs_1000b, c='tab:red', ls='dashed', label='P = 1000 bar')
29
30 ax.set_ylabel('Neutral pH')
31 ax.set_xlabel('Temperature [K]')
32 ax.set_xlim(273,500)
33 ax.set_ylim(5.5,7.5)
34 ax.legend(loc='upper right')
35 ax.grid(b=True, which='major', axis='both', color='#666666',
36       linestyle='-', alpha=0.8)
37 plt.savefig('pH_with_T.pdf')

```

## B.2 T adaptation calculations (Figure 3.4)

To plot these figures, we used NutMEG's `theory_estimates` submodule on a methanogen in Enceladus-like settings, as these are an in-built organism and reactor, saving set-up time.

```

1  import NutMEG as nm
2  from NutMEG.reactor.saved_systems.Enceladus import Enceladus
3  from NutMEG.culture.saved_organisms.TypicalOptimalMethanogen
4      import TypicalOptimalMethanogen as TOM
5  from uncertainties import ufloat as uf
6
7  Ts = range(270, 400)
8  rtr = Enceladus('EncT') # make a reactor object
9  org = TOM(rtr) # make an organism
10 TE = nm.apps_theory_estimates(org, rtr)
11
12 Tijhuis, TijhuisAerobe, TijhuisAnaerobe = [], [], []
13 Lever10pc, Lever2pc, Lever1AA = [], [], [] # in-built energy
14 Lever10pc_ces, Lever2pc_ces, Lever1AA_ces = [], [], [] # constant energy
15
16 for i, T in enumerate(Ts):
17     TE.loc.change_T(T)
18     TE.org.get_ESynth(AA=True) # update the synthesis energy
19     td = TE.temperature_defenses(T)
20     Tijhuis.append(uf(td['Tijhuis'], 0.29*td['Tijhuis']))
21     TijhuisAerobe.append(uf(td['TijhuisAerobe'], 0.41*td['TijhuisAerobe']))
22     TijhuisAnaerobe.append(uf(td['TijhuisAnaerobe'],
23         0.32*td['TijhuisAnaerobe']))
24     Lever1AA.append(td['Lever1/250'])
25     Lever10pc.append(td['Lever10pc'])
26     Lever2pc.append(td['Lever2pc'])
27
28     # Lever's Esynth, corrected for this cell size
29     TE.org.E_synth = 1.7e-11 *(org.dry_mass/29e-18)
30     td = TE.temperature_defenses(T)
31     Lever1AA_ces.append(td['Lever1/250'])
32     Lever10pc_ces.append(td['Lever10pc'])
33     Lever2pc_ces.append(td['Lever2pc'])

```

## B.3 pH adaptation calculations (Figures 3.5–3.7)

To plot these figures, we used NutMEG’s pHadaptations submodule. The following method returns a dictionary of fluxes and power demands for a 5000-long array of pH values between 0 and 14, for a given organism-like object:

```

1 def pH_flux_power(org, memb_pot, PermH, PermOH, v):
2     fluxH, fluxOH, pow = [], [], []
3     org.memb_pot = memb_pot
4     org.PermH = PermH
5     org.PermOH = PermOH
6     org.base_volume = v
7     org.surfacearea = (4*math.pi*((v*3)**2))**(1/3)
8     pHs = np.linspace(0,14, num=5000)
9     for i, pH in enumerate(pHs):
10         org.locale.update_pH(pH, _from='pH')
11         pHad = nm.pHadaptations(org)
12         org.maintenance.get_P_pH()
13         pow.append(org.maintenance.net_dict['pH'])
14         fluxH.append(abs(pHад._getfluxH()))
15         fluxOH.append(abs(pHад._getfluxOH()))
16     # return a dictionary of the pH values, fluxes, and power demand
17     return {'pH':pHs,
18         'fluxH':fluxH,
19         'fluxOH':fluxOH,
20         'pow':pow}

```

Then, arrays for the figures can be extracted by calling it. For example, for Figure 3.5 the calls are:

```

1 def_vals = pH_flux_power(org, -1e-3, 1e-10, 1e-10, org.base_volume)
2 high_phi = pH_flux_power(org, -1e-1, 1e-10, 1e-10, org.base_volume)
3 high_perms = pH_flux_power(org, -1e-3, 1e-5, 1e-5, org.base_volume)
4 bigger = pH_flux_power(org, -1e-3, 1e-10, 1e-10, org.base_volume*100)

```

## Appendix B. Availability of code and data

---



# APPENDIX C

---

## Supplemental material for Chapter 6

---

This Appendix contains the supplemental material which accompanies Chapter 6 and the paper it is based on [2]. Some supplemental figures from the original paper have been included in the main text so this appendix and figure numbering appears slightly different that of the manuscript. Scientific content is identical. The supplemental dataset for this work has been archived in Zenodo with doi: [10.6084/m9.figshare.14562144](https://doi.org/10.6084/m9.figshare.14562144)

### Sub-appendices

C.1	Captions for the data set .....	254
C.2	Supplemental tables .....	255
C.3	Supplementary figures .....	256

Supplemental information for this manuscript also included information on new NutMEG methods, but these are covered in detail in Chapter 4.

## C.1 Captions for the data set

---

Supplementary data sets have been uploaded to figshare with digital object identifier (doi): 10.6084/m9.figshare.14562144. The repository contains the following files:

- **nominal\_salts\_case.xlsx** contains the output from the chemical speciation model described in the main text for the nominal salt case, with  $[\text{Cl}] = 0.1 \text{ mol kg}^{-1}$  and  $[\text{DIC}] = 0.03 \text{ mol kg}^{-1}$ . DIC is the sum of the molalities of  $\text{CO}_2(\text{aq})$ ,  $\text{HCO}_3^- (\text{aq})$  and  $\text{CO}_3^{2-} (\text{aq})$ . The speciation was performed in intervals of 10 K and 0.5 pH units, between pH 7–12 and 273–473 K.
- **high\_salts\_case.xlsx** contains the output from the chemical speciation model described in the main text for the high salt case, with  $[\text{Cl}] = 0.2 \text{ mol kg}^{-1}$  and  $[\text{DIC}] = 0.1 \text{ mol kg}^{-1}$ . DIC is the sum of the molalities of  $\text{CO}_2(\text{aq})$ ,  $\text{HCO}_3^- (\text{aq})$  and  $\text{CO}_3^{2-} (\text{aq})$ . The speciation was performed in intervals of 10 K and 0.5 pH units, between pH 7–12 and 273–473 K.
- **low\_salts\_case.xlsx** contains the output from the chemical speciation model described in the main text for the low salt case, with  $[\text{Cl}] = 0.05 \text{ mol kg}^{-1}$  and  $[\text{DIC}] = 0.01 \text{ mol kg}^{-1}$ . DIC is the sum of the molalities of  $\text{CO}_2(\text{aq})$ ,  $\text{HCO}_3^- (\text{aq})$  and  $\text{CO}_3^{2-} (\text{aq})$ . The speciation was performed in intervals of 10 K and 0.5 pH units, between pH 7–12 and 273–473 K.
- **CO2\_activity\_uncertainty.xlsx** collects the activity of  $\text{CO}_2$  from the three files above into a single sheet. This is plotted in Supplemental Figure S2.
- **independent\_samples.zip** contains a further 20 figures which show the variance caused by solely each of  $[\text{CH}_4]$ ,  $[\text{H}_2]$ ,  $n_{\text{ATP}}$  and  $k$  at a fixed temperature or pH as indicated by the file name. These show the deviation from the nominal  $\log_{10}(\text{Power supply})$  e.g. Figure 3 in the main text if the named parameter were allowed to vary within its uncertainty defined in Table 1 in the main text.

## C.2 Supplemental tables

**Table C.1** Values of [DIC] (sum of the molalities of  $\text{CO}_2(\text{aq})$ ,  $\text{HCO}_3^-(\text{aq})$  and  $\text{CO}_3^{2-}(\text{aq})$ ) used to get the sum of  $[\text{HCO}_3^-]$  and  $[\text{CO}_3^{2-}]$  to match the constraint from Cassini observations. For each case, at all pH values higher than those listed in this table the DIC consists only of carbonates.

salts case	pH	DIC(mol kg <sup>-1</sup> )	[CO <sub>2</sub> ](mol kg <sup>-1</sup> )	[carbonates](mol kg <sup>-1</sup> )
<b>low-salts</b> <b>Cl = 0.05</b>	7	0.013	0.002877	0.010123
	7.5	0.011	0.0009061	0.0100939
	8	0.01	0.0002754	0.0097246
	8.5	0.01	0.0000878	0.00991218
<b>nominal</b> <b>Cl = 0.1</b>	7	0.037	0.007395	0.029605
	7.5	0.032	0.00234	0.02966
	8	0.031	0.0007509	0.0302491
	8.5	0.03	0.0002309	0.0297691
	9	0.03	0.0000705	0.02992948
<b>high-salts</b> <b>Cl = 0.2</b>	7	0.121	0.02073	0.10027
	7.5	0.107	0.006554	0.100446
	8	0.102	0.00205	0.099948
	8.5	0.101	0.0006406	0.1003594
	9	0.1	0.0001915	0.0998085

## C.3 Supplementary figures

---



appendicies/Supplements/Enc1/suppfig01\_stds\_Meth\_ATP.pdf

**Figure C.1** The standard free energy ( $\Delta G^\circ$ ) of methanogenesis and ATP production (Equations 2 and 3 in the main text) at various temperatures, and pressure 1 bar and 100 bar.



**Figure C.2** Activity of  $\text{CO}_2$  (top row) and bulk ocean pH at 273 K (bottom row) as the solution is warmed in the nominal case (lines) and in the limiting salt cases (filled regions). Also shown on the bottom row is the neutral pH of pure water with temperature at 1 bar (dashed line) and 100 bar (dotted line) for reference.

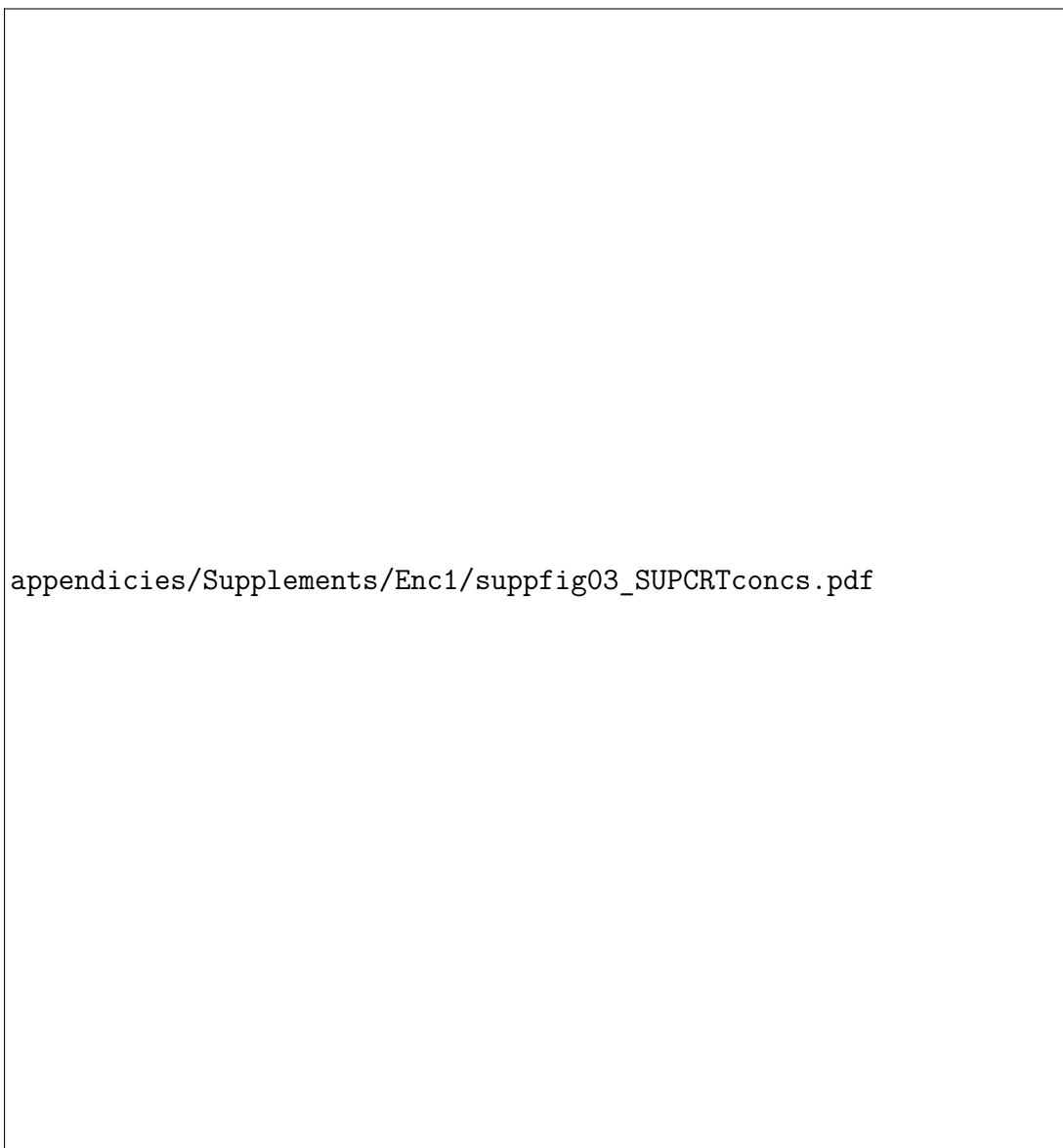


**Figure C.3** Estimates of the effect of pressure on the carbonate speciation using an SUPCRT model and the speciated  $\text{H}^+$  molality with temperatures (at 1 bar — lower-left plot of Fig S2). The equilibrium constants were calculated using SUPCRT92 at 1 bar (solid lines) and 100 bar (dashed lines) to estimate the difference in each as a fraction of total dissolved inorganic carbon [DIC]. Above 373 K the 1 bar estimate instead uses the saturation pressure of water. By comparison to Supplemental Figure S2, the effect of this pressure range is minor in comparison to that of the salt case or pH.



**Figure C.4** The free energy of ATP production  $\Delta G_{\text{ATP}}$  used for this work. The dashed and dotted lines show the yield per mole of  $\text{CO}_2$  for different values of  $n_{\text{ATP}}$ .



**Figure C.5** Total CH<sub>4</sub> production of methanogens considered in Higgins & Cockell (2020) (ref. in main text) along with the equivalent value drawn from the typical optimal methanogen in that work (solid line). The dashed lines show the effect of changing the rate constant of methanogenesis ( $k$ ) by  $\pm 1$  order of magnitude.





**Figure C.6** The Gibbs free energy of methanogenesis (equation 1 in main text) throughout the Enceladus ocean parameter space with different salt levels. Blue regions indicate where energy is available and red where it is not in each case. The solid contour line also reflects the nominal free energy yield in each case. The dotted contours show the total variation given by the chemical parameter space ( $a_{\text{H}_2}$  and  $a_{\text{CH}_4}$ ) with respect to the closest solid line.

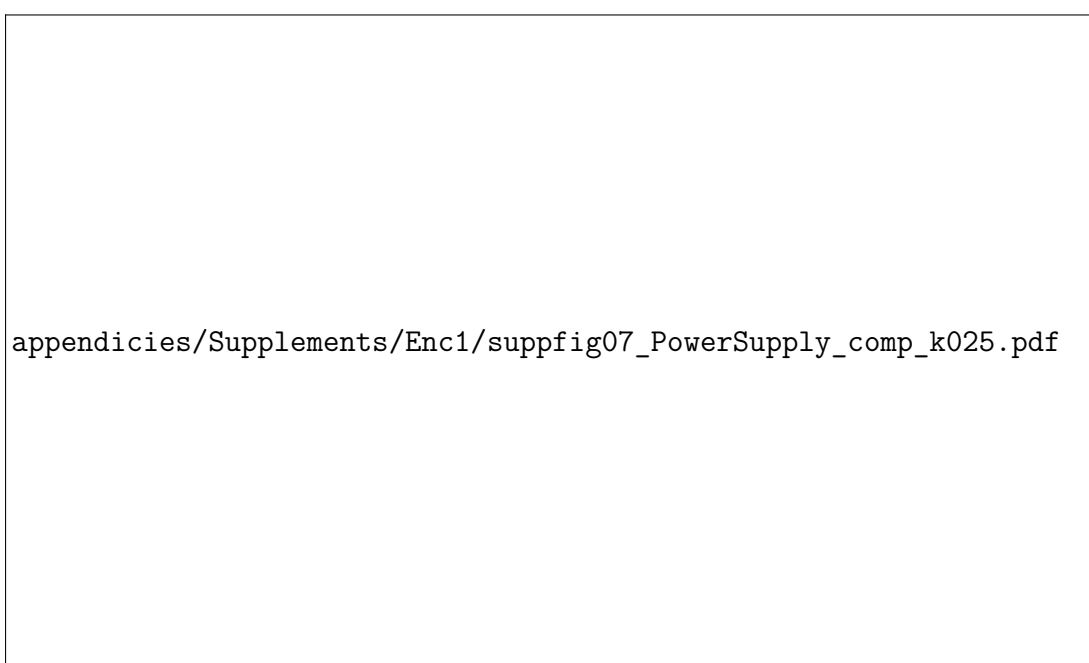


**Figure C.7** Power supply available to a methanogen at the limiting cases of the parameter space at various temperatures and bulk ocean pHs, as Figure 3 in the main text. Left) low salt endmember, minimised  $a_{\text{H}_2}$  and  $k$ , maximised  $a_{\text{CH}_4}$ . Right) high salt endmember, maximised  $a_{\text{H}_2}$  and  $k$ , minimised  $a_{\text{CH}_4}$ . Both at  $n_{\text{ATP}} = 0.25$ .

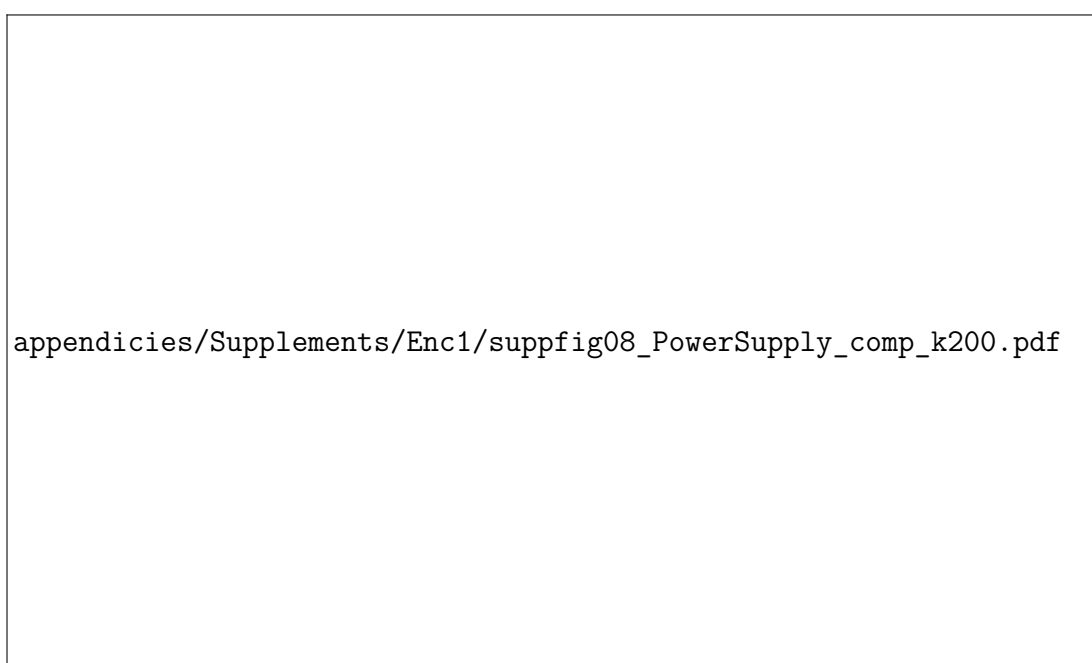


**Figure C.8** Power supply available to a methanogen at the limiting cases of the parameter space at various temperatures and bulk ocean pHs, as Figure 3 in the main text. Left) low salt endmember, minimised  $a_{\text{H}_2}$  and  $k$ , maximised  $a_{\text{CH}_4}$ . Right) high salt endmember, maximised  $a_{\text{H}_2}$  and  $k$ , minimised  $a_{\text{CH}_4}$ . Both at  $n_{\text{ATP}} = 2.0$ .



**Figure C.9** Power supply available in select pH and seawater temperature [T] combinations, with some estimates of power demands in those settings. The left hand column is at fixed T and changing pH, the right hand column is at fixed pH and changing T. Power supplies plotted are the nominal case (solid line), nominal high- and low-salt cases (dashed lines) and the endmembers that the composition may allow in those cases (dotted lines). This figure is for  $n_{\text{ATP}} = 0.25$ .

appendicies/Supplements/Enc1/suppfig10\_nominal2x3\_n200.pdf

**Figure C.10** Power supply available in select pH and seawater temperature [T] combinations, with some estimates of power demands in those settings. The left hand column is at fixed T and changing pH, the right hand column is at fixed pH and changing T. Power supplies plotted are the nominal case (solid line), nominal high- and low-salt cases (dashed lines) and the endmembers that the composition may allow in those cases (dotted lines). This figure is for  $n_{\text{ATP}} = 2.0$ . These power lines are truncated earlier than those on companion plots, because they reach a point at which power cannot be extracted sooner than at lower  $n_{\text{ATP}}$  values.



**Figure C.11** Areas of the parameter space which meet various criteria for habitability. Segments are filled when part of the parameter space's predicted power supply exceeds the power demand posed by one of four scenarios: top-left) exponential growth of methanogens; top-right) exponential growth of anaerobes; bottom-left) cost of protein repair after amino acid racemization; bottom-right) minimal power supplies to methanogens in Earth's subseafloor sediments. These cases are for  $n_{\text{ATP}} = 0.25$ .

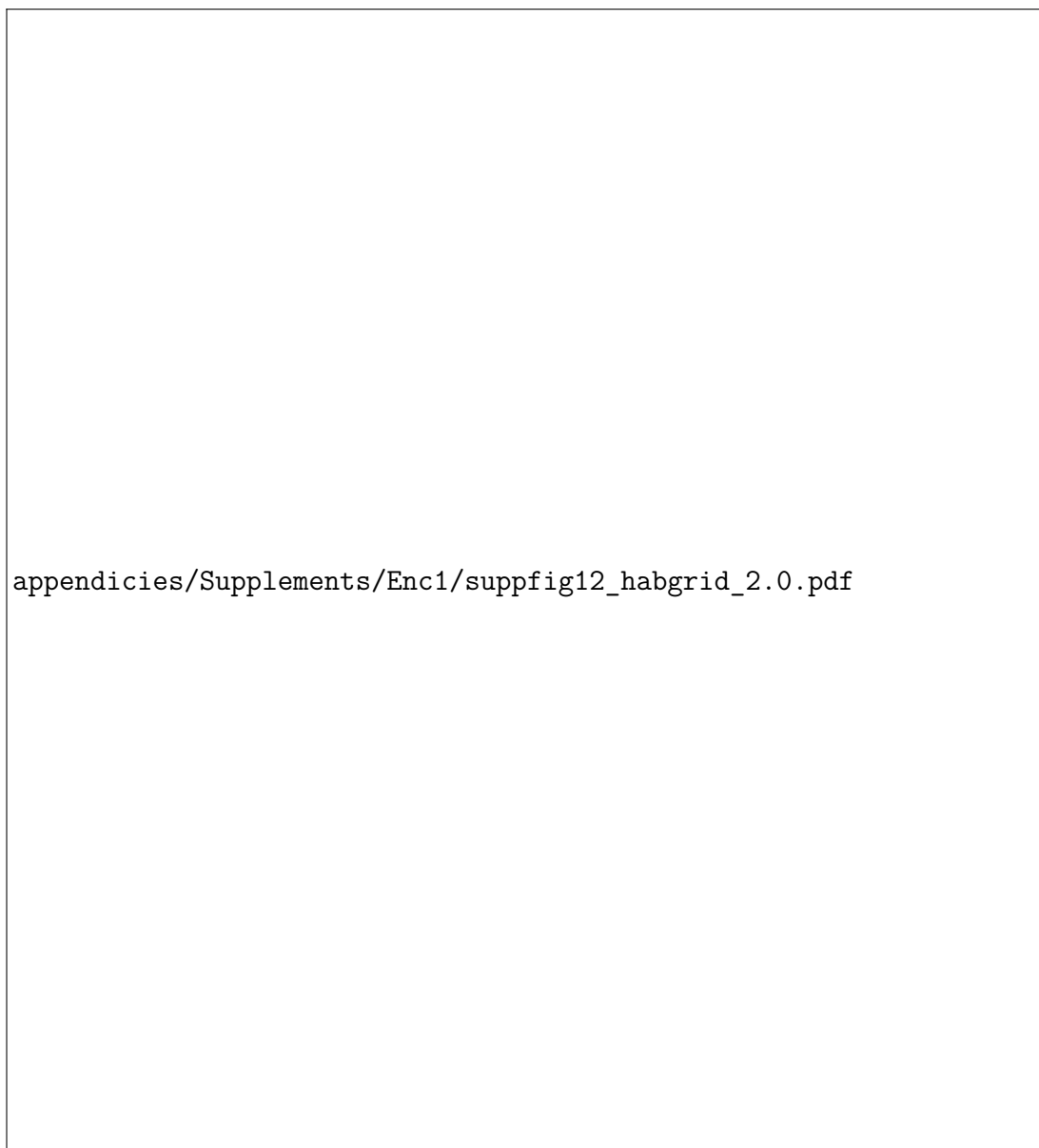


**Figure C.12** Areas of the parameter space which meet various criteria for habitability. Segments are filled when part of the parameter space's predicted power supply exceeds the power demand posed by one of four scenarios: top-left) exponential growth of methanogens; top-right) exponential growth of anaerobes; bottom-left) cost of protein repair after amino acid racemization; bottom-right) minimal power supplies to methanogens in Earth's subseafloor sediments. These cases are for  $n_{\text{ATP}} = 2.0$ .





---

## Bibliography

---

- [1] P. M. Higgins and C. S. Cockell. “A bioenergetic model to predict habitability, biomass and biosignatures in astrobiology and extreme conditions”. *Journal of The Royal Society Interface* **17**.171 (2020), p. 20200588. DOI: 10 . 1098 / rsif . 2020 . 0588.
- [2] P. M. Higgins, C. R. Glein, and C. S. Cockell. “Instantaneous Habitable Windows in the Parameter Space of Enceladus’ Ocean”. *Journal of Geophysical Research: Planets* **126**.11 (2021), e2021JE006951. DOI: 10 . 1029 / 2021JE006951.
- [3] P. M. Higgins. “NutMEG”. *Python package*. Available at: <https://github.com/pmhiggins/NutMEG>; Documentation: <https://nutmeg-astrobiology.readthedocs.io> (2021). DOI: 10.5281/zenodo.4746771.
- [4] C. S. Cockell, P. M. Higgins, and A. A. Johnstone. “Biologically Available Chemical Energy in the Temperate but Uninhabitable Venusian Cloud Layer: What Do We Want to Know?” *Astrobiology* **21**.10 (2021). DOI: 10 . 1089 / ast . 2020 . 2280.
- [5] L. M. R. Seeburger, P. M. Higgins, N. P. Whiteford, et al. “Linking methanogenesis in low-temperature hydrothermal systems to planetary spectra: CH<sub>4</sub> biosignatures on an Archean-Earth-like exoplanet”. *Astrobiology (in review)* (2022).
- [6] C. S. Cockell, R. Wordsworth, N. Whiteford, et al. “Minimum Units of Habitability and Their Abundance in the Universe”. *Astrobiology* **21**.4 (2021), pp. 481–489. DOI: 10 . 1089 / ast . 2020 . 2350.
- [7] S. Gault, P. M. Higgins, C. S. Cockell, et al. “A meta-analysis of the activity, stability, and mutational characteristics of temperature-adapted enzymes”. *Bioscience Reports* **41**.BSR20210336 (2021). DOI: 10 . 1042 / BSR20210336.
- [8] E. J. Ortega Arzola, P. M. Higgins, and C. S. Cockell. “Energetics of building cell structures: synthesizing proteomes, genomes, transcriptomes, and membranes”. *PNAS (in preparation)* (2022).
- [9] C. S. Cockell, T. Bush, C. Bryce, et al. “Habitability: A Review”. *Astrobiology* **16**.1 (2016), pp. 89–117. DOI: 10 . 1089 / ast . 2015 . 1295.

## Bibliography

---

- [10] T. M. Hoehler. “An Energy Balance Concept for Habitability”. *Astrobiology* **7.6** (2007), pp. 824–838. DOI: 10.1089/ast.2006.0095.
- [11] T. M. Hoehler, J. P. Amend, and E. L. Shock. “A “Follow the Energy” Approach for Astrobiology”. *Astrobiology* **7.6** (2007), pp. 819–823. DOI: 10.1089/ast.2007.0207.
- [12] E. L. Shock and M. E. Holland. “Quantitative Habitability”. *Astrobiology* **7.6** (2007), pp. 839–851. DOI: 10.1089/ast.2007.0137.
- [13] J. H. Waite, W. S. Lewis, B. A. Magee, et al. “Liquid water on Enceladus from observations of ammonia and  $^{40}\text{Ar}$  in the plume”. *Nature* **460**.7254 (2009), pp. 487–490. DOI: 10.1038/nature08153.
- [14] F. Postberg, S. Kempf, J. Schmidt, et al. “Sodium salts in E-ring ice grains from an ocean below the surface of Enceladus”. *Nature* **459**.7250 (2009), pp. 1098–1101. DOI: 10.1038/nature08046.
- [15] J. H. Waite, C. R. Glein, R. S. Perryman, et al. “Cassini finds molecular hydrogen in the Enceladus plume: Evidence for hydrothermal processes”. *Science* **356**.6334 (2017), pp. 155–159. DOI: 10.1126/science.aai8703.
- [16] M. L. Cable, M. Neveu, H. .-. Hsu, et al. “Enceladus”. *Planetary Astrobiology*. Ed. by V. S. Meadows, D. J. Des Marais, G. N. Arney, et al. Tucson, AZ: University of Arizona Press, 2020, pp. 217–246. ISBN: 978-0-8165-4006-8.
- [17] K. P. Hand, C. Sotin, A. Hayes, et al. “On the Habitability and Future Exploration of Ocean Worlds”. *Space Science Reviews* **216**.5 (2020), p. 95. DOI: 10.1007/s11214-020-00713-7.
- [18] A. R. Hendrix, T. A. Hurford, L. M. Barge, et al. “The NASA Roadmap to Ocean Worlds”. *Astrobiology* **19**.1 (2018), pp. 1–27. DOI: 10.1089/ast.2018.1955.
- [19] C. Ray, C. R. Glein, J. Hunter Waite, et al. “Oxidation processes diversify the metabolic menu on Enceladus”. *Icarus* (2020), p. 114248. DOI: 10.1016/j.icarus.2020.114248.
- [20] E. L. Steel, A. Davila, and C. P. McKay. “Abiotic and Biotic Formation of Amino Acids in the Enceladus Ocean”. *Astrobiology* **17**.9 (2017), pp. 862–875. DOI: 10.1089/ast.2017.1673.
- [21] A. Affholder, F. Guyot, B. Sauterey, et al. “Bayesian analysis of Enceladus’s plume data to assess methanogenesis”. *Nature Astronomy* (2021), pp. 1–10. DOI: 10.1038/s41550-021-01372-6.
- [22] C. S. Cockell. “Life in the lithosphere, kinetics and the prospects for life elsewhere”. *Philosophical Transactions of the Royal Society of London A: Mathematical, Physical and Engineering Sciences* **369**.1936 (2011), pp. 516–537. DOI: 10.1098/rsta.2010.0232.

- [23] T. M. Hoehler and B. B. Jørgensen. “Microbial life under extreme energy limitation”. *Nature Reviews Microbiology* **11.2** (2013), pp. 83–94. DOI: 10 . 1038/nrmicro2939.
- [24] D. A. Cowan. “The upper temperature for life—where do we draw the line?”. *Trends in microbiology* **12.2** (2004), pp. 58–60. DOI: 10 . 1016/j . tim . 2003 . 12 . 002.
- [25] P. B. Price and T. Sowers. “Temperature dependence of metabolic rates for microbial growth, maintenance, and survival”. *Proceedings of the National Academy of Sciences of the United States of America* **101.13** (2004), pp. 4631–4636. DOI: 10 . 1073/pnas . 0400522101.
- [26] K. Heremans. “High Pressure Effects on Proteins and other Biomolecules”. *Annual Review of Biophysics and Bioengineering* **11.1** (1982), pp. 1–21. DOI: 10 . 1146/annurev . bb . 11 . 060182 . 000245.
- [27] A. Oren. “Thermodynamic limits to microbial life at high salt concentrations”. *Environmental microbiology* **13.8** (2011), pp. 1908–1923. DOI: 10 . 1111/j . 1462–2920 . 2010 . 02365 . x.
- [28] T. A. Krulwich. “Alkaliphiles: ‘basic’ molecular problems of pH tolerance and bioenergetics”. *Molecular Microbiology* **15.3** (1995), pp. 403–410. DOI: 10 . 1111/j . 1365–2958 . 1995 . tb02253 . x.
- [29] M. A. Saito, T. J. Goepfert, and J. T. Ritt. “Some thoughts on the concept of colimitation: three definitions and the importance of bioavailability”. *Limnology and Oceanography* **53.1** (2008), pp. 276–290. DOI: 10 . 4319/lo . 2008 . 53 . 1 . 0276.
- [30] C. S. Cockell, A. H. Stevens, and R. Prescott. “Habitability is a binary property”. *Nature Astronomy* **3.11** (2019), pp. 956–957. DOI: 10 . 1038/s41550–019–0916–7.
- [31] R. Heller. “Habitability is a continuous property of nature”. *Nature Astronomy* **4.4** (2020), pp. 294–295. DOI: 10 . 1038/s41550–020–1063–x.
- [32] C. S. Cockell, T. Samuels, and A. H. Stevens. “Habitability Is Binary, But It Is Used by Astrobiologists to Encompass Continuous Ecological Questions”. *Astrobiology* (2021). DOI: 10 . 1089/ast . 2021 . 0038.
- [33] A. Lenardic and J. Seales. “Habitability: a process versus a state variable framework with observational tests and theoretical implications”. *International Journal of Astrobiology* **20.2** (2021), pp. 125–132. DOI: 10 . 1017 / S1473550420000415.

## Bibliography

---

- [34] E. L. Shock, E. H. Oelkers, J. W. Johnson, et al. "Calculation of the thermodynamic properties of aqueous species at high pressures and temperatures. Effective electrostatic radii, dissociation constants and standard partial molal properties to 1000 C and 5 kbar". *J. Chem. Soc., Faraday Trans.* **88.6** (1992), pp. 803–826. DOI: 10.1039/FT9928800803.
- [35] M. Bergkessel, D. W. Basta, and D. K. Newman. "The physiology of growth arrest: uniting molecular and environmental microbiology". *Nature Reviews Microbiology* **14.9** (2016), pp. 549–562. DOI: 10.1038/nrmicro.2016.107.
- [36] S. G. Wolf, D. Frenkiel, T. Arad, et al. "DNA protection by stress-induced biocrystallization". *Nature* **400.6739** (1999), pp. 83–85. DOI: 10.1038/21918.
- [37] M. A. Lever, K. L. Rogers, K. G. Lloyd, et al. "Life under extreme energy limitation: a synthesis of laboratory- and field-based investigations". *FEMS Microbiology Reviews* **39.5** (2015), pp. 688–728. DOI: 10.1093/femsre/fuv020.
- [38] R. Y. Morita. *Bacteria in oligotrophic environments: starvation-survival lifestyle*. Chapman & Hall microbiology series. New York: Chapman & Hall, 1997. ISBN: 978-0-412-10661-3.
- [39] D. E. LaRowe and J. P. Amend. "Catabolic rates, population sizes and doubling/replacement times of microorganisms in natural settings". *American Journal of Science* **315.3** (2015), pp. 167–203. DOI: 10.2475/03.2015.01.
- [40] D. E. LaRowe and J. P. Amend. "The energetics of anabolism in natural settings". *The ISME journal* **10.6** (2016), pp. 1285–1295. DOI: 10.1038/ismej.2015.227.
- [41] J. A. Bradley, J. P. Amend, and D. E. LaRowe. "Bioenergetic Controls on Microbial Ecophysiology in Marine Sediments". *Frontiers in Microbiology* **9** (2018), p. 180. DOI: 10.3389/fmicb.2018.00180.
- [42] J. A. Bradley, S. Arndt, J. P. Amend, et al. "Widespread energy limitation to life in global subseafloor sediments". *Science Advances* **6.32** (2020), eaba0697. DOI: 10.1126/sciadv.aba0697.
- [43] R. M. Jones, J. M. Goordial, and B. N. Orcutt. "Low Energy Subsurface Environments as Extraterrestrial Analogs". *Frontiers in Microbiology* **9** (2018). DOI: 10.3389/fmicb.2018.01605.
- [44] A. M. Semenov. "Physiological bases of oligotrophy of microorganisms and the concept of microbial community". *Microbial Ecology* **22.1** (1991), pp. 239–247. DOI: 10.1007/BF02540226.
- [45] C. P. Kempes, V. Bodegom, P. M., et al. "Drivers of Bacterial Maintenance and Minimal Energy Requirements". *Frontiers in Microbiology* **8** (2017), p. 31. DOI: 10.3389/fmicb.2017.00031.

- [46] T. A. Krulwich, G. Sachs, and E. Padan. "Molecular aspects of bacterial pH sensing and homeostasis". *Nature Reviews Microbiology* **9.5** (2011), pp. 330–343. DOI: 10.1038/nrmicro2549.
- [47] C. S. Cockell and S. Nixon. "The Boundaries of Life". *Astrochemistry and Astrobiology*. Ed. by I. W. M. Smith, C. S. Cockell, and S. Leach. Physical Chemistry in Action. Berlin, Heidelberg: Springer, 2013, pp. 211–241. ISBN: 978-3-642-31730-9. DOI: 10.1007/978-3-642-31730-9\_7.
- [48] M. C. Capece, E. Clark, J. K. Saleh, et al. "Polyextremophiles and the Constraints for Terrestrial Habitability". *Polyextremophiles: Life Under Multiple Forms of Stress*. Ed. by J. Seckbach, A. Oren, and H. Stan-Lotter. Cellular Origin, Life in Extreme Habitats and Astrobiology. Dordrecht: Springer Netherlands, 2013, pp. 3–59. ISBN: 978-94-007-6488-0. DOI: 10.1007/978-94-007-6488-0\_1.
- [49] H. M. Mader. "Observations of the water-vein system in polycrystalline ice". *Journal of Glaciology* **38.130** (1992), pp. 333–347. DOI: 10.3189/S0022143000002227.
- [50] P. B. Price. "A habitat for psychrophiles in deep Antarctic ice". *Proceedings of the National Academy of Sciences* **97.3** (2000), pp. 1247–1251. DOI: 10.1073/pnas.97.3.1247.
- [51] R. Jaenicke, H. Schurig, N. Beaucamp, et al. "Structure and stability of hyperstable proteins: glycolytic enzymes from hyperthermophilic bacterium *Thermotoga maritima*". *Advances in protein chemistry* **48** (1996), pp. 181–269. DOI: 10.1016/S0065-3233(08)60363-0.
- [52] K. Takai, K. Nakamura, T. Toki, et al. "Cell proliferation at 122 C and isotopically heavy CH<sub>4</sub> production by a hyperthermophilic methanogen under high-pressure cultivation". *Proceedings of the National Academy of Sciences* **105.31** (2008), pp. 10949–10954. DOI: 10.1073/pnas.0712334105.
- [53] B. Tauscher. "Pasteurization of food by hydrostatic high pressure: chemical aspects". *Zeitschrift für Lebensmittel-Untersuchung und -Forschung* **200.1** (1995), pp. 3–13. DOI: 10.1007/BF01192901.
- [54] D. Knorr, V. Heinz, and R. Buckow. "High pressure application for food biopolymers". *Biochimica et Biophysica Acta (BBA) - Proteins and Proteomics*. Proteins Under High Pressure **1764.3** (2006), pp. 619–631. DOI: 10.1016/j.bbapap.2006.01.017.
- [55] R. Winter and C. Jeworrek. "Effect of pressure on membranes". *Soft Matter* **5.17** (2009), pp. 3157–3173. DOI: 10.1039/B901690B.

## Bibliography

---

- [56] W. L. Nicholson, P. Fajardo-Cavazos, J. Fedenko, et al. "Exploring the Low-Pressure Growth Limit: Evolution of *Bacillus subtilis* in the Laboratory to Enhanced Growth at 5 Kilopascals". *Applied and Environmental Microbiology* **76.22** (2010), pp. 7559–7565. DOI: 10.1128/AEM.01126-10.
- [57] J. F. Miller, N. N. Shah, C. M. Nelson, et al. "Pressure and Temperature Effects on Growth and Methane Production of the Extreme Thermophile *Methanococcus jannaschii*". *Applied and Environmental Microbiology* **54.12** (1988), pp. 3039–3042.
- [58] A. M. M. Leal, D. A. Kulik, W. R. Smith, et al. "An overview of computational methods for chemical equilibrium and kinetic calculations for geochemical and reactive transport modeling". *Pure and Applied Chemistry* **89.5** (2017), pp. 597–643. DOI: 10.1515/pac-2016-1107.
- [59] D. A. McQuarrie and J. D. Simon. *Molecular Thermodynamics*. 1st ed. Sausalito, California: University Science Books, 1999. ISBN: 9781891389054.
- [60] L. Tijhuis, M. C. Van Loosdrecht, and J. J. Heijnen. "A thermodynamically based correlation for maintenance gibbs energy requirements in aerobic and anaerobic chemotrophic growth". *Biotechnology and Bioengineering* **42.4** (1993), pp. 509–519. DOI: 10.1002/bit.260420415.
- [61] J. P. Harrison, N. Gheeraert, D. Tsigelnitskiy, et al. "The limits for life under multiple extremes". *Trends in Microbiology* **21.4** (2013), pp. 204–212. DOI: 10.1016/j.tim.2013.01.006.
- [62] R. Jaenicke and R. Sterner. "Life at high temperatures". *The Prokaryotes*. Springer, 2006, pp. 167–209.
- [63] C. S. Cockell. *Astrobiology: Understanding Life in the Universe*. 1st ed. Chichester: Wiley, 2015. ISBN: 978-1-118-91333-8.
- [64] A. Oren. "Microbial life at high salt concentrations: phylogenetic and metabolic diversity". *Saline Systems* **4** (2008), p. 2. DOI: 10.1186/1746-1448-4-2.
- [65] S. G. Bratsch. "Standard electrode potentials and temperature coefficients in water at 298.15 K". *Journal of Physical and Chemical Reference Data* **18.1** (1989), pp. 1–21. DOI: 10.1063/1.555839.
- [66] A. C. Tikanen and W. R. Fawcett. "Application of the mean spherical approximation and ion association to describe the activity coefficients of aqueous 1:1 electrolytes". *Journal of Electroanalytical Chemistry* **439.1** (1997), pp. 107–113. DOI: 10.1016/S0022-0728(97)00376-8.
- [67] M. R. Fisk and S. J. Giovannoni. "Sources of nutrients and energy for a deep biosphere on Mars". *Journal of Geophysical Research: Planets* **104.E5** (1999), pp. 11805–11815. DOI: 10.1029/1999JE900010.

- [68] J. R. Michalski, J. Cuadros, P. B. Niles, et al. "Groundwater activity on Mars and implications for a deep biosphere". *Nature Geoscience* **6.2** (2013), pp. 133–138. DOI: 10.1038/ngeo1706.
- [69] J. Parnell, S. McMahon, and A. Boyce. "Demonstrating deep biosphere activity in the geological record of lake sediments, on Earth and Mars". *International Journal of Astrobiology* (2017), pp. 1–6. DOI: 10.1017/S1473550417000337.
- [70] A. H. Lobo, A. F. Thompson, S. D. Vance, et al. "A pole-to-equator ocean overturning circulation on Enceladus". *Nature Geoscience* **14.4** (2021), pp. 185–189. DOI: 10.1038/s41561-021-00706-3.
- [71] C. P. McKay. "Requirements and limits for life in the context of exoplanets". *Proceedings of the National Academy of Sciences* **111.35** (2014), pp. 12628–12633. DOI: 10.1073/pnas.1304212111.
- [72] J. B. Russell and G. M. Cook. "Energetics of bacterial growth: balance of anabolic and catabolic reactions." *Microbiological reviews* **59.1** (1995), pp. 48–62.
- [73] J. Monod. "The Growth of Bacterial Cultures". *Annual Review of Microbiology* **3.1** (1949), pp. 371–394. DOI: 10.1146/annurev.mi.03.100149.002103.
- [74] A. Holmberg. "On the practical identifiability of microbial growth models incorporating Michaelis-Menten type nonlinearities". *Mathematical Biosciences* **62.1** (1982), pp. 23–43. DOI: 10.1016/0025-5564(82)90061-X.
- [75] E. Bertolazzi. "A combination formula of Michaelis-Menten-Monod type". *Computers & Mathematics with Applications* **50.1** (2005), pp. 201–215. DOI: 10.1016/j.camwa.2004.10.045.
- [76] O. M. Neijssel and D. W. Tempest. "Bioenergetic aspects of aerobic growth of *Klebsiella aerogenes* NCTC 418 in carbon-limited and carbon-sufficient chemostat culture". *Archives of Microbiology* **107.2** (1976), pp. 215–221. DOI: 10.1007/BF00446843.
- [77] S. J. Pirt. "The maintenance energy of bacteria in growing cultures". *Proc. R. Soc. Lond. B* **163.991** (1965), pp. 224–231. DOI: 10.1098/rspb.1965.0069.
- [78] J. J. Heijnen and J. P. Van Dijken. "In search of a thermodynamic description of biomass yields for the chemotrophic growth of microorganisms". *Biotechnology and Bioengineering* **39.8** (1992), pp. 833–858. DOI: 10.1002/bit.260390806.
- [79] J. S. Liu, V. Vojinović, R. Patiño, et al. "A comparison of various Gibbs energy dissipation correlations for predicting microbial growth yields". *Thermochimica Acta* **458.1** (2007), pp. 38–46. DOI: 10.1016/j.tca.2007.01.016.

## Bibliography

---

- [80] C. C. Porco, P. Helfenstein, P. C. Thomas, et al. “Cassini Observes the Active South Pole of Enceladus”. *Science* **311**.5766 (2006), pp. 1393–1401. DOI: 10 . 1126/science.1123013.
- [81] K. K. Khurana, M. G. Kivelson, D. J. Stevenson, et al. “Induced magnetic fields as evidence for subsurface oceans in Europa and Callisto”. *Nature* **395**.6704 (1998), pp. 777–780. DOI: 10 . 1038/27394.
- [82] T. M. McCollom. “Methanogenesis as a potential source of chemical energy for primary biomass production by autotrophic organisms in hydrothermal systems on Europa”. *Journal of Geophysical Research: Planets* **104**.E12 (1999), pp. 30729–30742. DOI: 10 . 1029/1999JE001126.
- [83] S. D. Vance, M. P. Panning, S. Stähler, et al. “Geophysical Investigations of Habitability in Ice-Covered Ocean Worlds”. *Journal of Geophysical Research: Planets* **123**.1 (2018). DOI: 10 . 1002/2017JE005341.
- [84] M. J. Russell, A. E. Murray, and K. P. Hand. “The Possible Emergence of Life and Differentiation of a Shallow Biosphere on Irradiated Icy Worlds: The Example of Europa”. *Astrobiology* **17**.12 (2017), pp. 1265–1273. DOI: 10 . 1089/ast.2016.1600.
- [85] H.-W. Hsu, F. Postberg, Y. Sekine, et al. “Ongoing hydrothermal activities within Enceladus”. *Nature* **519**.7542 (2015), pp. 207–210. DOI: 10 . 1038 / nature14262.
- [86] C. R. Glein, J. A. Baross, and J. H. Waite. “The pH of Enceladus’ ocean”. *Geochimica et Cosmochimica Acta* **162** (2015), pp. 202–219. DOI: 10 . 1016 / j . gca . 2015 . 04 . 017.
- [87] C. R. Glein and J. H. Waite. “The Carbonate Geochemistry of Enceladus’ Ocean”. *Geophysical Research Letters* **47**.3 (2020), e2019GL085885. DOI: 10 . 1029/2019GL085885.
- [88] C. R. Glein, F. Postberg, and S. D. Vance. “The Geochemistry of Enceladus: Composition and Controls”. *Enceladus and the Icy Moons of Saturn*. Ed. by P. M. Schenk, R. N. Clark, C. J. A. Howett, et al. Tucson, AZ: University of Arizona Press, 2018, pp. 39–56. DOI: 10 . 2458/azu\_uapress\_9780816537075-ch003.
- [89] S. D. Vance. “The Habitability of Icy Ocean Worlds in the Solar System”. *Handbook of Exoplanets*. Ed. by H. J. Deeg and J. A. Belmonte. Cham: Springer International Publishing, 2018, pp. 1–23. ISBN: 978-3-319-30648-3. DOI: 10 . 1007/978-3-319-30648-3\_63-1.
- [90] B. A. Magee and J. H. Waite. “Neutral Gas Composition of Enceladus’ Plume — Model Parameter Insights from Cassini-INMS”. 2017.



- [91] J. F. Cooper, P. D. Cooper, E. C. Sittler, et al. “Old Faithful model for radiolytic gas-driven cryovolcanism at Enceladus”. *Planetary and Space Science. Surfaces and Atmospheres of the Outer Planets, Their Satellites and Ring Systems: Part V* **57.13** (2009), pp. 1607–1620. DOI: 10.1016/j.pss.2009.08.002.
- [92] J. R. Spencer and F. Nimmo. “Enceladus: An Active Ice World in the Saturn System”. *Annual Review of Earth and Planetary Sciences* **41.1** (2013), pp. 693–717. DOI: 10.1146/annurev-earth-050212-124025.
- [93] L. Iess, D. J. Stevenson, M. Parisi, et al. “The Gravity Field and Interior Structure of Enceladus”. *Science* **344**.6179 (2014), pp. 78–80. DOI: 10.1126/science.1250551.
- [94] G. Choblet, G. Tobie, C. Sotin, et al. “Powering prolonged hydrothermal activity inside Enceladus”. *Nature Astronomy* **1.12** (2017), pp. 841–847. DOI: 10.1038/s41550-017-0289-8.
- [95] D. J. Hemingway and T. Mittal. “Enceladus’s ice shell structure as a window on internal heat production”. *Icarus* **332** (2019), pp. 111–131. DOI: 10.1016/j.icarus.2019.03.011.
- [96] J. D. Goguen, B. J. Buratti, R. H. Brown, et al. “The temperature and width of an active fissure on Enceladus measured with Cassini VIMS during the 14 April 2012 South Pole flyover”. *Icarus* **226.1** (2013), pp. 1128–1137. DOI: 10.1016/j.icarus.2013.07.012.
- [97] S. D. Vance, S. Kedar, M. P. Panning, et al. “Vital Signs: Seismology of Icy Ocean Worlds”. *Astrobiology* **18.1** (2018), pp. 37–53. DOI: 10.1089/ast.2016.1612.
- [98] B. S. Southworth, S. Kempf, and J. Spitale. “Surface deposition of the Enceladus plume and the zenith angle of emissions”. *Icarus* **319** (2019), pp. 33–42. DOI: 10.1016/j.icarus.2018.08.024.
- [99] J. Schmidt, N. Brilliantov, F. Spahn, et al. “Slow dust in Enceladus’ plume from condensation and wall collisions in tiger stripe fractures”. *Nature* **451.7179** (2008), pp. 685–688. DOI: 10.1038/nature06491.
- [100] A. Bouquet, O. Mousis, J. H. Waite, et al. “Possible evidence for a methane source in Enceladus’ ocean”. *Geophysical Research Letters* **42.5** (2015), pp. 1334–1339. DOI: 10.1002/2014GL063013.
- [101] M. Y. Zolotov. “An oceanic composition on early and today’s Enceladus”. *Geophysical Research Letters* **34.23** (2007). DOI: <https://doi.org/10.1029/2007GL031234>.
- [102] G. M. Marion, J. S. Kargel, D. C. Catling, et al. “Modeling ammonia–ammonium aqueous chemistries in the Solar System’s icy bodies”. *Icarus* **220.2** (2012), pp. 932–946. DOI: 10.1016/j.icarus.2012.06.016.

## Bibliography

---

- [103] F. Postberg, J. Schmidt, J. Hillier, et al. “A salt-water reservoir as the source of a compositionally stratified plume on Enceladus”. *Nature* **474**.7353 (2011), pp. 620–622. DOI: 10.1038/nature10175.
- [104] F. Postberg, N. Khawaja, B. Abel, et al. “Macromolecular organic compounds from the depths of Enceladus”. *Nature* **558**.7711 (2018), pp. 564–568. DOI: 10.1038/s41586-018-0246-4.
- [105] N. Khawaja, F. Postberg, J. Hillier, et al. “Low-mass nitrogen-, oxygen-bearing, and aromatic compounds in Enceladean ice grains”. *Monthly Notices of the Royal Astronomical Society* **489**.4 (2019), pp. 5231–5243. DOI: 10.1093/mnras/stz2280.
- [106] M. Lingam and A. Loeb. “Is Extraterrestrial Life Suppressed on Subsurface Ocean Worlds due to the Paucity of Bioessential Elements?” *The Astronomical Journal* **156**.4 (2018), p. 151. DOI: 10.3847/1538-3881/aada02.
- [107] M. Čuk, L. Dones, and D. Nesvorný. “Dynamical evidence for a late formation of Saturn’s moons”. *The Astrophysical Journal* **820**.2 (2016), p. 97. DOI: 10.3847/0004-637X/820/2/97.
- [108] T. M. McCollom. “Geochemical Constraints on Sources of Metabolic Energy for Chemolithoautotrophy in Ultramafic-Hosted Deep-Sea Hydrothermal Systems”. *Astrobiology* **7**.6 (2007), pp. 933–950. DOI: 10.1089/ast.2006.0119.
- [109] J. P. Amend, T. M. McCollom, M. Hentscher, et al. “Catabolic and anabolic energy for chemolithoautotrophs in deep-sea hydrothermal systems hosted in different rock types”. *Geochimica et Cosmochimica Acta* **75**.19 (2011), pp. 5736–5748. DOI: 10.1016/j.gca.2011.07.041.
- [110] F. L. Sousa, T. Thiergart, G. Landan, et al. “Early bioenergetic evolution”. *Phil. Trans. R. Soc. B* **368**.1622 (2013), p. 20130088. DOI: 10.1098/rstb.2013.0088.
- [111] B. A. Lomstein, A. T. Langerhuus, S. D’Hondt, et al. “Endospore abundance, microbial growth and necromass turnover in deep sub-seafloor sediment”. *Nature* **484**.7392 (2012), pp. 101–104. DOI: 10.1038/nature10905.
- [112] M. Bär, J. Hardenberg, E. Meron, et al. “Modelling the survival of bacteria in drylands: the advantage of being dormant”. *Proceedings of the Royal Society of London B: Biological Sciences* **269**.1494 (2002), pp. 937–942. DOI: 10.1098/rspb.2002.1958.
- [113] S. M. Burrows, T. Butler, P. Jöckel, et al. “Bacteria in the global atmosphere – Part 2: Modeling of emissions and transport between different ecosystems”. *Atmos. Chem. Phys.* **9**.23 (2009), pp. 9281–9297. DOI: 10.5194/acp-9-9281-2009.

- [114] J. J. Middelburg. “Reviews and syntheses: to the bottom of carbon processing at the seafloor”. *Biogeosciences* **15.2** (2018), pp. 413–427. DOI: 10.5194/bg-15-413-2018.
- [115] E. S. Varnes, B. M. Jakosky, and T. M. McCollom. “Biological Potential of Martian Hydrothermal Systems”. *Astrobiology* **3.2** (2003), pp. 407–414. DOI: 10.1089/153110703769016479.
- [116] B. P. Weiss, Y. L. Yung, and K. H. Nealson. “Atmospheric energy for subsurface life on Mars?” *Proceedings of the National Academy of Sciences* **97.4** (2000), pp. 1395–1399. DOI: 10.1073/pnas.030538097.
- [117] E. G. Jones, C. H. Lineweaver, and J. D. Clarke. “An Extensive Phase Space for the Potential Martian Biosphere”. *Astrobiology* **11.10** (2011), pp. 1017–1033. DOI: 10.1089/ast.2011.0660.
- [118] C. R. Webster, P. R. Mahaffy, S. K. Atreya, et al. “Mars methane detection and variability at Gale crater”. *Science* **347.6220** (2015), pp. 415–417. DOI: 10.1126/science.1261713.
- [119] C. R. Webster, P. R. Mahaffy, S. K. Atreya, et al. “Low Upper Limit to Methane Abundance on Mars”. *Science* **342.6156** (2013), pp. 355–357. DOI: 10.1126/science.1242902.
- [120] A. H. Stevens, M. R. Patel, and S. R. Lewis. “Numerical modelling of the transport of trace gases including methane in the subsurface of Mars”. *Icarus* **250** (2015), pp. 587–594. DOI: 10.1016/j.icarus.2014.12.033.
- [121] S. L. Nixon, C. R. Cousins, and C. S. Cockell. “Plausible microbial metabolisms on Mars”. *Astronomy & Geophysics* **54.1** (2013), pp. 1.13–1.16. DOI: 10.1093/astrogeo/ats034.
- [122] A. G. Fairén, A. F. Davila, D. Lim, et al. “Astrobiology through the Ages of Mars: The Study of Terrestrial Analogues to Understand the Habitability of Mars”. *Astrobiology* **10.8** (2010), pp. 821–843. DOI: 10.1089/ast.2009.0440.
- [123] C. S. Cockell. “Trajectories of Martian Habitability”. *Astrobiology* **14.2** (2014), pp. 182–203. DOI: 10.1089/ast.2013.1106.
- [124] J. S. Greaves, A. M. S. Richards, W. Bains, et al. “Phosphine gas in the cloud decks of Venus”. *Nature Astronomy* (2020), pp. 1–10. DOI: 10.1038/s41550-020-1174-4.
- [125] S. Seager, W. Bains, and J. Petkowski. “Toward a List of Molecules as Potential Biosignature Gases for the Search for Life on Exoplanets and Applications to Terrestrial Biochemistry”. *Astrobiology* **16.6** (2016), pp. 465–485. DOI: 10.1089/ast.2015.1404.
- [126] E. Keles, J. L. Grenfell, M. Godolt, et al. “The Effect of Varying Atmospheric Pressure upon Habitability and Biosignatures of Earth-like Planets”. *Astrobiology* **18.2** (2018), pp. 116–132. DOI: 10.1089/ast.2016.1632.

## Bibliography

---

- [127] J. S. Yates, P. I. Palmer, B. Biller, et al. “Atmospheric Habitable Zones in Y Dwarf Atmospheres”. *The Astrophysical Journal* **836.2** (2017), p. 184. DOI: 10.3847/1538-4357/836/2/184.
- [128] V. S. Meadows, G. N. Arney, E. W. Schwieterman, et al. “The Habitability of Proxima Centauri b: Environmental States and Observational Discriminants”. *Astrobiology* **18.2** (2018), pp. 133–189. DOI: 10.1089/ast.2016.1589.
- [129] E. Schrödinger. *What is Life? The Physical Aspect of the Living Cell*. Cambridge University Press, 1944.
- [130] J. P. Amend, H. S. Aronson, J. Macalady, et al. “Another chemolithotrophic metabolism missing in nature: sulfur comproportionation”. *Environmental Microbiology* **22.6** (2020), pp. 1971–1976. DOI: <https://doi.org/10.1111/1462-2920.14982>.
- [131] J. P. Amend and D. E. LaRowe. “Minireview: demystifying microbial reaction energetics”. *Environmental Microbiology* **21.10** (2019), pp. 3539–3547. DOI: 10.1111/1462-2920.14778.
- [132] J. W. Johnson, E. H. Oelkers, and H. C. Helgeson. “SUPCRT92: A software package for calculating the standard molal thermodynamic properties of minerals, gases, aqueous species, and reactions from 1 to 5000 bar and 0 to 1000 C”. *Computers & Geosciences* **18.7** (1992), pp. 899–947. DOI: 10.1016/0098-3004(92)90029-Q.
- [133] K. R. Albe, M. H. Butler, and B. E. Wright. “Cellular concentrations of enzymes and their substrates”. *Journal of theoretical biology* **143.2** (1990), pp. 163–195. DOI: 10.1016/S0022-5193(05)80266-8.
- [134] B. Schink. “Synergistic interactions in the microbial world”. *Antonie van Leeuwenhoek* **81.1** (2002), pp. 257–261. DOI: 10.1023/A:1020579004534.
- [135] Q. Jin and C. M. Bethke. “The thermodynamics and kinetics of microbial metabolism”. *American Journal of Science* **307.4** (2007), pp. 643–677. DOI: 10.2475/04.2007.01.
- [136] D. E. LaRowe and J. M. Dick. “Calculation of the standard molal thermodynamic properties of crystalline peptides”. *Geochimica et Cosmochimica Acta* **80** (2012), pp. 70–91. DOI: 10.1016/j.gca.2011.11.041.
- [137] J. P. Amend, D. E. LaRowe, T. M. McCollom, et al. “The energetics of organic synthesis inside and outside the cell”. *Phil. Trans. R. Soc. B* **368**.1622 (2013), p. 20120255. DOI: 10.1098/rstb.2012.0255.
- [138] T. M. McCollom and J. P. Amend. “A thermodynamic assessment of energy requirements for biomass synthesis by chemolithoautotrophic microorganisms in oxic and anoxic environments”. *Geobiology* **3.2** (2005), pp. 135–144. DOI: 10.1111/j.1472-4669.2005.00045.x.

- [139] F. C. Neidhardt and H. E. Umbarger. *Escherichia coli and Salmonella: cellular and molecular biology*. Ed. by F. C. Neidhardt. Vol. 1. ASM Press, 1996.
- [140] Y. Ishihama, T. Schmidt, J. Rappsilber, et al. "Protein abundance profiling of the Escherichia coli cytosol". *BMC genomics* **9.1** (2008), p. 102. DOI: 10.1186/1471-2164-9-102.
- [141] B. Ho, A. Baryshnikova, and G. W. Brown. "Unification of Protein Abundance Datasets Yields a Quantitative *Saccharomyces cerevisiae* Proteome". *Cell Systems* (2018). DOI: 10.1016/j.cels.2017.12.004.
- [142] R. B. Martin. "Free energies and equilibria of peptide bond hydrolysis and formation". *Biopolymers* **45.5** (1998), pp. 351–353. DOI: 10.1002/(SICI)1097-0282(19980415)45:5<351::AID-BIP3>3.0.CO;2-K.
- [143] L. Brocchieri and S. Karlin. "Protein length in eukaryotic and prokaryotic proteomes". *Nucleic acids research* **33.10** (2005), pp. 3390–3400. DOI: 10.1093/nar/gki615.
- [144] C. Mathews, K. v. Holde, D. Appling, et al. *Biochemistry*. 4th edition. Toronto: Pearson, 2012. ISBN: 978-0-13-800464-4.
- [145] J. F. Nagle. "Theory of passive proton conductance in lipid bilayers". *Journal of Bioenergetics and Biomembranes* **19.5** (1987), pp. 413–426. DOI: 10.1007/bf00770027.
- [146] D. W. Deamer and J. Bramhall. "Permeability of lipid bilayers to water and ionic solutes". *Chemistry and Physics of Lipids* **40.2-4** (1986), pp. 167–188. DOI: 10.1016/0009-3084(86)90069-1.
- [147] D. W. Deamer and J. W. Nichols. "Proton flux mechanisms in model and biological membranes". *The Journal of Membrane Biology* **107.2** (1989), pp. 91–103. DOI: 10.1007/BF01871715.
- [148] T. E. Decoursey. "Voltage-Gated Proton Channels and Other Proton Transfer Pathways". *Physiological Reviews* **83.2** (2003), pp. 475–579. DOI: 10.1152/physrev.00028.2002.
- [149] W. Shinoda. "Permeability across lipid membranes". *Biochimica et Biophysica Acta (BBA) - Biomembranes* **1858.10** (2016), pp. 2254–2265. DOI: 10.1016/J.BBAMEM.2016.03.032.
- [150] H. Kugel, A. Mayer, G. O. Kirst, et al. "The energy requirements of pH homeostasis define the limits of pH regulation - a model". *Biochimica et Biophysica Acta (BBA) - Molecular Cell Research* **1054.1** (1990), pp. 33–40. DOI: 10.1016/0167-4889(90)90202-0.
- [151] N. Lakshminarayanaiah. *Equations of membrane biophysics*. Academic Press, 1984. ISBN: 0-12-434260-4.

## Bibliography

- [152] B. Hille. *Ion channels of excitable membranes*. Third edition.. Sunderland, Mass.: Sinauer, 2001. ISBN: 978-0-87893-321-1.
- [153] W. N. Konings, S.-V. Albers, S. Koning, et al. “The cell membrane plays a crucial role in survival of bacteria and archaea in extreme environments”. *Antonie van Leeuwenhoek* **81.1** (2002), pp. 61–72. DOI: 10.1023/A:1020573408652.
- [154] D. W. Deamer. “Proton permeation of lipid bilayers”. *Journal of Bioenergetics and Biomembranes* **19.5** (1987), pp. 457–479. DOI: 10.1007/bf00770030.
- [155] J. L. C. M. van de Vossenberg, A. J. M. Driessen, and W. N. Konings. “The essence of being extremophilic: the role of the unique archaeal membrane lipids”. *Extremophiles* **2.3** (1998), pp. 163–170. DOI: 10.1007/s007920050056.
- [156] T. M. McCollom. “Geochemical constraints on primary productivity in submarine hydrothermal vent plumes”. *Deep Sea Research Part I: Oceanographic Research Papers* **47.1** (2000), pp. 85–101. DOI: 10.1016/S0967-0637(99)00048-5.
- [157] R. M. Atlas. *Principles of microbiology*. Mosby, 1995. ISBN: 0-8016-7790-4.
- [158] M. Schulte, D. Blake, T. Hoehler, et al. “Serpentinization and Its Implications for Life on the Early Earth and Mars”. *Astrobiology* **6.2** (2006), pp. 364–376. DOI: 10.1089/ast.2006.6.364.
- [159] B. L. Ehlmann and C. S. Edwards. “Mineralogy of the Martian Surface”. *Annual Review of Earth and Planetary Sciences* **42.1** (2014), pp. 291–315. DOI: 10.1146/annurev-earth-060313-055024.
- [160] B. M. Jakosky and E. L. Shock. “The biological potential of Mars, the early Earth, and Europa”. *Journal of Geophysical Research: Planets* **103.E8** (1998), pp. 19359–19364. DOI: 10.1029/98JE01892.
- [161] S. F. Sholes, J. Krissansen-Totton, and D. C. Catling. “A Maximum Subsurface Biomass on Mars from Untapped Free Energy: CO and H<sub>2</sub> as Potential Antibiosignatures”. *Astrobiology* **19.5** (2019), pp. 655–668. DOI: 10.1089/ast.2018.1835.
- [162] E. L. Shock, M. Holland, D. Meyer-Dombard, et al. “Quantifying inorganic sources of geochemical energy in hydrothermal ecosystems, Yellowstone National Park, USA”. *Geochimica et Cosmochimica Acta* **74.14** (2010), pp. 4005–4043. DOI: 10.1016/j.gca.2009.08.036.
- [163] P. van Bodegom. “Microbial Maintenance: A Critical Review on Its Quantification”. *Microbial Ecology* **53.4** (2007), pp. 513–523. DOI: 10.1007/s00248-006-9049-5.
- [164] V. Chubukov, L. Gerosa, K. Kochanowski, et al. “Coordination of microbial metabolism”. *Nature Reviews Microbiology* **12.5** (2014), pp. 327–340. DOI: 10.1038/nrmicro3238.

- [165] R.-S. Taubner, C. Schleper, M. G. Firneis, et al. "Assessing the Ecophysiology of Methanogens in the Context of Recent Astrobiological and Planetological Studies". *Life* **5.4** (2015), pp. 1652–1686. DOI: 10.3390/life5041652.
- [166] B. Michał, P. Gagat, S. Jabłoński, et al. "PhyMet2 : a database and toolkit for phylogenetic and metabolic analyses of methanogens". *Environmental Microbiology Reports* **10.3** (2018), pp. 378–382. DOI: 10.1111/1758-2229.12648.
- [167] G. E. Powell. "Interpreting gas kinetics of batch cultures". *Biotechnology Letters* **5.7** (1983), pp. 437–440. DOI: 10.1007/BF00132224.
- [168] R. K. Thauer, K. Jungermann, and K. Decker. "Energy conservation in chemotrophic anaerobic bacteria." *Bacteriological reviews* **41.1** (1977), p. 100.
- [169] D. G. Nicholls and S. J. Ferguson. "5 - Respiratory Chains". *Bioenergetics (Fourth Edition)*. Ed. by D. G. Nicholls and S. J. Ferguson. 4th ed. Boston: Academic Press, 2013, pp. 91–157. ISBN: 978-0-12-388425-1. DOI: 10.1016/B978-0-12-388425-1.00005-1.
- [170] R. Milo and R. Phillips. *Cell Biology by the Numbers*. Garland Science, 2015. ISBN: 978-1-317-23069-4.
- [171] R. Milo. "What is the total number of protein molecules per cell volume? A call to rethink some published values". *BioEssays* **35.12** (2013), pp. 1050–1055. DOI: 10.1002/bies.201300066.
- [172] A. A. Esteves-Ferreira, M. Inaba, T. Obata, et al. "A Novel Mechanism, Linked to Cell Density, Largely Controls Cell Division in Synechocystis". *Plant Physiology* **174.4** (2017), pp. 2166–2182. DOI: 10.1104/pp.17.00729.
- [173] J. Shiloach and R. Fass. "Growing E. coli to high cell density—A historical perspective on method development". *Biotechnology Advances* **23.5** (2005), pp. 345–357. DOI: 10.1016/j.biotechadv.2005.04.004.
- [174] P. C. Thomas, R. Tajeddine, M. S. Tiscareno, et al. "Enceladus's measured physical libration requires a global subsurface ocean". *Icarus* **264** (2016), pp. 37–47. DOI: 10.1016/j.icarus.2015.08.037.
- [175] H. B. Smith, A. Drew, J. F. Malloy, et al. "Seeding Biochemistry on Other Worlds: Enceladus as a Case Study". *Astrobiology* **21.2** (2020), pp. 177–190. DOI: 10.1089/ast.2019.2197.
- [176] Y. Liao, F. Nimmo, and J. A. Neufeld. "Heat Production and Tidally Driven Fluid Flow in the Permeable Core of Enceladus". *Journal of Geophysical Research: Planets* **125.9** (2020), e2019JE006209. DOI: <https://doi.org/10.1029/2019JE006209>.
- [177] C. Bethke. *Geochemical and biogeochemical reaction modeling*. Second edition.. Geochemical & Biogeochemical Reaction Modeling. Cambridge: Cambridge : Cambridge University Press, 2008. ISBN: 978-0-521-15570-0.

## Bibliography

---

- [178] D. E. LaRowe and H. C. Helgeson. “Biomolecules in hydrothermal systems: Calculation of the standard molal thermodynamic properties of nucleic-acid bases, nucleosides, and nucleotides at elevated temperatures and pressures”. *Geochimica et Cosmochimica Acta* **70**.18 (2006), pp. 4680–4724. DOI: 10.1016/j.gca.2006.04.010.
- [179] E. L. Shock, H. C. Helgeson, and D. A. Sverjensky. “Calculation of the thermodynamic and transport properties of aqueous species at high pressures and temperatures: Standard partial molal properties of inorganic neutral species”. *Geochimica et Cosmochimica Acta* **53**.9 (1989), pp. 2157–2183. DOI: 10.1016/0016-7037(89)90341-4.
- [180] A. V. Plyasunov and E. L. Shock. “Correlation strategy for determining the parameters of the revised Helgeson-Kirkham-Flowers model for aqueous nonelectrolytes”. *Geochimica et Cosmochimica Acta* **65**.21 (2001), pp. 3879–3900. DOI: 10.1016/S0016-7037(01)00678-0.
- [181] Y. Sekine, T. Shibuya, F. Postberg, et al. “High-temperature water-rock interactions and hydrothermal environments in the chondrite-like core of Enceladus”. *Nature Communications* **6**.1 (2015), p. 8604. DOI: 10.1038/ncomms9604.
- [182] F. Meersman, I. Daniel, D. H. Bartlett, et al. “High-Pressure Biochemistry and Biophysics”. *Reviews in Mineralogy and Geochemistry* **75**.1 (2013), pp. 607–648. DOI: 10.2138/rmg.2013.75.19.
- [183] F. M. Lauro and D. H. Bartlett. “Prokaryotic lifestyles in deep sea habitats”. *Extremophiles* **12**.1 (2008), pp. 15–25. DOI: 10.1007/s00792-006-0059-5.
- [184] T. M. Hoehler. “Biological energy requirements as quantitative boundary conditions for life in the subsurface”. *Geobiology* **2**.4 (2004), pp. 205–215. DOI: <https://doi.org/10.1111/j.1472-4677.2004.00033.x>.
- [185] N. M. Mesbah, G. M. Cook, and J. Wiegel. “The halophilic alkalithermophile *Natranaerobius thermophilus* adapts to multiple environmental extremes using a large repertoire of Na<sup>+</sup> (K<sup>+</sup>)/H<sup>+</sup> antiporters”. *Molecular microbiology* **74**.2 (2009), pp. 270–281.
- [186] C. S. Cockell. “Vacant habitats in the Universe”. *Trends in Ecology & Evolution* **26**.2 (2011), pp. 73–80. DOI: 10.1016/j.tree.2010.11.004.
- [187] C. O’Neill and F. Nimmo. “The role of episodic overturn in generating the surface geology and heat flow on Enceladus”. *Nature Geoscience* **3**.2 (2010), pp. 88–91. DOI: 10.1038/ngeo731.
- [188] C. G. Wheat, A. T. Fisher, J. McManus, et al. “Cool seafloor hydrothermal springs reveal global geochemical fluxes”. *Earth and Planetary Science Letters* **476** (2017), pp. 179–188. DOI: 10.1016/j.epsl.2017.07.049.



- [189] T. Kulp, S. Han, C. Saltikov, et al. “Effects of imposed salinity gradients on dissimilatory arsenate reduction, sulfate reduction, and other microbial processes in sediments from two California soda lakes”. *Applied and environmental microbiology* **73**.16 (2007), pp. 5130–5137.
- [190] T. J. McGenity. “Methanogens and methanogenesis in hypersaline environments”. *Handbook of hydrocarbon and lipid microbiology*. Ed. by K. Timmis, T. McGenity, J. van der Meer, et al. Springer, 2010, pp. 665–680.
- [191] W. J. Brazelton, M. O. Schrenk, D. S. Kelley, et al. “Methane- and Sulfur-Metabolizing Microbial Communities Dominate the Lost City Hydrothermal Field Ecosystem”. *Applied and Environmental Microbiology* **72**.9 (2006), pp. 6257–6270. DOI: 10.1128/AEM.00574-06.
- [192] S. Tan, Y. Sekine, T. Shibuya, et al. “The role of hydrothermal sulfate reduction in the sulfur cycles within Europa: Laboratory experiments on sulfate reduction at 100 MPa”. *Icarus* **357** (2021), p. 114222. DOI: 10.1016/j.icarus.2020.114222.
- [193] J. M. McDermott, S. P. Sylva, S. Ono, et al. “Abiotic redox reactions in hydrothermal mixing zones: Decreased energy availability for the subsurface biosphere”. *Proceedings of the National Academy of Sciences* **117**.34 (2020), pp. 20453–20461. DOI: 10.1073/pnas.2003108117.
- [194] S. L. Worman, L. F. Pratson, J. A. Karson, et al. “Abiotic hydrogen (H<sub>2</sub>) sources and sinks near the Mid-Ocean Ridge (MOR) with implications for the seafloor biosphere”. *Proceedings of the National Academy of Sciences* **117**.24 (2020), pp. 13283–13293. DOI: 10.1073/pnas.2002619117.
- [195] C. Paranicas, E. Roussos, N. Krupp, et al. “Energetic charged particle weathering of Saturn’s inner satellites”. *Planetary and Space Science. Surfaces, atmospheres and magnetospheres of the outer planets and their satellites and ring systems: Part VII* **61**.1 (2012), pp. 60–65. DOI: 10.1016/j.pss.2011.02.012.
- [196] A. Bouquet, C. R. Glein, D. Wyrick, et al. “Alternative Energy: Production of H<sub>2</sub> by Radiolysis of Water in the Rocky Cores of Icy Bodies”. *The Astrophysical Journal* **840**.1 (2017), p. L8. DOI: 10.3847/2041-8213/aa6d56.
- [197] H. T. Smith, M. Shappirio, R. E. Johnson, et al. “Enceladus: A potential source of ammonia products and molecular nitrogen for Saturn’s magnetosphere”. *Journal of Geophysical Research: Space Physics* **113**.A11 (2008). DOI: <https://doi.org/10.1029/2008JA013352>.
- [198] R.-S. Taubner, P. Pappenreiter, J. Zwicker, et al. “Biological methane production under putative Enceladus-like conditions”. *Nature Communications* **9**.1 (2018), p. 748. DOI: 10.1038/s41467-018-02876-y.

## Bibliography

---

- [199] A. Zandanel, L. Truche, R. Hellmann, et al. “Short lifespans of serpentinization in the rocky core of Enceladus: Implications for hydrogen production”. *Icarus* **364** (2021), p. 114461. DOI: 10.1016/j.icarus.2021.114461.
- [200] S. M. MacKenzie, M. Neveu, A. F. Davila, et al. “The Enceladus Orbilander Mission Concept: Balancing Return and Resources in the Search for Life”. *The Planetary Science Journal* **2.2** (2021), p. 77. DOI: 10.3847/PSJ/abe4da.
- [201] M. L. Cable, C. Porco, C. R. Glein, et al. “The Science Case for a Return to Enceladus”. *The Planetary Science Journal* **2.4** (2021), p. 132. DOI: 10.3847/PSJ/abfb7a.
- [202] S. D. Vance, K. P. Hand, and R. T. Pappalardo. “Geophysical controls of chemical disequilibria in Europa”. *Geophysical Research Letters* **43.10** (2016), pp. 4871–4879. DOI: 10.1002/2016GL068547.
- [203] B. A. Cohen and C. F. Chyba. “Racemization of Meteoritic Amino Acids”. *Icarus* **145.1** (2000), pp. 272–281. DOI: 10.1006/icar.1999.6328.
- [204] A. Catenaccio, Y. Daruich, and C. Magallanes. “Temperature dependence of the permittivity of water”. *Chemical Physics Letters* **367.5** (2003), pp. 669–671. DOI: 10.1016/S0009-2614(02)01735-9.
- [205] R. A. Alberty. “Calculation of Standard Transformed Gibbs Energies and Standard Transformed Enthalpies of Biochemical Reactants”. *Archives of Biochemistry and Biophysics* **353.1** (1998), pp. 116–130. DOI: 10.1006/abbi.1998.0638.
- [206] R. F. Weiss. “Carbon dioxide in water and seawater: the solubility of a non-ideal gas”. *Marine Chemistry* **2.3** (1974), pp. 203–215. DOI: 10.1016/0304-4203(74)90015-2.